Universität Stuttgart

Institut für Wasser- und Umweltsystemmodellierung

Mitteilungen

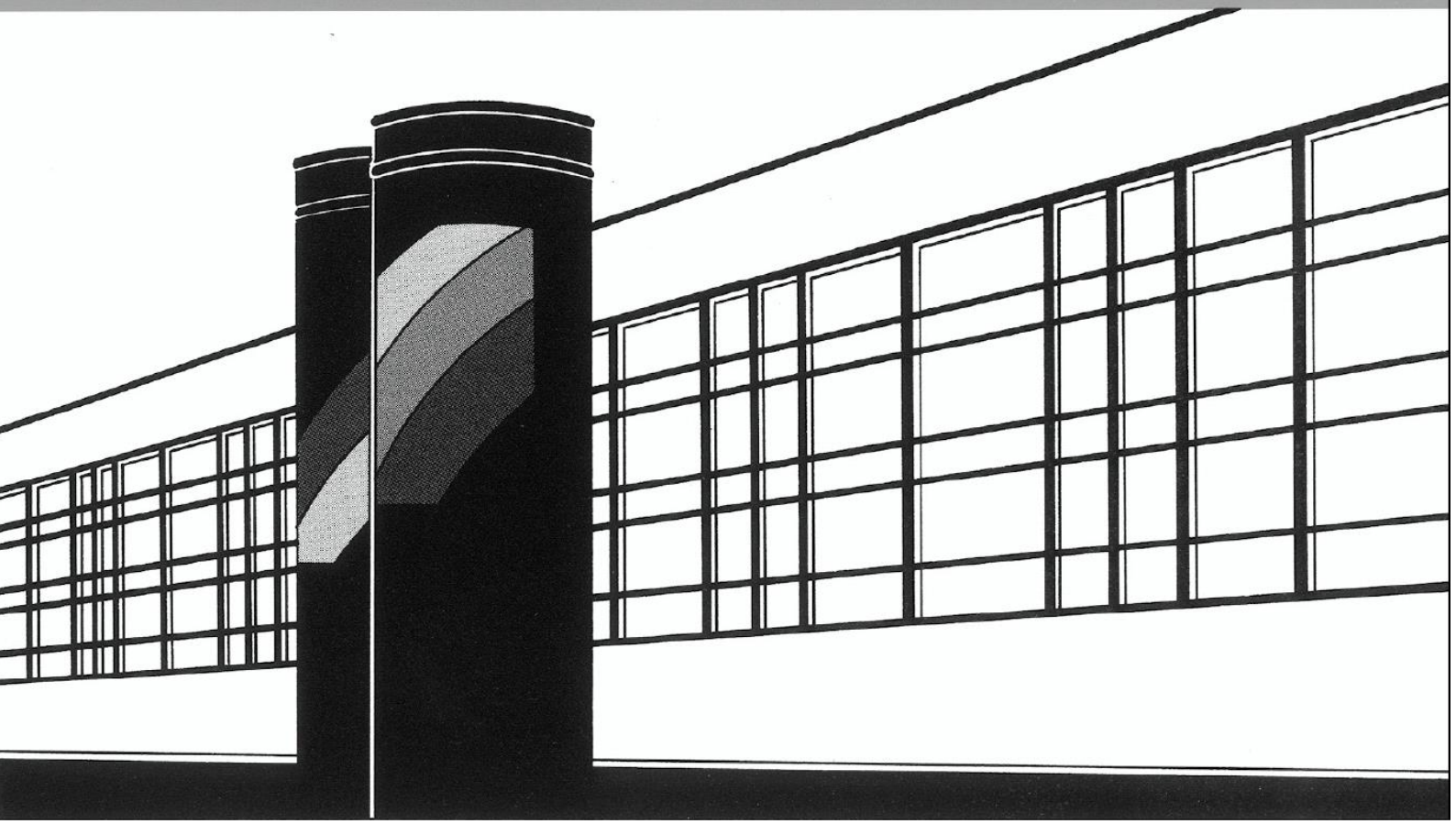

Heft 250 Stephen Oppong Kwakye

Study on the effects of climate change on the hydrology of the West African sub-region

Study on the effects of climate change on the hydrology of the West African sub-region

von der Fakultät Bau- und Umweltingenieurwissenschaften der Universität Stuttgart zur Erlangung der Würde eines Doktor-Ingenieurs (Dr.-Ing.) genehmigte Abhandlung

vorgelegt von

Stephen Oppong Kwakye

aus Kumasi

Hauptberichter:	Prof. Dr. rer. nat. Dr.-Ing. András Bárdossy
Mitberichter:	Prof. Dr. Harald Kunstmann

Tag der mündlichen Prüfung: 25.10.2016

Institut für Wasser- und Umweltsystemmodellierung
der Universität Stuttgart
2016

Heft 250

Study on the effects of climate change on the hydrology of the West African sub-region

von
Dr.-Ing.
Stephen Oppong Kwakye

Eigenverlag des Instituts für Wasser- und Umweltsystemmodellierung
der Universität Stuttgart

D93 Study on the effects of climate change on the hydrology of the West African sub-region

Bibliografische Information der Deutschen Nationalbibliothek
Die Deutsche Nationalbibliothek verzeichnet diese Publikation in der Deutschen Nationalbibliografie; detaillierte bibliografische Daten sind im Internet über http://www.d-nb.de abrufbar

Kwakye, Stephen Oppong:
Study on the effects of climate change on the hydrology of the West African sub-region, Universität Stuttgart. - Stuttgart: Institut für Wasser- und Umweltsystemmodellierung, 2016

(Mitteilungen Institut für Wasser- und Umweltsystemmodellierung, Universität Stuttgart: H. 250)
Zugl.: Stuttgart, Univ., Diss., 2016
ISBN 978-3-942036-54-2

NE: Institut für Wasser- und Umweltsystemmodellierung <Stuttgart>: Mitteilungen

Gegen Vervielfältigung und Übersetzung bestehen keine Einwände, es wird lediglich um Quellenangabe gebeten.

Herausgegeben 2016 vom Eigenverlag des Instituts für Wasser- und Umweltsystem-modellierung

Druck: Document Center S. Kästl, Ostfildern

Acknowledgment

I would like to thank and express my sincere gratitude to the following people and agencies that helped and supported me during my PhD programme.

Firstly, I would like to thank and appreciate Prof. Dr. rer.nat. Dr.-Ing. András Bárdossy and Prof. Dr. Harald Kunstmann for supervising this study. I tremendously appreciate their inputs, concerns, time, suggestions, guidance, encouragements and the overall supervision.

Many thanks to Dr. Jochen Seidel and my colleagues Tobias Mosthaf, Yingchun Huang, Dirk Schlabing, Thomas Müller, Suroso, Ning Wang, Faizan Anwar, Jieru Yan and many more. I really enjoyed the good working atmosphere, their suggestions and encouragements along the way.

I further extend my gratitude to Dr. Dominikus Heinzeller of Karlsruhe Institute of Technology (KIT) and to Antonio Rogmann of WASCAL for providing me the climate data for this study.

I appreciate the excellent and uncomplicated administrative help and work of Astrid Lemp.

The Ghanaian government, through the Ministry of Education, Ghana and the German Academic Exchange Service (DAAD) supported me financially during this work and I am much grateful to them.

Special thanks to all my friends and former colleagues in Stuttgart for the great academic and social life I enjoyed with you.

I am grateful to my family for their help throughout my educational career.

Last but not the least, to my mother-in-law for taking care of my children whiles I was doing this PhD with my wife.

Most of all, I would like to thank and appreciate my wife (Philomina Oppong Kwakye) and our kids for their continuous support, care, patience, prayers and everything during this research. I share this degree with them.

Contents

List of Figures III

List of Tables X

Abstract XI

Kurzfassung XV

1 Introduction 1
- 1.1 Motivation . . . 1
- 1.2 Aims and Objectives . . . 2
- 1.3 Innovation . . . 2
- 1.4 Methodology . . . 3
- 1.5 Structure of the Thesis . . . 3

2 Study Area Description and Literature Review 4
- 2.1 A brief description of the study area . . . 4
- 2.2 Climate . . . 7
- 2.3 Soils . . . 10
- 2.4 Geology . . . 11
- 2.5 Vegetation and Land Use . . . 12
- 2.6 Topography and Relief . . . 14
- 2.7 The climate trend in the West Africa sub-region . . . 16
- 2.8 Review of hydrological modeling in West Africa . . . 17
- 2.9 A brief review of studies on climate changes in West African . . . 19
- 2.10 A review of the effects of climate change on the hydrology of West Africa . . . 20

3 Analysis of Observed Climate and Hydrological Data 23
- 3.1 Introduction . . . 23
- 3.2 Precipitation . . . 23
  - 3.2.1 Annual cycle of rainfall . . . 24
  - 3.2.2 What influences rainfall in the catchment . . . 25
  - 3.2.3 Rainfall correlation between pairs of stations . . . 25
  - 3.2.4 Interpolation of mean monthly rainfall . . . 27
- 3.3 Temperature . . . 33
- 3.4 Discharge . . . 34
- 3.5 Potential Evapotranspiration . . . 36

4 Hydrological Modeling **39**
4.1 Introduction . . . 39
4.2 HBV − Hydrological Model . . . 40
4.2.1 Soil moisture accounting . . . 40
4.2.2 Evapotranspiration . . . 41
4.2.3 Runoff response process . . . 41
4.3 Model performance measures . . . 44
4.4 Robust Parameter Estimation (ROPE) . . . 46
4.5 Results . . . 46
4.5.1 Performance measures under different sub-catchments . . . 46
4.5.2 Calibrating on daily temporal scale and checking performance on different scales . . . 49
4.5.3 Calibration on different temporal scales . . . 49
4.5.4 Swapping of data for calibration and validation . . . 50
4.5.5 Calibrating on dry and validating on wet and vice versa . . . 51

5 Analysis of Climate Data from Regional Climate Models (RCMs) **59**
5.1 Introduction . . . 59
5.2 Definition of some Terminologies . . . 59
5.3 Data . . . 61
5.3.1 Climate data from IMK-IFU . . . 62
5.3.2 Climate data from CORDEX . . . 62
5.4 Results from the analysis of simulated climate data from IMK-IFU/WASCAL for the West Africa Sub-region . . . 63
5.5 Results from the analysis of simulated climate data from CORDEX . . . 71
5.6 Bias correction of climate simulations . . . 78
5.6.1 Introduction . . . 78
5.6.2 Linear Scaling method . . . 78
5.6.3 Quantile−Quantile mapping method . . . 79
5.6.4 Results of Bias-corrected climate simulations . . . 80

6 Effects of climate change (cc) on the hydrology of the sub-region **90**
6.1 Introduction . . . 90
6.2 The effects of CC on hydrology using CanESM driving model . . . 90
6.3 The effects of CC on hydrology using EC-EARTH driving model . . . 93
6.4 The effects of CC on hydrology using ECHAM driving model . . . 96
6.5 The effects of CC on hydrology using GFDL driving model . . . 98
6.6 The effects of CC on hydrology using MIROC driving model . . . 101

7 Summary and Conclusions **104**

Bibliography **107**

List of Figures

2.1 The Black Volta Basin with its riparian countries (Insert: Black Volta Basin showing digital elevation map and the rainfall gauge stations). 5
2.2 The Black Volta catchment (green) inside the Volta Basin 6
2.3 The aridity and climatic zones of the African Continent (The red box roughly indicates the study area). Source: World Meteorological Organization (WMO) 8
2.4 The movements of the ITCZ showing the wet and dry seasons of the West-Africa sub-region (The red box roughly shows the study area). Source: World Meteorological Organization (WMO) 9
2.5 Soil map of the Black Volta Basin (Adapted from the European Soil Data Centre) 11
2.6 Landcover map of the the Black Volta Basin for the year 2000 13
2.7 The NDVI map of the Black Volta Catchment for the year 2000 14
2.8 Digital elevation map of the Black Volta Basin 15
2.9 Runoff change (x axis, %) in West Africa based on all cases in the database (i.e., including different time period, rivers and models). The blue dashed line represents the median of the distribution; the red one is the mean. Focussed here only on the impact of climate change: this is the only changing parameter (no water use or land use change) Source: [Roudier et al., 2014] 21
2.10 Monthly mean discharge at Bonou (Benin) simulated with HBV, climate scenarios A2 (2000 to 2030) and B2 (2000 to 2030) compared to a reference period. Source: [Götzinger, 2007] 22

3.1 A DEM map of the catchment showing the locations of the 20 rainfall gauge stations (blue dot) 24
3.2 Left: annual rainfall cycle for a station in the north. Right: annual rainfall cycle for a station in the south 25
3.3 Correlation of northings of stations against monthly rainfalls 26
3.4 Correlation of eastings of stations against monthly rainfalls 26
3.5 Correlation of elevations of stations against monthly rainfalls 27
3.6 Correlation of rainfall between pairs of stations 27
3.7 Mean daily rainfall amounts in (mm) for the months of June (left) and July (right) for the period 1961−2005 30
3.8 Mean daily rainfall amounts in (mm) for the months of August (left) and September (right) for the period 1961−2005 30
3.9 Mean daily rainfall amounts in (mm) for the months of October(left) and November (right) for the period 1961−2005 31
3.10 Interpolated mean annual rainfall expressed in daily amounts (mm) 32
3.11 A map of the catchment showing the temperature stations 33

3.12 Annual temperature cycle for a station in the north (right) and a station in the south (left) of the catchment 34
3.13 Discharge stations on the Black Volta River of the catchment 35
3.14 Annual discharge cycles for two different stations in the catchment 35
3.15 Mean annual PET (mm) for the Black Volta basin. Primary souce: Global-PET geoportal) 38
3.16 Up: Mean monthly PET calculated using the Thornthwaite method and the data from Global-PET; Down: Mean daily PET estimated from the Global-PET 38

4.1 Smoothing of the generated runoff Qg to obtain Q. (source: [Hundecha and Bárdossy, 2004]) 43
4.2 Schematic representation of HBV−IWS model which is slightly modified for the study area. Adapted from Hundecha and Bárdossy [2004] 44
4.3 Hydrographs for sub-catchment Lawra showing both the calibration and validation periods 47
4.4 Hydrographs for sub-catchment Chache showing both the calibration and validation periods 48
4.5 Hydrograph for calibration of the model for gauge Chache using (NS +3LogNS) as the objective function 49
4.6 Hydrograph for validation of the model for gauge Chache using (NS +3LogNS) as the objective function 50
4.7 Hydrograph showing the model performance on the daily residuals after calibration on the daily scale 51
4.8 Hydrograph showing the model performance on the monthly simulations after calibration on the daily scale 52
4.9 Hydrograph showing the model performance on the monthly residuals after calibration on the daily scale 54
4.10 Hydrograph showing the model performance for gauge Chache when calibration was done on monthly scale 55
4.11 Hydrograph showing the model performance for gauge Chache when calibration was done on daily residuals. 56
4.12 Hydrograph showing model performance for gauge Chache on daily temporal scale for swapped calibration and validation data: Left (calibration), Right (Validation) 56
4.13 Hydrograph showing model performance for gauge Chache on monthly temporal scale for swapped calibration and validation data: Left (calibration), Right (Validation) 57
4.14 Hydrographs of split sampling for sub-catchment Lawra showing both the calibration and validation periods 57
4.15 Hydrographs of split sampling for sub-catchment Chache showing both the calibration and validation periods 58

5.1 Relationship between the new RCPs and the IPCC's Special Report on Emission Scenarios (SRES) (credit: [Stocker et al., 2013] 61

5.2 Schematic depiction of the first phase CORDEX experiment set-up (credit: [Giorgi et al., 2009]) . . . 63
5.3 Empirical cdf plots of observed and RCM runs using echam6 GCM driving model for temperature for historical (hist) and future (rcp) simulations for stations Bole and Wenchi . . . 64
5.4 Empirical cdf plots of observed and RCM runs using echam6 GCM driving model for temperature for historical (hist) and future (rcp) simulations for stations Babile and Bechem . . . 65
5.5 Annual cycle of observed and RCM runs using echam6 GCM driving model for temperature for historical (hist) and future (rcp) simulations for stations Wenchi and Bui . . . 65
5.6 Annual cycle of observed and RCM runs using echam6 GCM driving model for temperature for historical (hist) and future (rcp) simulations for stations Babile and Dedougou . . . 66
5.7 Empirical cdf plots for observed and RCM (echam6-GCM driving model) runs of daily rainfall less than 50mm for historical (hist) and future (rcp) simulations for stations Babile and Kintampo . . . 67
5.8 Empirical cdf plots for observed and RCM runs using Echam6 GCM driving model for daily rainfall greater than 20mm for historical and future simulations for stations Babile and Kintampo . . . 67
5.9 Empirical cdf plots for observed and Echam6 GCM driving model RCM runs of daily rainfall for historical and future simulations for stations Babile and Kintampo (N: number of events used, hist: historical simulations, rcp: future simulations, obs: observed measurements, Po: percentage of zero rainfall) . . 68
5.10 Empirical cdf plots for observed and Echam6-GCM driving model RCM runs of daily rainfall for historical and future simulations for stations Bagassi and Bui (N: number of events used, hist: historical simulations, rcp: future simulations, obs: observed measurements, Po: percentage of zero rainfall) . . . 68
5.11 Annual cycle before (left) and after smoothening (right) (i.e. noise removal) . 69
5.12 Annual cycle of observed and RCM runs using echam6 GCM driving model for rainfall for historical (hist) and future (rcp) simulations for station Kintampo and Bui . . . 69
5.13 Annual cycle of observed and RCM runs using echam6 GCM driving model for rainfall for historical (hist) and future (rcp) simulations for station Babile and Bagassi . . . 70
5.14 Annual cycle of observed and RCM runs using echam6 GCM driving model for rainfall for historical (hist) and future (rcp) simulations for station Bomborokuy . . . 70
5.15 Lorenz curve of RCM simulations of precipitation for different driving models as compared with the observed . . . 72
5.16 Lorenz curve for the RCM simulations of precipitation with different driving models as compared with the observed for station Kintampo . . . 73
5.17 Annual cycle of observed and RCM runs using CanESM GCM driving model for rainfall for historical (hist) and future (rcp) simulations for stations Bole and Bomborokuy . . . 74

5.18 Annual cycle of observed and RCM runs using EC-EARTH GCM driving model for rainfall for historical (hist) and future (rcp) simulations for stations Bole and Bomborokuy 74
5.19 Annual cycle of observed and RCM runs using GFDL GCM driving model for rainfall for historical (hist) and future (rcp) simulations for stations Bole and Bomborokuy 75
5.20 Annual cycle of observed and RCM runs using MIROC GCM driving model for rainfall for historical (hist) and future (rcp) simulations for stations Bole and Bomborokuy 75
5.21 Empirical cdf plots of observed and RCM runs using CanESM and EC-EARTH driving models for temperature of historical (hist) and future (rcp) simulations for station Babile 76
5.22 Empirical cdf plots of observed and RCM runs using ECHAM6 and GFDL driving models for temperature of historical (hist) and future (rcp) simulations for station Babile 76
5.23 Empirical cdf plots of observed and RCM runs using HadGEM and MIROC driving models for temperature of historical (hist) and future (rcp) simulations for station Babile 77
5.24 Bias correction procudure for ECHAM6 driving model using quantile-quantile mapping for station Babile. (The Gamma distribution of RCM-simulated daily precipitation (dashed blue) was shifted towards the Gamma distribution of the observations (red line)) 81
5.25 Bias correction procudure for ECHAM6 driving model using quantile-quantile mapping for station Wenchi. (The Gausssian distribution of RCM-simulated daily temperature (dashed blue) was shifted towards the Gaussian distribution of the observations (red line)). 82
5.26 Annual cycle of observed(obs), uncorrected historical and future rainfall RCM simulations (histUC and rcpUC) and bias corrected simulations (MC/QC) for the CanESM driving model. Left: Correction using Linear Scaling method (MC), Right: Correction using Quantile mapping method (QC) . 82
5.27 Annual cycle of observed(obs), uncorrected historical and future rainfall RCM simulations (histUC and rcpUC) and bias corrected simulations (MC/QC) for the EC-EARTH driving model. Left: Correction using Linear Scaling method (MC), Right: Correction using Quantile mapping method (QC) 83
5.28 Annual cycle of observed(obs), uncorrected historical and future rainfall RCM simulations (histUC and rcpUC) and bias corrected simulations (MC/QC) for the ECHAM driving model. Left: Correction using Linear Scaling method (MC), Right: Correction using Quantile mapping method (QC) . 83
5.29 Annual cycle of observed(obs), uncorrected historical and future rainfall RCM simulations (histUC and rcpUC) and bias corrected simulations (MC/QC) for the GFDL driving model. Left: Correction using Linear Scaling method (MC), Right: Correction using Quantile mapping method (QC) . 85

5.30 Annual cycle of observed(obs), uncorrected historical and future rainfall RCM simulations (histUC and rcpUC) and bias corrected simulations (MC/QC) for the MIROC driving model. Left: Correction using Linear Scaling method (MC), Right: Correction using Quantile mapping method (QC) . 85
5.31 Annual cycle of observed(obs), uncorrected historical and future temperature RCM simulations (histUC and rcpUC) and bias corrected simulations (MC/QC) for the CanESM driving model. Left: Correction using Linear Scaling method (MC), Right: Correction using Quantile mapping method (QC) . 86
5.32 Annual cycle of observed(obs), uncorrected historical and future temperature RCM simulations (histUC and rcpUC) and bias corrected simulations (MC/QC) for the EC-EARTH driving model. Left: Correction using Linear Scaling method (MC), Right: Correction using Quantile mapping method (QC) 86
5.33 Annual cycle of observed(obs), uncorrected historical and future temperature RCM simulations (histUC and rcpUC) and bias corrected simulations (MC/QC) for the ECHAM driving model. Left: Correction using Linear Scaling method (MC), Right: Correction using Quantile mapping method (QC) . 88
5.34 Annual cycle of observed(obs), uncorrected historical and future temperature RCM simulations (histUC and rcpUC) and bias corrected simulations (MC/QC) for the GFDL driving model. Left: Correction using Linear Scaling method (MC), Right: Correction using Quantile mapping method (QC) 88
5.35 Annual cycle of observed(obs), uncorrected historical and future temperature RCM simulations (histUC and rcpUC) and bias corrected simulations (MC/QC) for the MIROC driving model. Left: Correction using Linear Scaling method (MC), Right: Correction using Quantile mapping method (QC) . 89

6.1 Flow duration curves of simulated discharges (historical (hist) (1980−2005) *(blue)*; future (rcp)(2020−2045) *(green)*; observed (1980−2005)*(red)*; simulated (1980−2005) *(orange)*; bias-corrected rcm simulations using linear scaling (MC) method *dashed blue and green*) with CanESM as the driving model 92
6.2 Flow duration curves of simulated discharges (historical (hist) (1980−2005) *(blue)*; future (rcp)(2020−2045) *(green)*; observed (1980−2005)*(red)*; simulated (1980−2005) *(orange)*; bias-corrected rcm simulations using linear scaling (MC) method *dashed blue and green*) with CanESM as the driving model 93
6.3 Annual cycle of discharges (historical (hist) (1980−2005) *(blue)*; future (rcp)(2020−2045) *(green)*; bias-corrected rcm simulations using linear scaling (MC) (−left) and quantile mapping (QC) (−right) methods *dashed blue and green*) using CanESM as the driving model; observed (obs) (1980-2005) *(red)* and simulated discharges (sim) (1980−2005) *(black)*) 93
6.4 Flow duration curves of simulated discharges (historical (hist) (1980−2005) *(blue)*; future (rcp)(2020−2045) *(green)*; observed (1980−2005)*(red)*; simulated (1980−2005) *(orange)*; bias-corrected rcm simulations using Quantile mapping (QC) method *dashed blue and green*) with EC-EARTH as the driving model . . 94

6.5 Flow duration curves of simulated discharges (historical (hist) (1980−2005) *(blue)*; future (rcp)(2020−2045) *(green)*; observed (1980−2005)*(red)*; simulated (1980−2005) *(orange)*; bias-corrected rcm simulations using linear scaling (MC) method *dashed blue and green*) with EC-EARTH as the driving model . . 95
6.6 Annual cycle of discharges (historical (hist) (1980−2005) *(blue)*; future (rcp)(2020−2045) *(green)*; bias-corrected rcm simulations using linear scaling (MC) (−left) and quantile mapping (QC) (−right) methods *dashed blue and green*) using EC-EARTH as the driving model; observed (obs) (1980-2005) *(red)* and simulated discharges (sim) (1980−2005) *(black)*) 95
6.7 Flow duration curves of simulated discharges (historical (hist) (1980−2005) *(blue)*; future (rcp)(2020−2045) *(green)*; observed (1980−2005)*(red)*; simulated (1980−2005) *(orange)*; bias-corrected rcm simulations using Quantile mapping (QC) method *dashed blue and green*) with ECHAM as the driving model 96
6.8 Flow duration curves of simulated discharges (historical (hist) (1980−2005) *(blue)*; future (rcp)(2020−2045) *(green)*; observed (1980−2005)*(red)*; simulated (1980−2005) *(orange)*; bias-corrected rcm simulations using linear scaling (MC) method *dashed blue and green*) with ECHAM as the driving model 97
6.9 Annual cycle of discharges (historical (hist) (1980−2005) *(blue)*; future (rcp)(2020−2045) *(green)*; bias-corrected rcm simulations using linear scaling (MC) (−left) and quantile mapping (QC) (−right) methods *dashed blue and green*) using ECHAM as the driving model; observed (obs) (1980-2005) *(red)* and simulated discharges (sim) (1980−2005) *(black)*) 97
6.10 Flow duration curves of simulated discharges (historical (hist) (1980−2005) *(blue)*; future (rcp)(2020−2045) *(green)*; observed (1980−2005)*(red)*; simulated (1980−2005) *(orange)*; bias-corrected rcm simulations using Quantile mapping (QC) method *dashed blue and green*) with GFDL as the driving model 99
6.11 Flow duration curves of simulated discharges (historical (hist) (1980−2005) *(blue)*; future (rcp)(2020−2045) *(green)*; observed (1980−2005)*(red)*; simulated (1980−2005) *(orange)*; bias-corrected rcm simulations using linear scaling (MC) method *dashed blue and green*) with GFDL as the driving model 100
6.12 Annual cycle of discharges (historical (hist) (1980−2005) *(blue)*; future (rcp)(2020−2045) *(green)*; bias-corrected rcm simulations using linear scaling (MC) (−left) and quantile mapping (QC) (−right) methods *dashed blue and green*) using GFDL as the driving model; observed (obs) (1980-2005) *(red)* and simulated discharges (sim) (1980−2005) *(black)*) 100
6.13 Flow duration curves of simulated discharges (historical (hist) (1980−2005) *(blue)*; future (rcp)(2020−2045) *(green)*; observed (1980−2005)*(red)*; simulated (1980−2005) *(orange)*; bias-corrected RCM simulations using Quantile mapping (QC) method *dashed blue and green*) with MIROC as the driving model . 101
6.14 Flow duration curves of simulated discharges (historical (hist) (1980−2005) *(blue)*; future (rcp)(2020−2045) *(green)*; observed (1980−2005)*(red)*; simulated (1980−2005) *(orange)*; bias-corrected rcm simulations using linear scaling (MC) method *dashed blue and green*) with MIROC as the driving model 102

6.15 Annual cycle of discharges (historical (hist) (1980−2005) *(blue)*; future (rcp)(2020−2045) *(green)*; bias-corrected rcm simulations using linear scaling (MC) (−left) and quantile mapping (QC) (−right) methods *dashed blue and green*) using MIROC as the driving model; observed (obs) (1980-2005) *(red)* and simulated discharges (sim) (1980−2005) *(black)*) 102

List of Tables

4.1 Model parameter range for HBV model. Source: [Bárdossy and Singh, 2008] (max. and min. values were slightly modified for the study area) 43
4.2 Model performance for sub-catchment Lawra (size: 92,877 km^2) for calibration and validation 47
4.3 Model performance for sub-catchment Chache (size: 111,258 km^2) for calibration and validation 48
4.4 Calibration and validation results for Chache by calibrating on daily scale and checking performances on other temporal scales with (NS +3LogNS) as the objective function 51
4.5 Model performance on gauge Chache for calibration on different temporal scales using (NS+3LogNS)/4 and NS as the performance measurement functions 52
4.6 Model performance for gauge Chache for a swapped data for calibration and validation period 53
4.7 Model performance for Lawra on split sampling (calibration and validation) . 53
4.8 Model performance for Chache on split sampling (calibration and validation) 53

5.1 Summary of results for corrected and uncorrected rainfall simulations (areal) for historical period (1979−2005) and future (2019−2045). P0 and P20 represents the probability of zero precipitation and precipitation above 20mm respectively 84
5.2 Summary of results for corrected and uncorrected temperature simulations (areal) for historical period (1979−2005) and future (2019−2045) 87

Abstract

WATER is LIFE and the economy of many countries including the West African sub-region depends directly or indirectly on the water availability.

The Intergovernmental Panel on Climate Change (IPCC) reports predict and continues to predict global warming and a changing climate. Because there is a strong interconnection between the climate and the hydrological cycle, any changes that would occur in the climate system would also affect the hydrological cycle. As a result of the above and other reasons, a clear scientific research and understanding of the effects of the changing climate on the hydrology and water resources of an area is always eminent and crucial.

Western Africa is a fast developing sub-region within the African continent. It faces challenges like water scarcity, diseases, famine, unemployment and sometimes poor decisions on water related projects. Several studies by other researchers have revealed that, climate change has already made it's footprint in the sub-region.

In this study, I tried to ascertain further how much climate change is happening in the West Africa sub-region and to also determine its effect on the hydrology of the region. And in doing this, different latest climate models and simulations in conjunction with a conceptual lumped hydrological model were used in the study. The study was performed on the Black Volta Catchment in the sub-region which has an approximate area of 150,000 km^2.

Precipitation is a climate variable that influences the hydrology and water resources of an area. For any hydrological or climate model, one has to know the spatial and or temporal trend of this important variable (i.e. Precipitation) and how reliable it's observed and ground-truth data is. The observed annual rainfall cycles, rainfall correlation between pairs of stations, as well as what influences precipitation in the Black Volta Basin were investigated. Precipitation time series for about 20 stations ranging from 1961 to 2005 were used.

The analyzed observed climate depicted the different climates in the catchment which ranges from a sub-humid climate in the south to a semi-arid in the north of the basin. There is also a bi-modal annual rainfall cycle at the south of the catchment and a uni-modal cycle towards the north of the basin. The precipitation has a decreasing gradient towards the north of the basin which is all in consonant with previous studies and results by other researchers. A correlation analysis was performed on what influences precipitation in the catchment and at the end, it was revealed that the distances of the rain gauges from the coast influences precipitation and not the elevations. This knowledge was used as the external drift during the spatial interpolation of rainfall using external drift Kriging to produce maps of long-term monthly and annual rainfall mean for the study area.

Rainfall-runoff models are necessary and needed to predict water resources future development. And to investigate the water balance situations in the catchment, a lumped version

of the conceptual HBV−IWS version (Hydrologiska Byrans Vattenbalansavdelning) hydrological model was applied to the study area. The observed station data (i.e. rainfall and temperature) were obtained from the Meteorological agencies in Ghana and Burkina Faso and the Volta basin geoportal. Discharge measurements at two different locations were used to optimize the model parameters and to check the performance of the model.

In assessing how well the model performs, different optimization techniques ranging from Nash-Sutcliffe (NS), the logarithmic of the Nash-Sutcliffe (LogNS), the Nash-Sutcliffe with a bias constraint (NS-Bias) and the Kling−Gupta (KG) were used. The robust parameter estimation (ROPE) was used to generate and calibrate 10,000 best parameter sets in a computer framework with initially set model parameter ranges. The model performed well with an average NS of 0.75 and 0.6 for calibration and validation respectively. The performance also improved when a higher weight was given to the low-flows during the optimization.

Again, the robustness and steadiness of the HBV rainfall-runoff model was assessed by using various calibration and validation techniques. Results also show that the model reacts well to signals in that a split sampling of the data into dry and wet years used for calibration and validation and vice-versa yielded good results. The annual discharge cycle was subtracted from both the observed and modeled discharges and then the efficiency of the model was determined using the residual-discharges and the results were found to be encouraging.

Climate models such as General Circulation Models (GCMs) and Regional climate models (RCMs) are tools used to simulate the climate of the present and to also predict the future climate. The GCMs have coarser resolutions and they are mainly on the global scale and the RCMs are used on the regional to local scales.

In this study, GCM/RCM climate data from the Coordinated Regional Downscaling Experiment (CORDEX) and the Regional Climate Division of Institute of Meteorology and Climate research at Karlsruhe Institute of Technology (IMK-IFU) was used to determine how the climate in the West Africa sub-region will be in the future. Six (6) different GCM (CanESM2M, EC−EARTH, ECHAM6, HadGEM, GFDL and MIROC) driving models were used in the study. The Rossby Centre regional Atmospheric Climate model (RCA4) and the Weather Research and Forecasting (WRF) Model were used as the RCM for the data from CORDEX and IMK−IFU respectively. The analysis was performed on a daily temporal resolution and a spatial resolution of 50 km and 12 km respectively for the data from CORDEX and IMK−IFU.

The GCM/RCMs climate simulations showed biases, and they were corrected by using the Linear Scaling and the Quantile mapping methods of bias correction. In general, the results produced by the latter correction method produced better results than the former. It was then clear from the climate analysis that the future climate will change with respect to the temperature and the rainfall pattern and amounts. All the GCMs/RCMs predicted and confirmed a warmer future of about +1°C to +2°C. For precipitation, the models predicted both a slight increase and a decrease in the future rainfall. Similar climate trend was also observed in the bias corrected simulations.

The core of the research, which is to determine the effects of the changed climate on the

hydrology of the region, was performed using the robust and validated HBV hydrological model and the uncorrected and corrected climate simulations. The experiment was done on a daily temporal scale. It was found out that, out of the five (5) GCM driving models used for the impact analysis, four (4) of the models predicts a decrease in the discharge or hydrology of the sub-region and only one showed a slight increase. The corrected GCM/RCM climate simulations reproduced the same trend and signal as in the uncorrected data. And again, the bias corrected results showed a clear and better performance than the uncorrected climate simulations.

It was therefore concluded that climate change could negatively impact and decrease the hydrology of the sub-region in the future. The river flow could reduce and most of the rivers in the catchment will run dry in most months of the annual discharge cycle. But it should be stressed that, because only one climate scenario (the rcp45) was used for the analysis, care must be taken in using the results of the studies.

As a result of the decrease in river flow that will occur in the future as a result of climate change. This could tremendously affect the water resources of the sub-region and will also negatively impact on the socio-economic well-being of the people in the region. Hydropower is the main source of electricity for the region and this will also be negatively affected because of climate change. The people in the region are mainly farmers who use this scarce water resource to also irrigate their farms and they depend on this occupation for their sustenance and livelihood. The population of the sub-region is rising up at a growth rate of about 2.5% per annum which also put additional stress on the water resources in the area.

The above challenges and problems should prompt immediate proper adaptation and mitigation measures to be implemented so as to ameliorate the impact of these changes on the people and the economy of the region as a whole.

Kurzfassung

WASSER ist LEBEN. Auch deswegen hängt die Wirtschaft vieler Ländern, und speziell die der westafrikanischen Subregion, entscheidend von der Wasserversorgung ab.

Der Weltklimarat (Intergovernmental Panel on Climate Change, IPCC) sagt in seinen Sachstandsberichten zukünftige Klimaveränderungen und anhaltende globale Erwärmung voraus. Aufgrund der starken Kopplung von Klima und Wasserkreislauf werden die zukünftigen Klimaänderungen auch den Wasserkreislauf betreffen. Aus diesen Gründen sind wissenschaftlich fundierte Erkenntnisse über die Auswirkungen klimatischer Veränderungen auf die Hydrologie, und damit einhergehend tieferes Verständnis über Wasserressourcen wichtig und von eminenter Bedeutung.

Westafrika ist ein sich rasant entwickelnder Teil des afrikanischen Kontinents. Als Herausforderungen dieser Entwicklung sind unter anderem Wasserknappheit, Krankheiten, Hunger und Arbeitslosigkeit zu nennen. Nicht zuletzt werden bei wasserbezogenen Projekten außerdem manchmal schlechte Entscheidungen getroffen. In mehrere Studien wurde aus diesen Gründen schon bestätigt, dass der Klimawandel in Afrika bereits seine Fußabdrücke hinterlassen hat.

In der vorliegenden Arbeit vertiefe ich das Wissen darüber in welchem Maße der Klimawandel in der westafrikanische Subregion stattfindet und untersuche den Einfluss auf die Hydrologie in der Region. Als Grundlage für die Untersuchungen dienen die aktuellsten Klimamodelle und Simulationen in Kombination mit hydrologischen Wasserhaushaltsmodellen. Als Untersuchungsgebiet dient das Einzugsgebiet der Schwarzen Volta mit einer Gesamtfläche von ungefähr 150.000 km^2.

Eine Haupteinflussgröße auf die regionale Hydrologie und den Wasserhaushalt ist der Niederschlag. Für jedes hydrologische Modell ist also die räumliche und zeitliche Verteilung des Niederschlags und eine genaue Kenntnis der Datenlage und $-$qualität essentiell. Für das Untersuchungsgebiet stehen Niederschlagsdaten von ca. 20 Messeinrichtungen für den Zeitraum von 1961 bis 2005 zur Verfügung. Die Daten werden auf jährliche Zyklen ausgewertet; außerdem werden Korrelationen zwischen verschiedenen Niederschlagsmessstationen bestimmt um die Verteilung und externe Einflussgrößen des Niederschlags zu bestimmen.

Das Untersuchungsgebiet erstreckt sich über mehrere klimatische Zonen. Im Süden herrscht ein subhumides Klima während im Norden semiarides Klima vorherrschend ist. Damit einhergehend zeigen die Niederschlagsdaten einen bimodalen Jahresgang des Niederschlags im Süden der Richtung Norden in einen unimodalen Jahresgang übergeht. Die Niederschlagssummen weisen außerdem in übereinstimmung mit anderen Studien einen ab-

nehmenden Trend Richtung Norden des Einzugsgebiets auf. Als Ergebnis der Korrelationsuntersuchungen lässt sich festhalten, dass der Niederschlag hauptsächlich von der Entfernung zur Küste und nicht von der Geländehöhe abhängig ist. Diese Erkenntnisse können für die räumliche Interpolation (Kriging) von Monats- oder Jahressummen des Niederschlags als Trend (external drift) verwendet werden.

Um die zukünftige Entwicklung der Wasserressourcen zu modellieren wird in der vorliegenden Arbeit das Modell HBV−IWS (Hydrologiska Byrans Vattenbalansavdelning) verwendet. Die benötigten Wetterdaten (Niederschlag und Temperatur) werden von den meteorologischen Behörden Ghanas und Burkina Fasos sowie dem Geoportal des Volta-Einzugsgebiets zur Verfügung gestellt. Das Modell wird an das Untersuchungsgebiet von zwei unterschiedliche Flusspegeln angepasst um die Qualität der Modellierung zu beurteilen.

Für die Modellvalidierung werden verschiedene Optimierungsverfahren angewendet: Nash-Sutcliffe (NS), logarithmischer Nash-Sutcliffe (LogNS), Nash-Sutcliffe mit Bias-Nebenbedingung (NS-Bias) und Kling-Gupta (KG). Mit hilfe der computergestützten robusten Parameterschätzung (ROPE) werden die 10.000 besten Parametersätze innerhalb vorgegebenen obereb und unteren Grenzen generiert und kalibriert. Das Modell zeigt einen guten durchschnittlichen NS Koeffizient von 0,75 für die Kalibrierung und von 0,6 für die Validierung. Die Modellqualität verbesserte sich wenn bei der Kalibrierungden niedrigen Abflüsse mehr Gewichung gegeben wurde.

Die Robustheit und Stabilität des HBV-Niederschlag-Abfluss-Modell wurde unter Verwendung von verschiedenen Kalibrierungs- und Validierungstechniken bewertet. Die Aufteilung der Datenin trockene und feuchte Jahre und die Verwendung dieser Teilmengen jeweils zur Kalibrierung und zur Validierung zeigt, dass das Modell gut auf verschiedene Eingangsgrößen reagiert. Um die Effizienz des Modells über den Residualabfluss zu bestimmen wird der mittlere jährliche Abflusse vom modellierten sowie vom beobachteten Abfluss abgezogen auch diese Ergebnisse sprechen für die Güte des Modells.

Klimamodelle (General Circulation Models, GCMs) und Regionale Klimamodelle (RCMs) sind Instrumente, um das Klima der Gegenwart zu simulieren und das Klima der Zukunft vorhersagen. Die GCMs sind numerisch gröber aufgelöst und werden für Simulationen auf globalem Maßstab verwendet während RCMs für Modelle auf regionalem oder lokalem Maßstab verwendet werden. In dieser Arbeit werden GCM/RCM Klimadaten aus dem Coordinated Regional Downscaling Experiment (CORDEX) und der regionalen Klimaabteilung des Instituts für Meteorologie und Klimaforschung am Karlsruher Institut für Technologie (IMK-IFU) verwendet um zu bestimmen, welches Klima in Westafrika in der Zukunft vorherrschen wird. Außerdem werden sechs verschiedene GCMs verwendet (CanESM2M, EC-EARTH, ECHAM6, HadGEM, GFDL und Miroc). Das regionale atmosphärische Klimamodell des Rossby Zentrum (RCA4) und das Modell Weather Research and Forecasting (WRF) werden als RCMs für die Daten von CORDEX und IMK-IFU verwendet. Die Auswertung findet jeweils für die Daten von CORDEX und IMK-IFU statt auf einer täglichen zeitlichen Auflösung und einer räumlichen Auflösung von 50 km und 12 km.

Die GCM/RCM Klimasimulationen zeigen systematische Fehler. Diese werden unter Verwendung einer lineare Skalierung und anschließendem Quantile Mapping Bias-korrigiert. Im Allgemeinen sind die von diesem Korrekturverfahren erzeugten Daten realistischer als die unkorrigierten. ähnliche Klimatrends können aber sowohl in den originalen als auch in den Bias-korrigierten Simulationen beobachtet werden. Es zeigt sich, dass sich durch den Klimawandel in Zukunft auch die Niederschlags- und Temperaturverteilungen in Westafrika ändern werden. Alle GCMs/RCMs prognostizieren einen Temperaturanstieg von etwa +1°C bis +2°C. Beim Niederschlag ist das Bild uneinheitlich. Manche Modelle prognostizieren einen leichten Anstieg, andere eine Abnahme der Niederschläge in der Zukunft.

Die Kernuntersuchung der vorliegenden Arbeit, die Auswirkungen des veränderten Klimas auf die Hydrologie der Region zu bestimmen, basiert auf der Kombination der robusten und validierten HBV Modellen mit den unkorrigierte und korrigierte Klimasimulationen als Eingangsdaten. Es zeigt sich, dass vier von den fünf GCM Modellen zu sinkenden Abflüssen führen, und nur eins zu leicht steigenden Abflüssen führt. Mit korrigierten GCMs/RCMs zeigt sich der gleiche Trend wie mit den unkorrigierten Eingangs Daten. Es kann jedoch festgehalten werden, dass mit Bias-korrigierten Eingangsdaten klarere Ergebnisse erzielt werden.

Es kann also der Schluss gezogen werden, dass sich der Klimawandel negativ auf die Hydrologie des Volta-Einzugsgebietes auswirken könnte. Der Abfluss könnte sich prinzipiell reduzieren was dazu führen würde, dass viele Flüsse im Einzugsgebiet in den meisten Monaten des Jahres trocken fallen würden. Allerdings basieren die Ergebnisse nur auf einem einzelnen Klimaszenario (rcp45) und sollten deswegen mit Vorsicht verwendet werden.

Die Abnahme der Abflüsse, die in Zukunft als Folge des Klimawandels auftreten können, könnten die Wasserressourcen der Region allgemein beeinflussen und sich dadurch auch auf das sozioökonomische Wohlergehen der Menschen in der Region auswirken. Als Beispiel sei eine sinkende Stromerzeugung aus Wasserkraft genannt, welche die wichtigste Stromquelle der Regiond darstellt. Die Menschen, die in der Region leben, sind vor allem Landwirte, die die knappen Wasserressourcen nutzen, um ihre Felder zu bewässern und damit von ihnen abhängen um ihren Lebensunterhalt zu erwirtschaften. Zusätzlich wächst die Bevölkerung mit einer Wachstumsrate von etwa 2,5% pro Jahr, was zu einer zusätzliche Belastung für die Wasserressourcen führt.

Um den oben genannten Herausforderungen und Probleme zu begegnen sollten unverzüglich angemessene Anpassungs- und Klimaschutzmaßnahmen umgesetzt werden, die die Auswirkungen dieser Veränderungen für die Menschen und die Wirtschaft der Region als Ganzes verbessern.

1 Introduction

Undoubtedly, climate changes (cc) affect the hydrology and water resources of a region and therefore a deep understanding of the effects of it on the hydrology of an area is much needed. Water is life and the economy of many countries including the West African sub-region depends directly or indirectly on the water availability.

Moreover, a strong interconnection between the climate and the hydrological cycle exists. According to Speth et al. [2010], evidence shows that many natural systems are affected by Global Change, among which the hydrological system is predominately influenced.

The Intergovernmental Panel on Climate Change (IPCC) 2013 report states "Changes in the global water cycle in response to the warming over the 21st century will not be uniform. The contrast in precipitation between wet and dry regions and between wet and dry seasons will increase, although there may be regional exceptions" [Stocker et al., 2013].

And,

"Extreme precipitation events over most of the mid-latitude land masses and over wet tropical regions will very likely become more intense and more frequent by the end of this century, as global mean surface temperature increases" [Stocker et al., 2013].

1.1 Motivation

West Africa is a fast developing sub-region within the African continent with its challenges on water availability and variability. Hydropower is the main source of electricity in the sub-region and farming is the major occupation or source of income to the population of the sub-region. Surface water is also the main source of water supply for the region. On several occasions, Volta river authority (the operator) of the major hydropower in the sub-region (Volta River Authority) has to shut down most of their turbines because of low levels of water in the reservoir and many cities in the sub-region has to undergo what is termed "power rationing" which is a very unpleasant experience for both the Governments and the citizenry. In recent times, farmers have to lose their planting seeds, crops and harvest because of the delay in the onset of the rainy season and a prolonged dry period. Any changes in the climate and the hydrology of the region tremendously affect both the people and the economy of the sub-region as a whole.

Moreover, the Volta basin is the major water resource in the sub-region. And it is shared by several other countries in the region, namely Mali, Burkina Faso, Ghana, Ivory Coast, Togo

and Benin and for that matter any use of the basin upstream affects the other riparian countries downstream. This results in an increasing competing demand of this scarce resource in the sub-region.

The sub-region with its countries been in the lower to middle income economies have very scarce meteorological and hydrological data and because of that a scientifically proven model to be able to predict the future situations would be a great tool for the management of the water resources in the this region. Understanding the phenomenon of climate changes and its impact on the meteorology, the hydrology and the water resources of the sub-region may be very instrumental in helping policy makers and water resource managers to make important decisions on investment, development and management. A typical example is the Bui hydropower which was constructed in 2008 in the southern part of the Black Volta basin. Although it was planned to produce about 440 MW of power but currently producing just about one-third of its capacity, because of low levels of water in the dam.

1.2 Aims and Objectives

The aim of this study is to investigate climate changes in the West Africa sub-region and to ascertain its effects on the hydrology and water resources of the sub-region. And to achieve the above aim, the following research objectives were set:

- Review and discussion of the current knowledge on the impact of climate changes on the hydrology of the sub-region.
- Analysis of observed (measured) precipitation, temperature as well as river discharge time series.
- The setting up, calibration and validation of a hydrological model to investigate water balance situations for a catchment in the sub-region.
- Investigation of possible climate changes in the sub-region and downscaled to the study area.
- And finally, investigation of the effects of the changed climate on the hydrology of the sub-region.

1.3 Innovation

The study performed the following innovative works:

- Determining what influences precipitation in the sub-region and the information used as the external drift in the geostatistical interpolation of rainfall in a huge catchment with an extremely coarse observational data.
- A simple, but effective and not data demanding lumped conceptual hydrological model applied to a poorly gauged basin.

- Various latest GCM driving models with longer time spans are used in conjunction with the HBV model to predict the effects of climate change on hydrology.

1.4 Methodology

The following methodologies were used to accomplish the above objectives and innovations:

1. Climate data of regional climate models (RCMs) with different GCM driving models was obtained from the Regional Climate Division of Institute of Meteorology and Climate research at Karlsruhe Institute of Technology (IMK−IFU) and the Coordinated Regional Climate Downscaling Experiment (CORDEX). This data was used to determine possible climate changes in the sub-region.
2. The biases in the RCM simulations was then corrected using quantile−quantile mapping and linear scaling methods.
3. The outputs generated from the regional climate model (i.e., rainfall and temperature) was used as input to a hydrological model (HBV) which was setup, calibrated and validated with observed climate and hydrological data.
4. Finally, the effects of climate change on the hydrology of the sub-region was determined.

1.5 Structure of the Thesis

This thesis is structured in the following way: In Chapter 2, there is the description of the study area and a review of the current literature on the title of the thesis. Chapter 3 elaborates and discusses the observed climate and hydrological data for the study area. Rainfall−runoff modeling is discussed in Chapter 4 and the results of that presented. In Chapter 5, simulated RCM climate data from six (6) different GCM driving models are analyzed and presented. It is then followed by the results of the the effects of climate change on the hydrology of the sub-region which is presented in Chapter 6. The thesis then closes in Chapter 7 with a summary and conclusion of the study.

2 Study Area Description and Literature Review

2.1 A brief description of the study area

The study area is the Black Volta Basin in Western Africa and has a total catchment area of about 155,000 km^2 (figure 2.1) and is shared by four other West African countries. The portion of the basin lying within the boundaries of Ghana is approximately 28,000 km^2 (23%). The Black Volta River is the main river in the catchment which empties into the Volta Lake (which is one of the largest artificial lakes in the world). The Black Volta basin is about one-third of the entire Volta basin, which comprises the White, Black and Lower Voltas and the Oti subcatchment (figure 2.2). The major water resources usage in the catchment area includes hydropower, small scale irrigation and domestic water supply. The catchment lies in a data scarce environment. The main tributaries of the Black Volta river are Bougouriba, Gbongbo, Grand Bale, Voun Hou, Sourou, Wenare, Bambassou, Bondami, Tain and Poni rivers.

The basin can be found approximately between latitudes 7° N to 15° N and 5°30′W to 1° W. According to Shahin [2006], the Black Volta River used to join the White Volta River at the south-eastern part of Ghana but after the creation of the Volta Dam, the Black and White Voltas do not join each other anymore, instead each river enters the lake through a separate channel. The head water source of the Black Volta is in the Banfora Cliffs in Burkina Faso. The river then traverses on the left bank side of the Sourou (a north-south depression). Below the depression, the flow of the river is generally, in a southerly direction with a number of meanders in its course Shahin [2006].

Since the 1960s, tropical West Africa has suffered from declining rainfall and that several drought periods occurred in the early 1970s and in the first half of the 1980s [Speth et al., 2010]. According to Speth et al. [2010], there have been a decrease in the availability of fresh water in the sub-region and this has been compounded by a growing population of about 2.32% p.a., compared to a worldwide increase of 1.24% p.a. between 2000 and 2005. In Africa, the spatial and temporal variability of water resources is very high and it is linked directly to climate variability and population density [Speth et al., 2010].

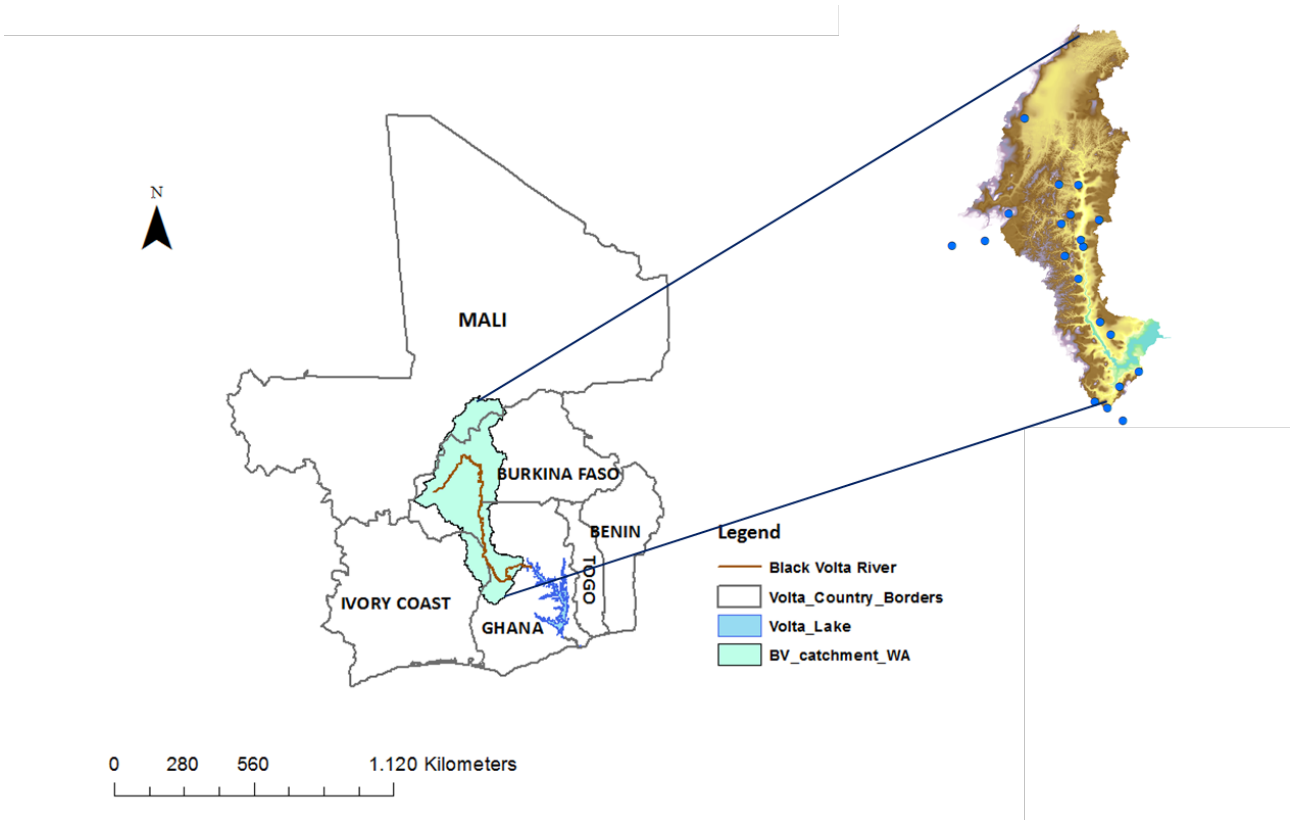

Figure 2.1: The Black Volta Basin with its riparian countries (Insert: Black Volta Basin showing digital elevation map and the rainfall gauge stations).

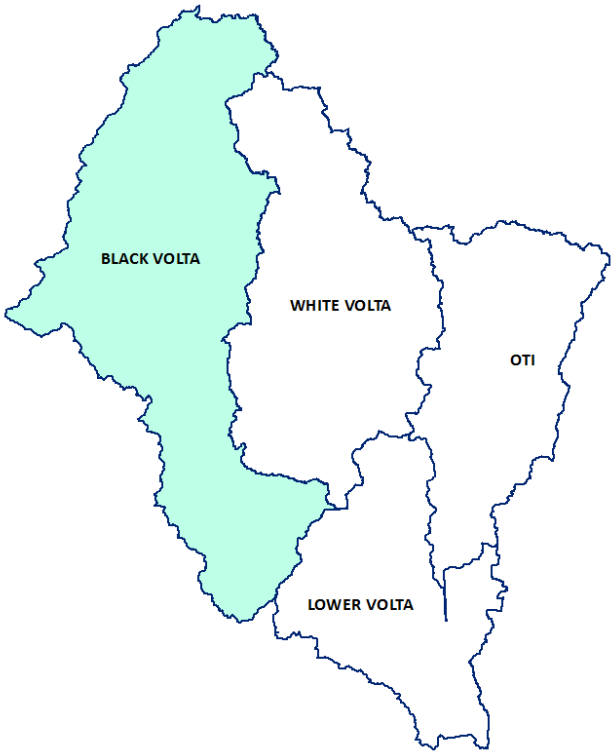

Figure 2.2: The Black Volta catchment (green) inside the Volta Basin

2.2 Climate

The climate of the study area (figure 2.3) ranges from a semi-arid in the northern part to a sub-humid in the southern part. The Sahel zone, which is in the region north of about 12.5°N, has a semi-arid climate. The Soudanian zone, between about 9 and 12.5°N, is sub-humid and parts of the Guinean Coast are humid [Speth et al., 2010]. The climatic pattern is fairly uniform in the northern part. The convergence of the monsoon and north-east air masses, locally known as Harmattan, is very important to explain the climate of the sub-region as a whole. From January to March (as seen in figure 2.4) is when the sub-region lies entirely on the path of the Harmattan air masses, the weather is dry and warm during the day and cool at night. The climatic condition however changes in June up to September when the weather is characterized by thunderstorms and heavy precipitation. By August, almost the whole of the catchment is covered under the monsoon air mass and most of the area including the northern part of the Black Volta basin has the maximum of their rainfall.

Speth et al. [2010] indicates that, as a consequence of the movement of the International-Tropical Convergence Zone (ITCZ), the Sahel and most parts of the Soudanian zone have a unimodal rainfall season that peaks in August whereas the Guinean coast shows a bimodal rainfall season with peaks in June and October. The second rainy season is less pronounced.

Two regimes of wet and dry seasons, occasioned by the northward and southward movement of the ITCZ as seen in figure 2.4, constitute the major climatic markers. This has created a remarkably clear south-north divide of climatic and vegetation zones that in turn have had significant influence on human activities, these being mainly agriculture. According to Amissah [1969] , changes in the climate of the sub-region, especially in that of Volta Basin are associated with the movement of the inter-Tropical boundary variation in the moisture content of the air masses, wind patterns and their frequencies.

Ferguson [1985] indicated that, the lowland climates of West Africa are characterized by uniformly high sunshine and high temperatures throughout the year; mean annual temperatures are usually above 18°C. Areas within 10° of the equator have a mean annual temperature of about 26°C with a range of 1.7°C to 2.8°C; the diurnal range is 5.6°C to 8.3°C. Between latitudes 10°N and the southern part of the Sahara mean monthly temperatures can rise to 30°C, but the annual range is 9°C and diurnal range 14° to 17°C. In the central Sahara temperatures in the shade in July may be as high as 58°C during the day and as low as 4°C at night; mean annual temperature ranges from 10° to 35°C. The skies in the higher latitudes in inland areas are usually cloudless as compared to areas close to the coast where skies are cloudier and night temperatures are higher [Ferguson, 1985].

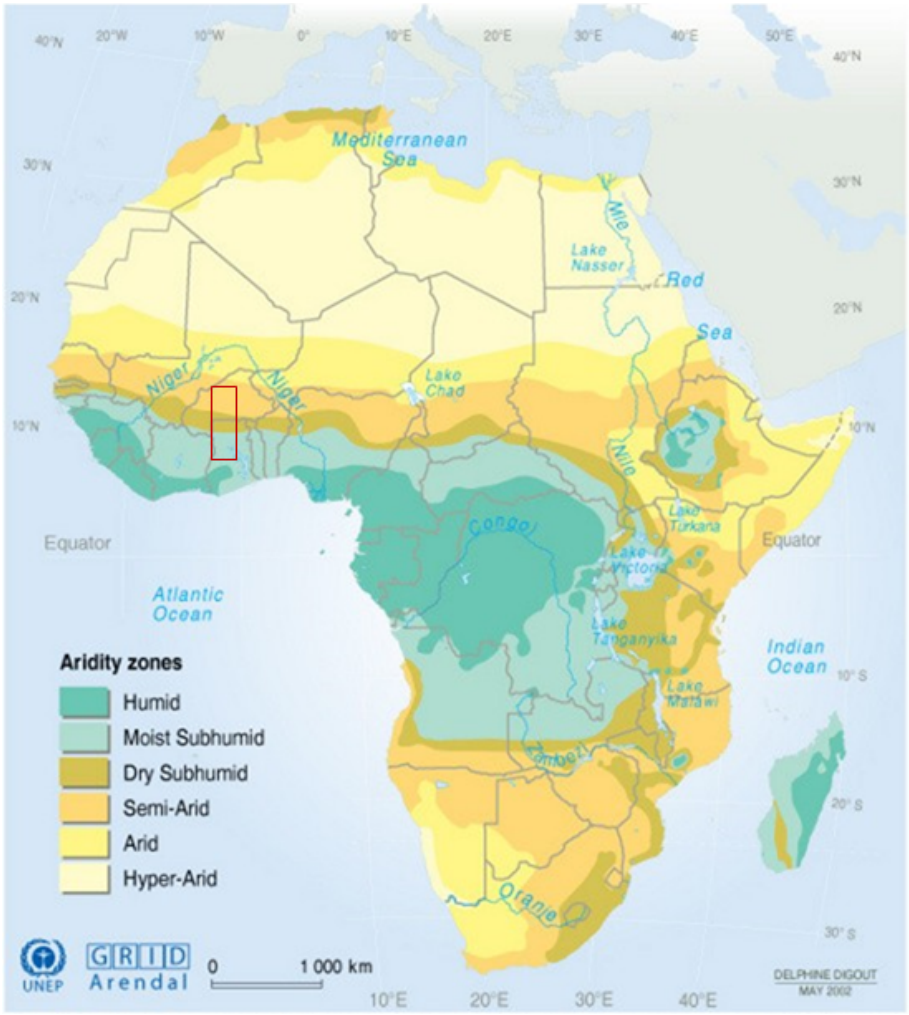

Figure 2.3: The aridity and climatic zones of the African Continent (The red box roughly indicates the study area). Source: World Meteorological Organization (WMO)

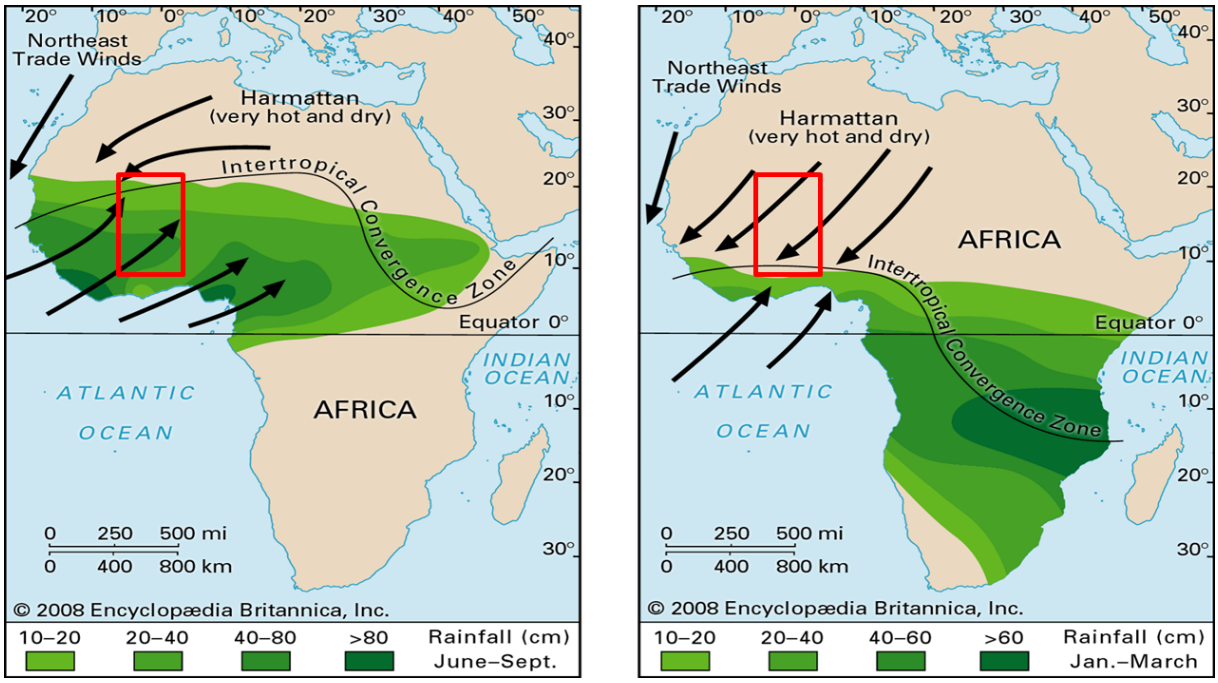

Figure 2.4: The movements of the ITCZ showing the wet and dry seasons of the West-Africa sub-region (The red box roughly shows the study area). Source: World Meteorological Organization (WMO)

2.3 Soils

According to Dewitte et al. [2013], the continent of Africa contains all but one of the world reference base (WRB) soil groups and illustrates great soil diversity. They also added that it is important to notice that over 60% of the soil types represent hot, arid or immature soil assemblages: Arenosols (22%), Leptosols (17%), Cambisols (11%), Calcisols (6%), Regosols (2%) and Solonchaks/Solonetz (2%). A further 20% or so are soils of a tropical or subtropical character: Ferralsols (10%), Plinthosols (5%), Lixisols (4%) and Nitisols (2%). A considerable area (6%) is occupied by a further 16 reference groups that cover an area of less than 1% of the African land mass. This fact illustrates that a considerable number of soil types are associated with local soil-forming factors such as volcanic activity, accumulations of gypsum or silica, waterlogging, etc. What is interesting is that unlike the other continents and that Africa does not exhibit large expanses of prairie or steppe-type soils (i.e. Kastanozems, Chernozems and Phaeozems) [Dewitte et al., 2013].

Soil data of Africa was downloaded from the European soil data centre and the data on the study area was clipped using ArcGIS. The clipped-map was modified in ArcGIS to obtain a raster image with 1km resolution (figure 2.5). This product was mapped with the harmonized world map from Food and Agriculture Organization (FAO) to obtain the properties and characteristics of the soil (i.e. soil texture, reference depth, available water storage capacity, soil drainage, etc). Figure 2.5 shows that, the type of soils in the basin includes the Planosols (0.2%), Plinthosols (46%), Regosols (3.7%), Luvisols (14%), Leptosols (3.4%), Lixisols (10.2%), Cambisols (6%), Nitosols (1.5%), Acrisols (1%), Fluvisols (1%).

Nachtergaele and Batjes [2012] have developed procedures for the estimation of Available Water Capacity in mm/m (AWC) in soils. In the catchment, 58% of the soils have AWCs of 150mm/m, 19% have AWC of 100mm/m, and 15% of the soils have AWC between 100 to 50 mm/m. From the guidelines to estimation of drainage classes based on soil type, texture, soil phase and a reference flat terrain (i.e., 0.0 to 0.5% slope), the drainage of the soils ranges from “moderately wel” to a “poor” drainage.

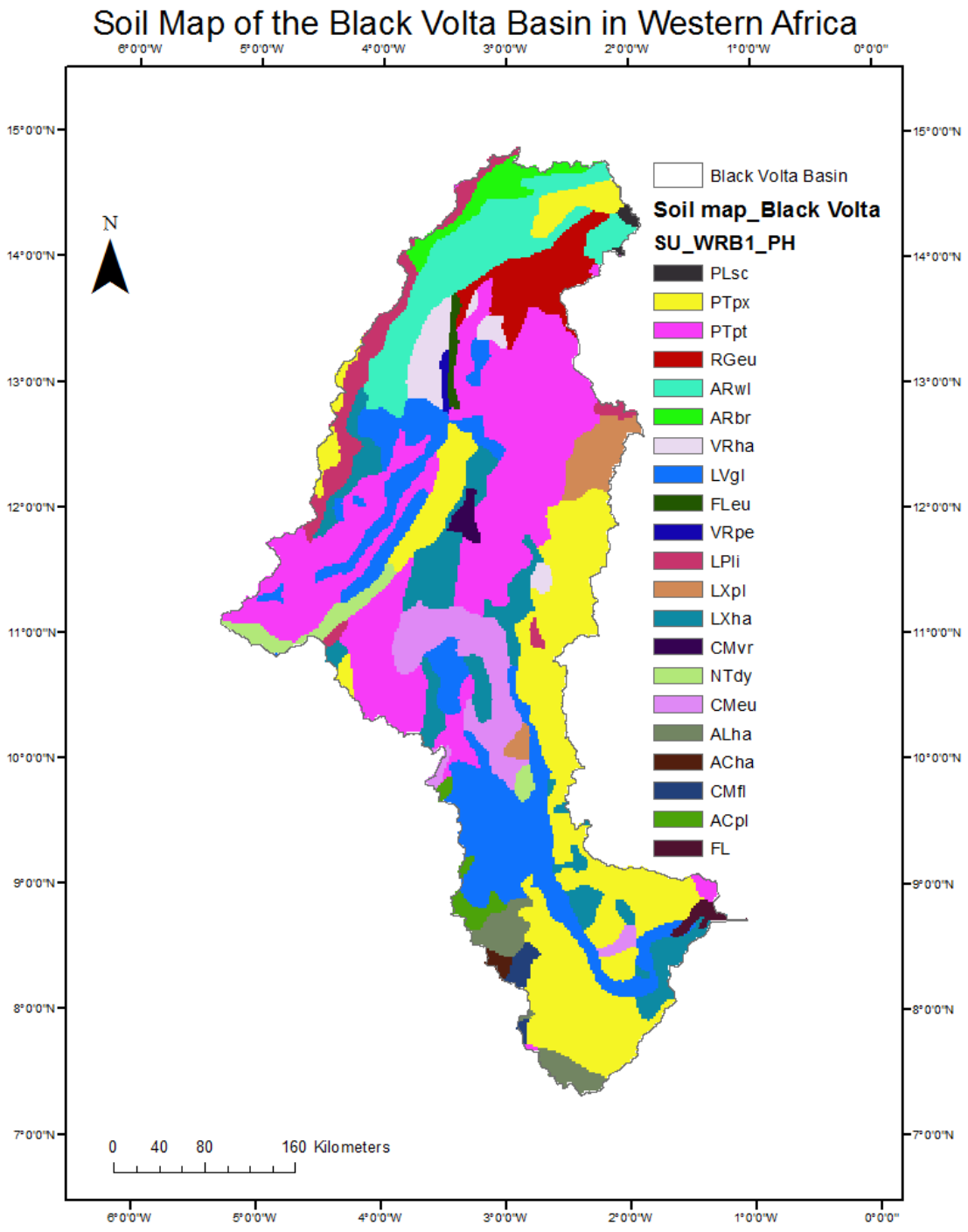

Figure 2.5: Soil map of the Black Volta Basin (Adapted from the European Soil Data Centre)

2.4 Geology

A Precambrian platform and a sedimentary layer are the dominant geological systems of the basin. Although it covers a large area in the Ghanaian part, is of minor importance for the

basin as a whole [Jung, 2006]. A study by Kortatsi [1997] on the Geology and underground water in the Volta Basin reveals that the Black Volta basin consists of mainly granitoids comprising of the Cape Coast and Dixcove granites, the Birimian and Voltaian systems and a little bit of the Tarkwaian system. He did also indicates that the Cape Coast Granite covers about 20 percent of the Black Volta Basin. The geographical coordinates of this formation stretches from latitude 9° N to 11° N and longitude 2° 25′W to 4° 40′ W [Kortatsi, 1997]. This type of geological formation is made up of well foliated, medium grained potash-rich muscovite-biotite granite, granodiorites, pegmatites, porphyroblastic-biotite gneiss and aplites. This parcel of land has many enclaves of schists and gneisses [Kortatsi, 1997].

Another geological characteristic of the Black Volta Basin is the Dixcove Granite that forms about 15 percent of the Basin. This stretches from latitude 8°N to 10° 31′ N and longitudes 2° W to 2° 50′W and is made up of soda-rich hornblende biotite granite, granodionites grading locally into quartz-diorite and hornblende-diorite. It forms non-foliated discordant to a semi-discordant bodies in the Upper Birimian metavolcanics rock which it is in contact with [Kortatsi, 1997]. Another geological formation known as the Granite undifferentiated that forms about 5 percent of the Basin and consists of rock is made up of Cape Coast and Dixcove-Granite [Kortatsi, 1997].

There is also Birimian Systems that is made up of Upper and Lower Birimian. The former is originated from volcanic and formed about 10 percent of the rock in the area, while the latter originates from pelitic and consists of great thickness of alternating shales, phyllites, greywacke and argillaceous beds with some tuffs and lavas. It covers about 20 percent of the basin. The Tarkwaian formation is also identified by Kortatsi [1997] as important geological formation of the Black Volta Basin. However, this is insignificant because it covers about 2 percent of the Basin around the South, West-North and East direction from Bepoasi across the Black Volta at Bui. Finally, the Voltaian Rocks system forms 33 percent of the Black Volta Basin and occurs in the South Eastern part of the basin and between latitudes 7° 31′ N to 9°5′ N and longitudes 1° 5′ W to 2° 10′ W. This geological formation is flat-lying late precambrian to paleozoic sandstones, shales, mudstone, pebbly beds and conglomerates with subordinate limestones attaining a total thickness of 150m [Kortatsi, 1997].

2.5 Vegetation and Land Use

Land cover/use data for the year 2000 which was derived from Landsat ETM+ and MODIS for the Volta basin was downloaded from the Volta Basin geoportal and a shape file of the Black Volta catchment was used to clip the area of interest with the help of ArcGIS in a resolution of 1km. The data had been aggregated to 10 classes and it is shown in Figure 2.6. From the map, about 44% of the land cover was Regularly flooded-woody-closed to open, followed by grassland which has 25% cover, cropland has 18% cover, Forest had just 5% cover and the rest are wetland (4%), Urban area (0.2%). The data shows that the yearly Land cover changes for this catchment are not significant. Figure 2.7 shows the Normalized Difference Vegetation Index (NDVI) for the catchment with higher NDVI values (0.52) in the southern part which indicates high presence of vegetation towards the southern part of

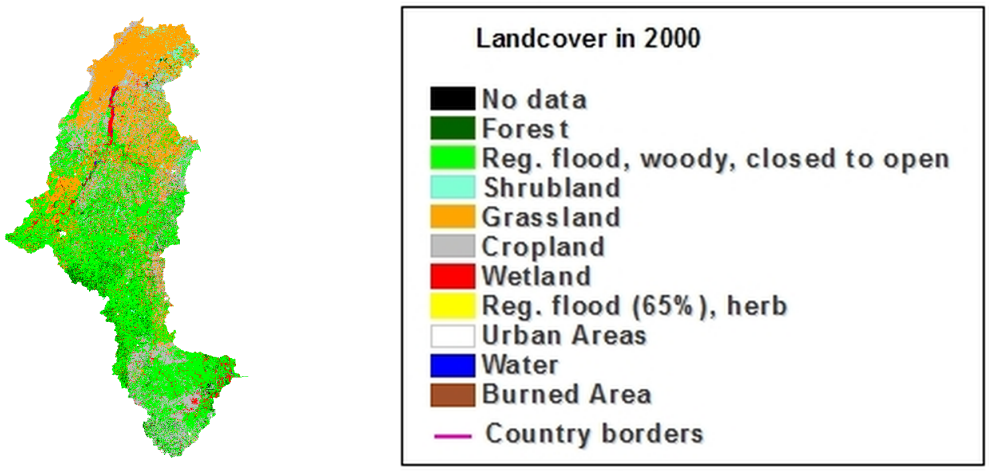

Figure 2.6: Landcover map of the the Black Volta Basin for the year 2000

the catchment and lower NDVIs (0.18) which shows desert areas at the northern part of the catchment. The sub-region has vegetation which grades with increasing latitude from the equatorial evergreen forest (in the southwest) to semi-deciduous tropical forest in the north of the forest zone, and through the forest Savannah transition zone to interior Savannah. It is within the interior Savannah zone that the Black Volta basin lies. The long dry (harmattan) season is the greatest climatic influence on the vegetation in the interior Savannah zone. The arboreal vegetation of this zone is typically composed of short branches of trees many less than twenty meters high, which do not usually form a close canopy and are often widely scattered [Agorsah, 2003]. The ground flora consists of an apparently continuous layer of grass, some species of which reach height of about five meters [Agorsah, 2003].

Agorsah [2003] emphasized that the interior Savannah vegetation zone is characterized by short grasses with the tussock grasses predominant in most palaces. When the grasses die off above the ground during the dry season, it is highly flammable. Annual bush fires, which sweep through the area, have given rise to trees that are fire resistant or fire-hardy and often characterized by thick barks and ability to reproduce from dormant buds [Agorsah, 2003]. After the fire has burnt through the area (December to March), and before rains begin, most of the trees in this zone form new leaves and some trees flower.

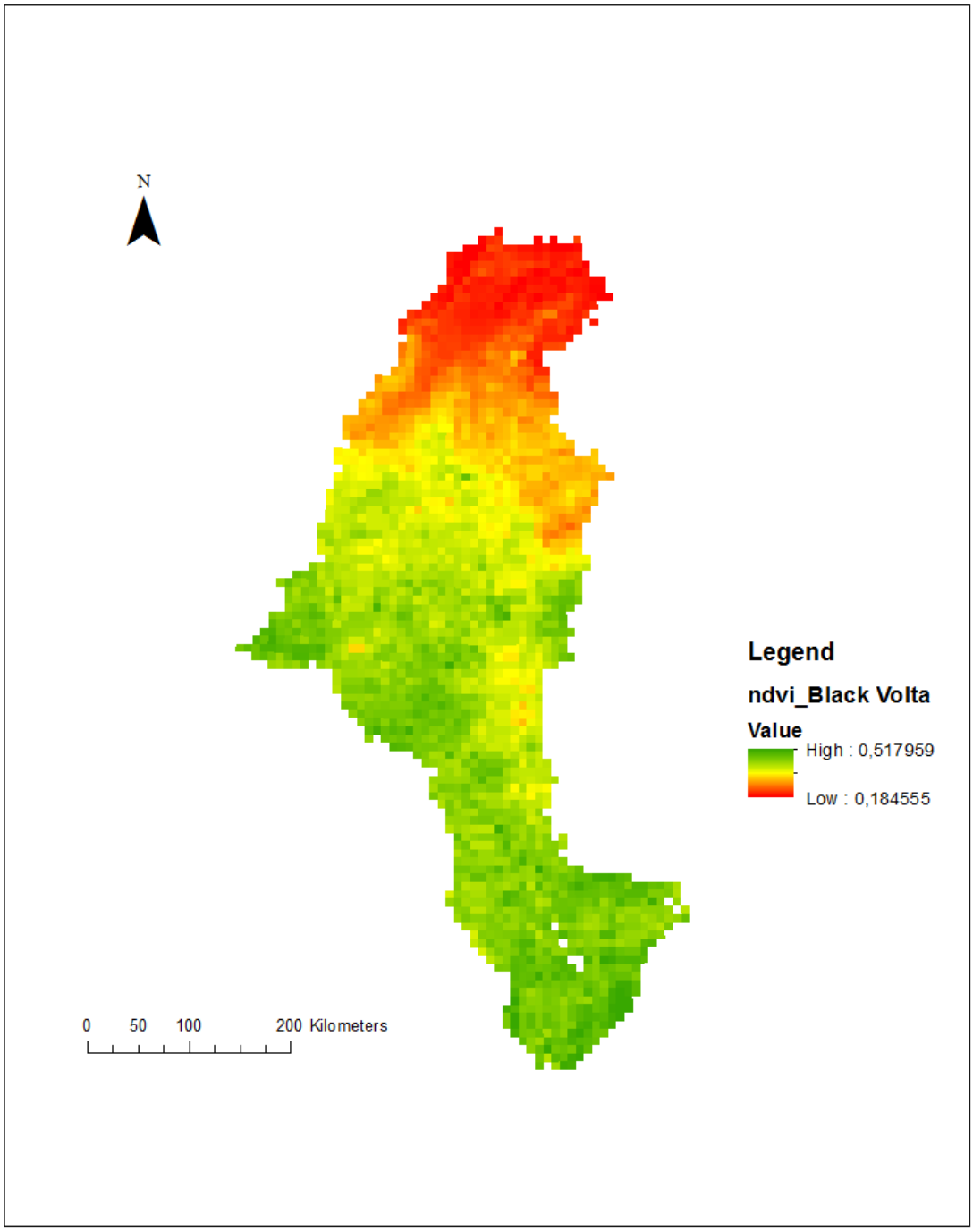

Figure 2.7: The NDVI map of the Black Volta Catchment for the year 2000

2.6 Topography and Relief

In knowing the terrain of the study area, a 30 arc second (approximately 1 km at the equator) digital elevation map (DEM) for the African continent was obtained from the USGS earth

explorer database. And once again the area of interest which is the Black Volta basin was clipped using ArcGIS with the help of a shape file of the catchment.

From the DEM map (Figure 2.8), the elevation ranges from 82 m to 887 m a.m.s.l. with the higher elevations around the western part of the catchment. The northern part of the catchment is almost flat with low elevations and slopes towards the central part where the Black Volta River is located. There is considerable variation in local relief of the Black Volta basin. The northern areas range between 300 m to 700 m above sea level and the southern sector are covered with water bodies or with height ranging from 0 to150 m above sea level. The Basin is gently undulating from the north to the south. Most part of the Black Volta basin falls under the savanna zone which is undulating with gentle slopes that promotes overland flow. Over the years, over grazing, bad methods of farming, and bush fires have combined negative effects on degradation of the vegetation that create large tracts of bare land which become highly susceptible to accelerated erosion. The low relief is also a cause for the poor surface drainage with a consequent flooding which characterize the desertification-prone areas during the rainy season.

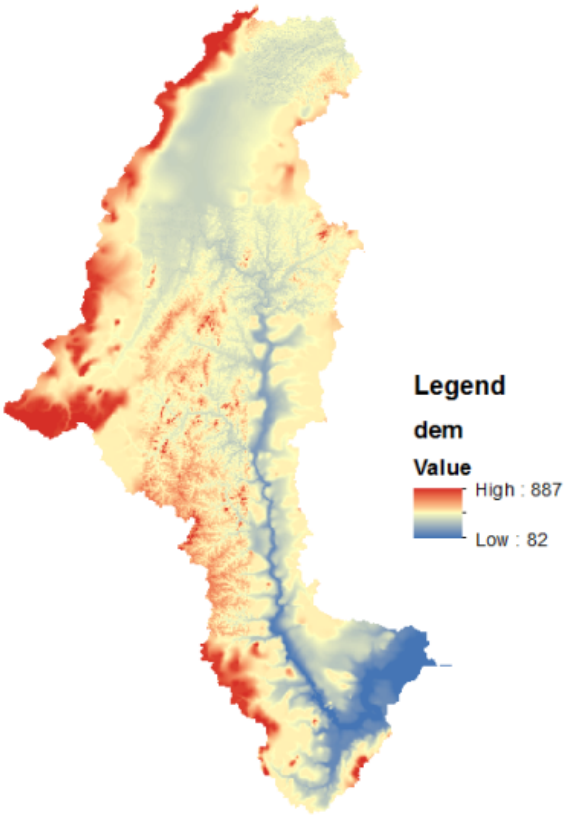

Figure 2.8: Digital elevation map of the Black Volta Basin

2.7 The climate trend in the West Africa sub-region

In addressing the issue of changing water availability in the Volta Basin, climate trends of temperature, precipitation and river discharge were analyzed by Neumann et al. [2007]. In their study, they showed that temperature time series showed dominantly positive significant trends and the conclusion was that there was an increase in temperature in the Volta Basin. In their study, the time series of precipitation showed both monthly negative and positive trends with only a few of them been significant. The significant trends were negative. However, they could not conclude a general trend towards decreasing precipitation in the Volta Basin. River discharge time series showed more negative significant trends for the dry season and more positive significant trends for the rainy season, leading to the conclusion that the rivers in the Volta Basin show a reduction trend of the discharge in the dry season and an increase in the rainy season. Moreover, they stated that the decrease in river discharge in the dry season cannot be directly connected to a decrease in precipitation and that it is more likely due to anthropogenic influences [Neumann et al., 2007].

It is important to note that Neumann et al. [2007] used annual and in some cases the monthly time series of the climate variables for their analysis and that the number of stations used in their analysis for this huge catchment (area: 400,000 square kilometers) was small. At the end, Neumann et al. [2007] deduced a clear climate change signal for the Volta Basin in general for temperature and it was in agreement with the general global signal. Again, the conclusion of a weak decrease of precipitation variability was drawn [Neumann et al., 2007].

Again, Kunstmann and Jung [2005] performed statistical analysis on the observed precipitation, temperature and river discharge time series to determine climatic trends within the Burkinabe part of the Volta Basin. In their work, they used annual and monthly means of temperature, precipitation and river discharge which were computed from daily observation data. Before the analysis, they in-filled gaps in temperature and river discharge time series but did not fill gaps in precipitation time series. In their trend analysis, only time series containing at least 25 years of usable data were included. The following results emerged from their study.

- There was a predominately positive trend of temperature time series with most of the trends statistically significant and therefore concluded that temperatures in the Burkina Faso are likely to be increasing [Kunstmann and Jung, 2005]
- Similar to the study conducted by Neumann et al. [2007], both negative and positive trends were shown in the precipitation time series with relatively few trends been significant which were all negative, with few exceptions. They stated that, the annual precipitation sums and monthly means all showed significant negative trends. However, they could not conclude that a clear trend towards decreasing precipitation is observed in Burkina Faso because only a small number of trends among those examined were statistically significant [Kunstmann and Jung, 2005].
- One could see negative trends in the discharge time series for the dry season and positive trends for the rainy season. The conclusion was that, the rivers in Burkina Faso trend towards a reduction of discharge in the dry season. The rainy season trends were

positive but no firm conclusion could be drawn as only a few trends were statistically significant [Kunstmann and Jung, 2005].

Furthermore, trends and variability analysis of hydroclimatology of the Volta Basin in West Africa from 1901 to 2002 which was performed by Oguntunde et al. [2006] revealed that the decadal average of rainfall showed that the wettest decade of the 20th century was the 1950s whereas the driest decade was 1980s. They also reported that rainfall variability index showed that 1968 was the wettest year while 1983 was the driest with the last three decades being drier than any other comparable period in the hydrological history of the Volta Basin. The monthly PET peaked in March, the hottest month in the region and the lowest value (average = 95 mm/month) was in August, the most humid month of the Basin. And that on the average maximum monthly rainfall was in August whereas the minimum was recorded in January. The river discharge has the lowest value of the three series and the discharge lagged precipitation by two months and remains very low for about 7 out of the 12 months of the year [Oguntunde et al., 2006].

Opoku-Ankomah and Amisigo [1998] analyzed the recent 40 years of rainfall and runoff records from the southwestern part of Ghana (part of Volta Basin) and showed that there is significant reduction in rainfall and runoff in the region, which have been linked to the influence of climate change. Studies by Lebel and Ali [2009] shows rain recovery in the eastern parts of West Africa and drought conditions in the western regions. There is a strong fluctuations in river discharge with a generally negative trend from 1960 to 2010 especially in Sudanian areas due to the variations in rainfall [Mahe et al., 2013].

Mahe et al. [2013] underscored the nonlinear effect of this rainfall decrease over much of West Africa, with a -20% decrease in rainfall resulting in a decrease of -60% in runoff. Several studies, for example, in Le Barbé et al. [2002] reveals that there is a decreasing rainfall amounts and increasing temperatures in West Africa over the past few decades. Nicholson [2000] reported a striking decrease in annual rainfall in the Sahel region of West Africa with a decrease of about 20 to 40% from $1931-60$ to $1968-97$ ([Nicholson, 2000]). It is rather interesting to know that, these trends do not match observed global results, which rather show an increase in precipitation over land areas (even though not strictly significant) [Solomon, 2007].

2.8 Review of hydrological modeling in West Africa

The application and advancement of rainfall-runoff models is limited in the lower latitudes like Western Africa due to the facts that these models were developed for the temperate conditions and moreover there is insufficient data availability. Nevertheless, after the review of some literature, I found some studies already done on the application of hydrological modeling in the sub-region. For example Niel et al. [2003] applied a lumped hydrological model to 17 west and central African catchments to study parameter stability related to climate change studies. Their study revealed that nonstationarity in rainfall or runoff series does not imply non-stability of the model parameters. Andersen et al. [2001] successfully applied and validated the physically$-$ based$-$distributed MIKE SHE model to the large Senegal

River basin. Moreover, a study performed by Paturel et al. [2003] using a semi-distributed empirical model showed reasonable results for rainfall-runoff modeling for different West African catchments. The results of Dezetter et al. [2008] demonstrated that the choice of soil datasets shows the highest sensitivity of the model, but no single data-model combination yielded the best results for all catchments under consideration. In their study, they used 49 West African catchments to investigate the effects of using different hydrological modeling approaches and input grids on the simulation of runoff. A good performance of monthly streamflow prediction was demonstrated by Amisigo et al. [2008] when he used a statistical model (NARMAX) for several subcatchments of the Volta Basin. Jung [2006] used a joint dynamical downscaling-hydrological modeling in her PhD work for climate impact studies for a basin in this region. Her study and the results is reported and discussed in a latter section of this chapter.

Wagner [2008], used the joint meteorological model (MM5) and WaSiM in his research for hydrological simulations in the White Volta Basin in West Africa and the results show a good performance for 2004 and a weaker one for 2005 due to precipitation overestimations. The results also showed that the performances of the hydrological simulations using the scaled TRMM product 3B42 were good. He also concluded that using station data as meteorological data source leads to a good and often best model efficiencies. Shaibu et al. [2012] used a simplified runoff model for the Black Volta Basin using an adjusted monthly TRMM input data and the results were encouraging.

From the review of literature, it was realized that so far the conceptual HBV hydrological model has only once been applied in a West Africa catchment by Götzinger [2007] during his PhD research. Although the physically based hydrological model WaSiM had been extensively applied in the sub-region [Jung et al., 2012; Jung, 2006; Wagner, 2008; Kasei, 2010]. In the study of Götzinger [2007], the modified distributed HBV was applied in the Ouémé basin in Benin (West Africa). The results was that, the total simulated discharge matches the scale and variability of the observations sufficiently well for water resources management planning and that the general seasonal behavior but not all observed flood peaks could be reproduced. At the outlet of the catchment, at gauge Bonou (51,543 square kilometers) the Nash-Sutcliffe model efficiency for daily discharge was 0.77 for calibration. The water balance of the whole Ouémé catchment could be reproduced with satisfactory accuracy considering the available data and their uncertainties. The average Nash-Sutcliffe coefficient of all sub-basins in the catchment for the validation period was 0.50 [Götzinger, 2007]. He revealed in the Ouémé basin that the model efficiencies themselves are acceptable but the variability of the discharge was not modelled well from an operational perspective. And that the model was not able to simulate all additional short-term fluctuations and the full extent of the dry season. This is one of the shortcomings that my research tried to overcome by looking at how well the hydrological model reacts to signals and seasonality and how steady the model might be by employing various techniques and methods for calibration and validation. He further stated that the modified HBV model was suitable for global change impact studies [Götzinger, 2007].

2.9 A brief review of studies on climate changes in West African

Jung [2006]; Jung and Kunstmann [2007]; Jung et al. [2012], used the mesoscale meteorological model MM5 to dynamically downscale the global ECHAM4 GCM data (scenario: IS92a) for two 10-years time slices (1991 to 2000) and (2030 to 2039) down to a resolution of 9 km and coupled it one-way to the physically based distributed hydrological model WaSiM in a resolution of 1km. Their studies revealed that the simulated temperature change clearly shows an increase of around 1.2 to 1.3°C with a high signal to noise ratio. However, precipitation change signal was largely not significant and lies within inter-annual variability. But in some cases the rainfall change signal was larger than inter-annual variability and therefore could indicate climate change [Jung, 2006]. The annual rainfall change showed a highly spatial heterogeneous trend in the future ranging from -20% to +50% (mean annual change) [Jung, 2006]. The non-linearity of the precipitation change signal in this region shows the complexity of the monsoonal system of West Africa which might be due to the lack of the influence of land-surface changes in the climate simulations. Because of this, more studies need to be done using current climate models and tools to properly predict the precipitation change signal in the West Africa sub-region. Jung [2006] discovered no major changes for the de Martonne aridtity index and a changed in evapotranspiration could only be explained by rainfall and temperature changes. A delay in the onset of the rainy season for this sub-region could also be noticed from the studies of Jung [2006]; Kunstmann and Jung [2005]. Similar results are described in Biasutti et al. [2009]; Patricola and Cook [2011]. The simulated change in mean monthly temperature is between 1°c and 3°C [Kunstmann and Jung, 2005]. They predicted a heterogeneous pattern of precipitation change ranging between -20% to +20% throughout the Volta Basin in West Africa. The change in monthly evapotranspiration ranged between -10% to +20% in this sub-region when ECHAM4 model was used for a regional downscaling experiment for time slices 1991 to 2000 and 2030 to 2039 [Kunstmann and Jung, 2005].

All Climate models agree on a projection of warming in West Africa even though its magnitude ranges from +2 to +6°C in 2100 [Christensen and Christensen]. However, these models do not agree on the sign of the future evolution of precipitation. Whiles almost half of the models predict an increase in rainfall, the other half predicts a decrease [Vigaud et al., 2011; Berg et al., 2013]. There is considerable uncertainty in relation to largescale precipitation changes simulated by GCMs for Africa [Joubert and Hewitson, 1997; Feddema, 1999].

A study was also done by McCartney et al. [2012], who used the A1B scenario in conjunction with the regional climate model COSMOCLM to determine climate projections for the Volta Basin for the period 1983 to 2100. It was observed in their study that, there will also be an increase in the annual average temperature of up to 3.6°C and a decrease in annual average rainfall of approximately 20% by the end of the twenty-first century across the basin.

Furthermore, Ibrahim et al. [2014] performed a similar study in determining the variability of the rainfall regime over Burkina Faso under the climate change condition using the A1B scenario for the reference period of 1971 to 2000 and the projected period of 2021 to 2050. Ibrahim et al. [2014] used five different RCMs for his analysis. Their results showed that two models CCLM and RCA, project a significant decrease in annual rainfall while HadRM3P

and RACMO project a significant increase in annual rainfall for the period 2021 to 2050 and REMO model produced no significant change in the pattern of the annual rainfall amount between the two periods. This result was similar to that of Paeth et al. [2011], which indicates that there is no agreement for nine different RCMs in terms of the future precipitation changes in Western and tropical Africa. From nine RCMs, three models projected a wetter climate; three models also predicted negative trends and the other three showed a more mixed signal [Paeth et al., 2011]. The ENSEMBLES RCMs altogether shows a prevailing drying tendency in sub-Saharan Africa [Paeth et al., 2011]. Paeth et al. [2011] stated that, "Statistical post-processing of simulated precipitation is a promising tool to reduce systematic model errors before application in impact studies". The IPCC (2007) document also reports of a positive, negative and no significant model spread of rainfall trends from global GCM projections over Africa.

Nikulin et al. [2012] performed a study of precipitation climatology in an ensemble of CORDEX-Africa regional climate simulations. Their studies summaries that the main details of the precipitation climatology over Africa is captured by the RCMs, although substantial biases depending on region, season and evaluation metric exists from individual models. The multimodel ensemble mean generally outperforms individual RCMs in terms of the annual cycle and the first CORDEX evaluation over Africa was overall encouraging.

Lastly, in the studies of Laprise et al. [2013] as part of their contribution to the CORDEX project. They analyzed the performance of the fifth-generation Canadian Regional Climate Model (CRCM5) in simulating current climate for the twenty-first century over Africa when driven by two different coupled GCMs (CanESM2 and MPI-ESM-LR) under the RCP4.5 emission scenario. From their results, there was the projection that the African continent will become progressively warmer towards the end of the twenty-first century from all the models. The simulated annual cycles in current and future climate showed no major changes, although there were some differences. The simulated diurnal cycle and daily precipitation intensity distributions also showed no significant changes in the projections by all of the models compared to the current climate [Laprise et al., 2013].

2.10 A review of the effects of climate change on the hydrology of West Africa

Precipitation and temperature variables are an integral part of the hydrological cycle. Therefore, any changes that occur in the climate might also affect the hydrological regime and that there is a direct connection between the climate and the hydrology of an area. West Africa is a fast developing sub-region of the African continent which depends largely on surface waters for its hydropower generation. Rain-fed agriculture is also the main source of occupation and livelihood for the population of the sub-region. From the above reasons, any slight changes in the hydrology of the basins in the sub-region will significantly affect the citizens and the economy of the area. The domestic water supply in West Africa is also been threatened because of change in rainfall patterns and the drying up of some of the major rivers. Although, population increases, pollution and land use changes could be factors for

these problems but one cannot rule out the adverse effects of climate change on the hydrology and water resources.

Jung [2006]; Jung and Kunstmann [2007]; Kunstmann and Jung [2005]; Jung et al. [2012] used a coupled climate-hydrology simulations to assess the effects of climate change on the hydrology of the Volta basin in Western Africa. The results showed a very heterogeneous response of river runoff to changes in climate variables. Their work showed that, there was no major change for the mean runoff regime of the future as compared with the current simulation. There was a slight increase in the simulated discharge due to an increase in rainfall. Most of the surplus rainfall evaporates due to an increase in temperature which leads to an increase in potential evapotranspiration [Kunstmann and Jung, 2005]. Kunstmann and Jung [2005] predicted an overall increase in total surface runoff of 18% for the decade 2020 to 2030 for the Volta basin in West Africa and a nonlinear response of surface runoff to precipitation.

Roudier et al. [2014] summarized the current state of knowledge on potential future streamflow evolutions in view of global warming in West Africa by creating a quantitative database of 301 points of information on the impact of climate change on runoff in the region. Their results showed no clear general pattern of future runoff evolution in this area. The median of the distribution was 0% with a mean of +5.2%, after considering different time horizons, different rivers, scenarios and models (see figure 2.9). Correlation analysis they performed revealed that runoff changes are tightly linked to changes in rainfall (R =0.49).

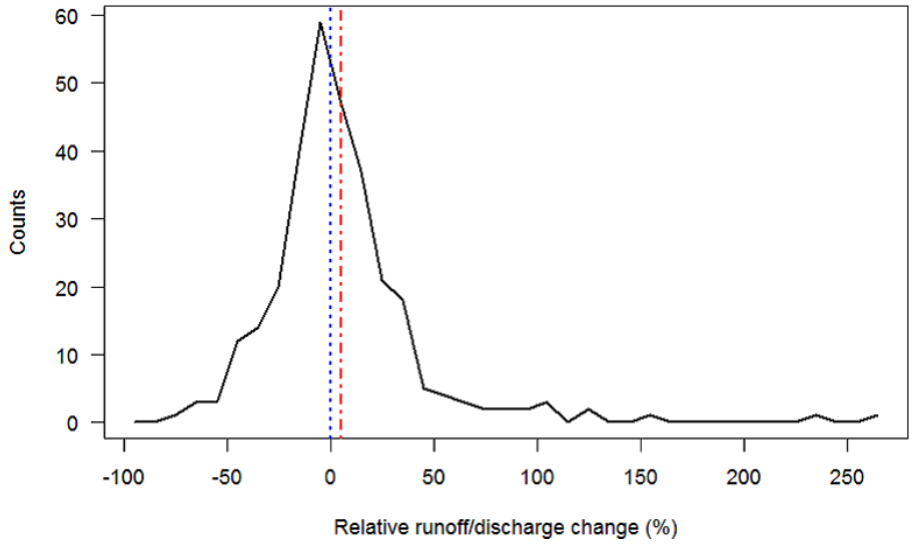

Figure 2.9: Runoff change (x axis, %) in West Africa based on all cases in the database (i.e., including different time period, rivers and models). The blue dashed line represents the median of the distribution; the red one is the mean. Focussed here only on the impact of climate change: this is the only changing parameter (no water use or land use change) Source: [Roudier et al., 2014]

However, Kankam-Yeboah et al. [2013] in their research rather projected a significant decrease in the projected mean annual streamflow for the future years 2020 and 2050 for the

White Volta and Pra Basins (all in Ghana). Similar results of a downward trend of streamflow in the future for the West Africa sub-region were obtained by McCartney et al. [2012]; Giertz et al. [2010]. Götzinger [2007] also showed similar results of a considerably reduced discharge, especially in the rainy season due to a reduced precipitation and increased temperature for two different climate scenarios which were simulated for a basin in Benin (West Africa) in comparison to a simulated historical period (see figure 2.10). In order to improve the acceptance of these results by the society and stakeholders, Götzinger [2007] recommended the continual update of the results with new models and scenarios.

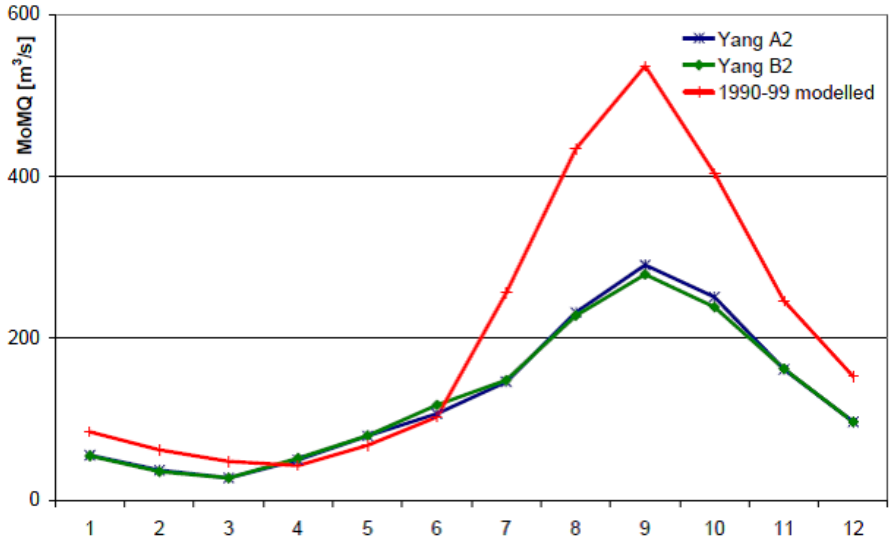

Figure 2.10: Monthly mean discharge at Bonou (Benin) simulated with HBV, climate scenarios A2 (2000 to 2030) and B2 (2000 to 2030) compared to a reference period. Source: [Götzinger, 2007]

3 Analysis of Observed Climate and Hydrological Data

3.1 Introduction

Western Africa been is a developing sub-region and lacks a dense network of both meteorological and hydrological data for analysis. The region is a data sparse environment. One could also notice a lot of gaps in the observed data. Satellite data (e.g. TRMM) also has its own peculiar challenges of under/overestimation of daily and monthly rainfall values for this area [Wagner, 2008; Nicholson et al., 2003]. Nonetheless, these challenges should not hinder a scientific research in the area. Meteorological and hydrological data sets were obtained from the Volta Basin Geoportal, Meteorological agencies of both Ghana and Burkina Faso and from the Hydrological Services Department of Ghana. A generic analysis performed on the main variables of meteorological and hydrological data time series produced the following results which were in consonant with previous studies and literature.

3.2 Precipitation

A total of 20 observed precipitation stations in and around the study area were used for the analysis. The duration of these time series is from 1961 to 2005 (45 years) with a daily temporal resolution. Out of this time series the annual rainfall cycles, what influences rainfall in the catchment and spatial interpolation using Kriging were performed. Some of the gauge stations were located in Ghana and the rest were in Burkina Faso and Ivory Coast. The names of the stations are Bechem, Sunyani, Berekum, Wenchi, Kintampo, Bui, Bole, Batie, Gaoua, Babile, Lawra, Baguera, Banfora Agri, Bob-Dioulasso, Diebougou, Dano, Boura, Boromo, Bagassi and Bomborokuy (see figure 3.1).

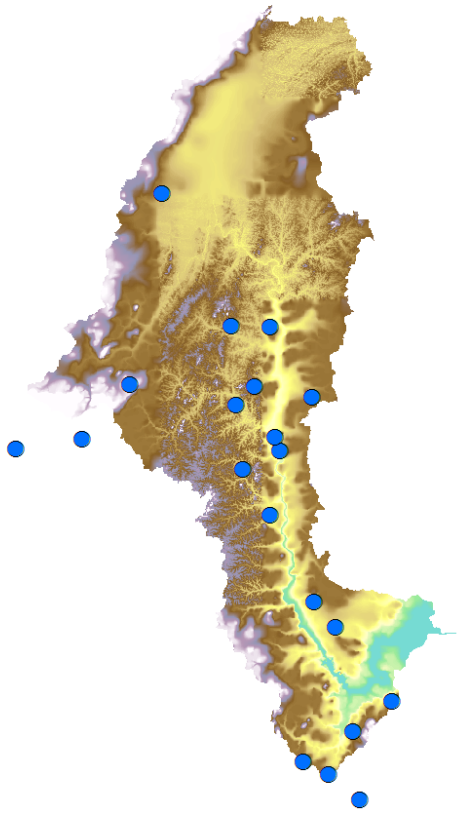

Figure 3.1: A DEM map of the catchment showing the locations of the 20 rainfall gauge stations (blue dot)

3.2.1 Annual cycle of rainfall

The mean daily rainfall values were calculated for the 45 years period for each station. Then a 10-day moving-weighting function was applied to smoothen the daily rainfall values and to remove the noises in the data. We could then have an annual cycle of rainfall for each gauge station.

From the results, there was a clear bi-modal rainfall cycle in the south of the catchment with rainfall seasons from April to July then September to October. And a uni-modal cycle in the north of the catchment with rainfall season from June to September. There is a negative gradient in rainfall as one move from the south to the north of the catchment. For a station in the north, the month of August has the highest amount of rainfall whiles January is the driest month in the year. A station in the south has the first rainfall season peaking in May/June whiles the second season peaks in September/October and the driest month is January (figure 3.2). The average daily rainfal was 9 mm for a station in the north and 7 mm for a station in the south. In the northern part of the sub-region, one could get on the average only four (4) months of rain in a year whiles there is about six (6) to seven (7) months of rain in a year in the southern part. And probably this could explain why there is more farming activities in the southern part of the catchment as compared to the north since the farming

in these areas are rain-fed.

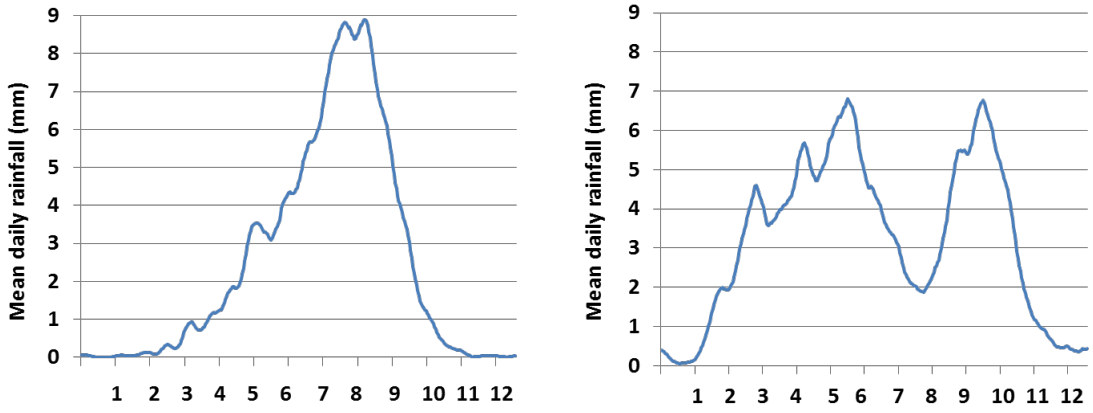

Figure 3.2: Left: annual rainfall cycle for a station in the north. Right: annual rainfall cycle for a station in the south

3.2.2 What influences rainfall in the catchment

In determining what influences rainfall in the catchment, a correlation matrix was calculated for the daily, monthly and seasonal amounts of rainfall against the northings, eastings and the elevations of rainfall stations. A histogram is then plotted for the number of months against the northings, eastings and elevations of the stations and the graphs are as shown in figures 3.3, 3.4 and 3.5. The graph of the station northings has the highest number of months that has higher correlations (although a negative correlation i.e. - 0.8, - 0.6). The eastings of the stations also have a positive correlation for higher number of months (0.4 and 0.6). In the graph of the station elevations the majority of the months have a weak correlation. The results of the daily and seasons behaved the same way.

It could therefore be concluded that the distances of the rain gauges from the coast (i.e. station northing's) rather has the strongest influence on rainfall in the catchment and that the correlation is negative which means that generally the amount of rainfall decreases as you move away from the coast. This knowledge was used during the interpolation of climate variables using external drift Kriging (EDK). The topography (elevations) of this sub-region doesn't influence the rainfall in the area. The type of rainfall experienced here is mainly convective rainfall and not orographic.

3.2.3 Rainfall correlation between pairs of stations

The Euclidean distance between station pairs were calculated and after that, a correlation matrix of rainfall against distances was evaluated. A graph is plotted to show how the correlation changes with distances. The correlation of rainfall between pair of stations was done to know the reliability of the station data. From the graph it could be seen that there is a

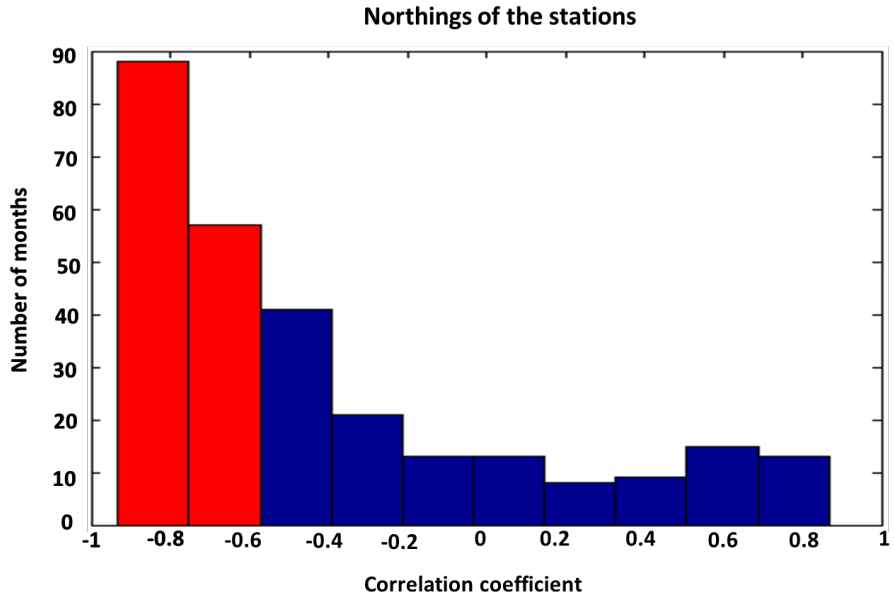

Figure 3.3: Correlation of northings of stations against monthly rainfalls

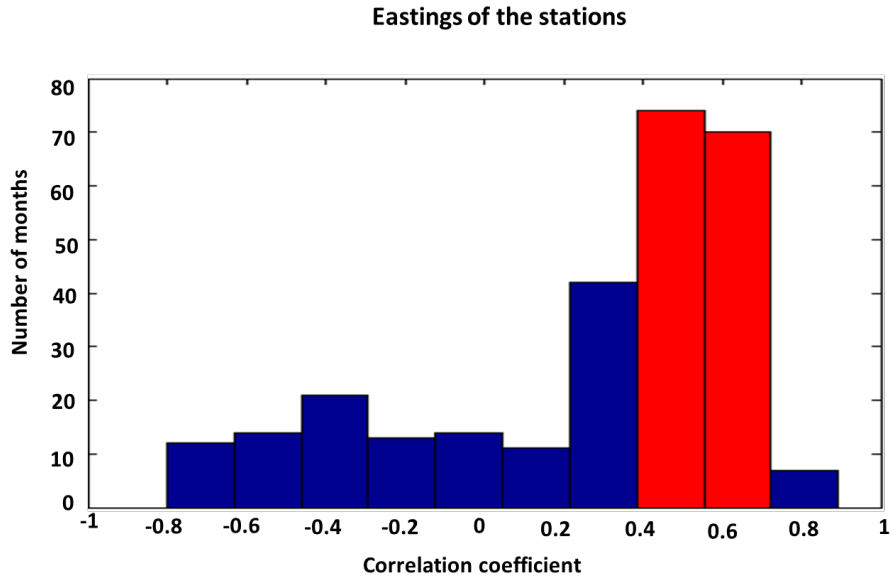

Figure 3.4: Correlation of eastings of stations against monthly rainfalls

strong correlation (R= 0.5) between rainfall and pair of stations and the correlation decreases as the distance between the pairs increase (figure 3.6). Similar results were seen when the data was split into wet and dry periods. About 90% of the gauge stations have distances between them ranging from 5 to 100 km.

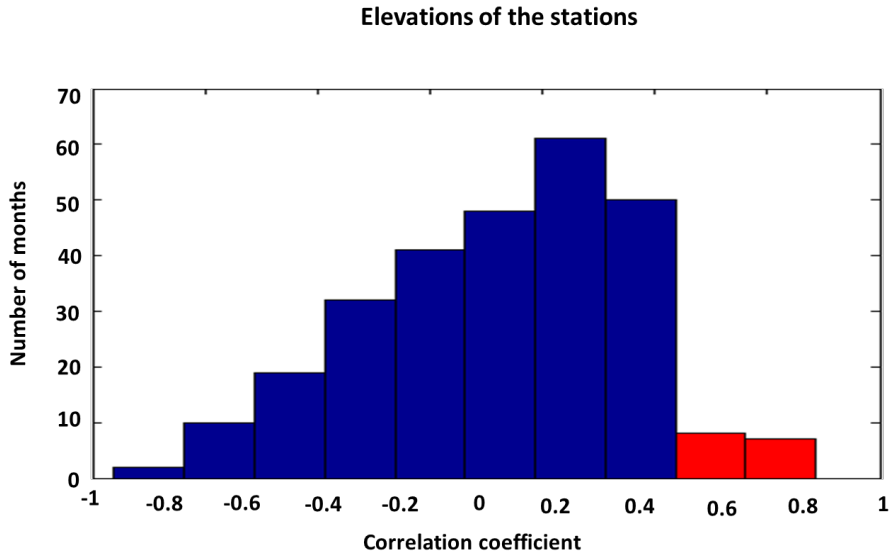

Figure 3.5: Correlation of elevations of stations against monthly rainfalls

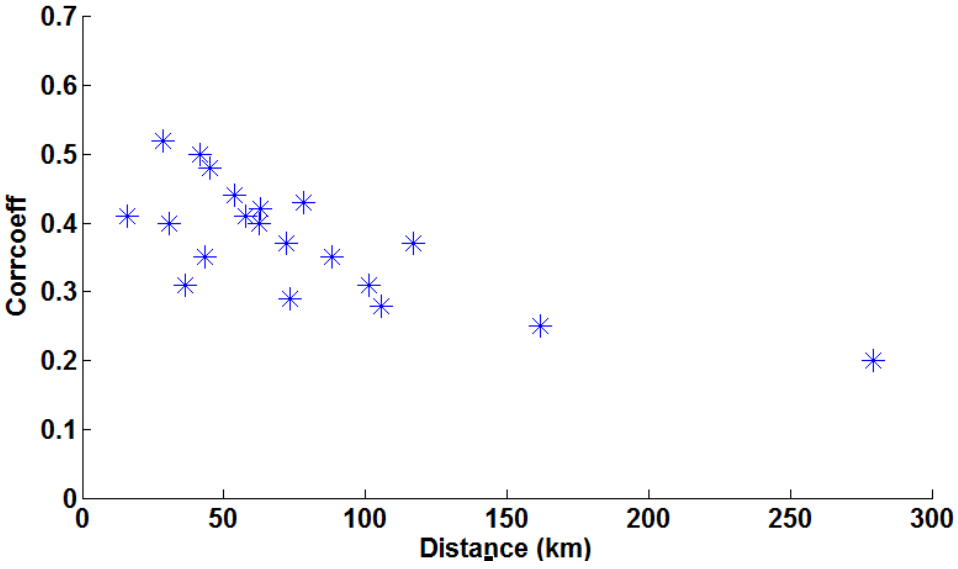

Figure 3.6: Correlation of rainfall between pairs of stations

3.2.4 Interpolation of mean monthly rainfall

Interpolation of mean monthly rainfall for the catchment was done on a 10 km x10 km grid spatial resolution using kriging .

Kriging is a geostatistical tool which uses a variogram function (i.e. the variance between pairs of points that lie at different distances apart) in the estimation of parameter values (precipitation/temperature) at unsampled locations, and/or the estimation of the average of the parameter over a certain area. In the application of the kriging method, the assumptions

of second order stationarity of the random function $Z(u)$ which consists of the following two conditions are made [Bárdossy, 2013]:

- The expected value of the random function $Z(u)$ is constant all over the domain D:

$$E[Z(u)] = m \text{ for all } u \in D \tag{3.1}$$

- The covariance of two random variables corresponding to two locations depends only on the vector h separating these two points:

$$E[(Z(u+h) - m)(Z(u) - m)] = C(h) \text{ for any } u, u+h \in D \tag{3.2}$$

$C(h)$ is the covariance function. In kriging one requires an experimental variogram for the estimation of the spatial variability of the variable. The experimental variogram is defined as:

$$\gamma(h) = \frac{1}{2N(h)} \sum_{i=1}^{N(h)} [Z(u_i) - Z(u_i + h)]^2 \tag{3.3}$$

The experimental variogram is fitted with a theoretical function to enable us estimate the variogram for any distance h. There exists several theoretical variograms which includes, the nugget, spherical, exponential and Gaussian theoretical variograms (equations 3.4 to 3.7). According to Cressie [2015], the nugget model is combined with another variogram to describe the microscale variation in the vicinity of its origin. In this study, the combination of the nugget and the spherical, the nugget and exponential, the nugget and the Gaussian models are used.

The pure nugget effect:

$$\gamma(h) = \begin{cases} 0 & \text{if } h = 0 \\ C & \text{if } h > 0 \end{cases} \tag{3.4}$$

The spherical variogram:

$$\gamma(h) = \begin{cases} \gamma(h) = C(\frac{3}{2}\frac{h}{a} - \frac{1}{2}\frac{h^3}{a^3}) & \text{if } h \leq a \\ C & \text{if } h > a \end{cases} \tag{3.5}$$

The exponential variogram:

$$\gamma(h) = C(1 - e^{-\frac{h}{a}}) \tag{3.6}$$

The gaussian variogram:

$$\gamma(h) = C(1 - e^{-\frac{h^2}{a^2}}) \tag{3.7}$$

where C is the sill and a is the range. Precipitation values at unsampled locations $Z^*(u)$ can be estimated using the the variogram results and Ordinary Kriging (OK) . OK uses weighted linear combinations of n neighbouring observations $Z(u_i)$ for the estimation at

unknown locations. λ_j are called the kriging weights. By introducing a Lagrange multiplier μ, the weights that minimize the $\sigma^2(u)$ are the solution of :

$$\begin{aligned} \sum_{j=1}^{n} \lambda_j \gamma(u_i - u_j) + \mu &= \gamma(u_i - u_0), \;\; i = 1, 2, ..., n \\ \sum_{j=1}^{n} \lambda_j &= 1 \end{aligned} \tag{3.8}$$

Equation 3.8 is called the kriging equation system.

External drift kriging (EDK) [Ahmed and De Marsily, 1987] was also applied apart from OK. In EDK, external knowledge is included in the system as external drift. In this case, it is supposed that an additional variable $Y(u)$ exists and is linearly related to $Z(u)$. Here, the estimator thus depends on the additional variable $Y(u)$. The secondary information $Y(u)$ has to be available at high spatial resolution. The linear kriging system with one external drift is:

$$\begin{aligned} \sum_{j=1}^{n} \lambda_j \gamma(u_i - u_j) + \mu_1 + \mu_2 Y(u_i) &= \gamma(u_i - u_0), \;\; i = 1, 2, ..., n \\ \sum_{j=1}^{n} \lambda_j &= 1 \\ \sum_{j=1}^{n} \lambda_j Y(u_j) &= Y(u_0) \end{aligned} \tag{3.9}$$

where μ_1 and μ_2 are Lagrange-multipliers.

In this study, OK and EDK were used to interpolate the mean monthly rainfalls on the 10km x10km grid size. For EDK, distance to sea information (i.e. station northings) is used as the external drift. Maps of mean monthly and mean annual rainfall were then produced. Figures 3.7, 3.8 and 3.9 show the EDK interpolated mean monthly rainfall maps for the rainfall months (June, July, August, September and October) and a dry month (November). In the month of June the southern part of the catchment experiences its rainfall (i.e. the monsoon rain). The rainfall band shits towards the middle and upper parts of the catchment in the months of July and August and again moves back to the south for the second rainy season in the months of September and October. Figure 3.10, shows the interpolated mean annual rainfall which was expressed in daily amounts by dividing the annual amounts by 365. In this graph, the clear south$-$north negative gradient of rainfall could be seen. The southern part experiences more rainfall and humidity than the northern part of the catchment, which brings about the sub$-$humid to semi$-$arid climate of the catchment. Expectedly, interpolation using EDK performed better than the OK(not shown).

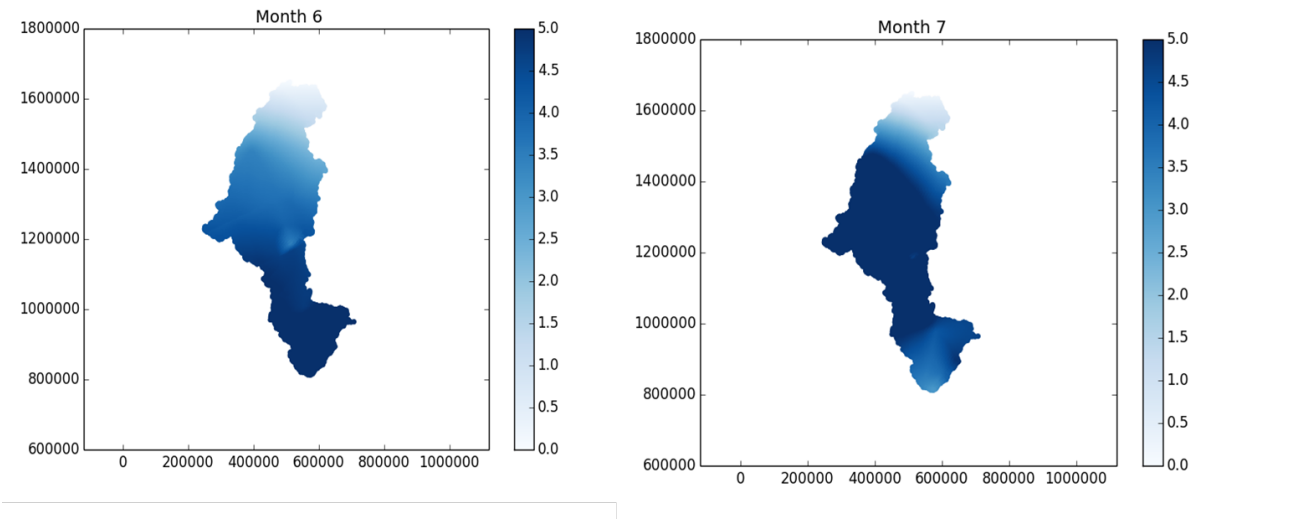

Figure 3.7: Mean daily rainfall amounts in (mm) for the months of June (left) and July (right) for the period 1961−2005

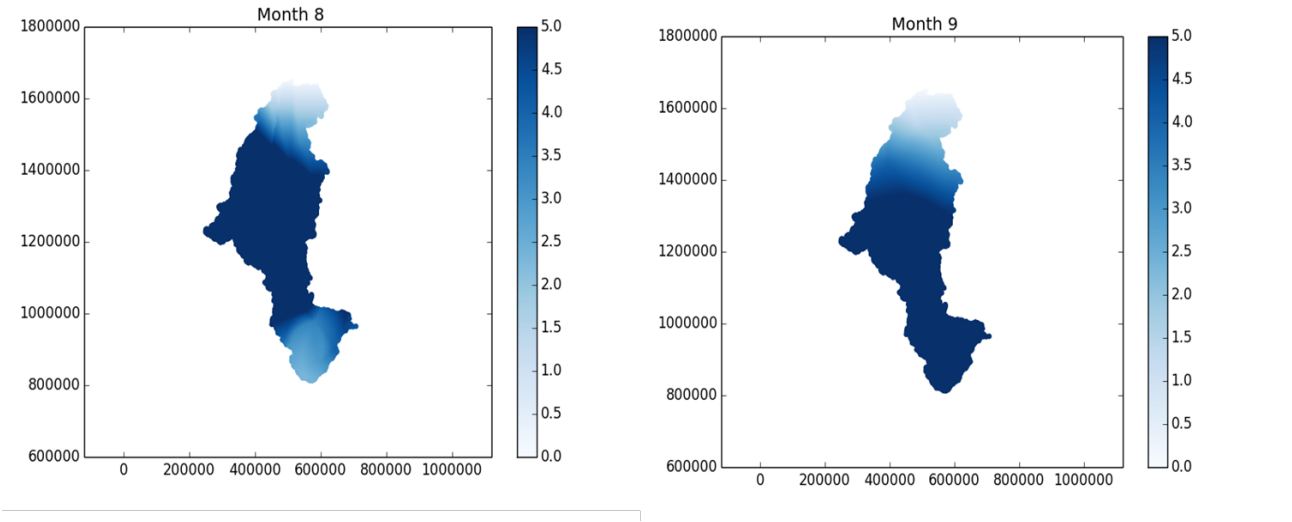

Figure 3.8: Mean daily rainfall amounts in (mm) for the months of August (left) and September (right) for the period 1961−2005

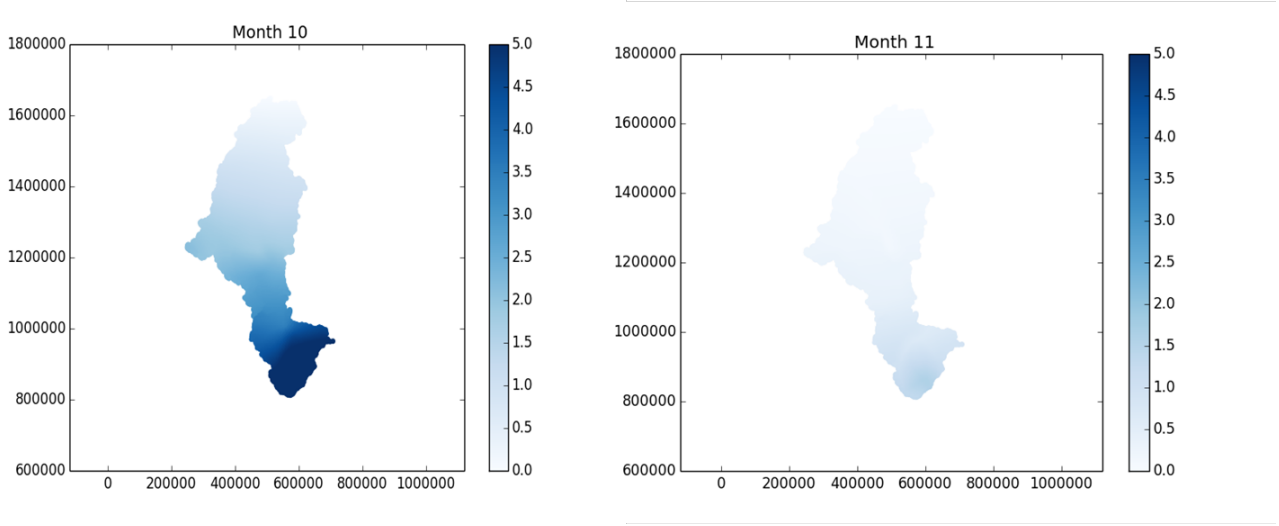

Figure 3.9: Mean daily rainfall amounts in (mm) for the months of October(left) and November (right) for the period 1961−2005

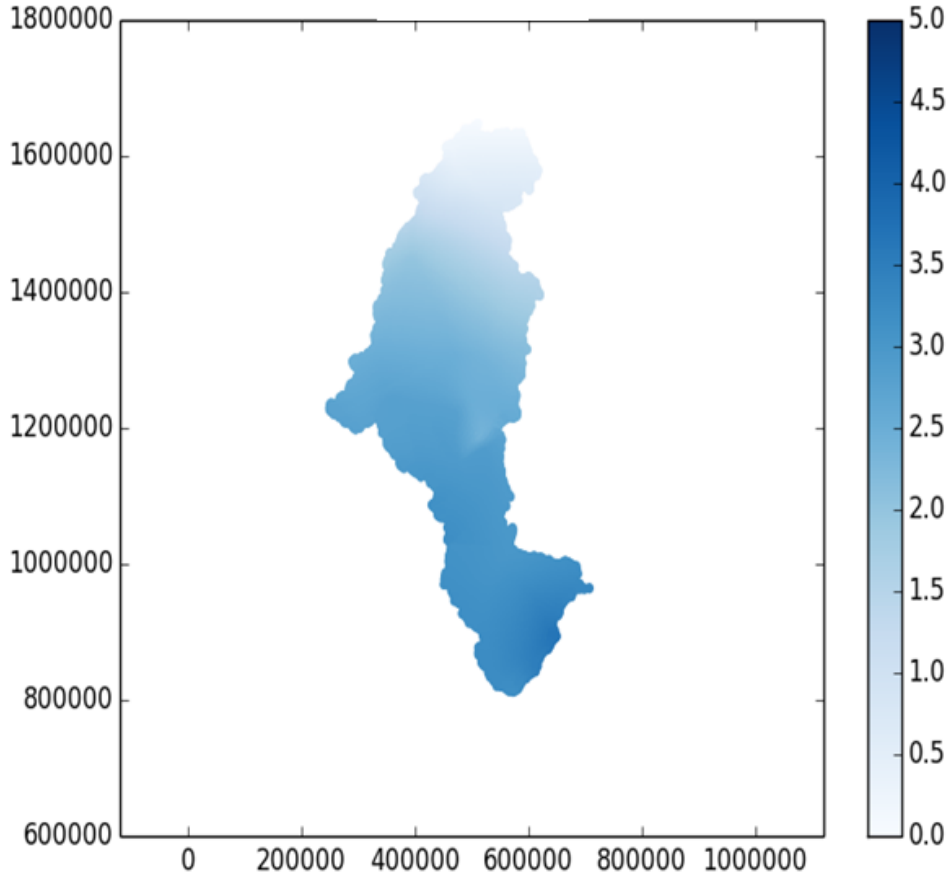

Figure 3.10: Interpolated mean annual rainfall expressed in daily amounts (mm)

3.3 Temperature

A brief analysis was performed on the temperature time series. The stations measuring temperature were fewer than the rainfall gauges in the catchment and there were eleven (11) temperature stations in the catchment (see figure 3.11) with daily resolution for the period 1961 to 2005. The annual cycles of temperature, mean daily temperature and temperature ranges for the study area was estimated. The temperature data was obtained from the Volta basin geoportal and the Meteorological agencies in Ghana and Burkina Faso. The gaps in the data were not filled. The mean maximum temperature for the north is about 34°C and for

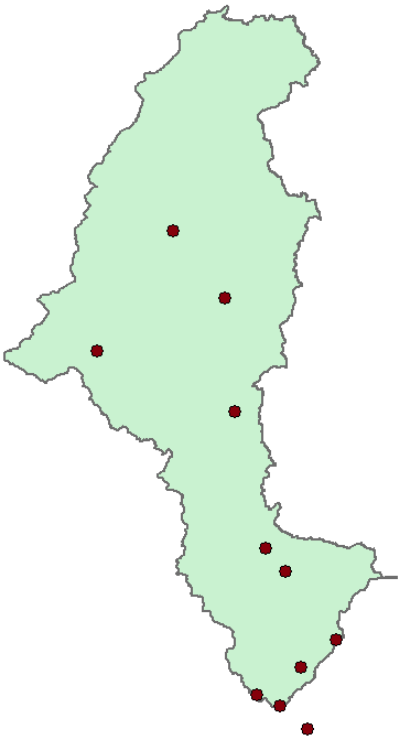

Figure 3.11: A map of the catchment showing the temperature stations

the south is about 29°C (as seen in figure 3.12). Overall, there is a small temperature range of about 7°C across the year and the mean annual temperature ranges from 24°C to 34°C across the catchment. The temperature values begins to decrease as the rainfall sets during the rainfall seasons and there is also a decrease in the daily temperature in the months of December and January due to the Harmattan winds from the Sahara desert. There is a positive temperature gradient as you move towards the northern part of the catchment. The temperature range in the south is smaller as compared with a station in the north.

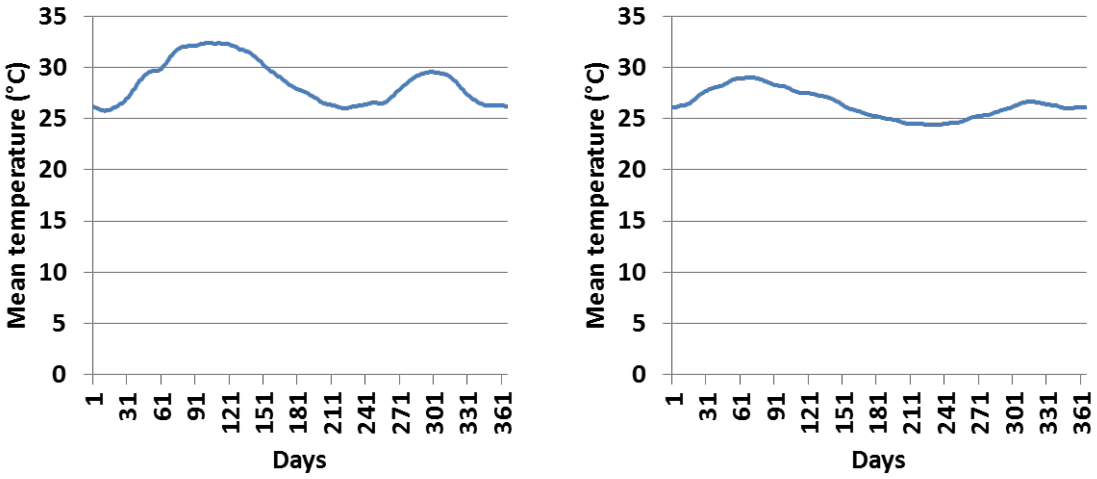

Figure 3.12: Annual temperature cycle for a station in the north (right) and a station in the south (left) of the catchment

3.4 Discharge

For the discharge time series, the annual cycles, annual sums and monthly means were determined. It was observed that, the discharge begins to increase when the rain starts to set in. Data from four (4) discharge stations namely, Chache, Lawra, Bui and Bamboi with daily resolution for the period 1961 to 2005 were used (see figure 3.13). All these gauges are located on the Black Volta River which flows to the Volta Lake. The mean maximum daily discharge for gauge station Lawra with an area of about 92,877 km^2 is 300 m^3/s whiles that of station Chache with a size of 111,258 km^2 is about 600m^3/s (figure 3.14). The discharge begins to rise in the month of May then peaks in August/September. It then subsides from October when the rains have stopped until the next rainy season in April.

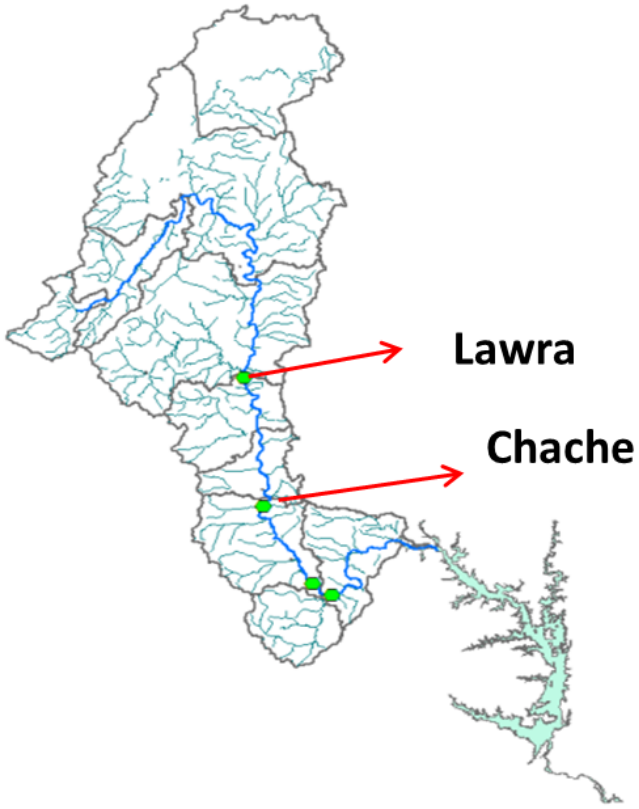

Figure 3.13: Discharge stations on the Black Volta River of the catchment

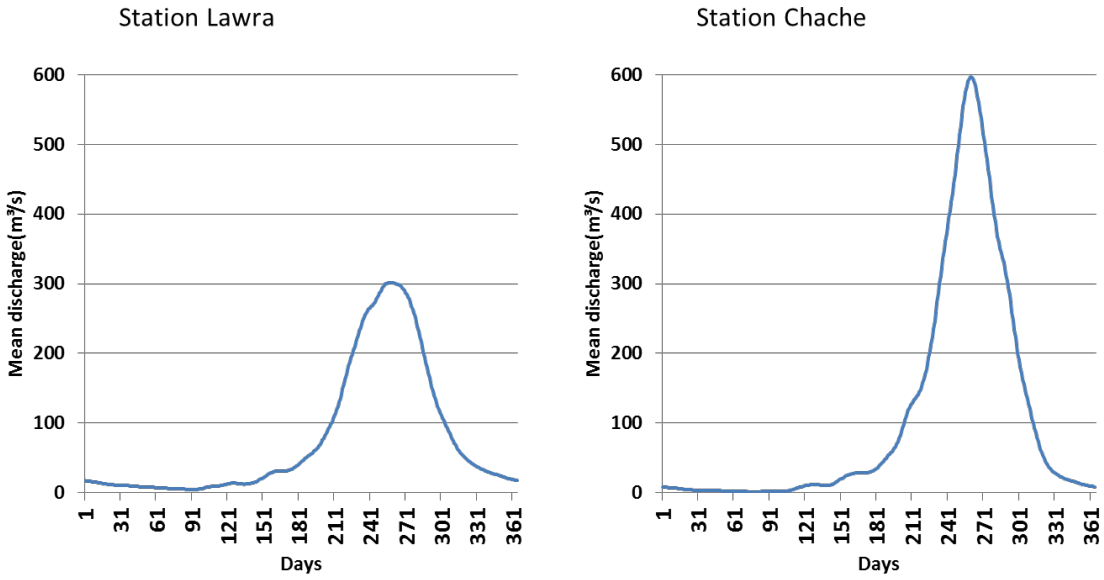

Figure 3.14: Annual discharge cycles for two different stations in the catchment

3.5 Potential Evapotranspiration

Potential evapotranspiration (PET) is a climate variable, which is not ease to measure on the field. Therefore, some equations and models have been developed to estimate it. The models range from the Hargreaves [1974]; Thornthwaite [1948]; Penman [1948]. Most of these models are site specific and are complex and require data which may not be available. Models that are easier to use are too general and produce highly variable results and the too complex are the ones that are considered to be more accurate [McCabe Jr, 1989]. The Thornthwaite potential evapotranspiration (PE) model is a temperature-based model which can essentially be used for any location because it only needs measurements of air temperature as inputs [Thornthwaite, 1948; Mather, 1954]. On a monthly and seasonal basis, the model has been found to produce reasonable estimates of PE [Penman, 1956; Bailey and Johnson, 1972; Garnier, 1956; Cohen, 1986]. PE is defined as the water loss from a large, homogeneous, vegetation-covered area which never suffers from a lack of water [Thornthwaite, 1948; Mather, 1954]. The equation of the Thornthwaite model is:

$$PE = 1.6[10T/I]^a \tag{3.10}$$

where PE is unadjusted potential evapotranspiration in cm/month, T is the mean monthly temperature in °C, I is the annual heat index for a location, and a is a constant. I is based on the sum of 12 monthly heat index values i which are calculated using the following equation:

$$i = (T/5)^{1.514} \tag{3.11}$$

where T is the mean monthly temperature in degrees Celsius. a is based on the annual heat index and is determined by:

$$a = (0.000000675 * I^3) - (0.0000771 * I^2) + (0.0179 * I) + 0.49 \tag{3.12}$$

Unadjusted PE represents water loss for a 30-day month with daylight periods of 12 hours. Unadjusted PE is multiplied by a correction factor to account for how the actual day and month length differ from these values [McCabe Jr, 1989]. It is very difficult to model actual evapotranspiration (ET) since it involves a lot of interrelated components of the environment. Thornthwaite [1948] stated that, there has not yet been an instrument perfected to measure the water movement from the earth to the atmosphere, and consequently we know next to nothing about the distribution of evapotranspiration in space and time [Thornthwaite, 1948]. Thus, models have been developed as surrogates for actual evapotranspiration. Generally, temperature is not a good indicator of available energy for evapotranspiration and this is the main drawback of the Thornwaite model since it is based solely on temperature [Pelton et al., 1960; Rosenberg et al., 1983]. The best indicator of available energy for evapotranspiration is the net radiation. Moreover, the relatively high need for specific data for a variety of variables (i.e. relative humidity, wind speed, solar radiation, etc.) is the major drawback of the Penman-Monteith equation. These parameters are reliably measured by a small number of meteorological stations around the globe, and are especially not available in developing countries [Droogers and Allen, 2002].

In this study, long-term mean monthly PET was estimated using the Thornthwaite approach with temperature as the only input. Again, PET datasets were obtained from the GeoPortal of the Consortium for Spatial Information (CSI) which is an initiative of the Consultative Group for International Agriculture Research (CGIAR) (http://www.csi.cgiar.org) for comparisons. The Global-PET datasets are provided in standard ESRI grid geospatial format, at 30 arc seconds or 1km at the equator [Trabucco and Zomer, 2009; Trabucco et al., 2008]. According to Trabucco and Zomer [2009]; Trabucco et al. [2008], the available data from the WorldClim Global Climate Data were used as the input data in modelling the Global-Aridity and Global-PET. The Hargreaves model is the most suitable to model PET globally [Trabucco and Zomer, 2009]; therefore it was used to model PET in the Global-PET dataset. This model performed almost as well as the Penman-Monteith, but required less parameterization, with significantly reduced sensitivity to error in climatic inputs [Hargreaves and Allen, 2003]. The equation used by Hargreaves to calculate PET is:

$$PET = 0.0023 * RA * (T_{mean} + 17.8) * TD * 0.5(mm/day) \tag{3.13}$$

where, $Tmean$ is the mean monthly temperature, TD is the mean monthly temperature range, and RA is the mean monthly extra-terrestrial radiation. This formula was used by Trabucco and Zomer [2009] to estimate the average monthly and annual PET (mm) layers at spatial resolution of 1km at the tropics for the 1959 to 2000 period. This data was obtained from the CGIAR-CSI Geoportal and then processed in ArcGIS to clip the catchment area to find the average monthly and annual PET (mm) for the study area (as seen in Figure 3.15). Because of the high values of temperature and for that matter energy in the northern part of the catchment, there are higher values of PET (approx. 2087mm) as compared with the southern part (approx. 1571mm). The annual PET pattern in the catchment is similar to that of the temperature. The monthly mean potential evapotranspiration (PET) for the study area using the Thornthwaite method and data from the Global-PET were calculated (see figure 3.16). The results show a slight difference between the two methods with March been the month with the highest PET (approx. 190 mm) and August the least PET (approx. 140 mm) according to the Global-PET (Hargreaves method). In March, the dry period reaches its peak and there are high temperatures resulting in higher PET. And in August, there is less energy due to low temperatures resulting into low values of PET. The daily mean PET ranges from 4 to 7 mm.

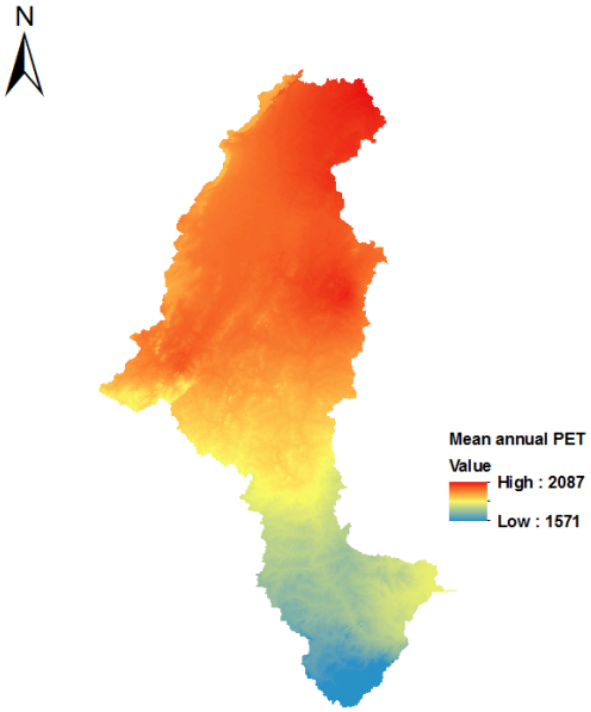

Figure 3.15: Mean annual PET (mm) for the Black Volta basin. Primary souce: Global-PET geoportal)

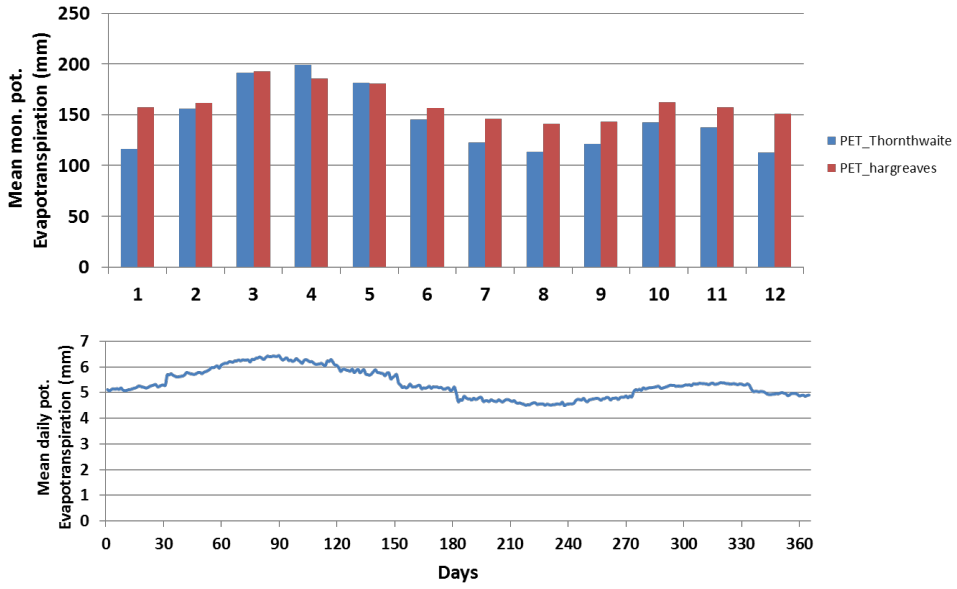

Figure 3.16: Up: Mean monthly PET calculated using the Thornthwaite method and the data from Global-PET; Down: Mean daily PET estimated from the Global-PET

4 Hydrological Modeling

4.1 Introduction

The most probable model that hydrologists spontaneously refer to when discussing hydrological models are runoff models. The basic principle in hydrological modeling is that the model is used to calculate river flow based on meteorological data, which are available in a catchment or in its vicinity. According to Beven [2011], the main reason why we need to model the rainfall-runoff processes of hydrology is the result of the limitations of hydrological measurement techniques. We are not able to measure all the things we would like to know about hydrological systems and that there is limited range of measurements in space and time. "We therefore need a means of extrapolating from those available measurements in both space and time, particularly to ungauged catchments (where measurements are not available) and into the future (where measurements are not possible) to assess the likely impact of future hydrological change" [Beven, 2011].

The types of hydrological models range from the empirical (e.g. Regression models) to the conceptual (e.g. HBV, HYMOD) and physically based models (e.g. TOPMODEL). The empirical models are purely based on analyzing observed input and output data (e.g. rainfall, discharge). Their advantages are that, they are simple in structure and parameter estimation and include empirical knowledge. The conceptual model has a conceptual description of important processes and that the model variable and parameters have an abstract meaning. It has the advantages of a simple processes description, a good performance especially at large scales and low amount of input data and number of parameters. The physically based model has its process description based on first principles and its parameters and state variables may be directly measured in the field. It has the merits of an advanced process description, good performance especially at small scales and a low number of calibration parameters.

In selecting the appropriate hydrological model for this study, the following criteria were considered:

- Because of the large size of the catchment and the coarse network of available data for the catchment, the chosen model should not be complex and data intensive. The requirement of data should be met by the available observations and measurements within the study area.
- There should not be too many parameters in the model structure.
- The structure of the model should describe and represent the most important runoff generating processes in a scientifically reasonable way.
- The model should be applicable to the study area.

As an investigation into the water balance situations in the catchment and based on the above criteria, the HBV model [Bergström, 1995] which is a lumped conceptual hydrological model was chosen for this study area. The model was set up, calibrated and validated for two different time spans and sub-catchment sizes.

4.2 HBV − Hydrological Model

The model was originally developed at the Swedish Meteorological and Hydrological Institute (SMHI) and was first applied in the early 1970s [Bergström and Forsman, 1973]. There have been some modifications to the model over time, but the philosophy behind the model has been unchanged [Lindström et al., 1997]. This model has been extensively applied in Europe and Götzinger [2007] also applied it in the Oueme Basin in Benin (West Africa). Slight modifications have been made to the original model by the Institute for Modelling Hydraulic and Environmental Systems (University of Stuttgart) and it is referred to as HBV−IWS model. In this study, the lumped version of the HBV−IWS model was used. The model consists essentially of four parts:

- Snow accumulation and melt
- Soil moisture and runoff generation
- Runoff concentration within the subcatchment and
- Flood routing in the river network

Because the study area is in the tropics, there is no precipitation as snow therefore the snow accumulation and melt module in the model was taken out.

4.2.1 Soil moisture accounting

The soil moisture accounting routine calculates the proportion of rainfall that reaches the soil surface that produces runoff. This is related to the soil moisture deficit and is calculated as:

$$\Delta Q/\Delta P = (SM/FC)^{\beta} \tag{4.1}$$

where,

ΔQ	is the contribution of the zone to runoff [mm]
ΔP	rainfall or snowmelt [mm]
SM	actual soil moisture [mm]
FC	maximum storage capacity of the soil [mm]
β	a model parameter

The remaining part of the rainfall is added to the soil moisture until the storage capacity of the soil (FC) is reached.

4.2.2 Evapotranspiration

The evapotranspiration in each month is computed by using the long term mean monthly evapotranspiration. The daily mean air temperature is used to adjust the daily values of potential evapotranspiration according to the relation:

$$PE_A = (1 + C_{ET}(T - T_M))PE_M \tag{4.2}$$

where,

PE_A adjusted potential evapotranspiration [mm/day]

PE_M long term mean evapotranspiration for a given month [mm/day]

T_M long term mean monthly air temperature [°C]

T mean daily air temperature [°C]

C_{ET} model parameter [°C^{-1}]

The actual evapotranspiration is calculated as:

$$E_A = \begin{cases} PE_A & \text{if} \quad \frac{SM}{CMAX} \geq \eta \\ \min\left(\frac{SM}{\eta.CMAX} PE_A, SM\right) & \text{else} \end{cases} \tag{4.3}$$

where,

E_A actual evapotranspiration from the soil zone [mm]

PE_A potential evapotranspiration from the soil zone

SM actual soil moisture [mm]

$CMAX$ limiting soil moisture at which potential evapotranspiration takes place [mm]

η water balance parameter

The relationship between potential and actual evapotranspiration can differ strongly due to water or energy limitations. Therefore, the parameter η is introduced to control the ratio between daily potential and actual evapotranspiration depending on the available water and depends on the long term water balance only. If there is enough water, you evaporate all the potential evapotranspiration as actual else the potential evapotranspiration is reduced by the factor $\left(\frac{SM}{\eta.CMAX}\right)$.

4.2.3 Runoff response process

The runoff response function is used to transform the runoff computed in the soil moisture accounting to discharge at the outlet of the catchment. It controls the time distribution of the generated runoff. The runoff response routine comprises of two conceptual reservoirs

cascaded over one another. The upper reservoir consists of two outlets which are used to conceptualize the direct runoff component from the upper soil zone and the inter-flow. Soil water is percolated to the lower (second) reservoir. The lower reservoir is a linear one whose outflow simulates the base flow component of the runoff. The response function is governed by three recession coefficients (K_0, K_1 and K_2), one percolation capacity (PERC), one threshold water level (L_1) and one parameter in the transformation function (MAXBAS): altogether six empirical parameters [Hundecha and Bárdossy, 2004; Singh and Bárdossy, 2012]. The upper reservoir is fed by the excess water from the soil moisture accounting routine and the flows at time step t from its two outlets are given by:

$$Q_0(t_i) = K_0(S_1 - L_1) \tag{4.4}$$

$$Q_1(t_i) = K_1 S_1 \tag{4.5}$$

where,

$Q_0(t_i)$ is the outflow from the near surface of the upper reservoir [mm/day], $Q_1(t_i)$ is outflow from the bottom outlet of the upper reservoir [mm/day], K_0, K_1 is recession coefficients of the near surface and inter flows respectively [day^{-1}], S_1 is effective depth of water in the upper reservoir [mm] and L_1 is the threshold water level for near surface flow [mm]

The lower reservoir is fed by a percolation rate controlled by a parameter PERC from the upper reservoir. The outflow from the lower reservoir at time step t_i is calculated as:

$$Q_2(t_i) = K_2 S_2 \tag{4.6}$$

where,

$Q_2(t_i)$ is the outflow from the lower reservoir [mm/day], K_2 is the recession coefficients of the lower reservoir [day^{-1}] and S_2 is the depth of water in the lower reservoir [mm].

The total runoff Q_g is computed as the sum of the outflows from the upper and the lower reservoirs as:

$$Q_g(t_i) = Q_0(t_i) + Q_1(t_i) + Q_2(t_i) \tag{4.7}$$

where,

$Q_g(t_i)$ total generated runoff at the outlet of a catchment [mm/day].

A triangular transformation function whose base is defined by a parameter MAXBAS [days] as shown in figure 4.1 is used to smooth the total runoff.

$$Q(t_i) = \sum_{j=0}^{T} \tau(j) Q_g(t_{i-j}) \tag{4.8}$$

where,

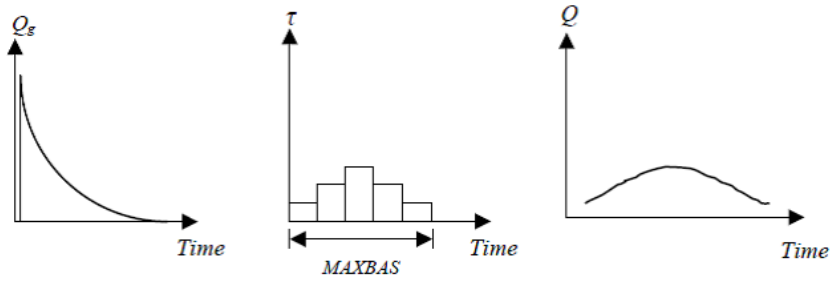

Figure 4.1: Smoothing of the generated runoff Qg to obtain Q. (source: [Hundecha and Bárdossy, 2004])

$Q(t_i)$ is the final transformed total runoff at the outlet of the catchment [mm/day], $\tau(j)$ is the weighting function at step jth time step and T is MAXBAS expressed as an integer multiple of the time-step used for runoff computation.

Figure 4.2 shows a schematic representation of the HBV-IWS version. There are 9 parameters to describe the model but because the snow accumulation and melt routine is taking out; it was left with 7 parameters which were used for calibration in this research (table 4.1). Table 4.1 also shows the model parameter range used in the HBV model.

Table 4.1: Model parameter range for HBV model. Source: [Bárdossy and Singh, 2008] (max. and min. values were slightly modified for the study area)

Parameter	Description	max	min
FC	Field capacity (mm)	600	50
BETA	Shape coefficient	8	0.2
K0	Near surface flow storage constant	0.8	0.02
K1	Interflow storage constant	0.25	0.01
K2	Baseflow storage constant	0.1	0.001
KD	Percolation storage constant	0.2	0.005
L1	Threshold water level for near surface flow (mm)	100	1

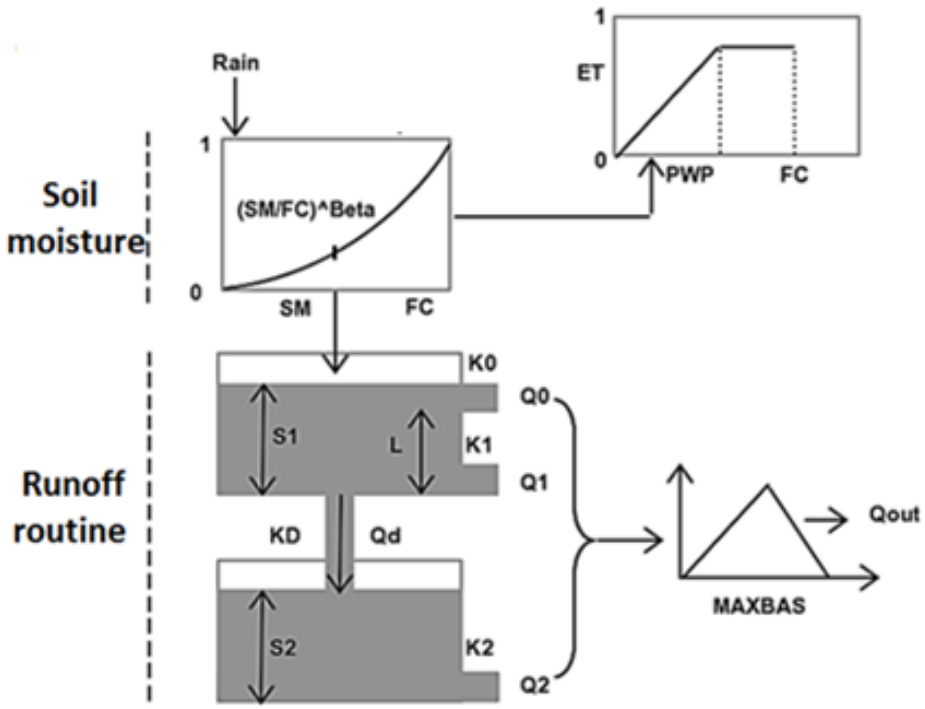

Figure 4.2: Schematic representation of HBV−IWS model which is slightly modified for the study area. Adapted from Hundecha and Bárdossy [2004]

4.3 Model performance measures

The performance of the model is determined by comparing simulated variables with observations. Different optimization functions ranging from Nash Sutcliffe coefficient (NS) to the Nash Sutcliffe coefficient of the logarithm of the discharge (LogNS) which focuses on the low flow condtions more than the traditional NS coefficient was used to determine how well the model performs. To equally concentrate on high and low flows, a combination of NS and LogNS was also used as the performance measure. The Nash Sutcliffe with a Bias constraint (NS−Bias) as proposed by Viney et al. [2009] and Correlation were also used. In order to take care of the water balances, a calibration using an explicit consideration of the correlation between the observed and simulated discharges which is similar to the approach of Kling and Gutpta (KG) ([Gupta et al., 2009]) was used.The equations below represent functions of the various performance measures used in the study. The best value for all the performance criterion is unity (1).

$$NS = 1 - \frac{\sum_{t=1}^{T}(Q_{obs}(t) - Q_{sim}(t))^2}{\sum_{t=1}^{T}(Q_{obs}(t) - \bar{Q})^2} \tag{4.9}$$

$$LogNS = 1 - \frac{\sum_{t=1}^{T}(ln(Q_{obs}(t)) - ln(Q_{sim}(t)))^2}{\sum_{t=1}^{T}(ln(Q_{obs}(t)) - ln(\bar{Q}))^2} \tag{4.10}$$

$$NS_{Bias} = NS - 5\,|ln(1 + Bias)|^{2.5} \tag{4.11}$$

where the Bias is calculated as:

$$Bias = \frac{\sum_{t=1}^{T} Q_{sim}(t) - \sum_{t=1}^{T} Q_{obs}(t)}{\sum_{t=1}^{T} Q_{obs}(t)} \tag{4.12}$$

where,

$Q_{obs}(t)$ and $Q_{sim}(t)$ represents the observed and simulated discharges at times (t) respectively and $\bar{Q}$ is the mean of the observed discharge. ln is the natural logarithm.

The Kling-Gupta equation is expressed as:

$$KG = 1 - (1 - r)^2 + \alpha(\frac{V_M - V_O}{V_O})^2 \tag{4.13}$$

where, r is the correlation between the observed discharge series and the one simulated with the model using parameter vector for the catchment. V_O is the observed total discharge and V_M is the one simulated with the model using parameter vector. α is the the weight of the balance error (which in this study a value of 5 is used).

Overall, a model is said to be good when: (1). It reproduces observations and (2). It reacts to signals in an appropriate manner. Some researchers only use the first point in assessing how well their model performs without considering the second important point of the model reacting to signals in an appropriate manner. In this study, we went further to ascertain how well the model reacts to signals and how steady it is, by introducing the following optimisation and calibration techniques:

1. Different objective functions were used for optimization. (e.g. NS, LogNS, Kling-Gupta, NS with a bias constraint, a combination of NS and LogNS and Correlation)
2. Using different sub-catchments
3. Calibrating on daily temporal scale and checking performance on different scales (i.e. daily, monthly and residual scales)
4. Calibration on different temporal scales (i.e. daily, monthly, residuals)
5. Swapping of data for calibration and validation
6. Calibrating on dry periods and validating on wet periods and vice versa

4.4 Robust Parameter Estimation (ROPE)

The robust parameter estimation (ROPE) algorithm, is an automatic calibration algorithm which generates best parameter sets based on a data depth function. According to Bárdossy and Singh [2008], these parameter sets are in the interior of the data depth and are themselves good, transferable and not very sensitive. They can be considered as a kind of compromise solution [Bárdossy and Singh, 2008].

Bárdossy and Singh [2008] reveals in their work that, the following procedure is used for modeling purposes in finding the set of good parameters and also the identification of the deep parameter vectors for robust modeling:

1. The range for the d selected parameters are identified
2. N random parameter vectors forming the set X_N are generated in the d dimensional rectangle bounded by the limits defined in 1
3. The model performances are calculated after the hydrological model is run for each parameter vector in X_N
4. The subset X_N^* of the best performing parameters is identified. This might be for example the best 10% of X_N
5. M random parameter sets forming the set Y_M are generated, such that for each parameter vector $\theta \in Y_M, D(\theta) \geq L$(with $L \geq 1$) where the depth is calculated with respect to the set X_N^*
6. The set Y_M is relabeled as X_N and steps 3-6 are repeated until the performance corresponding to X_N and Y_M does not differ much or until the pre-determined number of iterations is over.

Additional information about the ROPE algorithm can be found in Bárdossy and Singh [2008]. In this study, 10,000 best parameter sets was generated and calibrated in a computer framework using ROPE with the initially set model parameter ranges. The 90th quantile of the band of simulated discharges for 10,000 best parameter sets are analyzed and discussed in the subsequent section.

4.5 Results

4.5.1 Performance measures under different sub-catchments

Tables 4.2 and 4.3 summarizes the results of the model performance for two separate subcatchments (Lawra and Chache) all located in the study area. For subcatchment Lawra, the period used for calibration was 1992 to 1996 whiles 1997 to 2001 was used for the validation period. And for the subcatchment Chache, the periods 1996 to 2000 and 2001 to 2005 were used as calibration and validation periods respectively. In both cases, the first year was used as a warm-up period for the model.

Table 4.2: Model performance for sub-catchment Lawra (size: 92,877 km^2) for calibration and validation

Performance Measure	Calibration					Validation			
	MIN	MAX	MEAN	STD		MIN	MAX	MEAN	STD
NS - Bias	0.712	0.815	0.751	0.024		0.160	0.726	0.501	0.182
NS	0.712	0.815	0.750	0.022		0.219	0.731	0.566	0.148
LogNS	0.510	0.663	0.592	0.032		-	-	-	-
(NS+LogNS)/2	0.580	0.685	0.629	0.021		0.418	0.593	0.485	0.038
(NS+3LogNS)/4	0.612	0.723	0.668	0.015		0.402	0.588	0.495	0.027
Correlation	0.847	0.924	0.874	0.014		0.810	0.910	0.850	0.023
Kling-Gupta	0.976	0.994	0.984	0.004		0.964	0.992	0.977	0.007

The model performs quite well using NS as objective function with a mean value of 0.75 and 0.57 for calibration and validation respectively. However, it performed not better when using the Log NS or the addition of the two as the objective function. Moreover, using NS−Bias as the objective function did not have a significant change on the performance of the model. There was a slight improvement in the performance and better simulation of the low flows when a higher weight was given to the LogNS during its combination with NS (i.e. (NS + 3LogNS)/4).

The correlation and Kling Gupta values were all very high which justifies the notion that it is not good enough to use only correlation to describe how good a model is. Figures 4.3 and 4.4 shows hydrographs for both the calibration and validation periods for gauge stations Lawra and Chache respectively. In the hydrograph, it could be seen that the model overestimates the peaks in both the calibration and validation periods. The model performs rather slightly

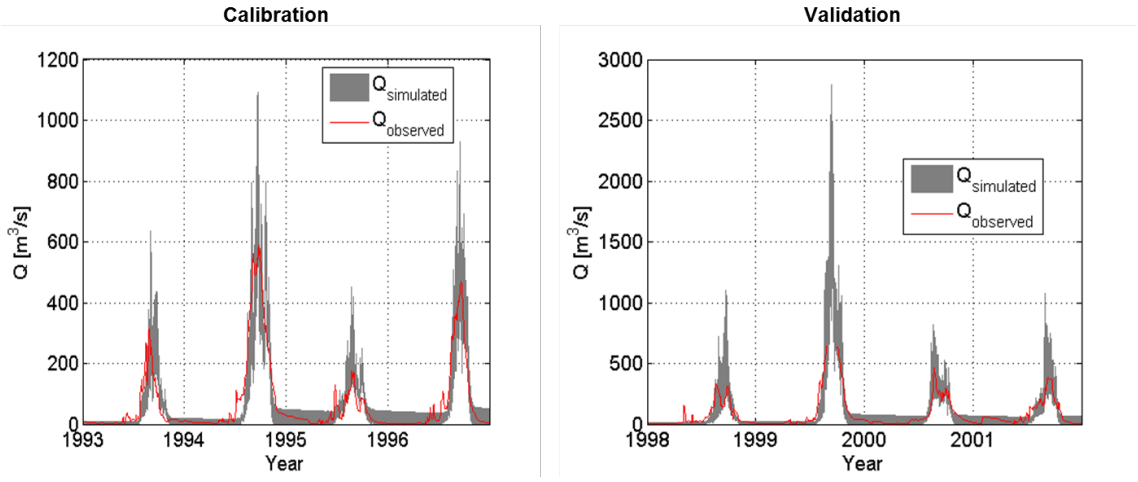

Figure 4.3: Hydrographs for sub-catchment Lawra showing both the calibration and validation periods

better when the sub-catchment size is increased as in the case of sub-catchment Chache

Table 4.3: Model performance for sub-catchment Chache (size: 111,258 km^2) for calibration and validation

Performance Measure	Calibration				Validation			
	MIN	MAX	MEAN	STD	MIN	MAX	MEAN	STD
NS - Bias	0.694	0.880	0.796	0.037	0.486	0.733	0.603	0.048
NS	0.682	0.880	0.792	0.041	0.472	0.737	0.598	0.052
LogNS	0.694	0.835	0.765	0.027	0.566	0.784	0.648	0.047
(NS+LogNS)/2	0.697	0.829	0.772	0.028	0.534	0.713	0.610	0.034
(NS+3LogNS)/4	0.750	0.821	0.790	0.021	0.604	0.685	0.641	0.015
Correlation	0.856	0.941	0.913	0.020	0.753	0.878	0.826	0.028
Kling-Gupta	0.979	0.997	0.991	0.004	0.938	0.985	0.968	0.010

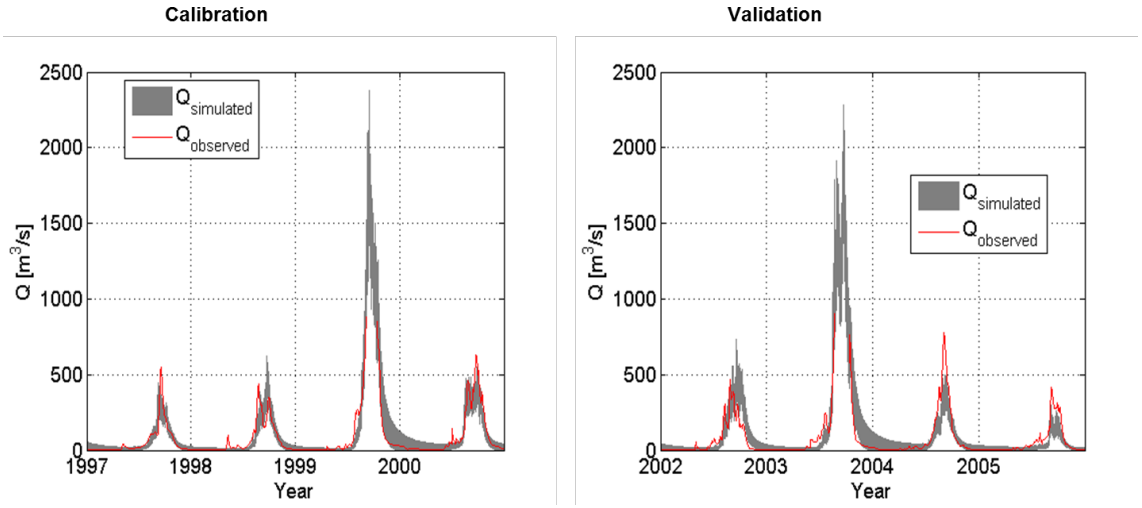

Figure 4.4: Hydrographs for sub-catchment Chache showing both the calibration and validation periods

(size: 111,258 km^2). This might be due to the less availability of input data for the bigger catchment. In the Chache sub-catchment, mean NS values are 0.80 and 0.60 for calibration and validation respectively. The estimation of the peaks is better in this sub-catchment. Again, there is not much difference in either using the Log NS or NS−Bias as the objective function but there is an improvement in the performance when a bigger weight is given to the LogNS in accounting for the low flows (figures 4.5 and 4.6). Better simulation of the low flows is very important in this study because the key objective of the model is for management of the water resources.

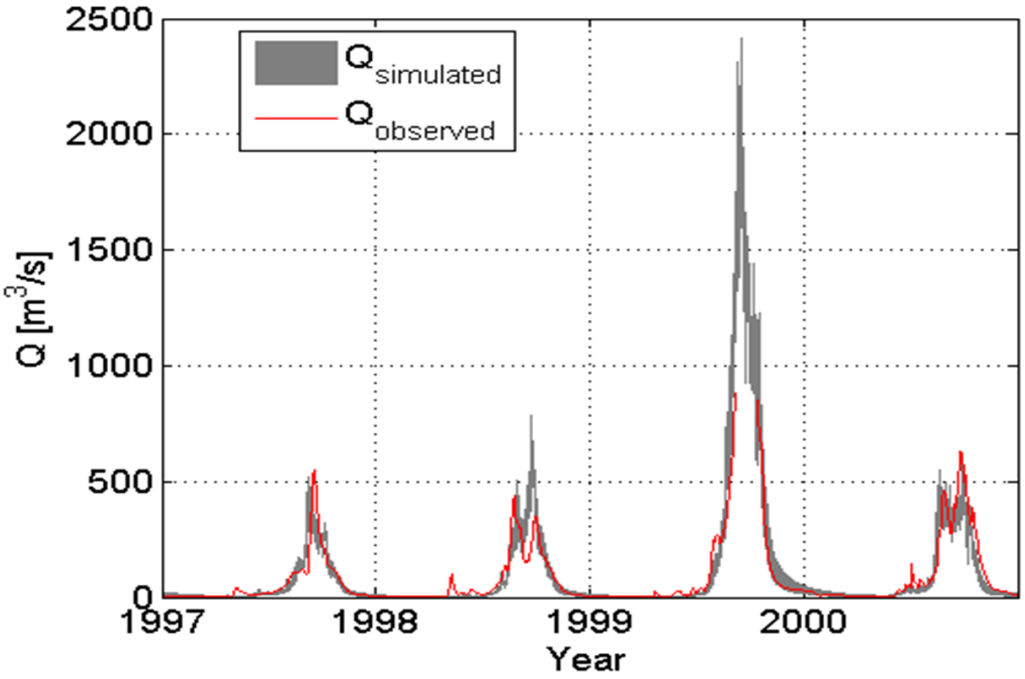

Figure 4.5: Hydrograph for calibration of the model for gauge Chache using (NS +3LogNS) as the objective function

4.5.2 Calibrating on daily temporal scale and checking performance on different scales

To determine how robust the model is and how well it reacts to signals, it was calibrated on the daily temporal scale and performances checked on the monthly and residuals or net discharge (obtained by subtracting the annual cycle from the daily data). The model was once again validated using different set of observed data.Table 4.4 and figures 4.7, 4.8 and 4.9 show the results for this case. In this case (NS+3LogNS)/4 was used as the objective function during the optimisation. From the results, it could be observed that the model performs better during calibration than the validation period. The model performed quite well when the annual cycle was deducted from the data (i.e. residuals or the net discharge) which signifies how the model reacts to signals. Obviously, the performance was improved when it was checked on the monthly scale and the monthly residuals. Hence, it performs well on different temporal scales and it's able to capture both deficit and surplus water volumes relative to the annual cycle.

4.5.3 Calibration on different temporal scales

In this case, calibration and validation was done for different temporal scales to determine how well the model performs on different scales. The results for this case could be seen in table 4.5 and figures 4.10 and 4.11. In this case, calibration was performed using both

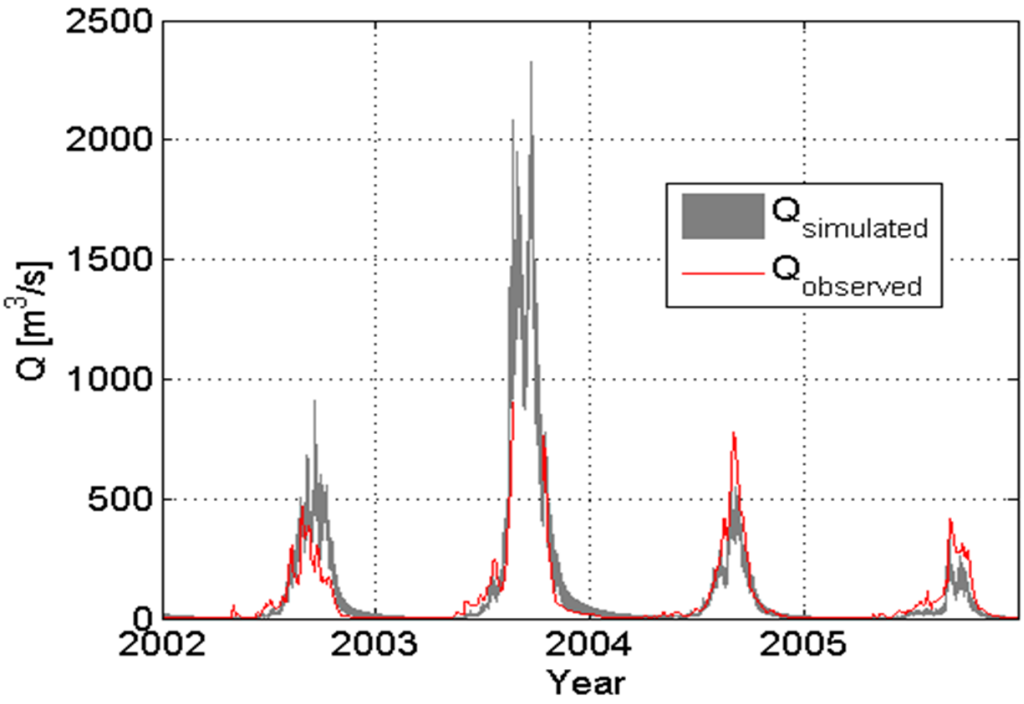

Figure 4.6: Hydrograph for validation of the model for gauge Chache using (NS +3LogNS) as the objective function

(NS+3LogNS)/4 and NS as objective functions. The model performs very well during the daily and monthly calibrations but loses some efficiency during the calibration on daily and monthly residuals. Calibrating on monthly scale has very high performance which makes the model suitable for water resource management. These performances exceed the daily calibration and checking performance on different scales discussed under subsection . Calibrating on monthly scale could reach a mean NS performance as high as 0.96 (see table 4.5.

4.5.4 Swapping of data for calibration and validation

The data used for calibration was swapped with that which was used for validation to again check how the model performs under different conditions and times. Table 4.6 and figures 4.12 and 4.13 show the results for the gauge station Chache when calibration was done on the daily and monthly scales respectively. It is interesting to know that the model performed creditably well during both scenarios for both calibration and validation for the daily and monthly scales. Almost the same performance (NS = 0.78) was realized for both swapped calibration years (i.e. 1996 to 2000 and 2001 to 2005). Meaning that, it doesn't matter which 5−year period used to calibrate the model the same performance results are obtained. The 5−year period (1996 to 2000) shows improved results for validation than the other period. Also, in that year period the validation results were unexpectedly slightly higher than the

Table 4.4: Calibration and validation results for Chache by calibrating on daily scale and checking performances on other temporal scales with (NS +3LogNS) as the objective function

Temporal Scales	Calibration (1996 - 2000)			Validation (2001 - 2005)		
	MIN	MAX	MEAN	MIN	MAX	MEAN
Daily	0.75	0.82	0.79	0.60	0.68	0.64
Daily Residual	0.17	0.52	0.35	0.11	0.40	0.26
Monthly	0.86	0.87	0.87	0.69	0.70	0.70
Monthly Residual	0.61	0.65	0.63	0.48	0.50	0.49

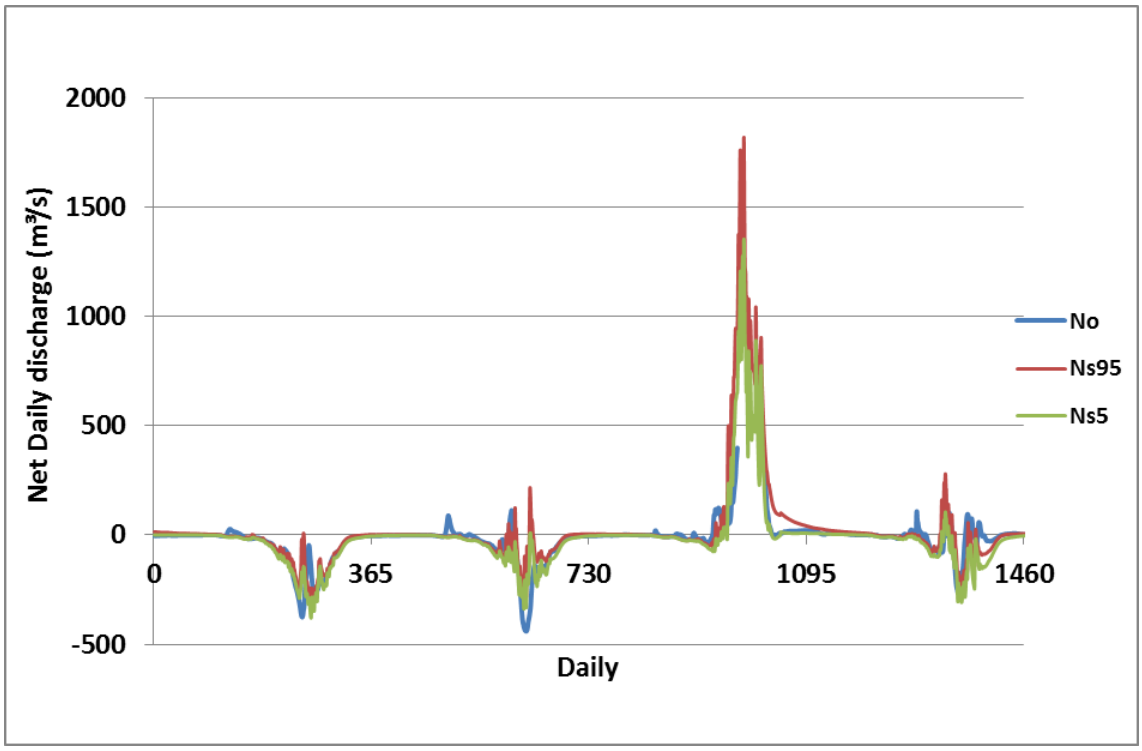

Figure 4.7: Hydrograph showing the model performance on the daily residuals after calibration on the daily scale

calibration results.

4.5.5 Calibrating on dry and validating on wet and vice versa

To investigate the transferability of the model to different years and catchment and to also know how it reacts to rainfall signals, the *split sampling* was done. In the split sampling, the data was split into two parts (namely the wet and dry years). A 3-year period was used for both the calibration and validation with the first year been a warm-up period for the model. Calibration of the model was done for wet years whiles validation was done for dry years and vice and versa. The results of this could be seen in tables 4.7 and 4.8 and figures 4.14

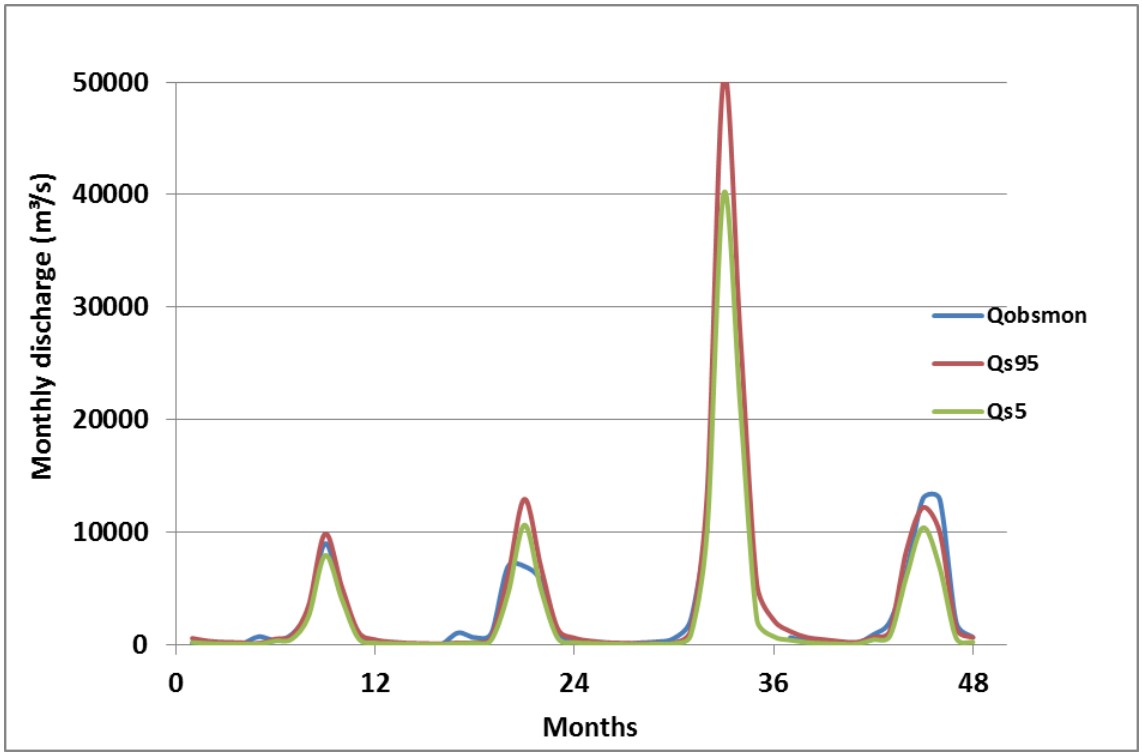

Figure 4.8: Hydrograph showing the model performance on the monthly simulations after calibration on the daily scale

and 4.15. The results of the split sampling emphasizes that the model reacts well to signals and it performs better in the wet conditions than the dry. The two subcatchments showed very encouraging results especially for the wet calibrations and validations. But, in both the dry calibration and wet validation, the model was slightly late and also overestimates the peak discharges.

Table 4.5: Model performance on gauge Chache for calibration on different temporal scales using (NS+3LogNS)/4 and NS as the performance measurement functions

Perf. measure: (NS+3LogNS)/4	Calibration (1996 - 2000)				Performance measure: NS	Calibration (2001 - 2005)		
	MIN	MAX	MEAN			MIN	MAX	MEAN
Daily	0.75	0.82	0.79		Daily	0.68	0.88	0.78
Monthly	0.87	0.93	0.90		Monthly	0.92	0.96	0.94
Daily Res.	-	-	-		Daily Res.	0.48	0.53	0.51
Monthly Res.	-	-	-		Monthly Res.	0.32	0.51	0.42

Table 4.6: Model performance for gauge Chache for a swapped data for calibration and validation period

Perf. measure: (NS+3LogNS)/4	Calibration (1996 - 2000)				Validation (2001 - 2005)		
	MIN	MAX	MEAN		MIN	MAX	MEAN
Daily	0.75	0.82	0.79		0.60	0.68	0.64
Monthly	0.87	0.93	0.90		0.63	0.88	0.76
Perf. measure: (NS+3LogNS)/4	Calibration (2001 - 2005)				Validation (1996 - 2000)		
	MIN	MAX	MEAN		MIN	MAX	MEAN
Daily	0.74	0.82	0.78		0.71	0.88	0.80
Monthly	0.61	0.89	0.75		0.73	0.93	0.83

Table 4.7: Model performance for Lawra on split sampling (calibration and validation)

Subcatchment Lawra								
	Calibration (Dry)				Validation (Wet)			
Perf. measure	MIN	MAX	MEAN	STD	MIN	MAX	MEAN	STD
NS	0.614	0.780	0.693	0.029	0.540	0.646	0.569	0.017
Correlation	0.819	0.936	0.849	0.022	0.737	0.808	0.761	0.013
	Calibration (Wet)				Validation (Dry)			
Perf. measure	MIN	MAX	MEAN	STD	MIN	MAX	MEAN	STD
NS	0.709	0.849	0.760	0.028	0.282	0.588	0.491	0.060
Correlation	0.852	0.936	0.879	0.015	0.618	0.692	0.675	0.014

Table 4.8: Model performance for Chache on split sampling (calibration and validation)

Subcatchment Chache								
Performance Measure	Calibration (Dry)				Validation (Wet)			
	MIN	MAX	MEAN	STD	MIN	MAX	MEAN	STD
NS	0.737	0.867	0.792	0.020	0.522	0.806	0.703	0.083
Correlation	0.877	0.943	0.897	0.011	0.832	0.953	0.892	0.026
Performance Measure	Calibration (Wet)				Validation (Dry)			
	MIN	MAX	MEAN	STD	MIN	MAX	MEAN	STD
NS	0.689	0.913	0.824	0.049	0.625	0.805	0.674	0.028
Correlation	0.848	0.967	0.926	0.029	0.864	0.924	0.888	0.011

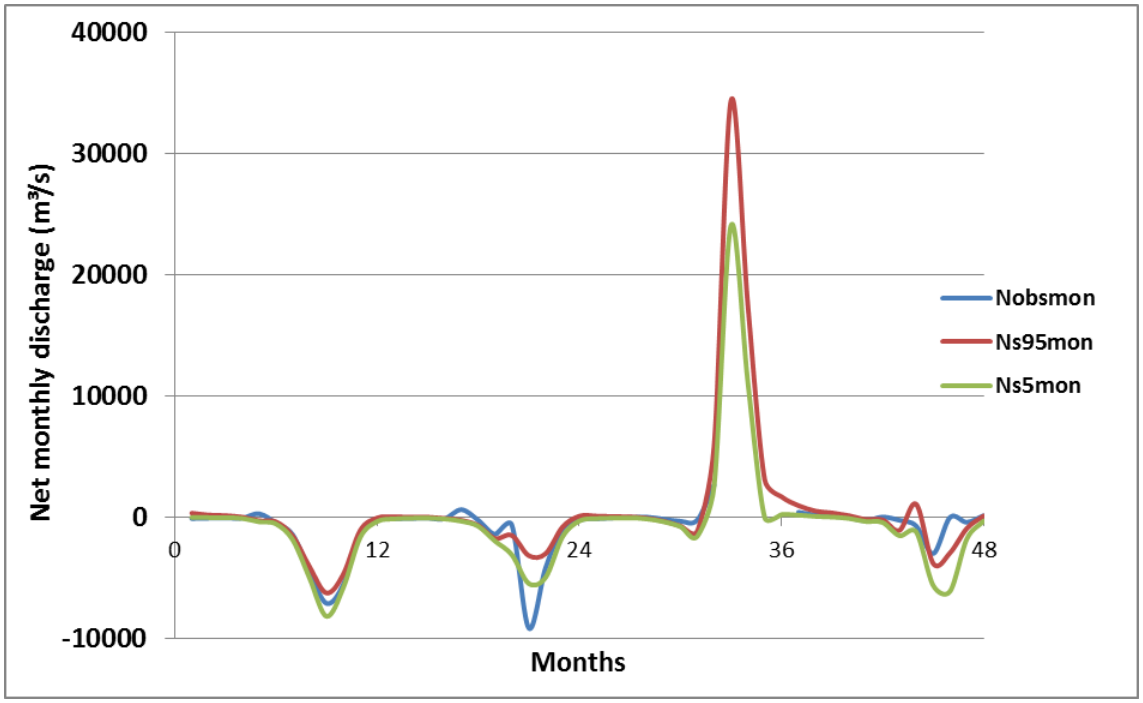

Figure 4.9: Hydrograph showing the model performance on the monthly residuals after calibration on the daily scale

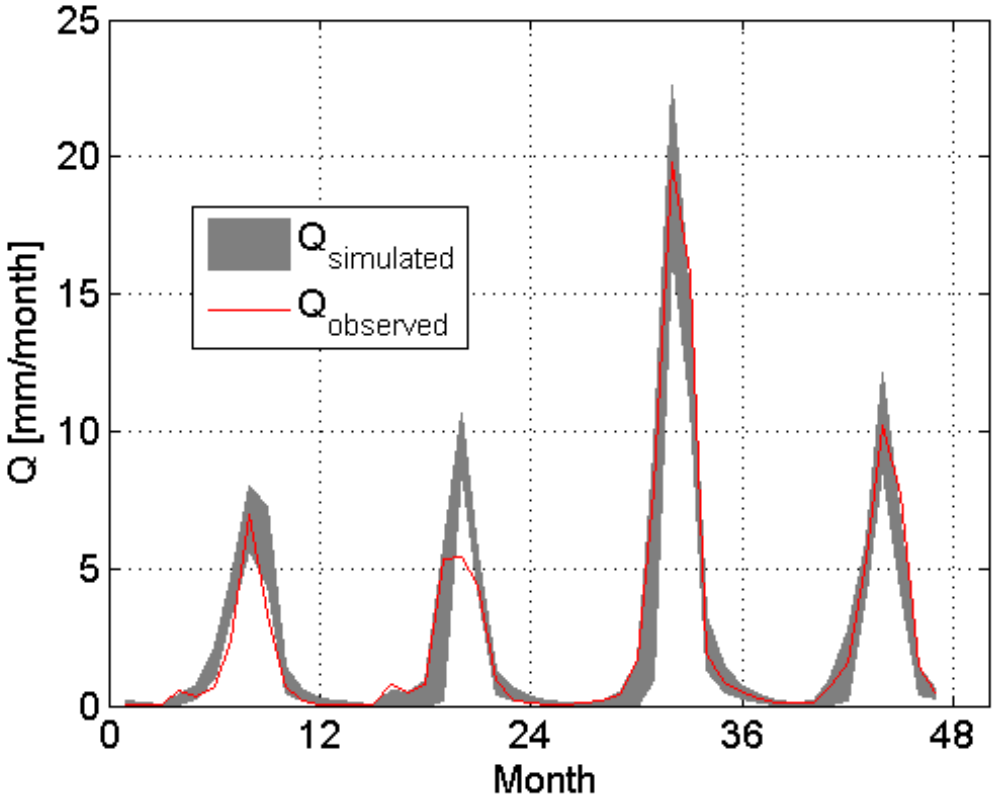

Figure 4.10: Hydrograph showing the model performance for gauge Chache when calibration was done on monthly scale

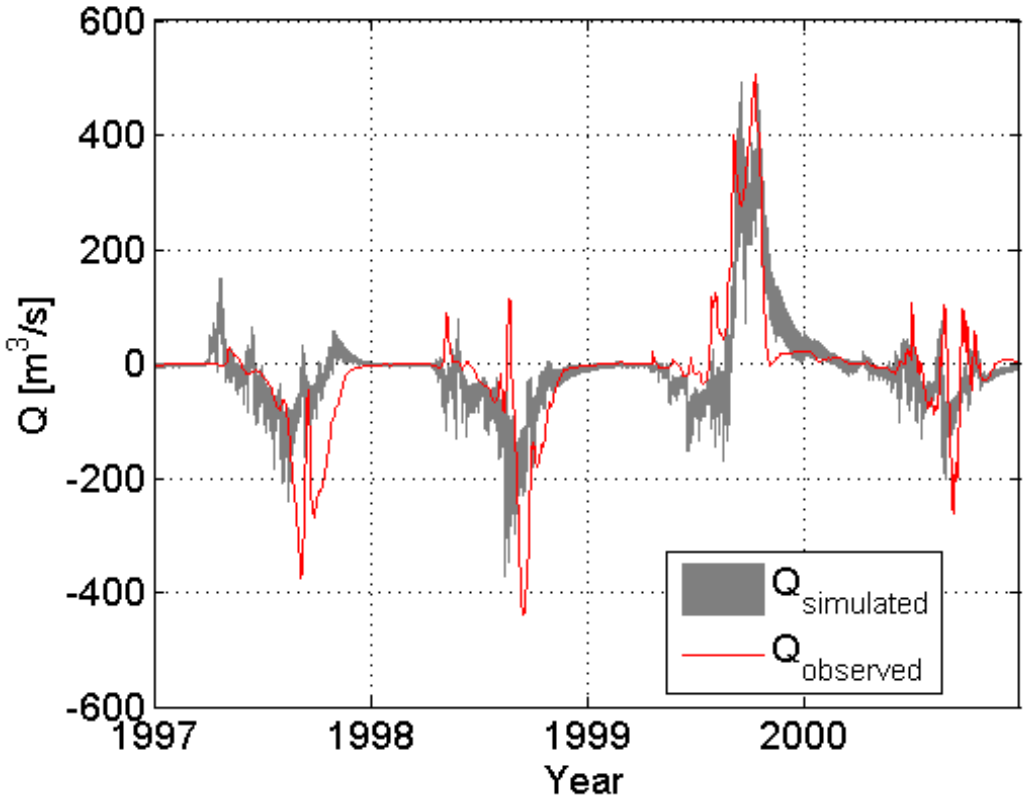

Figure 4.11: Hydrograph showing the model performance for gauge Chache when calibration was done on daily residuals.

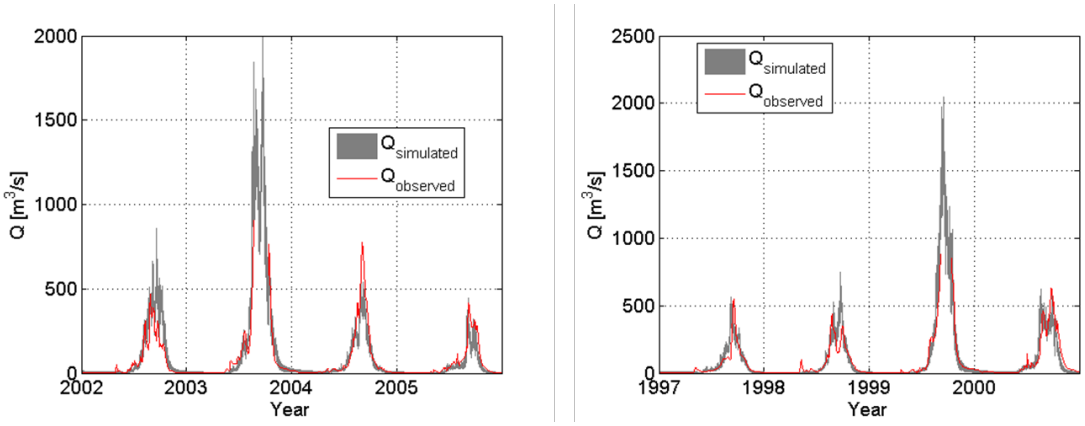

Figure 4.12: Hydrograph showing model performance for gauge Chache on daily temporal scale for swapped calibration and validation data: Left (calibration), Right (Validation)

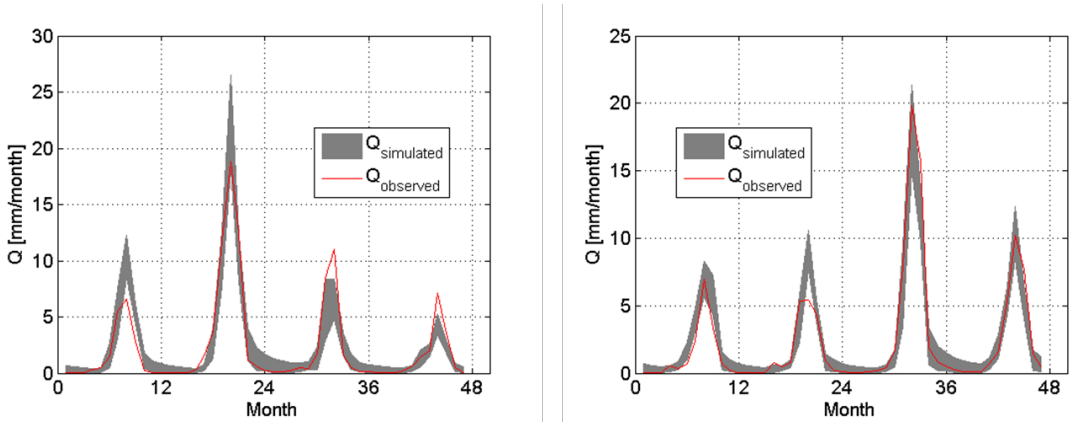

Figure 4.13: Hydrograph showing model performance for gauge Chache on monthly temporal scale for swapped calibration and validation data: Left (calibration), Right (Validation)

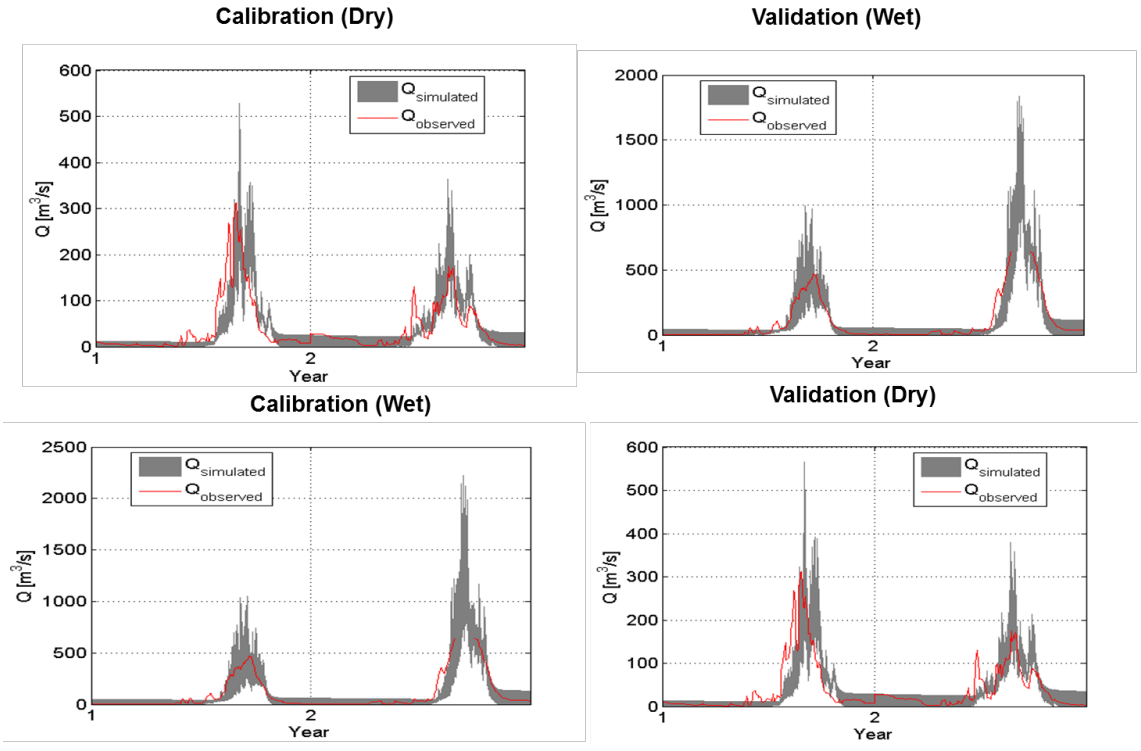

Figure 4.14: Hydrographs of split sampling for sub-catchment Lawra showing both the calibration and validation periods

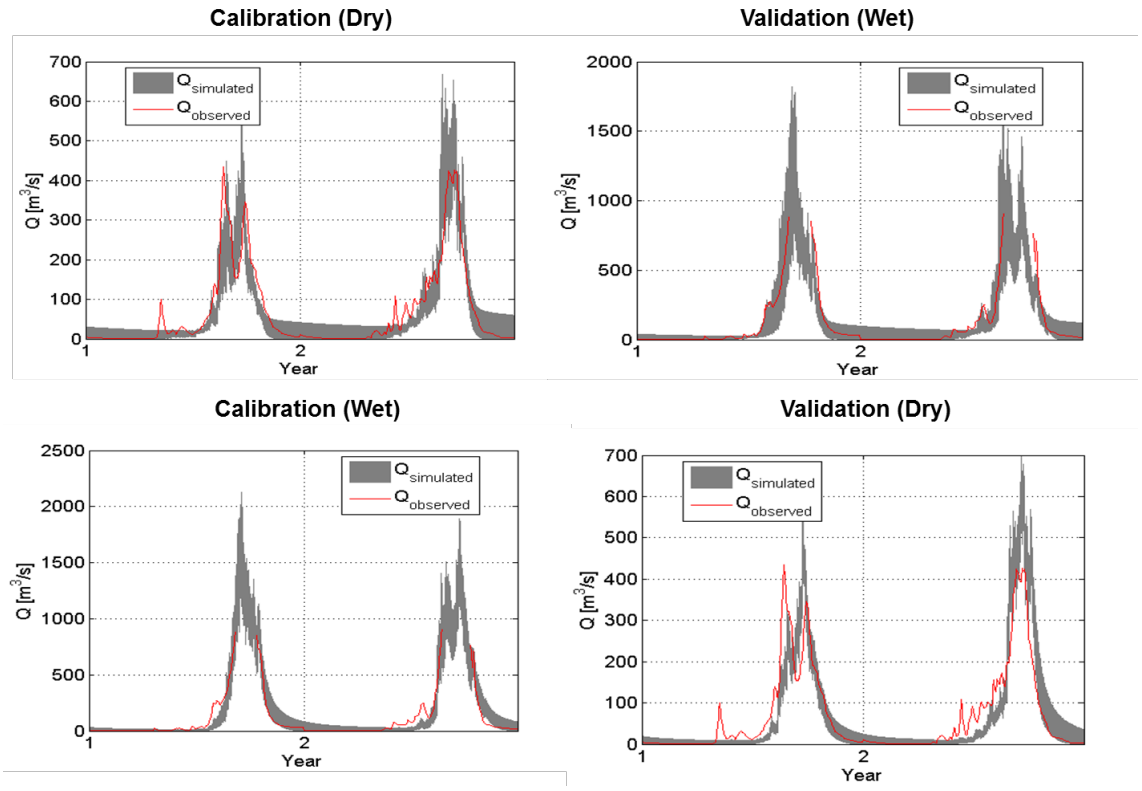

Figure 4.15: Hydrographs of split sampling for sub-catchment Chache showing both the calibration and validation periods

5 Analysis of Climate Data from Regional Climate Models (RCMs)

5.1 Introduction

The IPCC Climate Change 2013 report states that, "Warming of the climate system is unequivocal, and since the 1950s, many of the observed changes are unprecedented over decades to millennia. The atmosphere and ocean have warmed, the amounts of snow and ice have diminished, sea level has risen, and the concentrations of greenhouse gases have increased" [Stocker et al., 2013]. Various studies and reports [Bardossy and Caspary, 1990; Kunstmann and Jung, 2005; Jung and Kunstmann, 2007; Jung, 2006; Jung et al., 2012; Wagner, 2008; Bárdossy and Pegram, 2012; Giertz et al., 2010; Roudier et al., 2014; Nikulin et al., 2012; Christensen and Christensen; Stocker et al., 2013; Solomon, 2007] clearly indicate that, climate change has been happening and will continue to happen in the future.

Climate change drivers are the natural and anthropogenic substances and processes that alter the Earth's energy budget. Radiative forcing (RF) is used to quantify the change in energy fluxes. The largest contribution to total radiative forcing is caused by the increase in the atmospheric concentration of CO2 [Stocker et al., 2013]. Climate models have improved since the IPCC Assessment Report (AR)4 and that models can now reproduce observed continental scale surface temperature patterns and trends over many decades [Stocker et al., 2013]. Also, human influence on the climate system is evident.

According to Stocker et al. [2013], the global surface temperature change for the end of the 21st century is likely to exceed 1.5°C relative to 1850 to 1900 for all Representative Concentration Pathways (RCP) scenarios except RCP2.6.

5.2 Definition of some Terminologies

The following terms are frequently used in climate change studies.
Anthropogenic: Pollution or pollutants that come as a result of human activities.
Climate change: The Framework Convention on Climate Change (UNFCCC), in its Article 1, defines climate change as: "a change of climate which is attributed directly or indirectly to human activity that alters the composition of the global atmosphere and which is in addition to natural climate variability observed over comparable time periods".
Climate model: According to the IPCC Climate Change 2013 report, climate model is: "a numerical representation of the climate system based on the physical, chemical and biological

properties of its components, their interactions and feedback processes, and accounting for some of its known properties". The report further states that the current and most comprehensive model at the moment are Coupled Atmosphere−Ocean General Circulation Models (AOGCMs).
Climate projection: A climate projection is defined in the IPCC Climate Change 2013 report as: "the simulated response of the climate system to a scenario of future emission or concentration of greenhouse gases and aerosols, generally derived using climate models".
Downscaling: A method that obtains local− to regional scale (10 to 100 km) information from larger-scale models or data analyses is called downscaling [Stocker et al., 2013] . There exists dynamical and empirical/statistical downscaling. According to the IPCC Climate Change 2013 report, "the dynamical method uses the output of regional climate models, global models with variable spatial resolution or high-resolution global models and the empirical/statistical methods develop statistical relationships that link the large-scale atmospheric variables with local/ regional climate variables".
Regional Climate Model (RCM): The IPCC Climate Change 2013 report defines RCM as a climate model at higher resolution over a limited area and that such models are used in downscaling global climate results over specific regional domains.
Representative Concentration Pathways (RCPs): According to Moss et al. [2010], RCPs are "scenarios that include time series of emissions and concentrations of the full suite of greenhouse gases and aerosols and chemically active gases, as well as land use/land cover" [Moss et al., 2010].

At the moment, the IPCC 2013 report indicates the existence of four RCPs which were produced from the Integrated Assessment Models and are used for the climate predictions and projections [Stocker et al., 2013] and they are shown in figure 5.1. *RCP2.6* is a pathway where radiative forcing peaks at approximately 3 W m−2 before 2100 and then declines. *RCP4.5* and *RCP6.0* are two intermediate stabilization pathways in which radiative forcing is stabilized at approximately 4.5 W m−2 and 6.0 W m−2 after 2100. *RCP8.5* is one high pathway for which radiative forcing reaches greater than 8.5 W m−2 by 2100 and continues to rise for some amount of time (the corresponding ECP assuming constant emissions after 2100 and constant concentrations after 2250).
Figure 5.1 explains the relationship between the new RCPs and the IPCC's Special Report on Emission Scenarios (SRES)

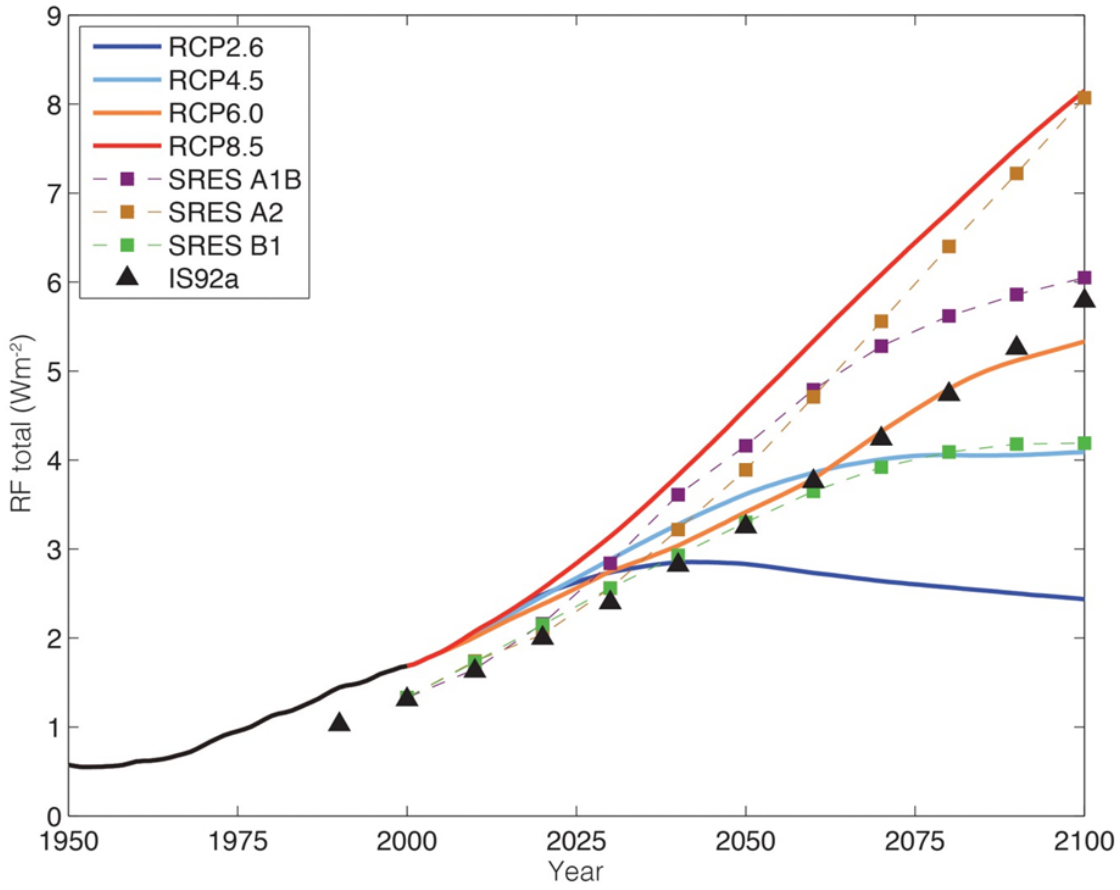

Figure 5.1: Relationship between the new RCPs and the IPCC's Special Report on Emission Scenarios (SRES) (credit: [Stocker et al., 2013]

5.3 Data

RCM data for the West Africa sub-region was obtained from CORDEX [Giorgi et al., 2009] and the Regional Climate Division of the Institute of Meteorology and Climate research at Karlsruhe Institute of Technology (IMK−IFU). Climate simulations from the RCA 4 dynamical downscaling model from Swedish Meteorological and Hydrological Institute, Rossby Centre (SMHI) using different driving models was obtained from one of the CORDEX nodes. Precipitation and temperature variables were used for this analysis with a daily temporal resolution and a 50 km spatial resolution. In the case of the RCM data from IMK−IFU, the Weather Research and Forecasting (WRF) RCM model was used to downscale the Max Planck Institute Earth System model (MPI−ESM) ECHAM6 GCM model to a spatial resolution of 12 km.

The data from IMK−IFU was pre-processed by aggregating the 3 hourly data to daily and also converting the temperatures from Kelvin to degrees Celsius. The original data is in a 12 x 12 km spatial grid resolution in a netcdf file format where a simple computer program was written in Python programming language to locate the nearest grid point to an existing

gauge station. Both data consists of historical simulations of climate variables (precipitation and temperature) from 1979−2005 and future simulations from 2019−2049 with the representative concentrations pathway (RCP 4.5).

5.3.1 Climate data from IMK-IFU

The IMK−IFU is working in collaboration with the West African Science Service Center on Climate Change and Adapted Land Use (WASCAL) which is funded by the German Federal Ministry of Education and Research (BMBF). WASCAL is a large scale research-focused Climate Service Center. It is designed to help solve the challenge of developing effective adaptation and mitigation measures against a threatening climate change which is happening in the West Africa sub-region. This is done by pooling scientific excellence of West African researchers and linking in the expertise and the financial and computational capabilities of Germany (www.wascal.org).

The simulations from WASCAL/IMK-IFU are based on the RCP4.5 emission scenario with a grid spacing of 12 km and 3-hourly data for a large number of climate variables. The first results from the WASCAL team show an increase in temperature of 2 to 2.5°C in continental West Africa [Heinzeller et al., 2014]. Precipitation simulations from the team shows an increase in annual rainfall for the Coast of Guinea and the Soudan-Sahel until the end of the 21st century as compared with the 1980 - 2010 mean [Heinzeller et al., 2014].

5.3.2 Climate data from CORDEX

According to Giorgi et al. [2009], CORDEX is an initiative of the World Climate Research Programme (WRCP) of the World Meteorological Organization (WMO). It was set up among other mandates to develop a framework to evaluate and improve regional climate downscaling (RCD) techniques for use in downscaling global climate projections. It's other mandate is to foster an international coordinated effort to produce improved multi-model RCD-based high resolution climate-change information over regions worldwide for input to impact work and to the IPCC Fifth Assessment Report (AR5) [Giorgi et al., 2009]. According to Giorgi et al. [2009], CORDEX was set up to bridge the spatial gap that exists between the climate information provided by AOGCMs and the input needed for impact assessment work. It has five domains covering the entire African, Australian, South American, North American and European continents. Figure 5.2 shows a schematic representation of the first phase CORDEX experiment set-up. CORDEX climate projection framework is based on the set of new global model simulations of the IPCC Fifth Assessment Report (referred to as CMIP5) [Taylor et al., 2009]. Africa was selected as the first target region in the CORDEX experiment because of various reasons. And key among the reasons is that, Africa is very vulnerable to climate change because of the dependence of vital sectors like (agriculture, water management, health) on climate variability and because of the relatively low adaptive capacity of its economies [Giorgi et al., 2009]. Additional information on CORDEX could be seen in [Giorgi et al., 2009].

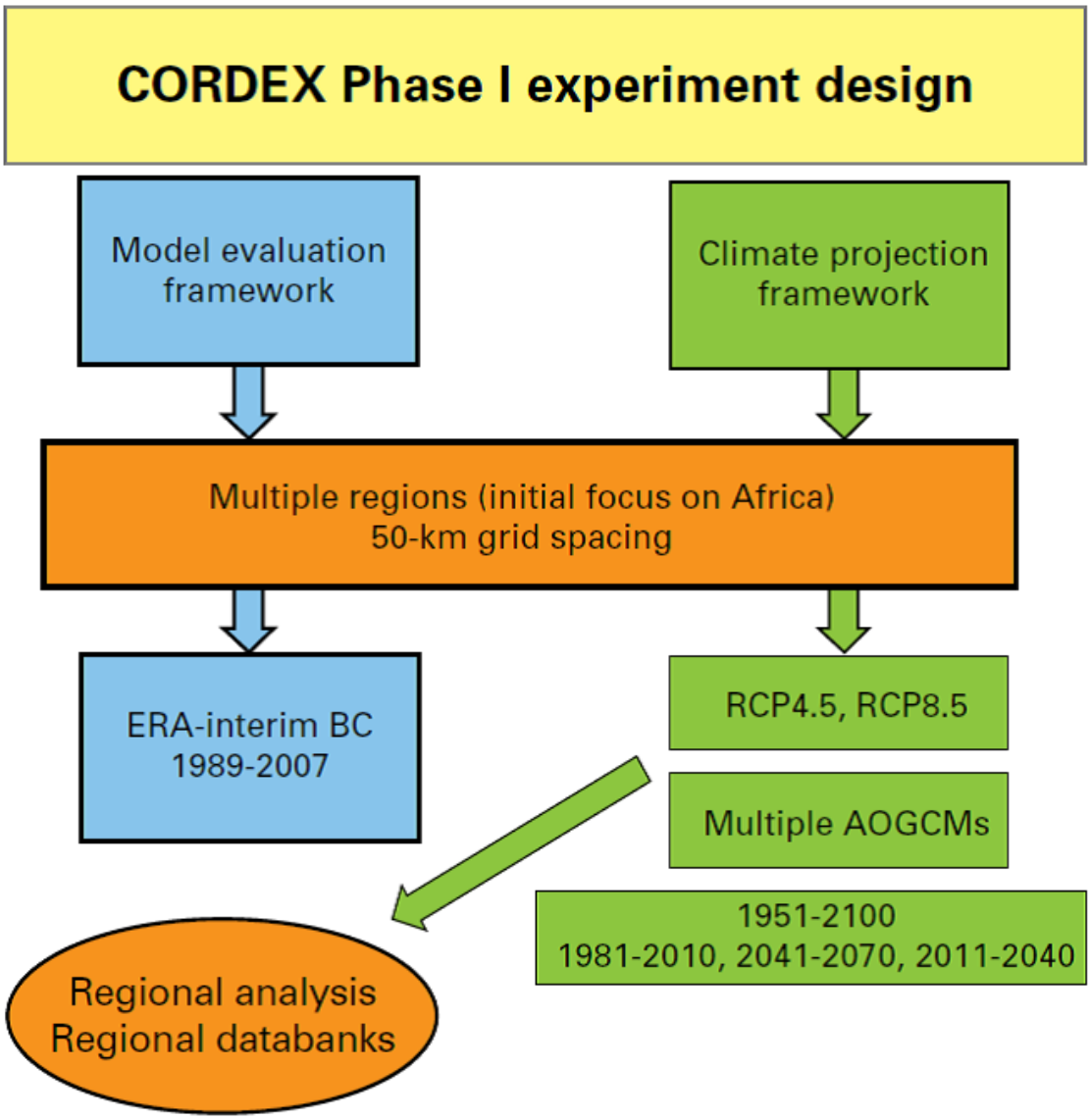

Figure 5.2: Schematic depiction of the first phase CORDEX experiment set-up (credit: [Giorgi et al., 2009])

5.4 Results from the analysis of simulated climate data from IMK-IFU/WASCAL for the West Africa Sub-region

It can clearly be seen from the cdf plots of the precipitation that there will be a decrease of about 10% in the amount of rainfall in the future and also the number of dry-days in the future will increase to about 7%. Therefore, a drier future is predicted. The results confirm current rainfall trend which shows a decrease in the rainfall amounts and drier climate [Neumann et al., 2007; Opoku-Ankomah and Amisigo, 1998; Oguntunde et al., 2006; Kunstmann and Jung, 2005]. The duration of the rainy season shortens as one move towards

the northern part of the catchment. All the stations in the catchment show a slight decrease in rainfall for the future and can therefore be concluded that, there would be drier climate in the future. There is a mean daily rainfall of 4.85 mm for historical simulations as compared with 4.31 mm mean-daily rainfall for the future simulation for station Kintampo in the southern part of the study area.

In the cdf plots for temperature, as expected there is a rise in temperature in the future with an amount of about 1.5 °C. This result is in agreement with the results by other researchers and it's in consonant with global temperature rise and some CORDEX simulations performed by other researchers. It would be warmer towards the northern part of the catchment with a mean maximum temperature of 36.8°C as compared with 32.8°C in the southern part.

The RCM data is compared with the observed gauge station data and the results are as followed.

Temperature

The temperature simulations of the RCM data from IMK-IFU show that the historical run is very close to the observed temperature measurements for most of the stations. For station Bole (as seen in figure 5.3), daily temperatures less than 27° C were well simulated as the two cdf curves coincide. The daily mean of the observed temperature for this station is 26.9° C whiles that of the simulated historical period is 26.8° C. However, some stations (e.g. Babile and Bechem) have a large bias in the historical simulations as compared with the observed temperature (figure 5.4).

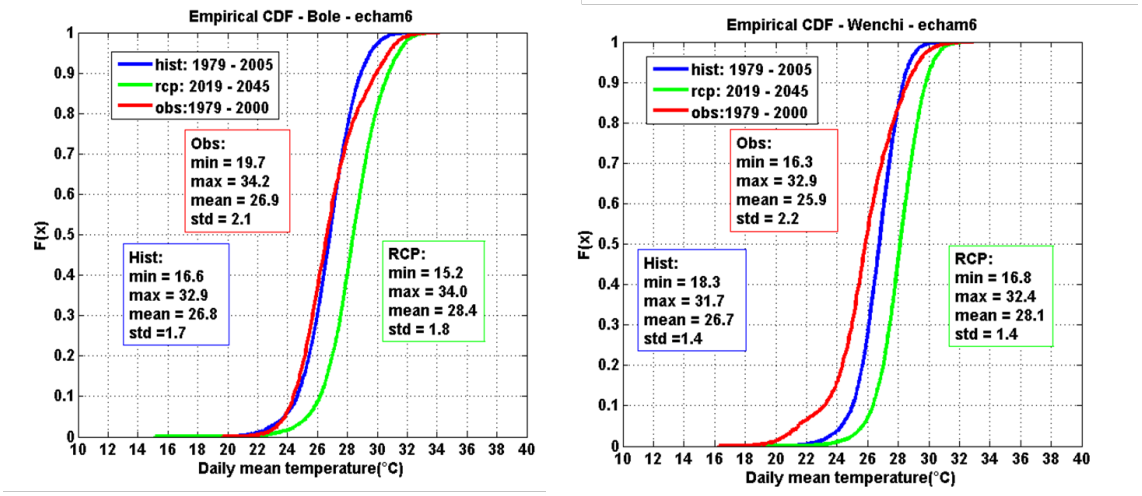

Figure 5.3: Empirical cdf plots of observed and RCM runs using echam6 GCM driving model for temperature for historical (hist) and future (rcp) simulations for stations Bole and Wenchi

Figures 5.5 and 5.6 show the annual cycle of the RCM data obtained from IMK-IFU/WASCAL for five (5) different stations (Kintampo, Wenchi, Bui, Babile and Dedougou

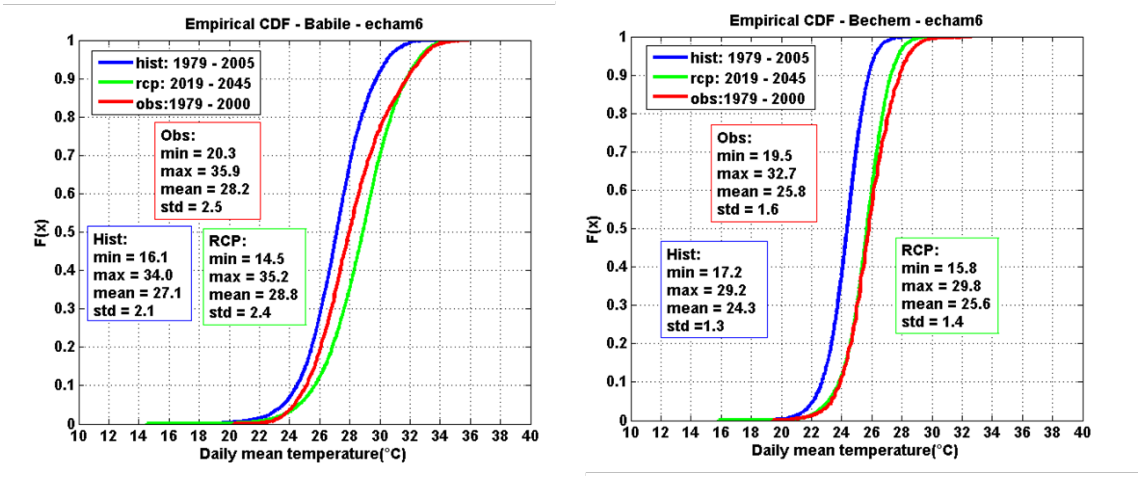

Figure 5.4: Empirical cdf plots of observed and RCM runs using echam6 GCM driving model for temperature for historical (hist) and future (rcp) simulations for stations Babile and Bechem

which are spread across the study area. The figures also depict how the simulations performed compared with the observed climate data. All the stations show an increase in the future temperature as compared with the present up to a magnitude of about 2° C. This confirms the global change of about 2° C in the future. The historical (present) simulations of temperature mimiced very well the observed time series for stations Kintampo and Bui and fairly well for station Babile. But didn't perform well for the other two stations. This results suggest the need for the application of bias correction for the climate simulations before they are used for impact studies.

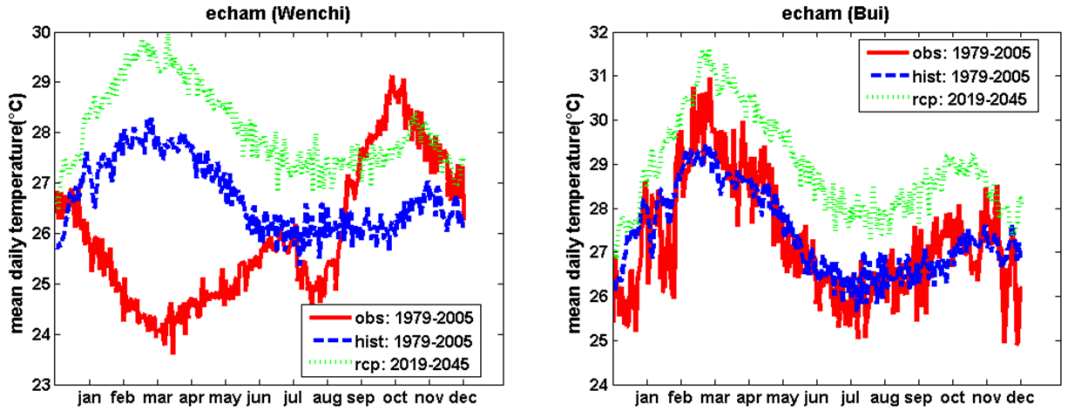

Figure 5.5: Annual cycle of observed and RCM runs using echam6 GCM driving model for temperature for historical (hist) and future (rcp) simulations for stations Wenchi and Bui

Rainfall

The cdf curves of the daily rainfall show that the observed values show more dry periods

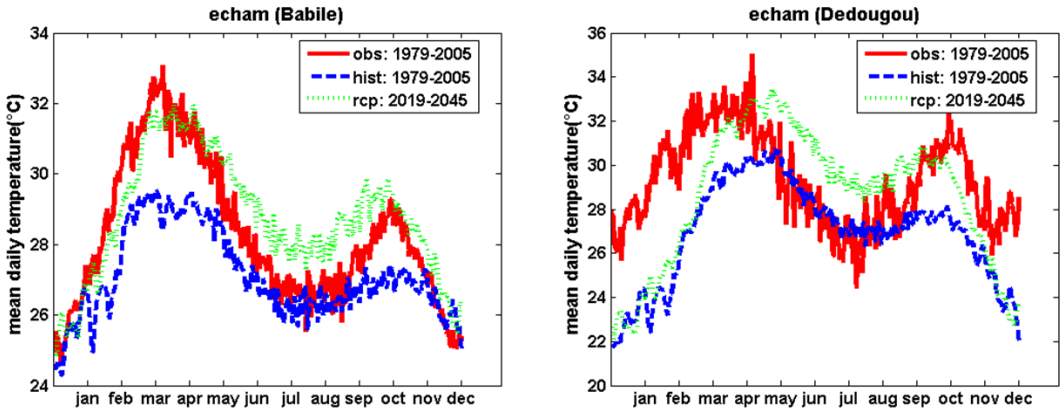

Figure 5.6: Annual cycle of observed and RCM runs using echam6 GCM driving model for temperature for historical (hist) and future (rcp) simulations for stations Babile and Dedougou

than the historical simulations of the RCM. The days of zero precipitation is about 80% and 45% for the observed and historical runs respectively (figure 5.7). And this shows the occurrence of too many wet days with low-intensity rain which is typical biases with RCM outputs [Ines and Hansen, 2006]. The observed time series seems to get closer to the historical runs only for rainfall values above 15 mm/day (as seen in figure 5.8). There is overestimation of rainfall for the historical simulation as compared with the observed rainfall.

General under- or overestimation and incorrect seasonal variations of precipitation is also synonymous with outputs of RCMs [Christensen et al., 2008; Terink et al., 2009; Teutschbein and Seibert, 2010]. Therefore, bias correction methods are needed to help correct the various problems with biased RCM output. Overall, the results shows that only about 45 % of the observed and RCM simulations data has daily rainfall values exceeding 20 mm per day. One could then use the so called "quantile− quantile mapping" [Bárdossy and Pegram, 2011; Boé et al., 2007; Déqué et al., 2007; Johnson and Sharma, 2011] as the method to bias correct the RCM simulations since this method truncates the extreme values. For station Babile, the mean daily rainfalls for the observed, RCM-historical and RCM-future are 2.8, 4.9, and 4.1 mm respectively (figure 5.9). Implying that the observed rainfall amount are less than the RCM-historical runs. With their corresponding maximum amounts been 119.6 (observed), 219.5 (RCM-historical) and 209.7 mm (RCM-historical) respectively. Similar results could be seen for the rest of the stations as observed in figure 5.10.

The annual cycles of the rainfall time series are shown in figures 5.12, 5.13 and 5.14. The mean daily values were smoothen (i.e. to remove the noise) by applying a weighting function on a 10 day moving window with the day in particular having a weight of 1.0 and decreasing to 0.1 for the last 10 day in both directions. A typical example of a graph before and after applying the smoothening function could be seen in figure 5.11.

The annual cycle figures show a slight decrease in the future rainfall as compared with the present (figures 5.12, 5.13 and 5.14). The simulations were able to model the uni-modal cycle of rainfall in station Bomborokuy, Bagassi and Babile. But unfortunately, not able to show

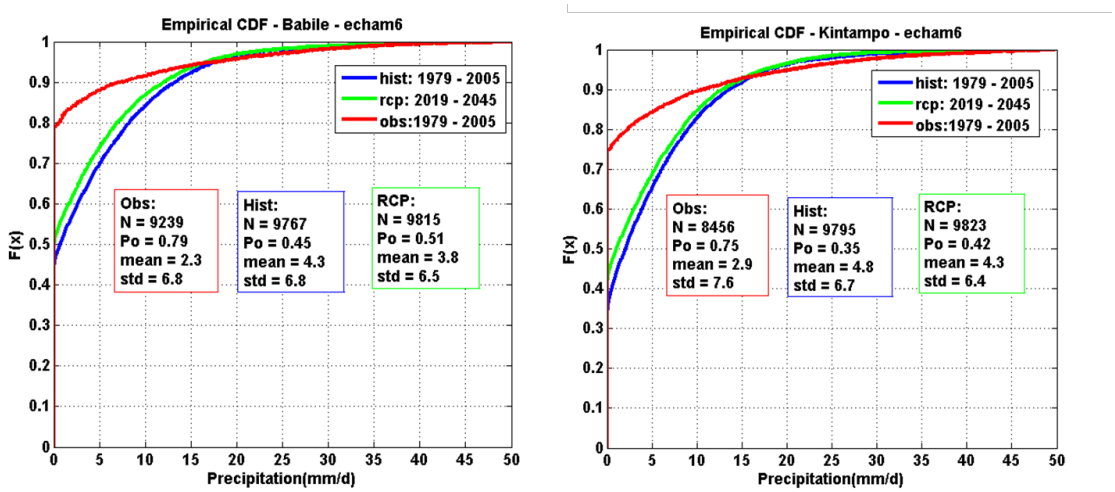

Figure 5.7: Empirical cdf plots for observed and RCM (echam6-GCM driving model) runs of daily rainfall less than 50mm for historical (hist) and future (rcp) simulations for stations Babile and Kintampo

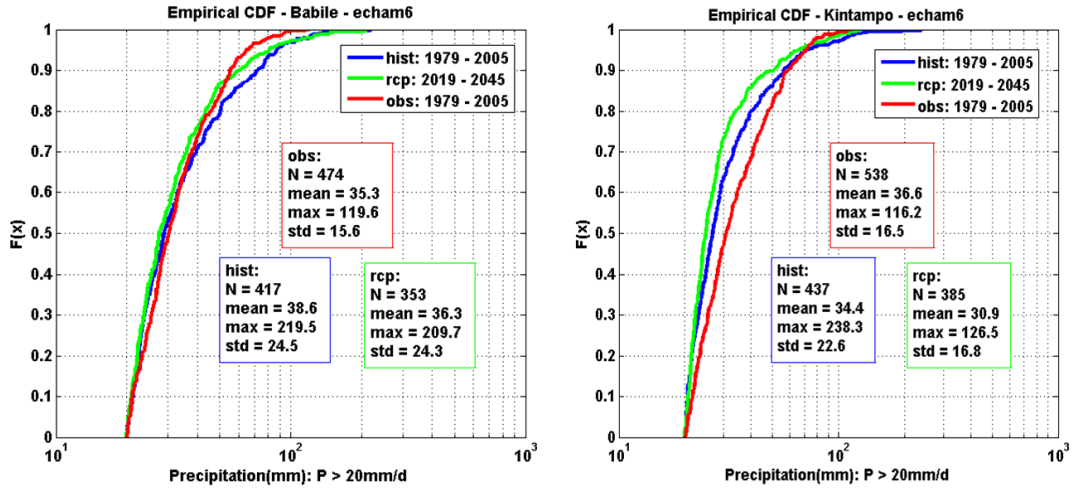

Figure 5.8: Empirical cdf plots for observed and RCM runs using Echam6 GCM driving model for daily rainfall greater than 20mm for historical and future simulations for stations Babile and Kintampo

the bi-modal rainfall cycle in the southern part of the catchment, as shown in stations Bui and Kintampo. It tried to reproduce the annual cycle but failed in both the timing and the magnitudes of the rain (figure 5.12).

The simulations show a late start in the rainfall season (the months of April and May) in the future for all the stations.

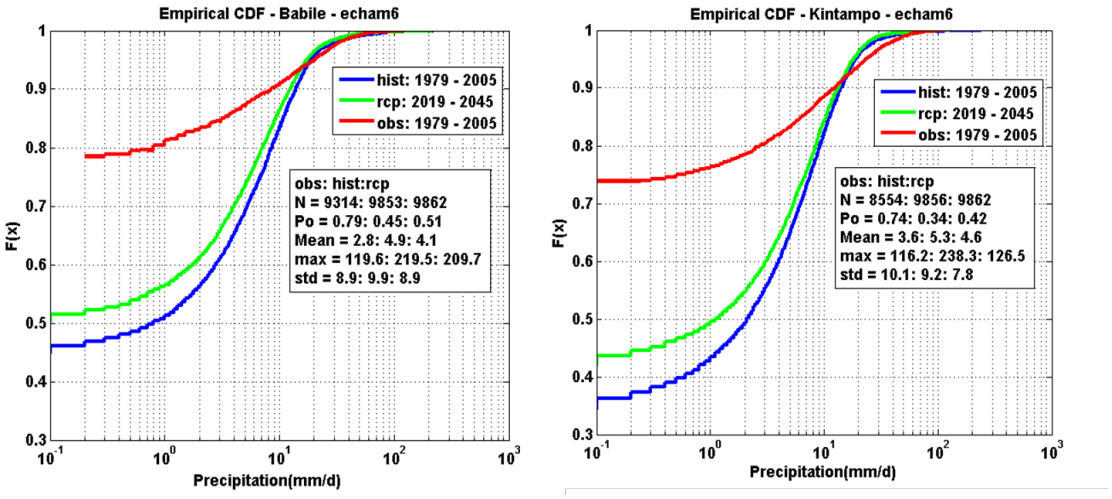

Figure 5.9: Empirical cdf plots for observed and Echam6 GCM driving model RCM runs of daily rainfall for historical and future simulations for stations Babile and Kintampo (N: number of events used, hist: historical simulations, rcp: future simulations, obs: observed measurements, Po: percentage of zero rainfall)

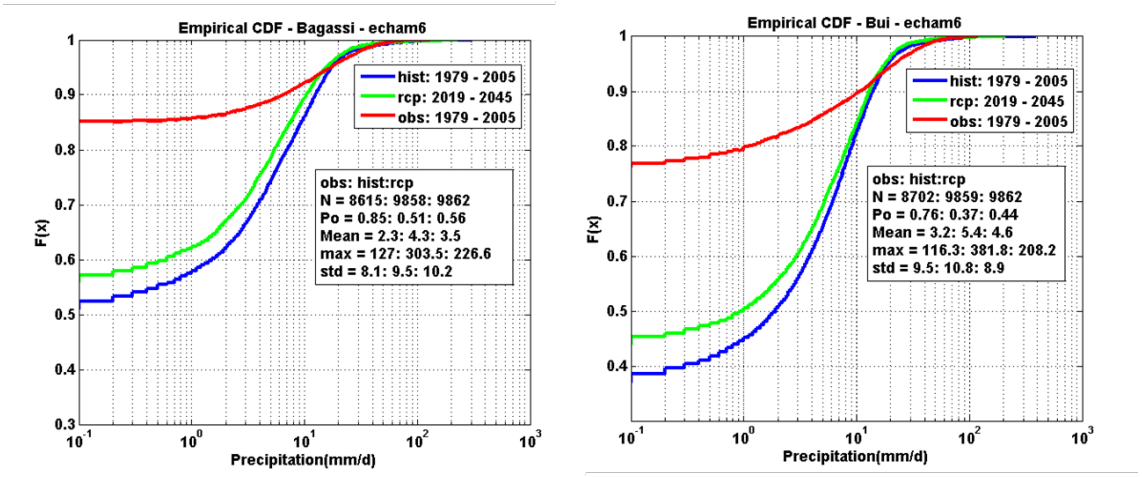

Figure 5.10: Empirical cdf plots for observed and Echam6-GCM driving model RCM runs of daily rainfall for historical and future simulations for stations Bagassi and Bui (N: number of events used, hist: historical simulations, rcp: future simulations, obs: observed measurements, Po: percentage of zero rainfall)

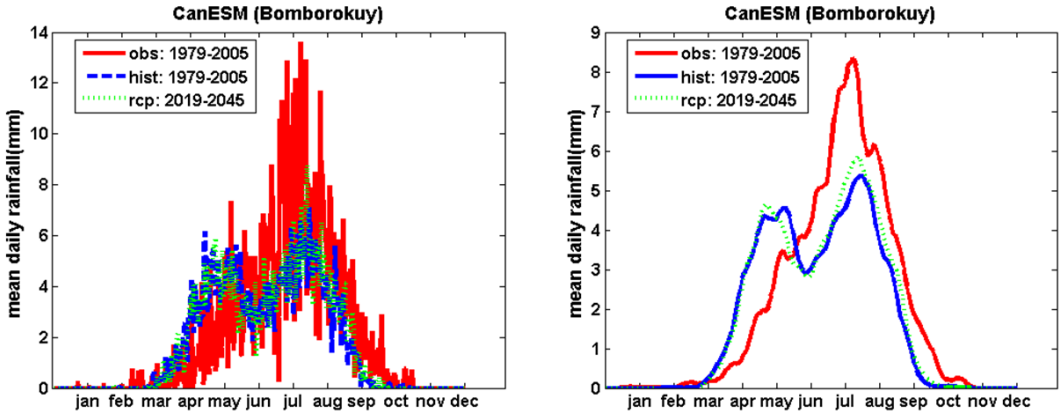

Figure 5.11: Annual cycle before (left) and after smoothening (right) (i.e. noise removal)

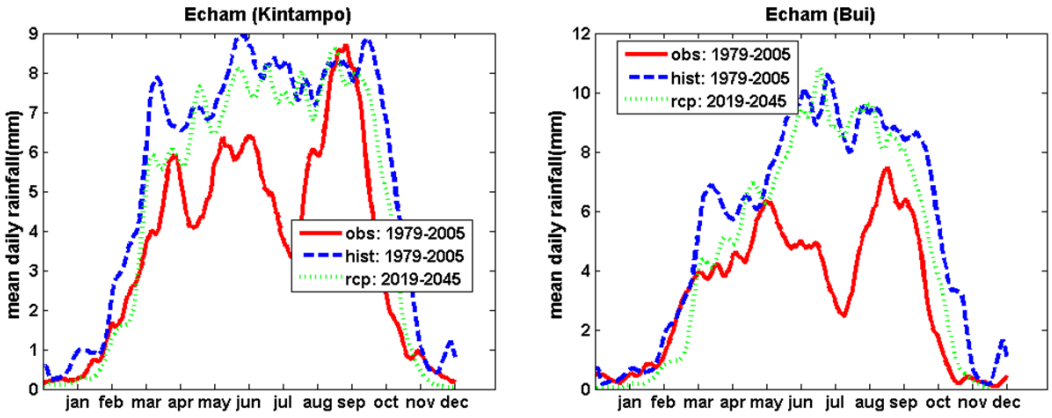

Figure 5.12: Annual cycle of observed and RCM runs using echam6 GCM driving model for rainfall for historical (hist) and future (rcp) simulations for station Kintampo and Bui

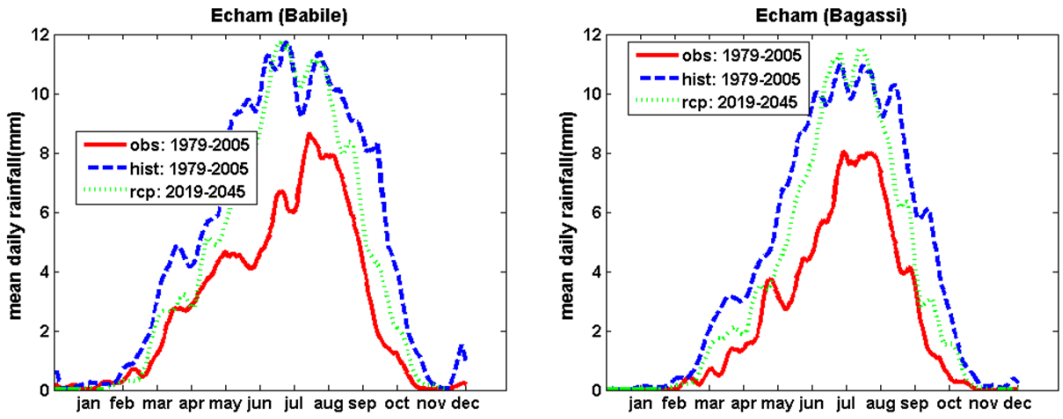

Figure 5.13: Annual cycle of observed and RCM runs using echam6 GCM driving model for rainfall for historical (hist) and future (rcp) simulations for station Babile and Bagassi

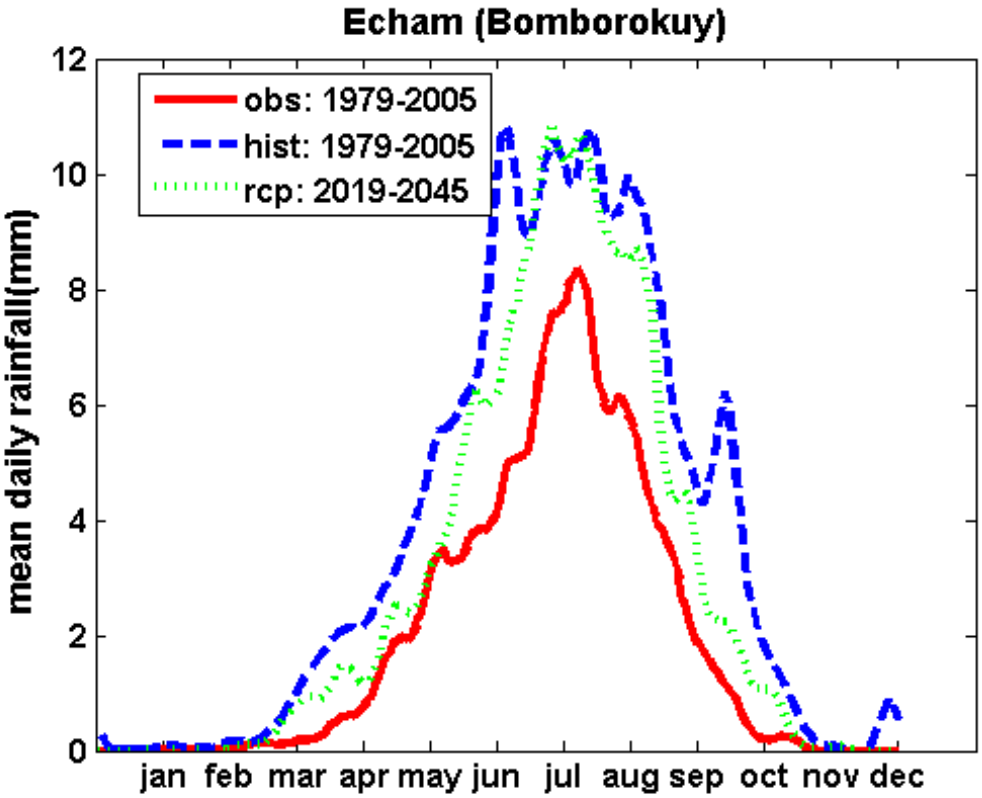

Figure 5.14: Annual cycle of observed and RCM runs using echam6 GCM driving model for rainfall for historical (hist) and future (rcp) simulations for station Bomborokuy

5.5 Results from the analysis of simulated climate data from CORDEX

RCM data from various driving GCMs on Africa was downloaded from CORDEX for this analysis. Daily rainfall and temperature simulations at a spatial resolution of approximately 50 km were used with the same year span as with the RCM data from IMK-IFU and the observed data. In exploring how the rainfall variable is distributed in the study area, Lorenz curves (figures 5.15 and 5.16) were plotted for the RCMs with the following GCM driving models:

- Hadly Centre Global Environmental Model (HadGEM2) by the Meteorological office Hadley Centre (MOHC)
- Canadian Earth System model (CanESM2) by the Canadian center for climate modelling and analysis (CCCma)
- Geophysical Fluid Dynamics Laboratory Earth system model (GFDL−ESM2M)
- the Model for Interdisciplinary Research on Climate (MIROC5)
- the European Earth System Model (EC−EARTH)
- the the ERA-Interim reanalysis data (ERAINT)
- the RCM data from IMK−IFU

With the exception of the data from IMK−IFU which used WRF-RCM model, the rest of the data were downscaled by SMHI using the Rossby Centre Regional Climate model (RCA4). The data were downloaded from one of the nodes of CORDEX.

Lorenz Curves
Lorenz curves are graphical representation of the distribution of some variables like income, wealth or rainfall (as in this case). They are commonly used in Economics and it was developed by Max O. Lorenz in 1905 for representing inequality of the wealth distribution ($https://en.wikipedia.org/wiki/Lorenzcurve$). The concept describes the inequality among the population of some variables, where the cumulative proportion of the variable population is plotted against the cumulative proportion of the amount or magnitude of the variable.

The curve shows on its horizontal axis a defined population (e.g., rainfall), which are broken down into percentiles and ordered from left to right on the horizontal axis, from the minimum to the maximum percentile. The vertical axis of the Lorenz curve shows the cumulative percentage of the variable (e.g. rainfall) amount. It should be noted that the Lorenz curve can be used for many other distributions.

Points on the Lorenz curve represent statements like the bottom 25% of the entire population has 10% of the total rainfall amount. Both the horizontal and the vertical axis of the Lorenz curve go from 0% to 100%. There is a perfectly equal distribution of the variable if every population has the same variable amount. In this case, the bottom K% of the variable population would always have K% of the variable amount or magnitude. This can be depicted

by the straight line y=x (i.e. the line of perfect equality). Deviations of the actual cumulative distribution (i.e. the Lorenz curve), from the line of perfect equality then depicts the degree of inequality of the variable being explored. If the line of the Lorenz curve is more bent, it means the distribution of the variable across the population is more unequal.

Rainfall

Figures 5.15 and 5.16 show a plot of the Lorenz curves for the same RCM simulations (RCA4) with different driving models for some of the stations in the catchment. The Lorenz curve of

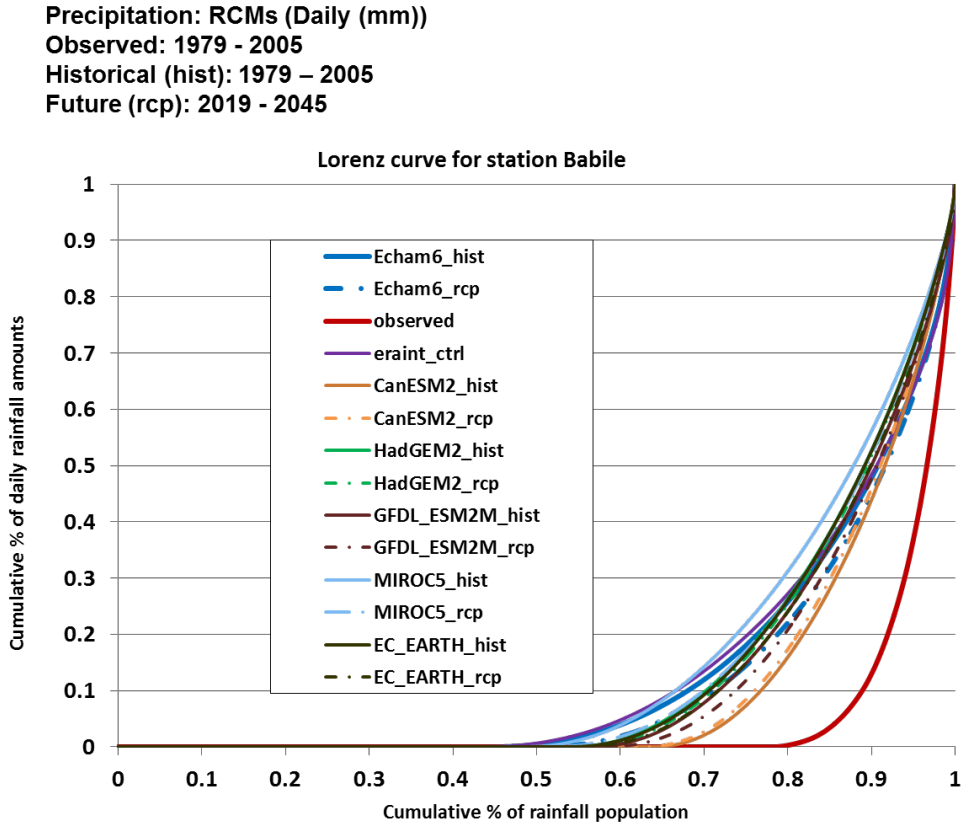

Figure 5.15: Lorenz curve of RCM simulations of precipitation for different driving models as compared with the observed

station Babile shows that between $40 - 50\%$ of the daily data has zero precipitation (i.e. dry days) for the various driving models with CanESM2 having about 65% zero precipitation. It can also be observed that about 75% of the data have their daily rainfall values in the lower 25%. And in all, there wasn't a big difference in the historical and future simulations of the rainfall for most of the driving models.

In assessing how these other five (5) driving models predict the future climate in this area, annual cycles of rainfall for different stations were constructed. They are shown in figures 5.17 to 5.20. CanESM driving model was able to simulate the bi-modal rainfall annual cycle in the southern part (figure 5.17) but was unable to time it rightly. It showed the rain peaks in the months of April and July instead of June and August as seen in the observed data.

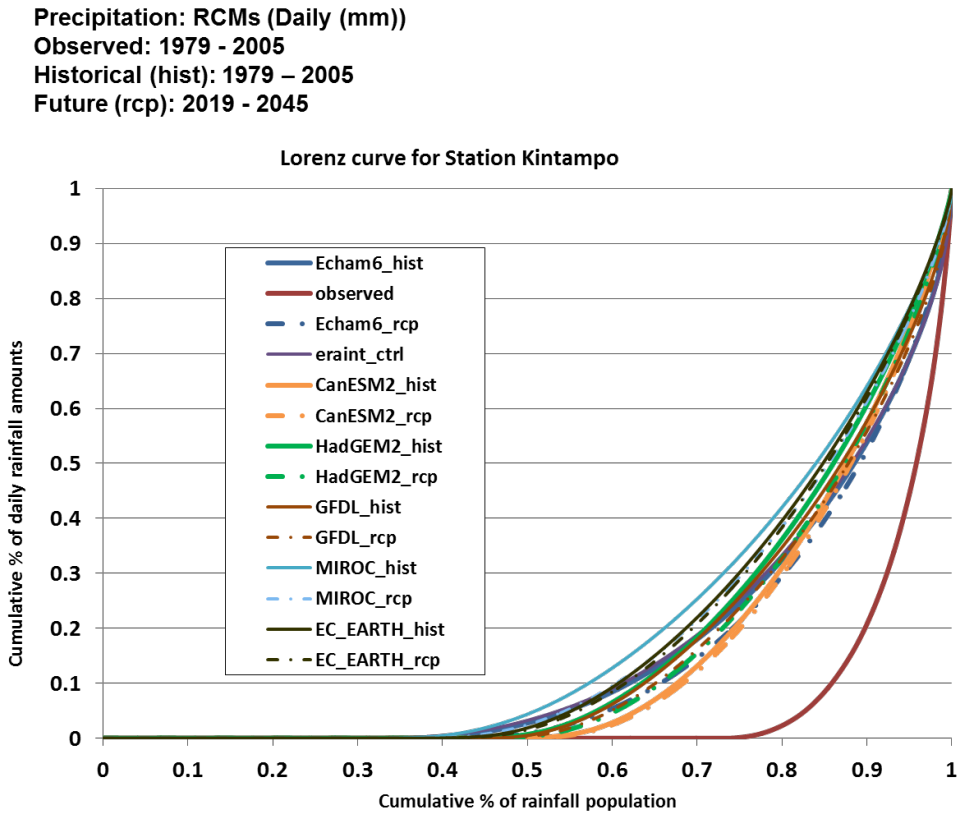

Figure 5.16: Lorenz curve for the RCM simulations of precipitation with different driving models as compared with the observed for station Kintampo

It also showed a bi-modal cycle instead of a uni-modal for the station in the northern part (Bomborokuy) of the catchment (figure 5.17). The EC-EARTH model also shows a bimodal annual cycle in the south (station Bole) and in the north (station Bomborokuy) as seen in figure 5.18. The results from GFDL and MIROC models (figures 5.19 and 5.20) tried to reproduce the two peak cycles in the southern part and the uni-modal in the northern part (figures 5.19 and 5.20).

For climate change signals, CanESM shows a slight decrease of rainfall in the south and the northern part of the catchment. EC-EARTH did not show a significant difference between the present and the future in terms of rainfall. And, GFDL shows a slight increase in rain in the future in the southern part and a decrease in the northern part. MIROC driving model predicts a slight decrease in the first rainfall season and an increase in the second season. All the driving models shows a deviation of the historical runs from the observed data which necessitates the application of bias corrections.

Temperature

From figures 5.21, 5.22 and 5.23 of temperature simulations for the various GCM driving models, the following deductions could be made:

- CanESM depicts a daily mean temperature increase of about 2.5°C in the future.

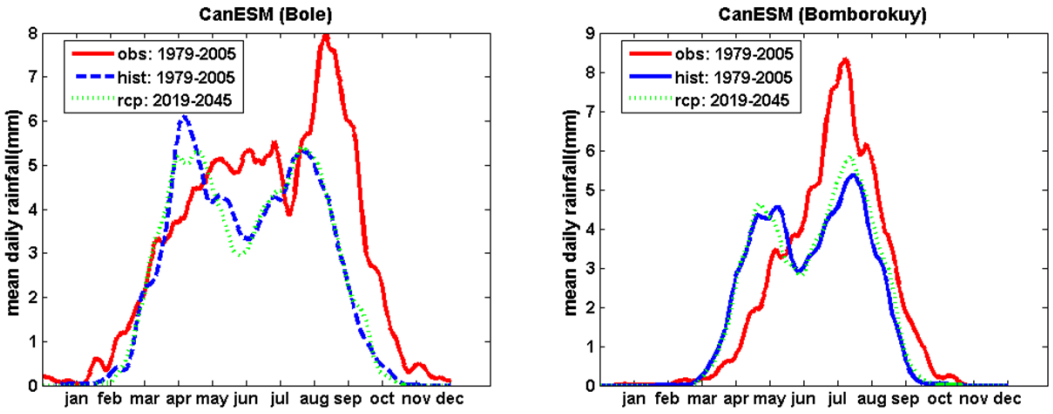

Figure 5.17: Annual cycle of observed and RCM runs using CanESM GCM driving model for rainfall for historical (hist) and future (rcp) simulations for stations Bole and Bomborokuy

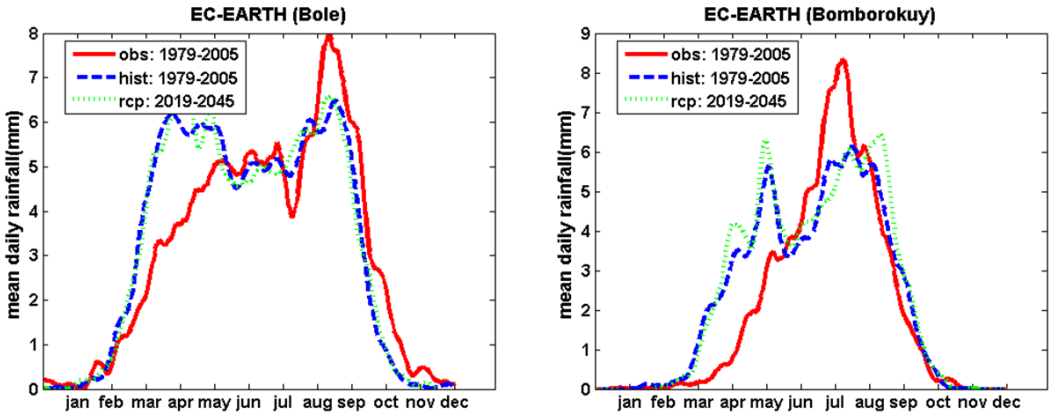

Figure 5.18: Annual cycle of observed and RCM runs using EC-EARTH GCM driving model for rainfall for historical (hist) and future (rcp) simulations for stations Bole and Bomborokuy

- A temperature increase of 1.2°C is suggested by EC-EARTH.
- ECHAM shows an increase of about 1.7°C in the future.
- GFDL rather predicts an increase of about 1.2°C in the future.
- Both HadGEM and MIROC predict an increase of about 1.5°C.

For extreme cases, the CanESM model predicts the highest temperature of about 37.5°C in the future whiles EC-EARTH shows the least maximum temperature of about 33.5°C. Overall, the CanESM and ECHAM models are better simulators of the observed temperature than the rest of the models. Very similar results were also realized in the other stations (as seen in figures 5.22 and 5.23).

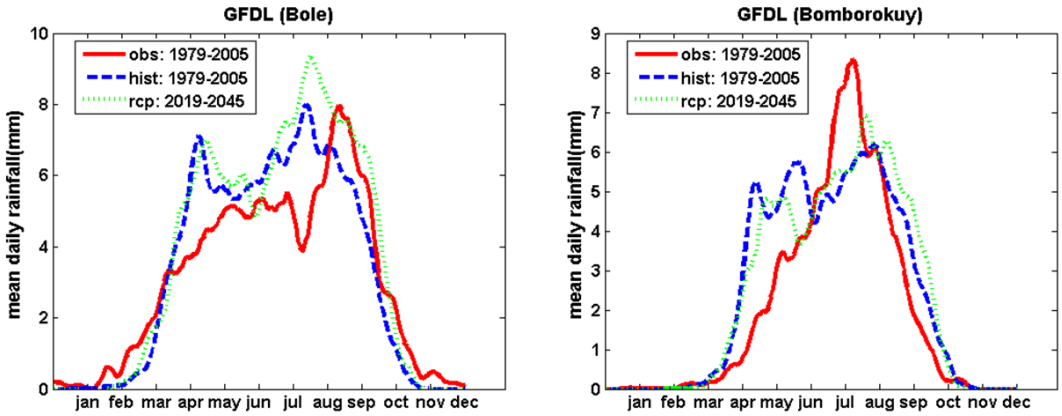

Figure 5.19: Annual cycle of observed and RCM runs using GFDL GCM driving model for rainfall for historical (hist) and future (rcp) simulations for stations Bole and Bomborokuy

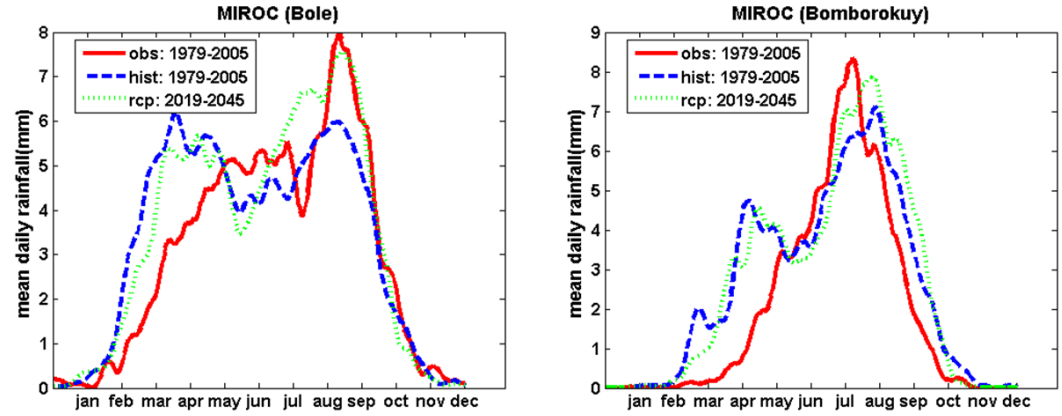

Figure 5.20: Annual cycle of observed and RCM runs using MIROC GCM driving model for rainfall for historical (hist) and future (rcp) simulations for stations Bole and Bomborokuy

Potential Evapotranspiration (PET)

Daily potential evapotranspiration was calculated based on daily temperature, long-term averages of temperature and the PET calculated using the data from Global – PET.

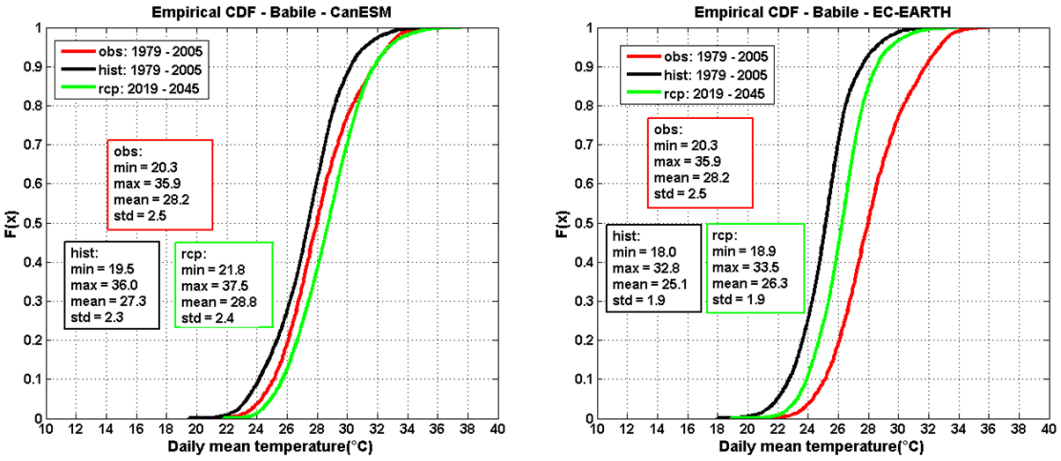

Figure 5.21: Empirical cdf plots of observed and RCM runs using CanESM and EC-EARTH driving models for temperature of historical (hist) and future (rcp) simulations for station Babile

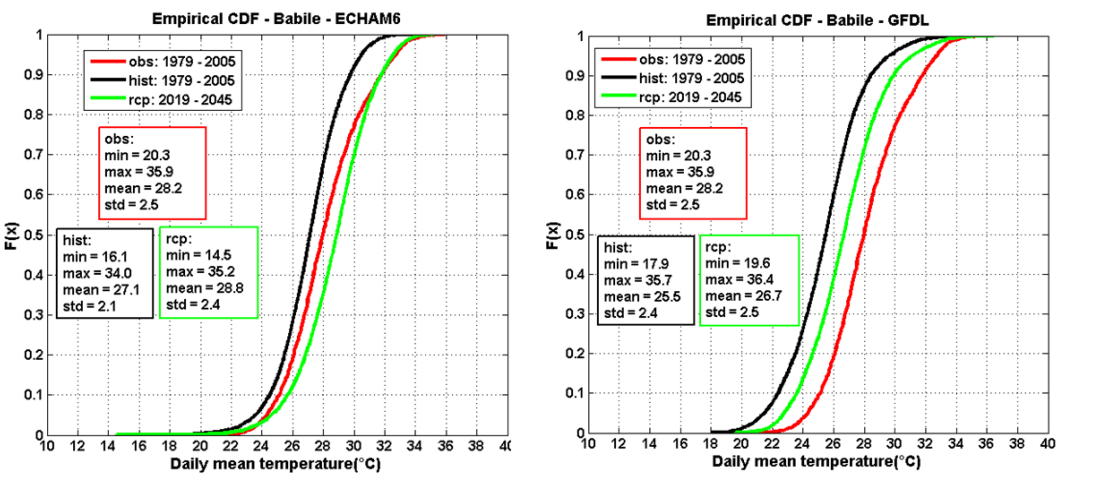

Figure 5.22: Empirical cdf plots of observed and RCM runs using ECHAM6 and GFDL driving models for temperature of historical (hist) and future (rcp) simulations for station Babile

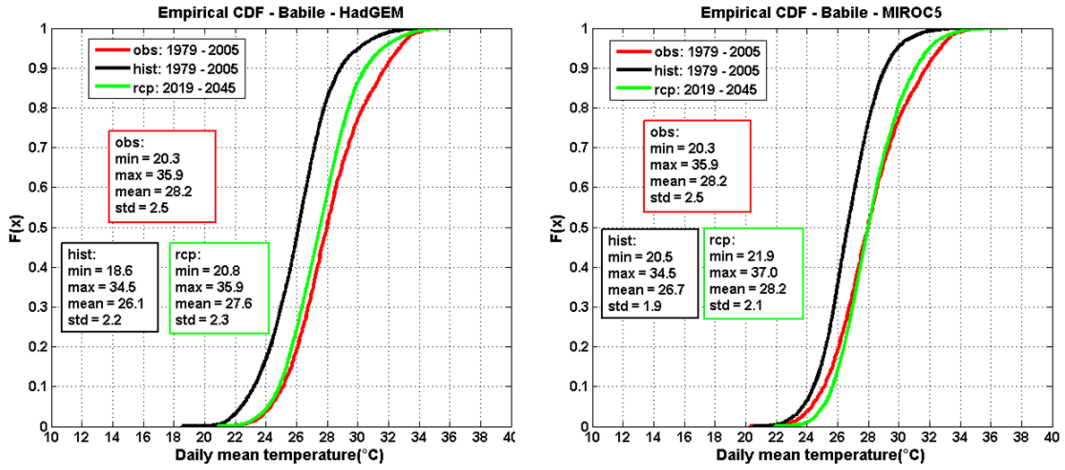

Figure 5.23: Empirical cdf plots of observed and RCM runs using HadGEM and MIROC driving models for temperature of historical (hist) and future (rcp) simulations for station Babile

5.6 Bias correction of climate simulations

5.6.1 Introduction

RCM simulations of temperature and precipitation often show biased representations of observed climate and therefore must be handled with caution [Christensen et al., 2008; Teutschbein and Seibert, 2010; Varis et al., 2004]. According to Teutschbein and Seibert [2012], systematic model errors caused by imperfect conceptualization, discretization and spatial averaging within grid cells are the reasons for such biases. To help remedy the various problems associated with RCM output, bias correction methods are employed [Teutschbein and Seibert, 2012]. The occurrence of too many wet days with low-intensity rain or incorrect estimation of extreme temperatures [Ines and Hansen, 2006] and general under-or overestimation and incorrect seasonal variations of precipitation [Christensen et al., 2008; Terink et al., 2009; Teutschbein and Seibert, 2010] are the typical biases in an RCM output. There are several bias correction methods which range from simple scaling methods to sophisticated approaches employing probability mapping or weather generators. The procedures employ a transformation algorithm for adjusting the RCM output.

The idea behind the correction procedure is the identification of possible biases between observed and simulated climate variables, which serves as the basis for correcting both control and future scenario RCM runs [Teutschbein and Seibert, 2012]. In bias correction, it is assumed that the correction algorithm and its parameterization for current climate conditions are also valid for future conditions [Teutschbein and Seibert, 2012].

A review of literature shows the existence of the following bias correction methods which is used to adjust RCM simulations: (1) linear scaling, (2) local intensity scaling, (3) power transformation, (4) variance scaling, (5) distribution mapping and (6) the delta-change method. In this study, the linear scaling and the distribution mapping approach which is also referred to as "probability mapping" [Block et al., 2009; Ines and Hansen, 2006], "quantile−quantile mapping" [Boé et al., 2007; Johnson and Sharma, 2011; Sun et al., 2011; Bárdossy and Pegram, 2011; Pegram and Bárdossy, 2013], "statistical downscaling" [Piani et al., 2010] and "histogram equalization" [Rojas et al., 2011; Sennikovs and Bethers, 2009] were used to bias correct the RCM outputs. A precipitation threshold (for a day to be considered wet, precipitation should be greater than 0.1mm) as used by Piani et al. [2010] in their studies was also used to adjust the wet-day frequencies of precipitation time series. The linear scaling and distribution (quantile−quantile) mapping method are further described in the subsequent sub-sections.

5.6.2 Linear Scaling method

The linear-scaling method works with monthly correction values which are based on the differences between observed and historical simulated values [Teutschbein and Seibert, 2012]. According to Teutschbein and Seibert [2012], the correction of precipitation is done with a factor based on the ratio of long-term monthly mean observed and historical (control) run

data:

$$P^*_{hist}(d) = P_{hist}(d).\left[\frac{\mu_m(P_{obs}(d))}{\mu_m(P_{hist}(d))}\right] \tag{5.1}$$

$$P^*_{rcp}(d) = P_{rcp}(d).\left[\frac{\mu_m(P_{obs}(d))}{\mu_m(P_{hist}(d))}\right] \tag{5.2}$$

where,
P^*_{hist} is the corrected precipitation values of the control or historical simulation
P_{hist} is the uncorrected control or historical simulation
P^*_{rcp} is the corrected precipitation values of the future simulation
P_{rcp} is the uncorrected future simulation
$\mu_m(P_{obs}(d))$ is the long-term monthly mean of observed data
$\mu_m(P_{hist}(d))$ is the long-term monthly mean of historical simulation

Temperature is corrected using an additive term which is based on the difference of long-term monthly mean of observed and historical run data.

$$T^*_{hist}(d) = T_{hist}(d) + \mu_m(T_{obs}(d)) - \mu_m(T_{hist}(d)) \tag{5.3}$$

$$T^*_{rcp}(d) = T_{rcp}(d) + \mu_m(T_{obs}(d)) - \mu_m(T_{hist}(d)) \tag{5.4}$$

It should be noted that the applied correction factors and terms are assumed to remain constant even for future conditions.

5.6.3 Quantile−Quantile mapping method

Quantile-quantile mapping is to correct the distribution function of RCM-simulated climate values to agree with the observed distribution function and it is done by the creation of a transfer function to shift the occurrence distributions of precipitation and temperature [Sennikovs and Bethers, 2009].

Various literatures [Block et al., 2009; Ines and Hansen, 2006; Piani et al., 2010; Watterson and Dix, 2003] reveal that the Gamma distribution [Thom, 1958] with shape parameter α and scale parameter β is often assumed to be suitable and effective for distributions of precipitation events:

$$f_\gamma\left(\mathrm{x} \mid \alpha, \beta\right) = \mathrm{x}^{\alpha-1} \cdot \frac{1}{\beta^\alpha \cdot \Gamma\left(\alpha\right)} \cdot e^{\frac{-\mathrm{x}}{\beta}};\ \mathrm{x} \geq 0; \quad \alpha, \beta > 0 \tag{5.5}$$

The Gaussian distribution [Cramér, 1945] with location parameterμ and scale parameterσ is usually to best fit temperature time series [Teutschbein and Seibert, 2012; Schoenau and Kehrig, 1990; Thom, 1952]:

$$f_N\left(\mathrm{x} \mid \mu, \sigma^2\right) = \mathrm{x}^{\mu-1} \cdot \frac{1}{\sigma \cdot \sqrt{2\pi}} \cdot e^{\frac{-(\mathrm{x}-\mu)^2}{2\sigma^2}};\ \mathrm{x} \in \Re \tag{5.6}$$

In this study, cumulative distribution functions (CDFs) were constructed for both the observed and the RCM-simulated climate variables (1979−2005) for all days within a certain

month (figures 5.24 and 5.25). The value of the RCM-simulated precipitation/temperature of day d within month m was then searched on the empirical CDF of the RCM simulations together with its corresponding cumulative probability (figures 5.24 and 5.25). The value of precipitation/temperature was thereafter located on the empirical CDF of observations. This value was finally used as the corrected value for the RCM control run (1979−2005). For precipitation, this approach can be expressed mathematically in terms of the Gamma CDF (F_γ) and its inverse (F_γ^{-1}) as:

$$P^*_{hist}(d) = F_\gamma^{-1}(F_\gamma(P_{hist}(d) \mid \alpha_{hist,m}, \beta_{hist,m}) \mid \alpha_{obs,m}, \beta_{obs,m}) \tag{5.7}$$

$$P^*_{rcp}(d) = F_\gamma^{-1}(F_\gamma(P_{rcp}(d) \mid \alpha_{hist,m}, \beta_{hist,m}) \mid \alpha_{obs,m}, \beta_{obs,m}) \tag{5.8}$$

where,
P^*_{hist} is the corrected precipitation values of the control or historical simulation
P_{hist} is the uncorrected control or historical simulation
P^*_{rcp} is the corrected precipitation values of the future simulation
P_{rcp} is the uncorrected future simulation

The same approach can be used in terms of the Gaussian (normal) CDF (F_N) and its inverse (F_N^{-1}) for the temperature time series as:

$$T^*_{hist}(d) = F_N^{-1}(F_N(T_{hist}(d) \mid \mu_{hist,m}, \sigma^2_{hist,m}) \mid \mu_{obs,m}, \sigma^2_{obs,m}) \tag{5.9}$$

$$T^*_{rcp}(d) = F_N^{-1}(F_N(T_{rcp}(d) \mid \mu_{hist,m}, \sigma^2_{hist,m}) \mid \mu_{obs,m}, \sigma^2_{obs,m}) \tag{5.10}$$

where,
T^*_{hist} is the corrected temperature values of the control or historical simulation
T_{hist} is the uncorrected control or historical simulation
T^*_{rcp} is the corrected temperature values of the future simulation
T_{rcp} is the uncorrected future simulation

The shape and scale parameters for each of the distributions were determined using the maximum likelihood estimation.

5.6.4 Results of Bias-corrected climate simulations

Rainfall
Figures 5.26 to 5.30 indicates the performance of the two different bias correction methods applied on the five (5) diffferent GCM driving models used for this study. These figures show the annual cycle of areal rainfall for both methods with their uncorrected data for the various driving models.

Overall, the linear scaling (MC) approach was well-able to bring the historical simulations to the observed whiles maintaining the change signal between the present and the future. The linear scaling method destroys part of the distribution in the uncorrected data in the process. The quantile mapping method (QC) maintains the change signal during the correction and

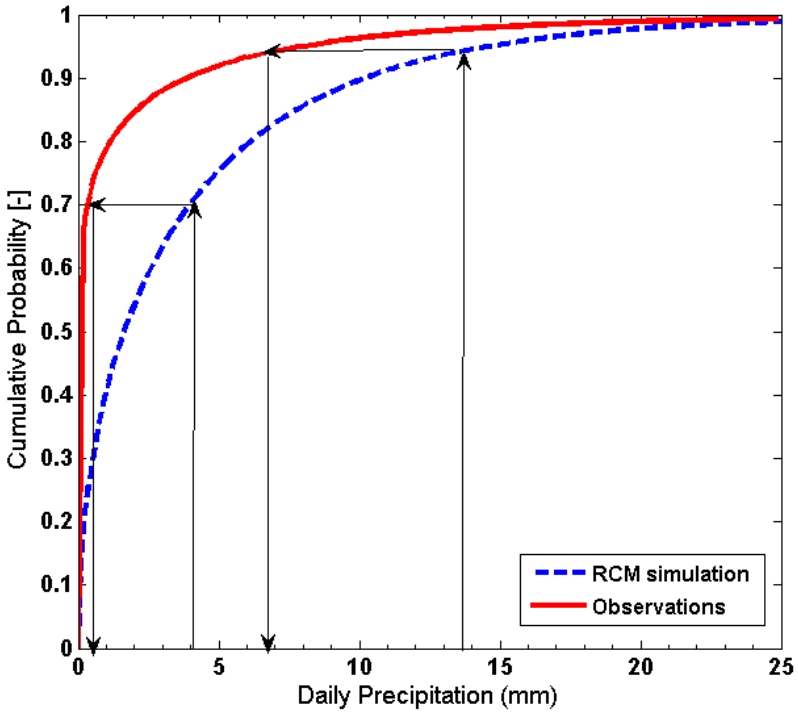

Figure 5.24: Bias correction procudure for ECHAM6 driving model using quantile-quantile mapping for station Babile. (The Gamma distribution of RCM-simulated daily precipitation (dashed blue) was shifted towards the Gamma distribution of the observations (red line))

also reproduces the distribution in the data. As a result, the corrected historical data from the MC method fits better on the observed curve than the QC method. In all the GCM driving models and the correction methods, the change signal between the historical and the future are correctly reproduced. This shows the efficacy of the bias correction methods.

Table 5.1 shows a summary of the results in terms of the means, variance, maximum rainfall and probability of dryness (P0) for the areal precipitation for the study area produced by the uncorrected and corrected climate simulations.

It is observed in table 5.1 that, CanESM driving model shows an insignificant change in the future precipitation according to the mean rainfall and the percentage of dryness for the present and the future in the uncorrected and corrected simulations. On the other hand, EC-EARTH indicates a slight increase in the future (2019−2045) precipitation in both the uncorrected and corrected RCM simulations. However, the signal for the probability of dryness remains unchanged in this driving model. There is a negative rainfall signal from the ECHAM driving model and an increase in the percentage of dryness for the future. GFDL, shows a slight increase in the future rainfall and an insignificant change in the probability of dryness. And lastly, the MIROC model predicts a slight increase of rainfall in both the uncorrected and corrected RCM simulations. Table 5.1 indicates that the change in the

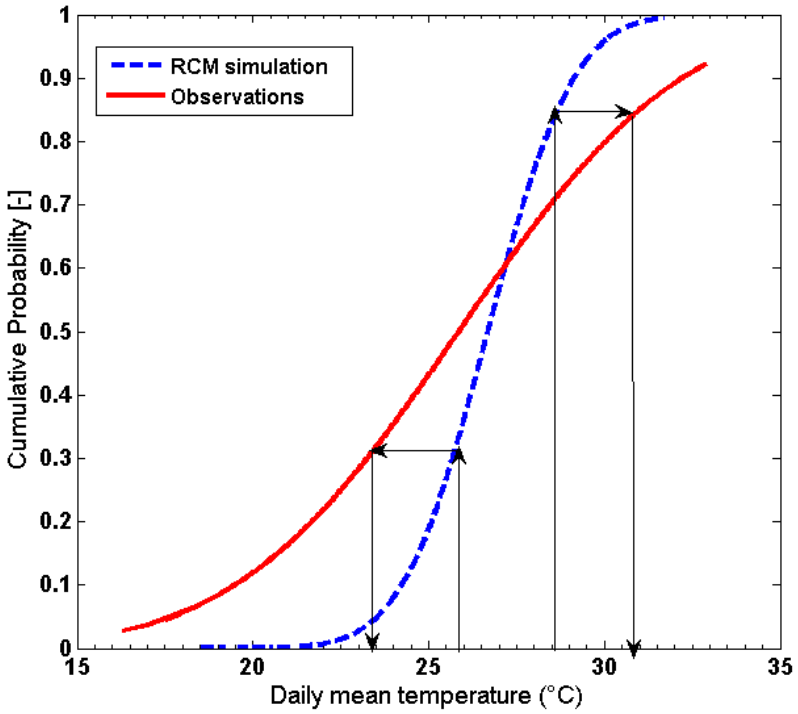

Figure 5.25: Bias correction procudure for ECHAM6 driving model using quantile-quantile mapping for station Wenchi. (The Gausssian distribution of RCM-simulated daily temperature (dashed blue) was shifted towards the Gaussian distribution of the observations (red line)).

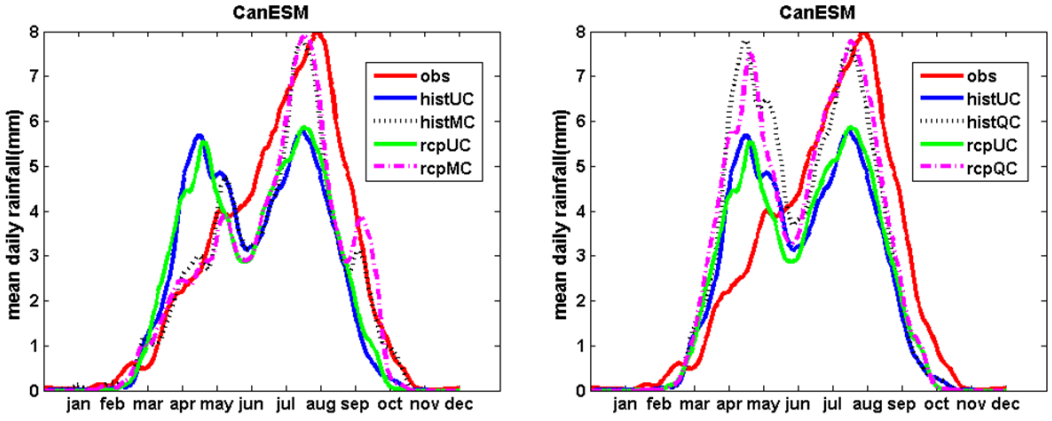

Figure 5.26: Annual cycle of observed(obs), uncorrected historical and future rainfall RCM simulations (histUC and rcpUC) and bias corrected simulations (MC/QC) for the CanESM driving model. Left: Correction using Linear Scaling method (MC), Right: Correction using Quantile mapping method (QC)

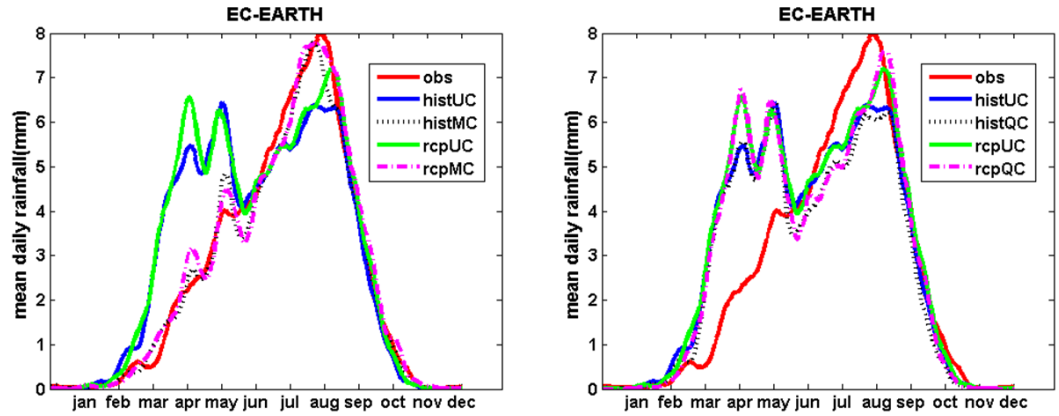

Figure 5.27: Annual cycle of observed(obs), uncorrected historical and future rainfall RCM simulations (histUC and rcpUC) and bias corrected simulations (MC/QC) for the EC-EARTH driving model. Left: Correction using Linear Scaling method (MC), Right: Correction using Quantile mapping method (QC)

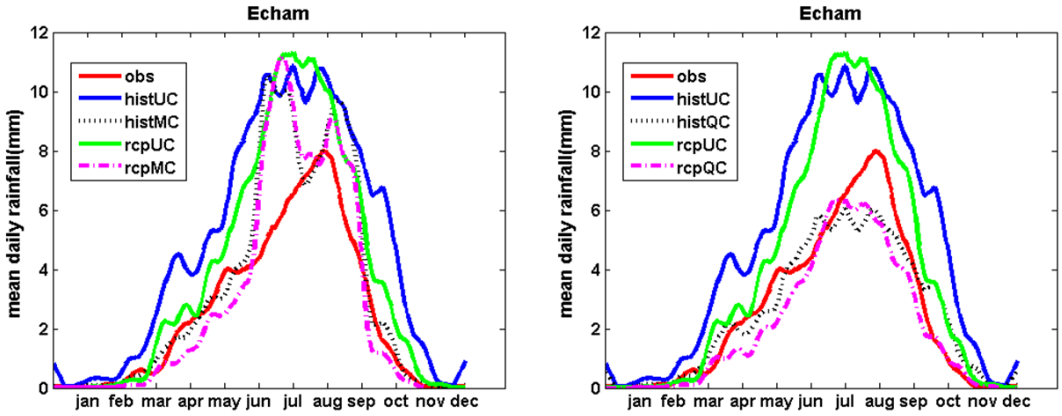

Figure 5.28: Annual cycle of observed(obs), uncorrected historical and future rainfall RCM simulations (histUC and rcpUC) and bias corrected simulations (MC/QC) for the ECHAM driving model. Left: Correction using Linear Scaling method (MC), Right: Correction using Quantile mapping method (QC)

probability of rainfall exceeding 20 mm/day in the future is insignificant. ECHAM has the highest variance in the data (71.73 $(mm/day)^2$) for the uncorrected data and CanESM has the minimum variance.

Temperature

Figures 5.31 to 5.35 shows that both the corrected and uncorrected RCM simulations predict a warmer future of about 1 - 2 degrees celsius. This signal is maintained in the data obtained from the application of the two bias correction methods. The annual cycles also indicate that the RCM simulations reproduce the two peaks in the annual temperature cycle for the months of March and October. All the driving models capture the low temperature season in

Table 5.1: Summary of results for corrected and uncorrected rainfall simulations (areal) for historical period (1979−2005) and future (2019−2045). P0 and P20 represents the probability of zero precipitation and precipitation above 20mm respectively

Scenario	GCM	RCM	Mean	Variance	Max	P0	P20
			mm/day	(mm/day)	mm/day		
Observed			2.52	27.18	55.91	0.54	0.0199
Uncorrected historical runs	CanESM	RCA4	2.10	11.46	37.94	0.483	0.0015
	EC-EARTH	RCA4	2.88	17.62	67.93	0.4088	0.0045
	ECHAM	WRF	4.76	71.73	286.50	0.2743	0.0327
	GFDL	RCA4	3.03	22.54	63.89	0.4539	0.0079
	MIROC	RCA4	3.13	16.87	74.28	0.3268	0.003
Uncorrected future runs	CanESM	RCA4	2.13	10.79	25.61	0.4767	3.04E-04
	EC-EARTH	RCA4	3.01	23.28	88.05	0.4088	0.0054
	ECHAM	WRF	3.87	58.74	150.86	0.4292	0.0282
	GFDL	RCA4	3.26	27.79	72.58	0.4531	0.0118
	MIROC	RCA4	3.30	24.24	79.19	0.3479	0.0085
Bias Corrected historical runs using linear scaling method	CanESM	RCA4	2.16	13.27	37.09	0.483	0.0035
	EC-EARTH	RCA4	2.45	14.97	67.93	0.4088	0.004
	ECHAM	WRF	3.19	45.36	286.50	0.2743	0.0219
	GFDL	RCA4	2.55	18.30	64.77	0.4539	0.0069
	MIROC	RCA4	2.47	13.82	74.28	0.3268	0.0021
Bias Corrected future runs using linear scaling method	CanESM	RCA4	2.19	13.03	35.34	0.4767	0.0025
	EC-EARTH	RCA4	2.56	20.32	83.42	0.4088	0.0048
	ECHAM	WRF	2.81	41.26	111.94	0.4292	0.0206
	GFDL	RCA4	2.78	23.36	72.58	0.4531	0.0105
	MIROC	RCA4	2.77	22.94	94.05	0.3479	0.0092
Bias Corrected historical runs using quantile mapping method	CanESM	RCA4	2.67	24.50	66.81	0.5371	0.0138
	EC-EARTH	RCA4	2.67	24.03	106.42	0.4984	0.011
	ECHAM	WRF	2.48	28.22	198.91	0.3858	0.0126
	GFDL	RCA4	2.64	25.13	82.83	0.5235	0.0095
	MIROC	RCA4	2.63	24.61	129.44	0.4496	0.0084
Bias Corrected future runs using quantile mapping method	CanESM	RCA4	2.68	22.33	43.27	0.5299	0.0106
	EC-EARTH	RCA4	2.88	37.48	141.09	0.5053	0.0118
	ECHAM	WRF	2.03	22.18	102.67	0.5106	0.0101
	GFDL	RCA4	2.94	32.39	95.10	0.5263	0.0162
	MIROC	RCA4	3.03	41.81	138.98	0.4836	0.0187

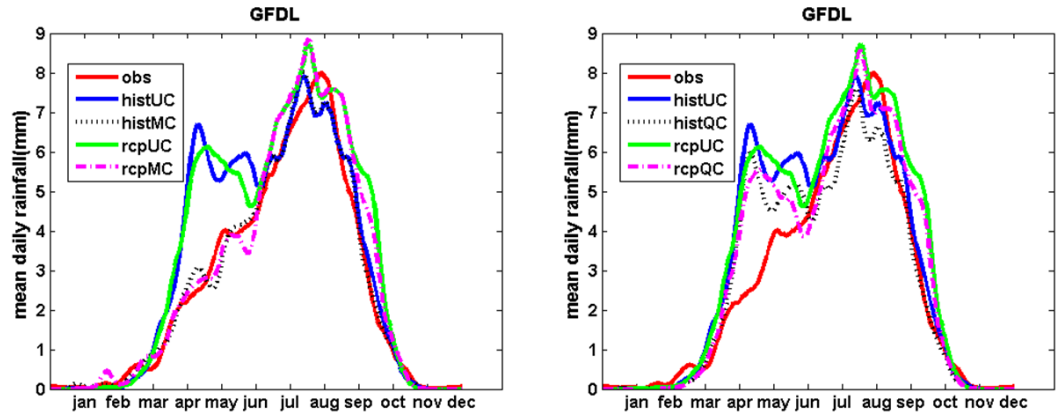

Figure 5.29: Annual cycle of observed(obs), uncorrected historical and future rainfall RCM simulations (histUC and rcpUC) and bias corrected simulations (MC/QC) for the GFDL driving model. Left: Correction using Linear Scaling method (MC), Right: Correction using Quantile mapping method (QC)

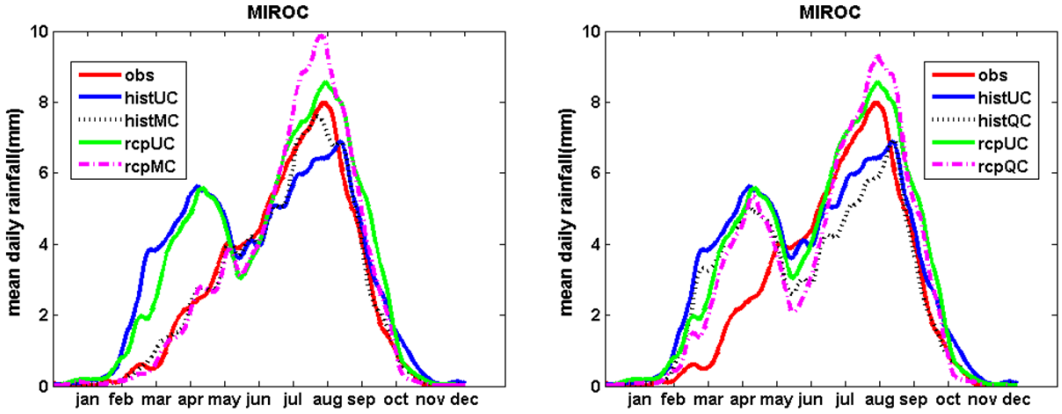

Figure 5.30: Annual cycle of observed(obs), uncorrected historical and future rainfall RCM simulations (histUC and rcpUC) and bias corrected simulations (MC/QC) for the MIROC driving model. Left: Correction using Linear Scaling method (MC), Right: Correction using Quantile mapping method (QC)

the months of July and August. The low temperature in the Harmattan season (December to February) is also well captured in the annual cycles produced by the various driving models.

Looking at the annual cycle figures, it is however difficult to determine which bias correction method performed better. In the corrected data, the magnitude of the temperature change in the future is narrowed after the correction. The data corrected using quantile mapping shows a less magnitude of temperature increase than the corrected data using linear scaling method.

Table 5.2 shows a summary of the areal mean, variances and maximum daily temperature values for the study area. It could be again observed from table5.2 that all the GCM/RCM

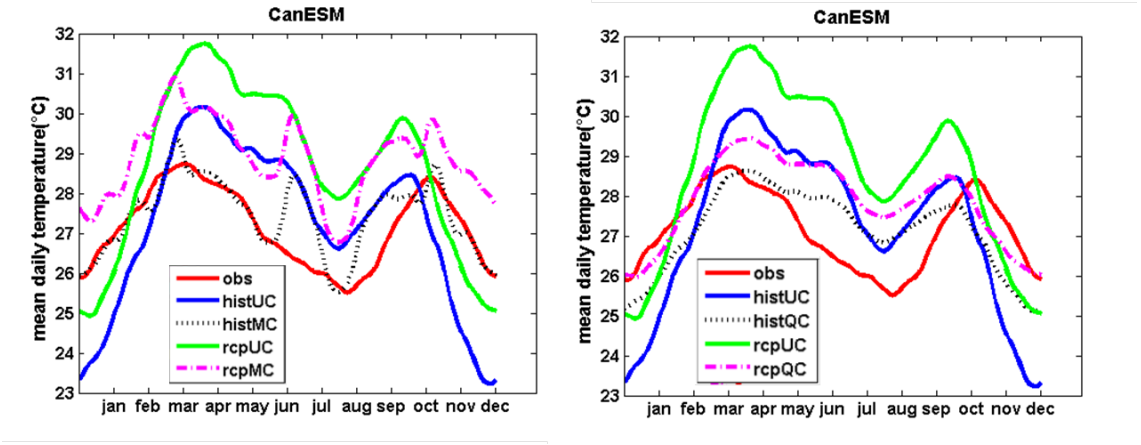

Figure 5.31: Annual cycle of observed(obs), uncorrected historical and future temperature RCM simulations (histUC and rcpUC) and bias corrected simulations (MC/QC) for the CanESM driving model. Left: Correction using Linear Scaling method (MC), Right: Correction using Quantile mapping method (QC)

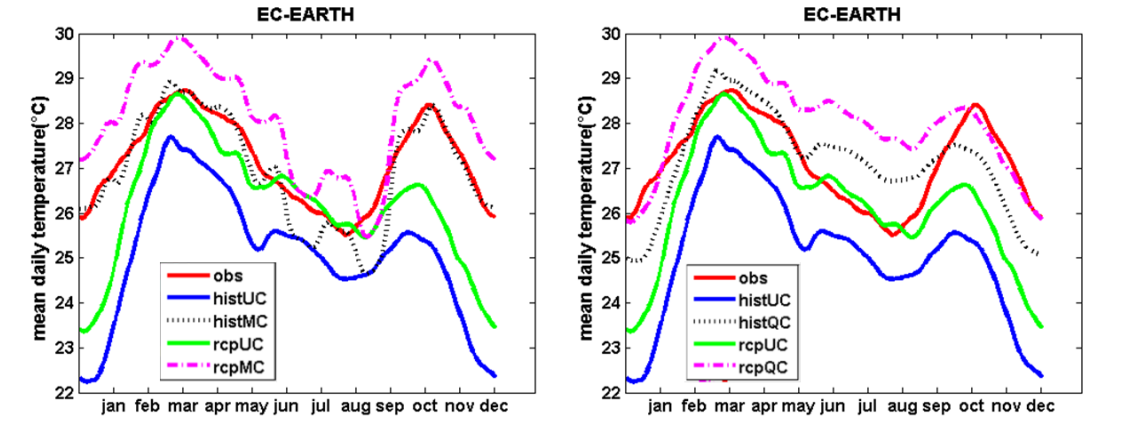

Figure 5.32: Annual cycle of observed(obs), uncorrected historical and future temperature RCM simulations (histUC and rcpUC) and bias corrected simulations (MC/QC) for the EC-EARTH driving model. Left: Correction using Linear Scaling method (MC), Right: Correction using Quantile mapping method (QC)

models predict a warmer future which ranges from approximately +1°C to +2°C. All the GCM/RCMs also indicates an increase in the extreme temperatures as observed in table 5.2. The simulations are obviously improved after the bias correction and that there is a higher variance in the uncorrected simulations but it is reduced after the bias correction. Correction using quantile mapping predicts a less warmer future and a smaller variance than the correction using linear scaling method.

Table 5.2: Summary of results for corrected and uncorrected temperature simulations (areal) for historical period (1979−2005) and future (2019−2045)

Scenario	GCM	RCM	Mean	Variance	Max
			C/day	(C/day)	C/day
Observed			27.15	2.79	33.89
Uncorrected historical runs	CanESM	RCA4	27.2519	5.4909	35.01
	EC-EARTH	RCA4	25.10	3.58	31.45
	ECHAM	WRF	26.76	5.03	33.55
	GFDL	RCA4	25.40	5.86	33.80
	MIROC	RCA4	26.74	3.24	33.39
Uncorrected future runs	CanESM	RCA4	28.69	5.52	36.01
	EC-EARTH	RCA4	26.23	3.40	32.71
	ECHAM	WRF	28.40	6.83	34.84
	GFDL	RCA4	26.69	6.16	35.69
	MIROC	RCA4	28.19	4.11	36.21
Bias Corrected historical runs using linear scaling method	CanESM	RCA4	27.43	2.45	34.44
	EC-EARTH	RCA4	26.96	3.09	33.08
	ECHAM	WRF	27.21	3.90	33.36
	GFDL	RCA4	27.02	3.35	34.09
	MIROC	RCA4	27.17	2.55	33.32
Bias Corrected future runs using linear scaling method	CanESM	RCA4	28.87	2.46	34.92
	EC-EARTH	RCA4	28.08	3.07	34.04
	ECHAM	WRF	28.85	4.59	34.60
	GFDL	RCA4	28.31	3.47	36.40
	MIROC	RCA4	28.63	3.46	36.14
Bias Corrected historical runs using quantile mapping method	CanESM	RCA4	27.15	1.42	31.10
	EC-EARTH	RCA4	27.15	2.18	32.10
	ECHAM	WRF	27.15	1.55	30.92
	GFDL	RCA4	27.15	1.33	31.16
	MIROC	RCA4	27.15	2.41	32.89
Bias Corrected future runs using quantile mapping method	CanESM	RCA4	27.89	1.43	31.61
	EC-EARTH	RCA4	28.03	2.07	33.08
	ECHAM	WRF	28.07	2.10	31.64
	GFDL	RCA4	27.77	1.40	32.06
	MIROC	RCA4	28.41	3.05	35.32

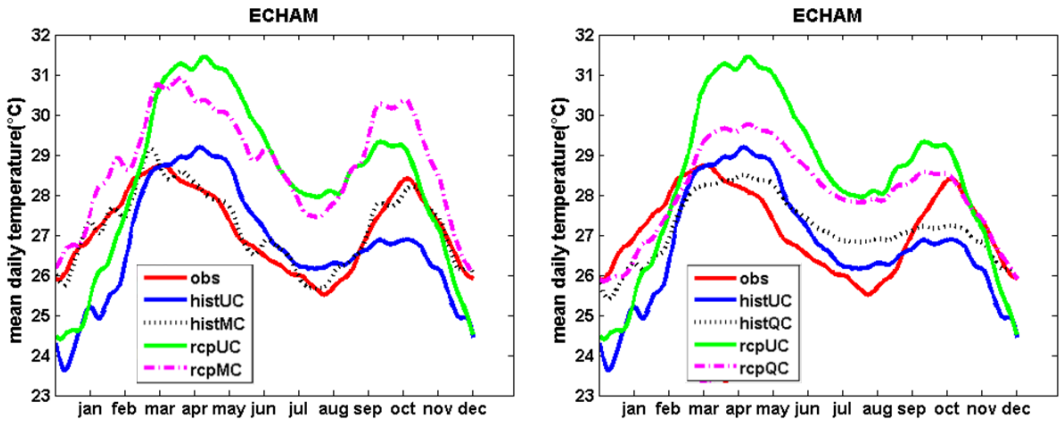

Figure 5.33: Annual cycle of observed(obs), uncorrected historical and future temperature RCM simulations (histUC and rcpUC) and bias corrected simulations (MC/QC) for the ECHAM driving model. Left: Correction using Linear Scaling method (MC), Right: Correction using Quantile mapping method (QC)

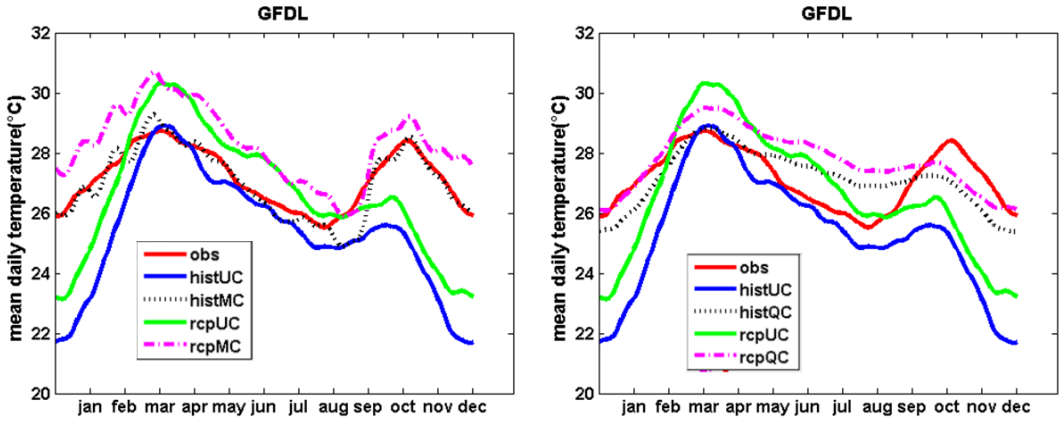

Figure 5.34: Annual cycle of observed(obs), uncorrected historical and future temperature RCM simulations (histUC and rcpUC) and bias corrected simulations (MC/QC) for the GFDL driving model. Left: Correction using Linear Scaling method (MC), Right: Correction using Quantile mapping method (QC)

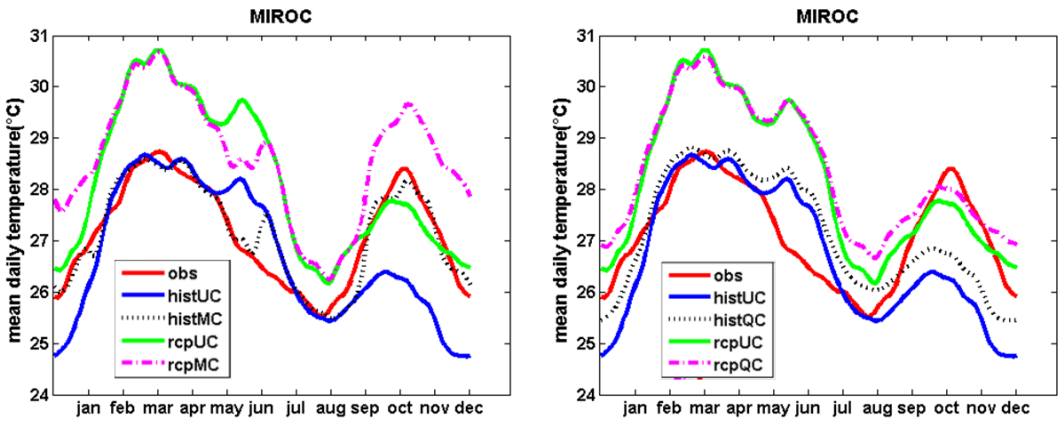

Figure 5.35: Annual cycle of observed(obs), uncorrected historical and future temperature RCM simulations (histUC and rcpUC) and bias corrected simulations (MC/QC) for the MIROC driving model. Left: Correction using Linear Scaling method (MC), Right: Correction using Quantile mapping method (QC)

6 Effects of climate change (cc) on the hydrology of the sub-region

6.1 Introduction

The hydrological cycle is directly connected to the climate system, therefore changes that occur in the climate also have effects on the hydrology of a region. From the preceding chapters, it is clear and unambiguous that climate change is having its footprint on the West Africa sub-region. Because the sub-region largely depends on rainfall and river flow for its agriculture, domestic water supply and energy production, changes in these variables will significantly affect the economy and the people of this sub-region. For the rapid development of the African Continent and its sub-regions, agriculture, water supply and energy production are key and vital to the realization of this dream.

Huge investments has been made in hydropower generation in this sub-region over the past one to two decades but has yielded small results in terms of electricity production. An example is the Bui hydropower in Ghana which is working far below the designed capacity because of low-levels of water in the reservoir of the dam. The Volta river authority which operates the Akosombo dam which is the main source of electricity for most of the countries in the sub-region also has to shut down most of its turbines during the last decade as the result of less rainfall during the period. All these could be attributed to climate change and its effects on the sub-region. Furthermore, the people in the northern part of the sub-region are peasant farmers who depend solely on rain-fed agriculture for their sustenance. Therefore, climate change will also promote more rural-urban and international migration of people in the sub-region which has its own negative consequences.

In this chapter, we tried to ascertain the effects of climate change on the hydrology of the sub-region. To do this, we used the RCM simulations obtained from CORDEX and IMK−IFU in conjunction with the calibrated and validated HBV hydrological model to determine the effects of the changed climate on the hydrology of the Black Volta Basin. Five (5) of the GCM driving models used to determine climate change in the preceding chapter were used to find out the effects of climate change on hydrology.

6.2 The effects of CC on hydrology using CanESM driving model

The CanESM2M is the second edition of the climate model for the Canadian Center for Climate Modeling and Analysis (CCCma). The areal precipitation, temperature and potential

evapotranspiration were used as inputs for the lumped HBV hydrological model to get the river flow (discharge) as the output for the historical (control) and the future (rcp) time periods. Flow duration curves (FDCs) and annual cycles were constructed and the results could be seen in figures 6.1 and 6.3 respectively.

The FDC in figure 6.1 shows that for the uncorrected (UC) RCM simulations, the discharge (River flow) in the future will slightly increase. With magnitudes slightly higher for mean daily flow which are less than $100m^3/s$. For the flows which are higher than 100 m^3/s, the increase is very minimal. However, the curve of the historical discharge simulations was quite different from the observed discharge curve and the reasons might be from the errors in observations and wrong parameterization of the climate and/or the hydrological models. It could also be seen from the curve that, for 25% of the time the daily discharge obtained from the RCM simulations equaled or exceeded 100 m^3/s. This number reduces to about $10-20$ m^3/s for the 50% exceedance probability and reduces further to $2-3$ m^3/s for the 75% exceedance probability. This therefore shows that, the Rivers in this catchment virtually dries up for about $25-30$% of the times. The peak discharge is about 300 m^3/s and this is equaled or exceeded for about 10% of the time.

Figure 6.1 also shows the results from the bias corrected simulations using Quantile mapping method. They are shown in dashed blue and dashed green colours for historical ($1980-2005$) and future ($2020-2045$) periods respectively. The corrected data clearly predicts an increase in the future discharge(river flow) as compared with the historical. The increase is more pronounced with the corrected than the uncorrected data (figure 6.1). For example, in 50% of the time a discharge of $3m^3/s$ and $12m^3/s$ is equaled or exceeded in the corrected historical and future respectively. The positive singal is reduced in higher discharges (i.e. flows greater than $100m^3/s$).

In comparing the results to the other bias correction method (i.e. linear scaling (MC)), figure 6.2 shows the fdc obtained using linear scaling as the correction method. In this method (figure 6.2) the increase is not huge and is closer to what the uncorrected data predicts. In all the three scenarios (i.e. the uncorrected (UC), corrected using quantile mapping (QC) and corrected using linear scaling (MC)), the change signal is maintained and reproduced.

The simulated discharge curve (sim) which is shown in orange colour as seen in figures 6.1 and 6.2 is the simulation obtained by using the observed climate as input data in the hydrological model to produce the runoff (discharge). This curve is close to the observed discharge but it underestimate the low flows and also overestimate the high flows as was also discussed in section 4.5.

A time series plot (not shown) of the simulated discharges of the RCMs shows an increase in the peaks of the discharge for the future as compared with the present. It is however striking to know that some years in the future rather shows less discharge as compared with the present. One could also notice a mixture of an early and late accumulation of the discharge. And with the exception of discharge years 1989, 1992, 1993, 1997 and 2002 for the historical simulation and 2029, 2032, 2033, 2037 and 2042 for the future, all the discharges were less than the 600 m^3/s mark.

The graph of the annual cycle (figure 6.3) of the discharge from the RCM simulations using

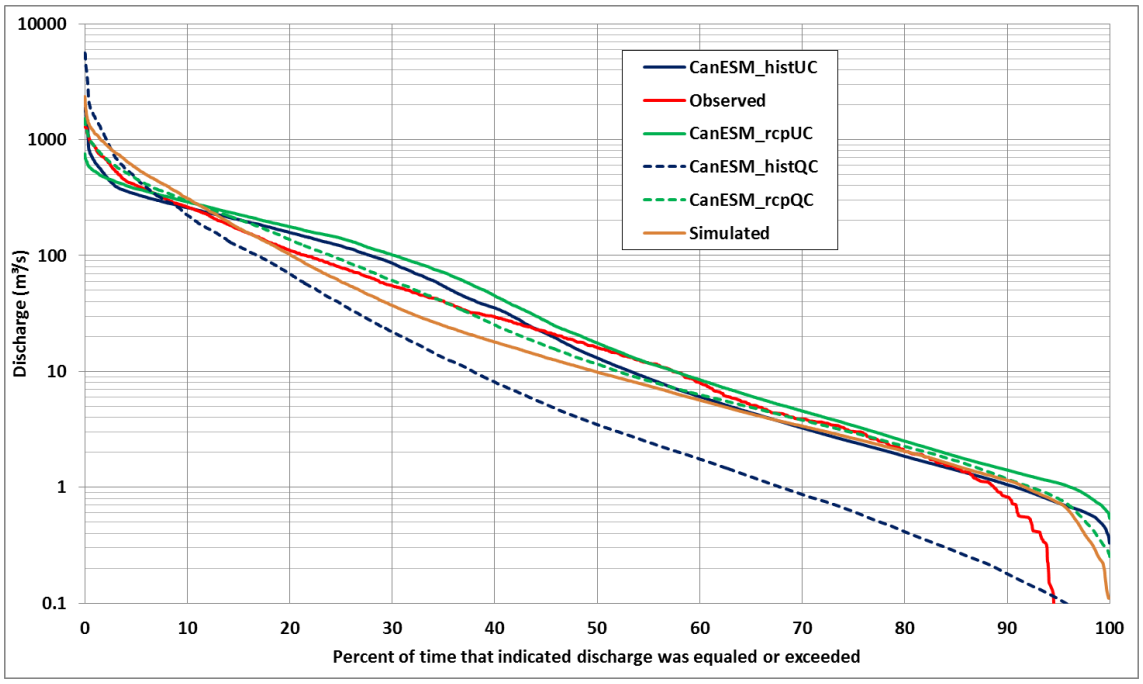

Figure 6.1: Flow duration curves of simulated discharges (historical (hist) (1980−2005) *(blue)*; future (rcp)(2020−2045) *(green)*; observed (1980−2005)*(red)*; simulated (1980−2005) *(orange)*; bias-corrected rcm simulations using linear scaling (MC) method *dashed blue and green*) with CanESM as the driving model

CanESM driving model shows a bi-modal discharge cycle for the uncorrected (UC) and corrected data using quantile mapping (QC). The first peak is in May and the second one in August. The observed annual cycle and the corrected data using linear scaling method (MC) rather shows a uni-modal discharge cycle which peaks in August/September. From the RCM simulations, there is a decrease in the discharge for the first cycle and an increase during the second cycle for the future as compared with the historical simulation. It could be inferred that there will be a decreased discharge in the first or minor discharge cycle and an increased discharge during the second or the major discharge cycle in the future. The rivers dry up for about 4 months of the year. Both the uncorrected and corrected data shows the discharge cycle reaching its highest amount in the month of August

Furthermore, the discharge from the historical RCM simulations didn't quite represent the observed discharge as seen in figure 6.3. It could be seen in figure 6.3 that, the simulated discharge (sim) outperformed the discharge resulting from the historical rcm simulations. Whiles the simulated discharge showed a uni-modal annual cycle which is what happens in the observed data, the historical showed a bi-modal cycle. Again, it could be seen from the annual cycle that there is slight underestimation of the low flows and overestimation of the peaks in the simulated discharge.

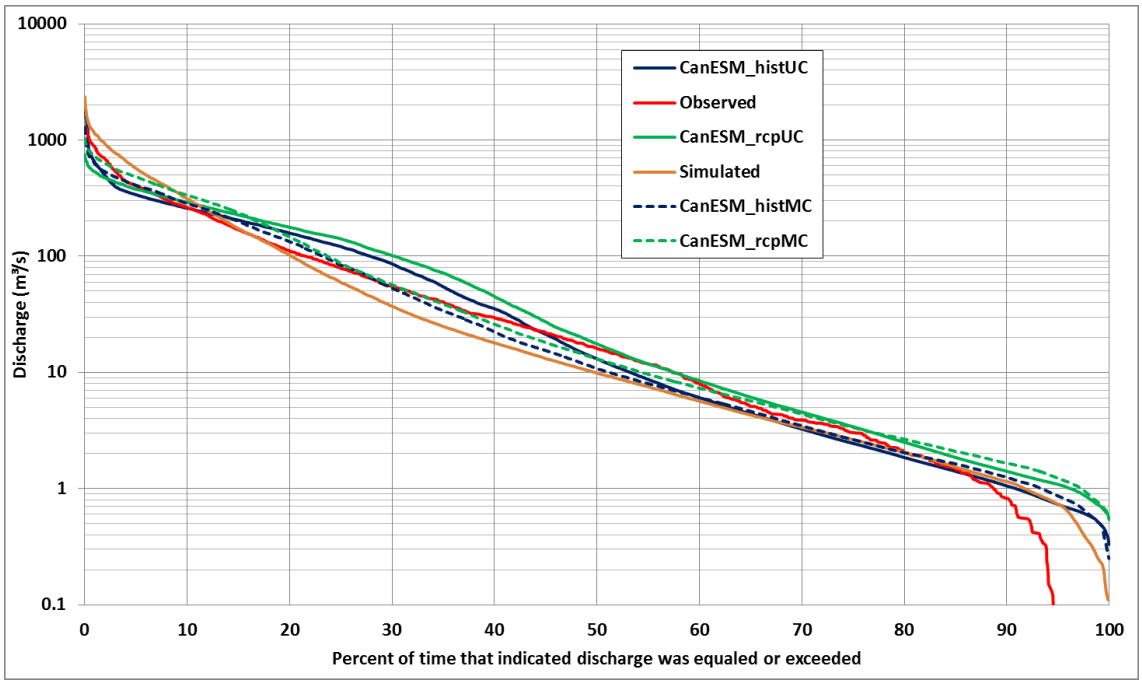

Figure 6.2: Flow duration curves of simulated discharges (historical (hist) (1980−2005) *(blue)*; future (rcp)(2020−2045) *(green)*; observed (1980−2005)*(red)*; simulated (1980−2005) *(orange)*; bias-corrected rcm simulations using linear scaling (MC) method *dashed blue and green*) with CanESM as the driving model

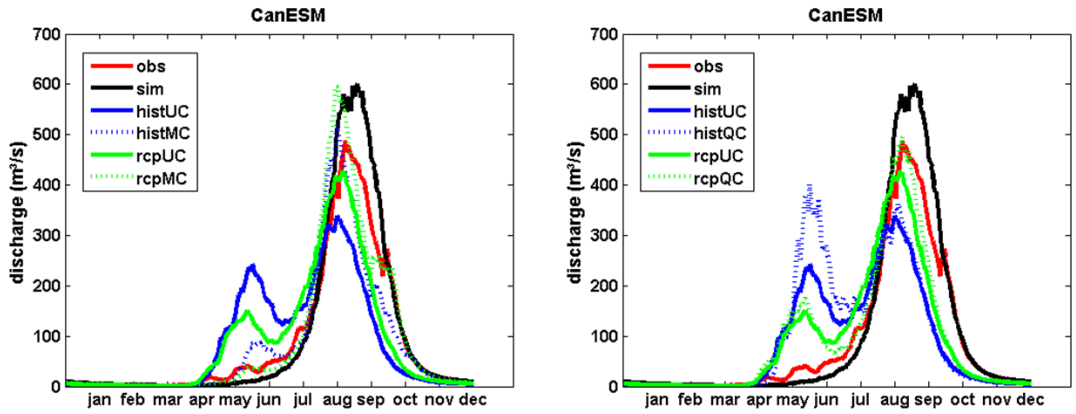

Figure 6.3: Annual cycle of discharges (historical (hist) (1980−2005) *(blue)*; future (rcp)(2020−2045) *(green)*; bias-corrected rcm simulations using linear scaling (MC) (−left) and quantile mapping (QC) (−right) methods *dashed blue and green*) using CanESM as the driving model; observed (obs) (1980-2005) *(red)* and simulated discharges (sim) (1980−2005) *(black)*)

6.3 The effects of CC on hydrology using EC-EARTH driving model

EC-EARTH is an Earth System model (ESM) which was developed and maintained by a consortium of European climate modelers. It brings together 27 research institutes from 10

European countries to collaborate on the development of an Earth System Model (www.ec-earth.org). Figures 6.4, 6.5 and 6.6 show and describe the effects of climate change on the hydrology of the West Africa sub-region using this model.

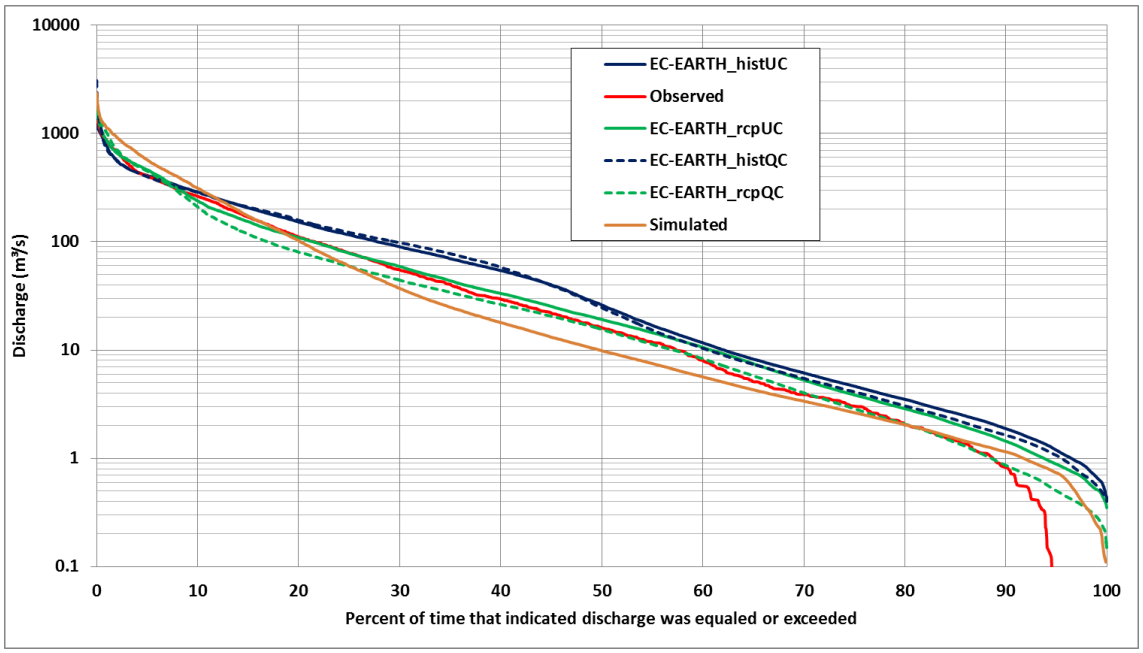

Figure 6.4: Flow duration curves of simulated discharges (historical (hist) (1980−2005) *(blue)*; future (rcp)(2020−2045) *(green)*; observed (1980−2005)*(red)*; simulated (1980−2005) *(orange)*; bias-corrected rcm simulations using Quantile mapping (QC) method *dashed blue and green*) with EC-EARTH as the driving model

The FDC of the discharge using EC−EARTH driving model reveals that, the discharge will decrease slightly in the future as compared with the present which is a direct opposite of what the CanESM model predicted. This case also shows that, at 25% of the times a discharge of $70m^3/s$ is equaled or exceeded, whiles $20m^3/s$ is for 50% exceedance probability and $4m^3/s$ is for 75% in the future.

Figures 6.4 and 6.5 shows that the bias corrected data also predicts a negative signal for the hydrology of the future. The future discharge for 50% exceedeence probability is $20m^3/s$ and $8m^3/s$ for the quantile mapping and linear scaling methods for bias correction respectively. The corrected data from linear scaling (MC) method predicts lower discharges as compared with that from the quantile mapping (QC). In this case, the bias corrected historical data using linear scaling method performed better than its counterpart (QC) method (as seen in figure 6.5).

The annual cycle of discharge (figure 6.6) for the EC-EARTH driving model also confirms a slight decrease in the discharge in the future. It also shows one discharge cycle and not two as previously observed with the case of the CanESM model. The discharge begins to increase in the month of April when the rainy season begins. It then peaks in August/September and then subsides in October to March the following year. The high uncertainty in the

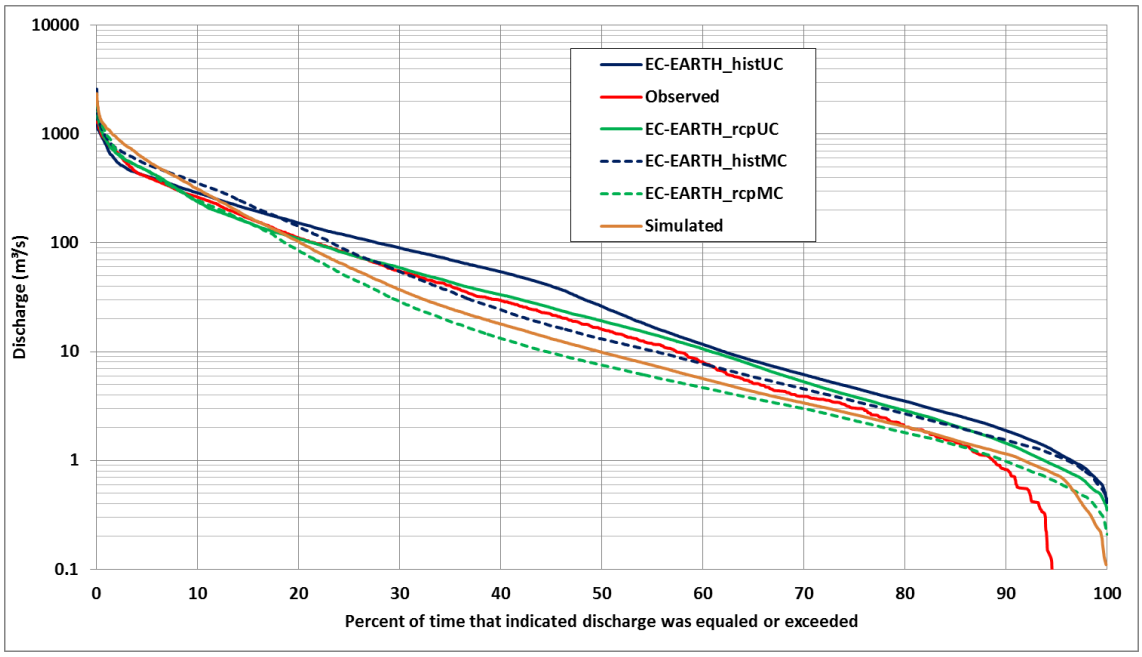

Figure 6.5: Flow duration curves of simulated discharges (historical (hist) (1980−2005) *(blue)*; future (rcp)(2020−2045) *(green)*; observed (1980−2005)*(red)*; simulated (1980−2005) *(orange)*; bias-corrected rcm simulations using linear scaling (MC) method *dashed blue and green*) with EC-EARTH as the driving model

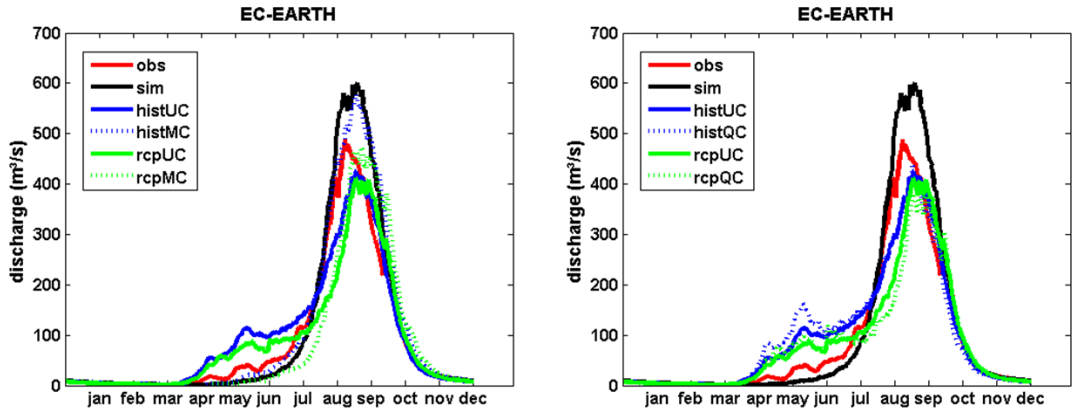

Figure 6.6: Annual cycle of discharges (historical (hist) (1980−2005) *(blue)*; future (rcp)(2020−2045) *(green)*; bias-corrected rcm simulations using linear scaling (MC) (−left) and quantile mapping (QC) (−right) methods *dashed blue and green*) using EC-EARTH as the driving model; observed (obs) (1980-2005) *(red)* and simulated discharges (sim) (1980−2005) *(black)*)

first discharge months (April−June) is evident in both the historical, observed and future discharges. The negative signal is maintained in the results from the bias corrected data. Both the MC and QC correction methods shows a negative discharge singnal in the future.

The MC bias correction method predicted lesser discharges in the low flows and higher discharges in the peak flows as compared the QC correction method (figure 6.6). This also shows the uncertainties in the bias correction methods.

6.4 The effects of CC on hydrology using ECHAM driving model

ECHAM is an atmospheric general circulation model, developed by the Max Planck Institute (MPI) for Meteorology and it forms the atmospheric component of the MPI−ESM. The current version is ECHAM6 which was used for this study. The FDC from this model (figure 6.7) shows a decrease in the future discharge as compared with the historical. The decrease is rather huge as compared with what the CanESM predicted. Overall, this model yields higher discharges in comparison with the other models. For example, the 25%, 50% and 75% exceedance probabilities give discharges of $400m^3/s$, $40m^3/s$ and $10m^3/s$ respectively.

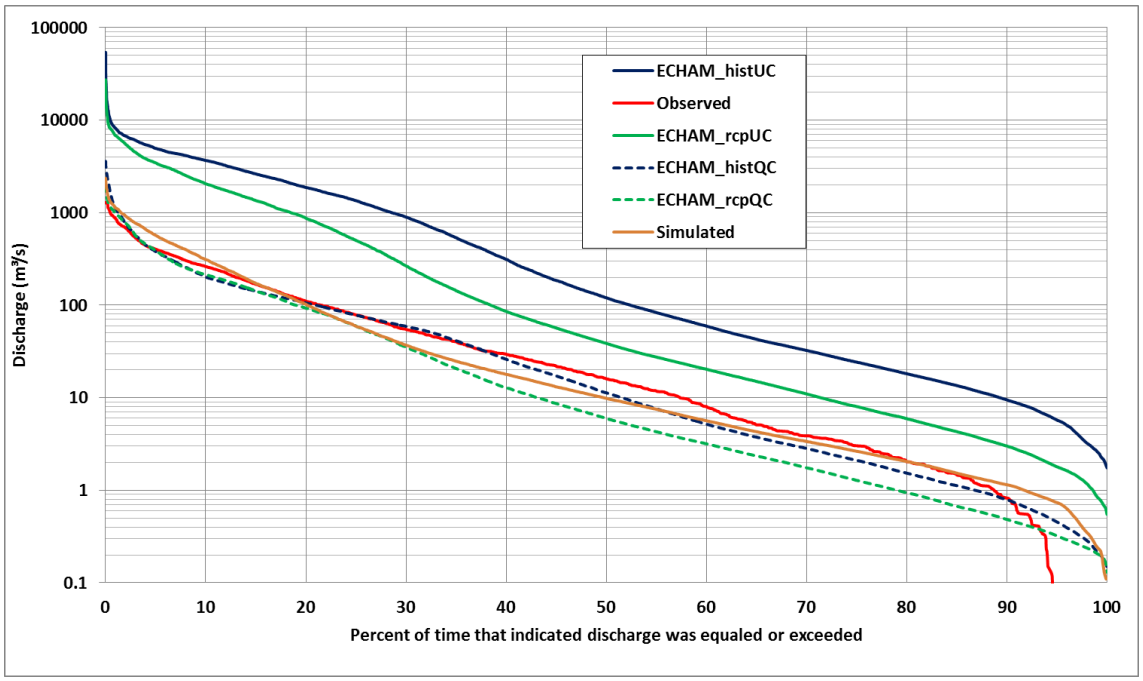

Figure 6.7: Flow duration curves of simulated discharges (historical (hist) (1980−2005) *(blue)*; future (rcp)(2020−2045) *(green)*; observed (1980−2005)*(red)*; simulated (1980−2005) *(orange)*; bias-corrected rcm simulations using Quantile mapping (QC) method *dashed blue and green*) with ECHAM as the driving model

The discharge curve obtained from the historical RCM simulations as input is far away from the discharge curve of the observations.

In figures 6.7 and 6.8 the curves obtained using corrected RCMs as input data yielded better results than the uncorrected RCM data. Both the two bias correction methods maintains the negative impact change signal as seen in figures 6.7 and 6.8. The decrease in the discharge narrows for high discharges (flows above $100m^3/s$) which occurs in 20% of the times.

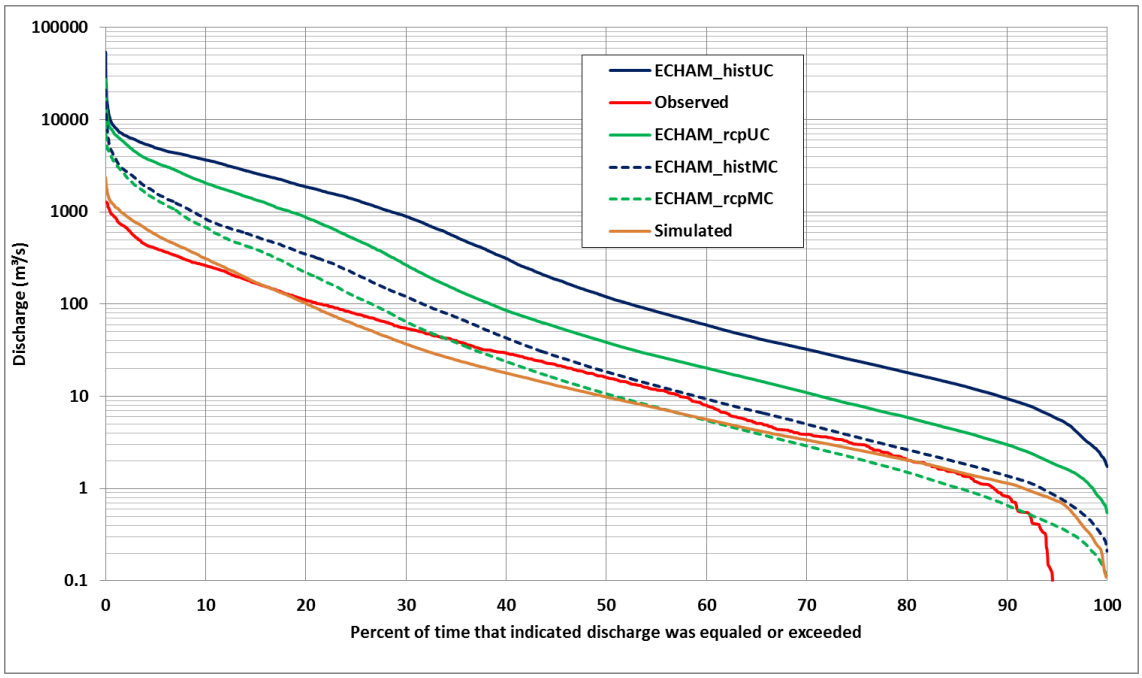

Figure 6.8: Flow duration curves of simulated discharges (historical (hist) (1980−2005) *(blue)*; future (rcp)(2020−2045) *(green)*; observed (1980−2005)*(red)*; simulated (1980−2005) *(orange)*; bias-corrected rcm simulations using linear scaling (MC) method *dashed blue and green*) with ECHAM as the driving model

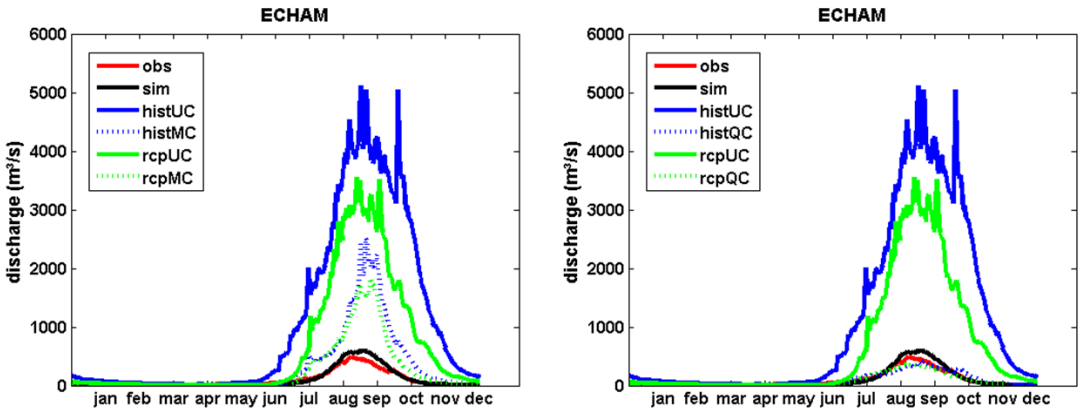

Figure 6.9: Annual cycle of discharges (historical (hist) (1980−2005) *(blue)*; future (rcp)(2020−2045) *(green)*; bias-corrected rcm simulations using linear scaling (MC) (−left) and quantile mapping (QC) (−right) methods *dashed blue and green*) using ECHAM as the driving model; observed (obs) (1980-2005) *(red)* and simulated discharges (sim) (1980−2005) *(black)*)

The historical discharge as a result of the correction using QC outperformed the discharge as a result of the MC correction method. The 50% exceedance probabilities for future un-

corrected, future corrected using MC method and future corrected using QC method are $40m^3/s$, $6m^3/s$ and $10m^3/s$ respectively.

The annual cycle (figure 6.9) also shows a decrease in the discharge in the future and a unimodal discharge cycle. Surprisingly, very huge discharges are the product of this driving model and can clearly be seen from figure 6.9 that whiles the peak discharge of the observed is about 600 m^3/s. That from the historical simulation is 4000 m^3/s, which is a clear overestimation of the discharge. The discharge cycle starts rather late (in June) and peaks in the middle of August. The high discrepancies and uncertainties resulting from the discharge for this driving model could be due to the higher spatial resolution (12 km) for this model as compared with the data from CORDEX, which has a resolution of 50 km.

The annual cycle again shows that the corrected data using QC method performed better than that using MC method as seen in figure6.9. Figure 6.9 also shows the bias corrected data performed better than the uncorrected data.

6.5 The effects of CC on hydrology using GFDL driving model

GFDL Climate and Earth System Models (GFDL−ESM) was developed by the Geophysical Fluid Dynamics Laboratory (GFDL) which is a laboratory in the National Oceanic and Atmospheric Administration (NOAA) office of Oceanic and Atmospheric Research (OAR) (www.gfdl.noaa.gov).

The flow duration curve that resulted from this model can be seen in figure 6.10. The uncorrected climate data shows a mixture of both an increased and decreased flow in the future as compared with the historical. In about 50% of the time, the flow for the future was less than that of the historical and vice versa. For 25% of the time a flow of 80 m^3/s was equaled or exceeded in the uncorrected data whiles 10 m^3/s is for 50% exceedance probability and 2 m^3/s is for 75% exceedance probability.

However, the discharges resulting from the corrected RCM simulations (figures 6.10 and 6.11 show a better results and a decrease in the future discharge as compared with the corrected historical simulations. The QC method corrected data performed better than the MC method. In 50% of the time, the discharges from the QC and MC method corrected data indicates that a discharge of $5m^3/s$ will be equaled or exceeded in the future as compared with $15-20m^3/s$ in the historical/present period.

The annual cycle shows a slight increase in the peak discharges for the future as compared with the historical (figure 6.12). The discharge for the historical period has similar flow pattern with the observed discharge but the peak discharge is almost doubled in the month of September. The month of the peak discharge is shifted from August in the observed discharge cycle to September in both the historical and future discharge cycles.

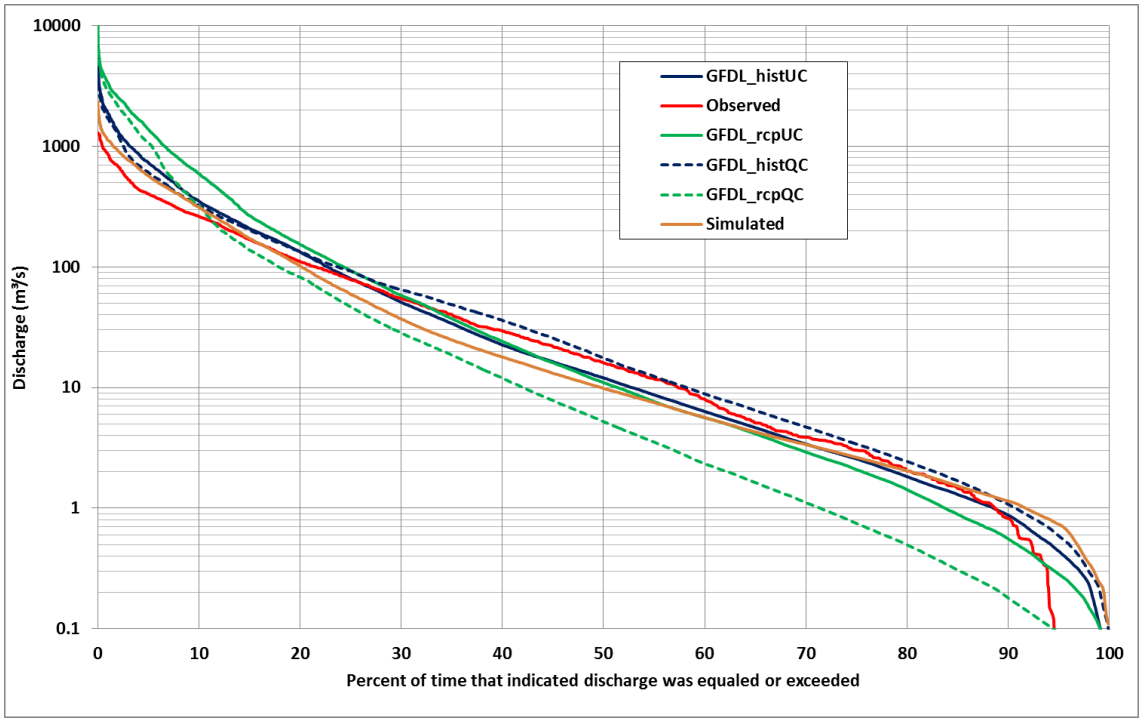

Figure 6.10: Flow duration curves of simulated discharges (historical (hist) (1980−2005) *(blue)*; future (rcp)(2020−2045) *(green)*; observed (1980−2005)*(red)*; simulated (1980−2005) *(orange)*; bias-corrected rcm simulations using Quantile mapping (QC) method *dashed blue and green*) with GFDL as the driving model

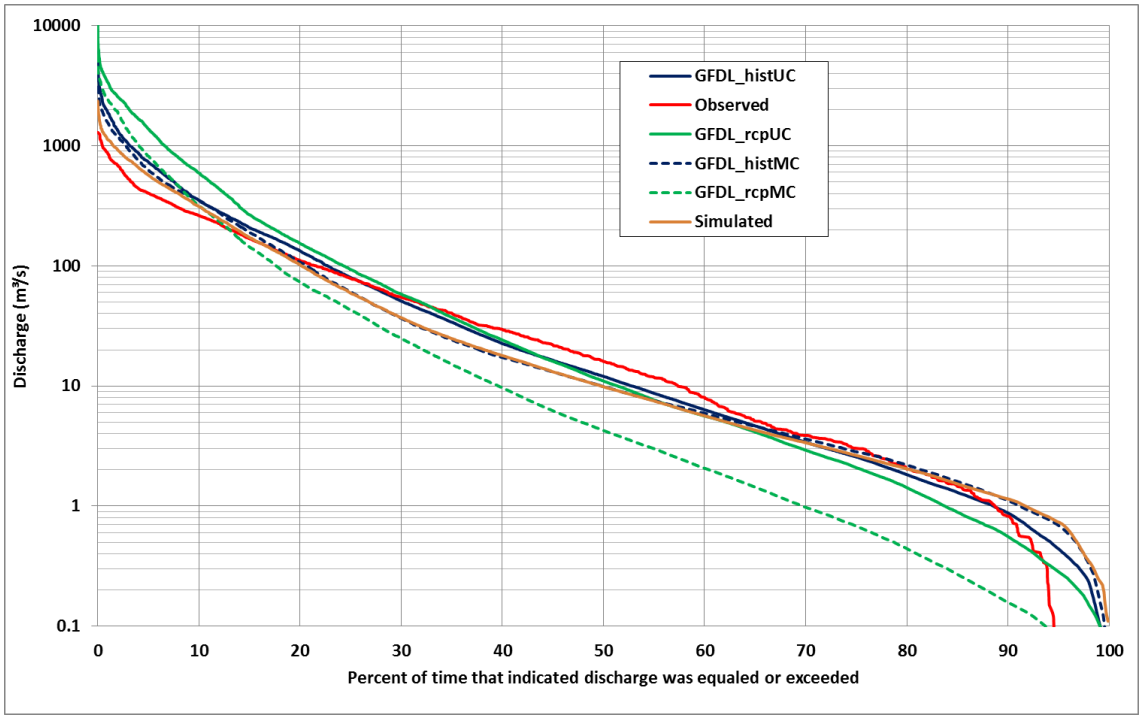

Figure 6.11: Flow duration curves of simulated discharges (historical (hist) (1980−2005) *(blue)*; future (rcp)(2020−2045) *(green)*; observed (1980−2005)*(red)*; simulated (1980−2005) *(orange)*; bias-corrected rcm simulations using linear scaling (MC) method *dashed blue and green*) with GFDL as the driving model

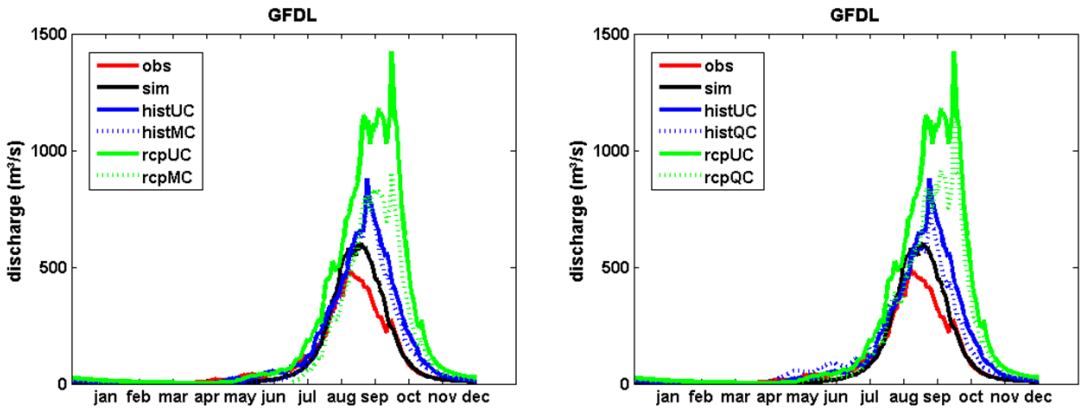

Figure 6.12: Annual cycle of discharges (historical (hist) (1980−2005) *(blue)*; future (rcp)(2020−2045) *(green)*; bias-corrected rcm simulations using linear scaling (MC) (−left) and quantile mapping (QC) (−right) methods *dashed blue and green*) using GFDL as the driving model; observed (obs) (1980-2005) *(red)* and simulated discharges (sim) (1980−2005) *(black)*)

6.6 The effects of CC on hydrology using MIROC driving model

MIROC is the climate model developed by the Center for Climate System Research in Japan. Figure 6.13 shows the flow duration curve obtained when the results of this model was used as the input to the hydrological model. From this driving model, it could be observed that the discharge/flow for the future will decrease as compared with the present and the amount decreased would be very high for the low flows (flows less than 100 m^3/s). The observed flow is better simulated by the historical simulations produced by the RCMs. The 25%, 50% and 75% exceedance probabilities produced discharges of 30 m^3/s, 6 m^3/s and 2 m^3/s respectively in the future.

The corrected data also predicts a negative impact signal on the hydrology of the catchment in the future (figures 6.13 and 6.14). The correction using quantile mapping method performed better than the linear scaling method for the historical corrected simulations. For the 50% exceedance probability, the QC and MC corrected future data predicts a discharge of $5m^3$/s as against a discharge of $10-20m^3$/s for the historical/present period.

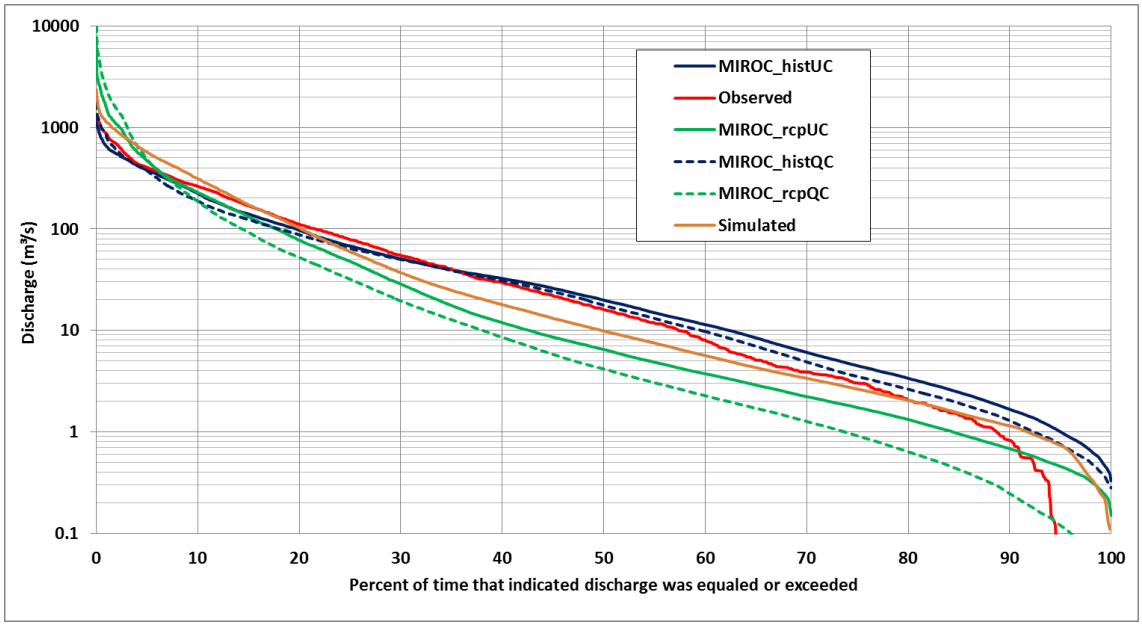

Figure 6.13: Flow duration curves of simulated discharges (historical (hist) (1980−2005) *(blue)*; future (rcp)(2020−2045) *(green)*; observed (1980−2005)*(red)*; simulated (1980−2005) *(orange)*; bias-corrected RCM simulations using Quantile mapping (QC) method *dashed blue and green*) with MIROC as the driving model

The annual discharge cycle (figure 6.15) for both the corrected and uncorrected data also shows the same decrease in flows for the future for the flows below $150m^3$/s from January to the middle of August. Then for the flows exceeding $300m^3$/s which occurs around August/September, there is an increase discharge for the future as compared with the present. It could therefore be concluded in this case that in the future, the dry periods becomes drier

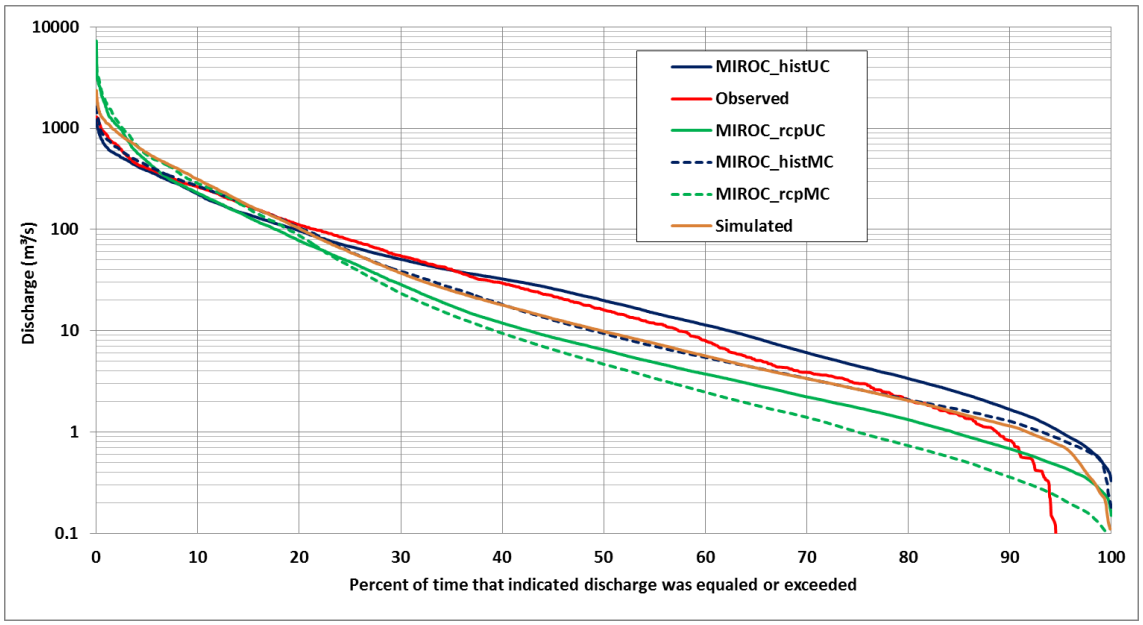

Figure 6.14: Flow duration curves of simulated discharges (historical (hist) (1980−2005) *(blue)*; future (rcp)(2020−2045) *(green)*; observed (1980−2005)*(red)*; simulated (1980−2005) *(orange)*; bias-corrected rcm simulations using linear scaling (MC) method *dashed blue and green*) with MIROC as the driving model

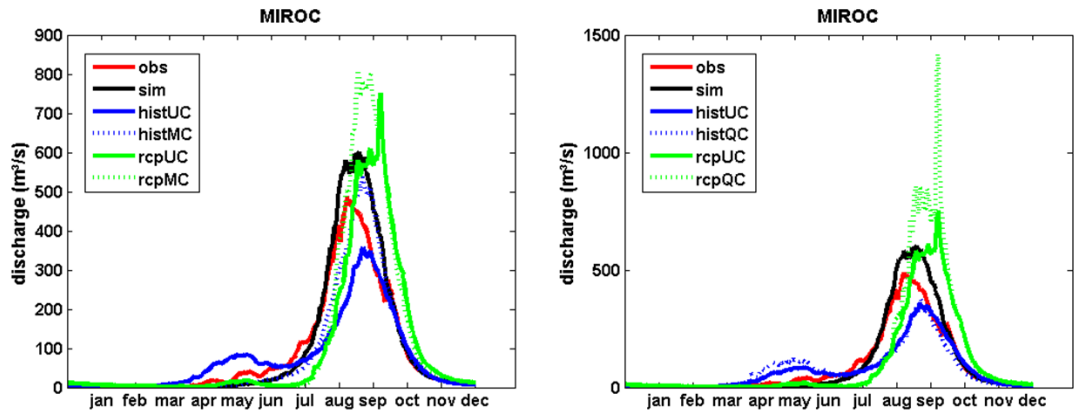

Figure 6.15: Annual cycle of discharges (historical (hist) (1980−2005) *(blue)*; future (rcp)(2020−2045) *(green)*; bias-corrected rcm simulations using linear scaling (MC) (−left) and quantile mapping (QC) (−right) methods *dashed blue and green*) using MIROC as the driving model; observed (obs) (1980-2005) *(red)* and simulated discharges (sim) (1980−2005) *(black)*)

and the wet periods become wetter with more extreme cases happening. The month for the peak discharge is shifted from August to September as seen in the observed discharge curve.

The future from this GCM driving model shows that from the months of November to April

there is very little flows and the rivers in the catchment virtually dries up. The flow begins to increase from the month of July which is very late as compared with the observed and historical cycle. This indicates a shorten discharge regime from 6−7 months to just 4 months which might have dire consequences on the agriculture, hydropower and water supply of the countries in this sub-region.

7 Summary and Conclusions

From the review of literature, it was undoubtful that climate change (*cc*) has already and will continue to have its footprint on the sub-region. And to ameliorate the impacts of *cc* on the hydrology and water resources of this region, a scientifically proven model and assessment needed to be done.

Again, for the proper management of the water resources in this area and for good policy decisions and investments in water related projects, the impact of *cc* on hydrology and water resources is very essential and crucial for the region. West Africa been a developing sub-region needs to make good and plausible decisions on water-related issues and management so as to acquire the needed and anticipated benefits from all investments made in this regard. It is imperative to stress that, the Bui hydropower which is in this sub-region constructed at a cost of 790 million US dollars for an installed capacity (IC) of 400 MW (source: www.buipower.com) is currently working to about 20% of the IC. This problem is mainly due to low levels of water in the reservoir. This could be as a result of *cc* on the hydrology and water resources of the sub-region which was not taken into account during the design and construction of the hydropower. To possibly avert this blunder in the future, there is the need to incorporate the effects of *cc* on all water related projects (wrp) in the region as to optimize the benefits of all wrps in the future.

Preliminary analysis of observed hydro-climatic data of the region showed that, results were in consonant with previous studies and research. The southern part of the catchment has a bi-modal rainfall cycle whiles the northern part shows a uni-modal cycle. Rainfall is influenced by the distance from the coast (ie northings) and it has a negative trend as one move away from the coast. There is a positive temperature trend towards the northern part of this region. The temperature difference throughout the year is very minimal (range: +34°C to +19°C). There is more vegetation in the southern part as compared to the north. The sub-region been in the lower to middle income economies has scarce meteorological and hydrological observed data.

Water balance analysis in this sub-region using the HBV model showed a good water balance for the Black Volta Catchment (size: 150,000 km^2) in this region. The lumped conceptual HBV model was able to capture and well predict the dynamics in the catchment. At the end, a good model performance was achieved by using different optimization and model performance measures. The optimization method which uses a combination of Nash Sutcliffe (NS) and the logarithm of the discharges (LogNS) achieved the most desirable results. The HBV rainfall-runoff model was able to react to signals with a fairly good performance. The weak point of the model is the overestimation of the peaks at certain times.

Climate change in the sub-region was investigated using five (5) different GCM driving models with the RCA4 RCM model and one GCM model with the WRF model using the

RCP4.5. Expectedly, all the driving models and RCMs showed an increase in the mean daily temperature for the future (2019 − 2045) as compared with the historical simulations (1979 − 2005). The temperature change ranged from +1.0°C to 2.5°C across the various driving models. The Canadian Earth System Model (CanESM2M) predicts a hotter climate in the future (increase of +2.5°C) whiles the EC-EARTH and GFDL models predicted an increase of 1.2°C each.

The bias corrected temperature RCM simulations for temperature yielded better results as compared with the uncorrected data and also reproduced the positive temperature change signal for all the models. For example, the mean daily temperature increase for the future was reduced from approximately +2°C in the uncorrected data to +1.6°C and +1°C in the linear scaling and quantile mapping methods of bias correction respectively for the ECHAM driving model. In all the models, the bias corrections reduced the future temperature increase with the quantile method predicting a moderate warmer future than the linear scaling method and the uncorrected data.

For precipitation change signal, the CanESM model doesn't show any clear change signal. The EC-EARTH, GFDL and the MIROC driving models predict a slight positive change signal in both the uncorrected and the bias corrected GCM/RCM simulations. On the other hand, the ECHAM model indicates a slight decrease in the future precipitation in both the uncorrected and bias corrected simulations. Therefore, the future precipitation change signal is difficult to predict for this catchment. However, this information should be used with caution because; only RCP4.5 climate scenario was used to arrive at this conclusion. Different GCM and RCM models with other climate scenarios need to be investigated in further studies.

Lastly, on the effects of these changes on the hydrology of the sub-region, four (4) (EC-EARTH, ECHAM, GFDL and MIROC) out of the five (5) models showed a clear decrease in discharge for the future. The decrease (negative impact) is more pronounced and clearer in the bias corrected data. Only the CanESM model showed an increase in the future discharge. It could therefore be concluded that climate change will negatively affect and impact the hydrology of this sub-region because there would be a decrease in the future discharge for the study area.

It is also worthwhile to state that the Quantile mapping bias correction method produced better results than the linear scaling method in most cases.

In conclusion, the study reveals that *cc* could negatively affect the hydrology of the sub-region. Therefore, proper adaptation and water resources management measures need to be put in place to mitigate or ameliorate the effects of *cc* on the hydrology and water resources of the region. It is also recommended for the region to possibly look for alternative sources of electricity, because, there would not be enough water in the reservoirs for Hydropower production in the future. The negative effects of *cc* on the water resources is also a regional security threat because, it may lead to loss of jobs, occupation and farming harvest. This may subsequently destabilize the already vulnerable sub-region and increase food insecurity and poverty. To mitigate food insecurity and poverty in the sub-region, more irrigation dams needs to be constructed to store the less future water resource for farming activities.

Lastly, the population of the sub-region is on the increase (growth rate: 2.5% per annum) and this puts additional stress on the scarce water resources. And, proper adaptation measures and solutions could help reduce the impact of cc on the hydrology of the region.

Bibliography

Emmanuel Kofi Agorsah. *An Ethnoarchaeological Analysis of Human Functional Dynamics in the Volta Basin of Ghana: Before and After the Akosombo Dam*, volume 2. Edwin Mellen Press, 2003.

Shakeel Ahmed and Ghislain De Marsily. Comparison of geostatistical methods for estimating transmissivity using data on transmissivity and specific capacity. *Water resources research*, 23(9):1717–1737, 1987.

BA Amisigo, N Van de Giesen, C Rogers, WEI Andah, and J Friesen. Monthly streamflow prediction in the volta basin of west africa: A siso narmax polynomial modelling. *Physics and Chemistry of the Earth, Parts A/B/C*, 33(1):141–150, 2008.

AN Amissah. De heer (1969). some possible climatic changes that may be caused by the volta lake. *Man-Made Lakes*, pages 73–82, 1969.

Jens Andersen, Jens C Refsgaard, and Karsten H Jensen. Distributed hydrological modelling of the senegal river basinmodel construction and validation. *Journal of Hydrology*, 247(3): 200–214, 2001.

HP Bailey and CW Johnson. Potential evapotranspiration in relation to annual waves of temperature. *Thornthwaite Memorial Volume I, Papers on Evapotranspiration and the Climatic. Water Balance*, pages 4–12, 1972.

A Bardossy and HJ Caspary. Detection of climate change in europe by analyzing european atmospheric circulation patterns from 1881 to 1989. *Theoretical and Applied Climatology*, 42 (3):155–167, 1990.

A. Bárdossy and S. K. Singh. Robust estimation of hydrological model parameters. *Hydrology and Earth System Sciences*, 12(6):1273–1283, 2008.

András Bárdossy. Lecture notes: Concepts of geostatistics, 2013.

András Bárdossy and Geoffrey Pegram. Downscaling precipitation using regional climate models and circulation patterns toward hydrology. *Water Resources Research*, 47(4), 2011.

András Bárdossy and Geoffrey Pegram. Multiscale spatial recorrelation of rcm precipitation to produce unbiased climate change scenarios over large areas and small. *Water Resources Research*, 48(9), 2012.

A Berg, N de Noblet-Ducoudré, Benjamin Sultan, Matthieu Lengaigne, and M Guimberteau. Projections of climate change impacts on potential c4 crop productivity over tropical regions. *Agricultural and Forest Meteorology*, 170:89–102, 2013.

S. Bergström. *The HBV model. In: Computer Models of Watershed Hydrology*. Water Resources Publications, Littleton, Colorado, USA, 1995.

S. Bergström and A. Forsman. Development of a conceptual deterministic rainfall-runoff model. *Nordic Hydrology*, 4:174–190, 1973.

Keith J Beven. *Rainfall-runoff modelling: the primer*. John Wiley & Sons, 2011.

Michela Biasutti, Adam H Sobel, and Suzana J Camargo. The role of the sahara low in summertime sahel rainfall variability and change in the cmip3 models. *Journal of Climate*, 22(21):5755–5771, 2009.

Paul J Block, Francisco Assis Souza Filho, Liqiang Sun, and Hyun-Han Kwon. A streamflow forecasting framework using multiple climate and hydrological models1, 2009.

J Boé, L Terray, F Habets, and E Martin. Statistical and dynamical downscaling of the seine basin climate for hydro-meteorological studies. *International Journal of Climatology*, 27(12): 1643–1655, 2007.

Jens H Christensen, Fredrik Boberg, Ole B Christensen, and Philippe Lucas-Picher. On the need for bias correction of regional climate change projections of temperature and precipitation. *Geophysical Research Letters*, 35(20), 2008.

JH Christensen and OB Christensen. Coauthors, 2007: Regional climate projections. climate change 2007: The physical science basis, s. solomon et al., eds.

Stewart J Cohen. Impacts of co2-induced climatic change on water resources in the great lakes basin. *Climatic Change*, 8(2):135–153, 1986.

Harald Cramér. *Mathematical methods of statistics*, volume 9. Princeton university press, 1945.

Noel Cressie. *Statistics for spatial data*. John Wiley & Sons, 2015.

M Déqué, DP Rowell, D Lüthi, F Giorgi, JH Christensen, B Rockel, D Jacob, Erik Kjellström, M De Castro, and BJJM van den Hurk. An intercomparison of regional climate simulations for europe: assessing uncertainties in model projections. *Climatic Change*, 81(1):53–70, 2007.

Olivier Dewitte, Arwyn Jones, Otto Spaargaren, Henrik Breuning-Madsen, Michel Brossard, Almami Dampha, Jozef Deckers, Tahar Gallali, Stephen Hallett, Robert Jones, et al. Harmonisation of the soil map of africa at the continental scale. *Geoderma*, 211:138–153, 2013.

Alain Dezetter, S Girard, Jean-Emmanuel Paturel, Gilles Mahé, Sandra Ardoin-Bardin, and Eric Servat. Simulation of runoff in west africa: Is there a single data-model combination that produces the best simulation results? *Journal of Hydrology*, 354(1):203–212, 2008.

Peter Droogers and Richard G Allen. Estimating reference evapotranspiration under inaccurate data conditions. *Irrigation and drainage systems*, 16(1):33–45, 2002.

Johannes J Feddema. Future african water resources: interactions between soil degradation and global warming. *Climatic change*, 42(3):561–596, 1999.

W Ferguson. Integrating crops and livestock in west africa. *FAO Animal Production and Health Paper*, 41, 1985.

BJ Garnier. A method of computing potential evapotranspiration in west africa. *Bulletin de l'Institut Français d'Afrique Noire*, 18(3):665–676, 1956.

S Giertz, C Hiepe, B Höllermann, and B Diekkrüger. Impacts of global change on water resources and soil degradation in benin. *Impacts of global change on the hydrological cycle in West and Northwest Africa. Springer, Berlin (accepted for publication)*, 2010.

Filippo Giorgi, Colin Jones, Ghassem R Asrar, et al. Addressing climate information needs at the regional level: the cordex framework. *World Meteorological Organization (WMO) Bulletin*, 58(3):175, 2009.

Jens Götzinger. *Distributed conceptual hydrological modelling-simulation of climate, land use change impact and uncertainty analysis*. PhD thesis, University of Stuttgart, Germany, 2007.

Hoshin V Gupta, Harald Kling, Koray K Yilmaz, and Guillermo F Martinez. Decomposition of the mean squared error and nse performance criteria: Implications for improving hydrological modelling. *Journal of Hydrology*, 377(1):80–91, 2009.

George H Hargreaves. Estimation of potential and crop evapotranspiration. *Transactions of the ASAE*, 17(4):701–0704, 1974.

George H Hargreaves and Richard G Allen. History and evaluation of hargreaves evapotranspiration equation. *Journal of Irrigation and Drainage Engineering*, 129(1):53–63, 2003.

Dominikus Heinzeller, Cornelia Klein, Joel Arnault, Jan Bliefernicht, Luitpold Hingerl, and Harald Kunstmann. On the bias correction of forcing global model data for regional climate simulations over west africa. In *EGU General Assembly Conference Abstracts*, volume 16, page 1151, 2014.

Yeshewatesfa Hundecha and András Bárdossy. Modeling of the effect of land use changes on the runoff generation of a river basin through parameter regionalization of a watershed model. *Journal of Hydrology*, 292(1):281–295, 2004.

Boubacar Ibrahim, Harouna Karambiri, Jan Polcher, Hamma Yacouba, and Pierre Ribstein. Changes in rainfall regime over burkina faso under the climate change conditions simulated by 5 regional climate models. *Climate Dynamics*, 42(5-6):1363–1381, 2014.

Amor VM Ines and James W Hansen. Bias correction of daily gcm rainfall for crop simulation studies. *Agricultural and forest meteorology*, 138(1):44–53, 2006.

Fiona Johnson and Ashish Sharma. Accounting for interannual variability: A comparison of options for water resources climate change impact assessments. *Water Resources Research*, 47(4), 2011.

AM Joubert and BC Hewitson. Simulating present and future climates of southern africa using general circulation models. *Progress in physical geography*, 21(1):51–78, 1997.

Gerlinde Jung. *Regional climate change and the impact on hydrology in the Volta Basin of West Africa*. PhD thesis, University of Augsburg, Germany, 2006.

Gerlinde Jung and Harald Kunstmann. High-resolution regional climate modeling for the volta region of west africa. *Journal of Geophysical Research: Atmospheres*, 112(D23), 2007.

Gerlinde Jung, Sven Wagner, and Harald Kunstmann. Joint climate–hydrology modeling: an impact study for the data-sparse environment of the volta basin in west africa. *Hydrology Research*, 43(3):231–248, 2012.

Kwabena Kankam-Yeboah, Emmanuel Obuobie, Barnabas Amisigo, and Yaw Opoku-Ankomah. Impact of climate change on streamflow in selected river basins in ghana. *Hydrological Sciences Journal*, 58(4):773–788, 2013.

Raymond Abudu Kasei. Ecology and development series no. 69, 2010. 2010.

B Kortatsi. Ghana water resources management study. *Information Building Block*, 1997.

H Kunstmann and G Jung. Impact of regional climate change on water availability in the volta basin of west africa. regional hydrological impacts of climate variability and change. In *Proceedings of symposium S6 for the seventh IAHS scientific assembly. Foz de Iguacu, Brazil*, 2005.

René Laprise, Leticia Hernández-Díaz, Kossivi Tete, Laxmi Sushama, Leo Šeparović, Andrey Martynov, Katja Winger, and Michel Valin. Climate projections over cordex africa domain using the fifth-generation canadian regional climate model (crcm5). *Climate Dynamics*, 41 (11-12):3219–3246, 2013.

Luc Le Barbé, Thierry Lebel, and Dominique Tapsoba. Rainfall variability in west africa during the years 1950-90. *Journal of climate*, 15(2):187–202, 2002.

Thierry Lebel and Abdou Ali. Recent trends in the central and western sahel rainfall regime (1990–2007). *Journal of Hydrology*, 375(1):52–64, 2009.

Göran Lindström, Barbro Johansson, Magnus Persson, Marie Gardelin, and Sten Bergström. Development and test of the distributed hbv-96 hydrological model. *Journal of hydrology*, 201(1):272–288, 1997.

Gil Mahe, G Lienou, Luc Descroix, F Bamba, Jean-Emmanuel Paturel, Alain Laraque, M Meddi, H Habaieb, O Adeaga, Claudine Dieulin, et al. The rivers of africa: witness of climate change and human impact on the environment. *Hydrological Processes*, 27(15): 2105–2114, 2013.

John Russell Mather. *The measurement of potential evapotranspiration*. Johns Hopkins University, Laboratory of Climatology, 1954.

Gregory J McCabe Jr. A parabolic function to modify thornthwaite estimates of potential evapotranspiration for the eastern united states. *Physical Geography*, 10(2):176–189, 1989.

Matthew McCartney, Gerald Forkuor, Aditya Sood, Barnabas Amisigo, Fred Hattermann, and Lal Muthuwatta. *The water resource implications of changing climate in the Volta River Basin*, volume 146. IWMI, 2012.

Richard H Moss, Jae A Edmonds, Kathy A Hibbard, Martin R Manning, Steven K Rose, Detlef P Van Vuuren, Timothy R Carter, Seita Emori, Mikiko Kainuma, Tom Kram, et al. The next generation of scenarios for climate change research and assessment. *Nature*, 463 (7282):747–756, 2010.

Freddy Nachtergaele and Niels Batjes. *Harmonized world soil database*. FAO Rome, Italy, 2012.

Rebekka Neumann, Gerlinde Jung, Patrick Laux, and Harald Kunstmann. Climate trends of temperature, precipitation and river discharge in the volta basin of west africa. *International Journal of River Basin Management*, 5(1):17–30, 2007.

Sharon E Nicholson. The nature of rainfall variability over africa on time scales of decades to millenia. *Global and planetary change*, 26(1):137–158, 2000.

Sharon E Nicholson, B Some, J McCollum, E Nelkin, D Klotter, Y Berte, BM Diallo, I Gaye, G Kpabeba, O Ndiaye, et al. Validation of trmm and other rainfall estimates with a high-density gauge dataset for west africa. part ii: Validation of trmm rainfall products. *Journal of Applied Meteorology*, 42(10):1355–1368, 2003.

Hélène Niel, Jean-Emmanuel Paturel, and Eric Servat. Study of parameter stability of a lumped hydrologic model in a context of climatic variability. *Journal of Hydrology*, 278(1): 213–230, 2003.

Grigory Nikulin, Colin Jones, Filippo Giorgi, Ghassem Asrar, Matthias Büchner, Ruth Cerezo-Mota, Ole Bøssing Christensen, Michel Déqué, Jesus Fernandez, Andreas Hänsler, et al. Precipitation climatology in an ensemble of cordex-africa regional climate simulations. *Journal of Climate*, 25(18):6057–6078, 2012.

Philip G Oguntunde, Jan Friesen, Nick van de Giesen, and Hubert HG Savenije. Hydroclimatology of the volta river basin in west africa: trends and variability from 1901 to 2002. *Physics and Chemistry of the Earth, Parts A/B/C*, 31(18):1180–1188, 2006.

Y Opoku-Ankomah and BA Amisigo. Rainfall and runoff variability in the southwestern river system of ghana. *Variabilité Des Ressources en Eau en Afrique Au XXème Siècle*, (252): 307, 1998.

Heiko Paeth, Nicholas MJ Hall, Miguel Angel Gaertner, Marta Dominguez Alonso, Sounmaïla Moumouni, Jan Polcher, Paolo M Ruti, Andreas H Fink, Marielle Gosset, Thierry Lebel, et al. Progress in regional downscaling of west african precipitation. *Atmospheric science letters*, 12(1):75–82, 2011.

CM Patricola and KH Cook. Sub-saharan northern african climate at the end of the twenty-first century: forcing factors and climate change processes. *Climate dynamics*, 37(5-6):1165–1188, 2011.

JE Paturel, M Ouedraogo, G Mahé, E Servat, A Dezetter, and S Ardoin. The influence of distributed input data on the hydrological modelling of monthly river flow regimes in west africa. *Hydrological sciences journal*, 48(6):881–890, 2003.

Geoffrey Pegram and András Bárdossy. Downscaling regional circulation model rainfall to gauge sites using recorrelation and circulation pattern dependent quantile–quantile transforms for quantifying climate change. *Journal of Hydrology*, 504:142–159, 2013.

WL Pelton, KM King, and CB Tanner. An evaluation of the thornthwaite and mean temperature methods for determining potential evapotranspiration. *Agronomy Journal*, 52(7): 387–395, 1960.

H L_ Penman. Estimating evaporation. *Eos, Transactions American Geophysical Union*, 37(1): 43–50, 1956.

Howard Latimer Penman. Natural evaporation from open water, bare soil and grass. In *Proceedings of the Royal Society of London A: Mathematical, Physical and Engineering Sciences*, volume 193, pages 120–145. The Royal Society, 1948.

C Piani, JO Haerter, and E Coppola. Statistical bias correction for daily precipitation in regional climate models over europe. *Theoretical and Applied Climatology*, 99(1-2):187–192, 2010.

R Rojas, L Feyen, A Dosio, and D Bavera. Improving pan-european hydrological simulation of extreme eventsthrough statistical bias correction of rcm-driven climatesimulations. *Hydrology and Earth System Sciences*, 15(8):2599, 2011.

Norman J Rosenberg, Blaine L Blad, and Shashi B Verma. *Microclimate: the biological environment*. John Wiley & Sons, 1983.

Philippe Roudier, Agnès Ducharne, and Luc Feyen. Climate change impacts on runoff in west africa: a review. *Hydrol. Earth Syst. Sci.*, 18:2789–2801, 2014.

Greg J Schoenau and Robert A Kehrig. Method for calculating degree-days to any base temperature. *Energy and Buildings*, 14(4):299–302, 1990.

J Sennikovs and U Bethers. Statistical downscaling method of regional climate model results for hydrological modelling. In *Proc. 18 th World IMACS/MODSIM Congress, Cairns, Australia*. Citeseer, 2009.

Mamdouh Shahin. *Hydrology and water resources of Africa*, volume 41. Springer Science & Business Media, 2006.

Salamatu Shaibu, Samuel Nii Odai, Kwaku Amaning Adjei, Edward Matthew Osei, and Frank Ohene Annor. Simulation of runoff for the black volta basin using satellite observation data. *International journal of river basin management*, 10(3):245–254, 2012.

Shailesh Kumar Singh and András Bárdossy. Calibration of hydrological models on hydrologically unusual events. *Advances in Water Resources*, 38:81–91, 2012.

Susan Solomon. *Climate change 2007-the physical science basis: Working group I contribution to the fourth assessment report of the IPCC*, volume 4. Cambridge University Press, 2007.

Peter Speth, Michael Christoph, and Bernd Diekkrüger. *Impacts of global change on the hydrological cycle in West and Northwest Africa*. Springer Science & Business Media, 2010.

TF Stocker, D Qin, GK Plattner, M Tignor, SK Allen, J Boschung, A Nauels, Y Xia, B Bex, and BM Midgley. Ipcc, 2013: climate change 2013: the physical science basis. contribution of working group i to the fifth assessment report of the intergovernmental panel on climate change. 2013.

Fubao Sun, Michael L Roderick, Wee Ho Lim, and Graham D Farquhar. Hydroclimatic projections for the murray-darling basin based on an ensemble derived from intergovernmental panel on climate change ar4 climate models. *Water Resources Research*, 47(12), 2011.

Karl E Taylor, Ronald J Stouffer, and Gerald A Meehl. A summary of the cmip5 experiment design. *PCDMI Rep*, 33, 2009.

W Terink, RTWL Hurkmans, PJJF Torfs, and R Uijlenhoet. Bias correction of temperature and precipitation data for regional climate model application to the rhine basin. *Hydrology and Earth System Sciences Discussions*, 6(4):5377–5413, 2009.

Claudia Teutschbein and Jan Seibert. Regional climate models for hydrological impact studies at the catchment scale: a review of recent modeling strategies. *Geography Compass*, 4 (7):834–860, 2010.

Claudia Teutschbein and Jan Seibert. Bias correction of regional climate model simulations for hydrological climate-change impact studies: Review and evaluation of different methods. *Journal of Hydrology*, 456:12–29, 2012.

HCS Thom. Seasonal degree-day statistics for the united states 1. *Monthly Weather Review*, 80(9):143–147, 1952.

Herbert CS Thom. A note on the gamma distribution. *Monthly Weather Review*, 86(4):117–122, 1958.

Charles Warren Thornthwaite. An approach toward a rational classification of climate. *Geographical review*, 38(1):55–94, 1948.

A Trabucco and RJ Zomer. Global aridity index (global-aridity) and global potential evapotranspiration (global-pet) geospatial database. *CGIAR Consortium for Spatial Information. Published online, available from the CGIAR-CSI GeoPortal at: http://www. csi. cgiar. org/(2009). Global Aridity Index (Global-Aridity) and Global Potential Evapo-Transpiration (Global-PET) Geospatial Database. In. CGIAR Consortium for Spatial Information*, 2009.

Antonio Trabucco, Robert J Zomer, Deborah A Bossio, Oliver van Straaten, and Louis V Verchot. Climate change mitigation through afforestation/reforestation: a global analysis of hydrologic impacts with four case studies. *Agriculture, ecosystems & environment*, 126 (1):81–97, 2008.

Olli Varis, Tommi Kajander, and Risto Lemmelä. Climate and water: from climate models to water resources management and vice versa. *Climatic Change*, 66(3):321–344, 2004.

Nicolas Vigaud, Pascal Roucou, Bernard Fontaine, Sivarajan Sijikumar, and Sophie Tyteca. Wrf/arpege-climat simulated climate trends over west africa. *Climate dynamics*, 36(5-6): 925–944, 2011.

NR Viney, JM Perraud, J Vaze, FHS Chiew, DA Post, and A Yang. The usefulness of bias constraints in model calibration for regionalisation to ungauged catchments. In *18th World IMACS Congress and MODSIM09 International Congress on Modelling and Simulation*, pages 13–17. Modelling and Simulation Society of Australia and New Zealand and International Association for Mathematics and Computers in Simulation: Cairns, 2009.

Sven Wagner. *Water balance in a poorly gauged basin in West Africa using atmospheric modelling and remote sensing information*. PhD thesis, University of Stuttgart, Germany, 2008.

IG Watterson and MR Dix. Simulated changes due to global warming in daily precipitation means and extremes and their interpretation using the gamma distribution. *Journal of Geophysical Research: Atmospheres*, 108(D13), 2003.

Institut für Wasser- und Umweltsystemmodellierung
Universität Stuttgart

Pfaffenwaldring 61
70569 Stuttgart (Vaihingen)
Telefon (0711) 685 - 64717/64749/64752/64679
Telefax (0711) 685 - 67020 o. 64746 o. 64681
E-Mail: iws@iws.uni-stuttgart.de
http://www.iws.uni-stuttgart.de

Direktoren
Prof. Dr. rer. nat. Dr.-Ing. András Bárdossy
Prof. Dr.-Ing. Rainer Helmig
Prof. Dr.-Ing. Silke Wieprecht
Prof. Dr.-Ing. Wolfgang Nowak

Vorstand *(Stand 1.3.2016)*
Prof. Dr. rer. nat. Dr.-Ing. A. Bárdossy
Prof. Dr.-Ing. R. Helmig
Prof. Dr.-Ing. S. Wieprecht
Prof. Dr. J.A. Sander Huisman
Jürgen Braun, PhD
apl. Prof. Dr.-Ing. H. Class
Dr.-Ing. H.-P. Koschitzky
Dr.-Ing. M. Noack
Prof. Dr.-Ing. W. Nowak
Dr. rer. nat. J. Seidel
Dr.-Ing. K. Terheiden
Dr.-Ing. habil. Sergey Oladyshkin

Emeriti
Prof. Dr.-Ing. habil. Dr.-Ing. E.h. Jürgen Giesecke
Prof. Dr.h.c. Dr.-Ing. E.h. Helmut Kobus, PhD

Lehrstuhl für Wasserbau und Wassermengenwirtschaft
Leiter: Prof. Dr.-Ing. Silke Wieprecht
Stellv.: Dr.-Ing. Kristina Terheiden
Versuchsanstalt für Wasserbau
Leiter: Dr.-Ing. Markus Noack

Lehrstuhl für Hydromechanik und Hydrosystemmodellierung
Leiter: Prof. Dr.-Ing. Rainer Helmig
Stellv.: apl. Prof. Dr.-Ing. Holger Class

Lehrstuhl für Hydrologie und Geohydrologie
Leiter: Prof. Dr. rer. nat. Dr.-Ing. András Bárdossy
Stellv.: Dr. rer. nat. Jochen Seidel
Hydrogeophysik der Vadosen Zone
(mit Forschungszentrum Jülich)
Leiter: Prof. Dr. J.A. Sander Huisman

Lehrstuhl für Stochastische Simulation und Sicherheitsforschung für Hydrosysteme
Leiter: Prof. Dr.-Ing. Wolfgang Nowak
Stellv.: Dr.-Ing. habil. Sergey Oladyshkin

***VEGAS,* Versuchseinrichtung zur Grundwasser- und Altlastensanierung**
Leitung: Jürgen Braun, PhD, AD
Dr.-Ing. Hans-Peter Koschitzky, AD

Verzeichnis der Mitteilungshefte

1 Röhnisch, Arthur: *Die Bemühungen um eine Wasserbauliche Versuchsanstalt an der Technischen Hochschule Stuttgart*, und
Fattah Abouleid, Abdel: *Beitrag zur Berechnung einer in lockeren Sand gerammten, zweifach verankerten Spundwand*, 1963

2 Marotz, Günter: *Beitrag zur Frage der Standfestigkeit von dichten Asphaltbelägen im Großwasserbau*, 1964

3 Gurr, Siegfried: *Beitrag zur Berechnung zusammengesetzter ebener Flächentragwerke unter besonderer Berücksichtigung ebener Stauwände, mit Hilfe von Randwert- und Lastwertmatrizen*, 1965

4 Plica, Peter: *Ein Beitrag zur Anwendung von Schalenkonstruktionen im Stahlwasserbau*, und

Petrikat, Kurt: *Möglichkeiten und Grenzen des wasserbaulichen Versuchswesens*, 1966

5 Plate, Erich: *Beitrag zur Bestimmung der Windgeschwindigkeitsverteilung in der durch eine Wand gestörten bodennahen Luftschicht*,
und
Röhnisch, Arthur; Marotz, Günter: *Neue Baustoffe und Bauausführungen für den Schutz der Böschungen und der Sohle von Kanälen, Flüssen und Häfen; Gestehungskosten und jeweilige Vorteile*, sowie
Unny, T.E.: *Schwingungsuntersuchungen am Kegelstrahlschieber*, 1967

6 Seiler, Erich: *Die Ermittlung des Anlagenwertes der bundeseigenen Binnenschiffahrtsstraßen und Talsperren und des Anteils der Binnenschiffahrt an diesem Wert*, 1967

7 *Sonderheft anläßlich des 65. Geburtstages von Prof. Arthur Röhnisch mit Beiträgen von* Benk, Dieter; Breitling, J.; Gurr, Siegfried; Haberhauer, Robert; Honekamp, Hermann; Kuz, Klaus Dieter; Marotz, Günter; Mayer-Vorfelder, Hans-Jörg; Miller, Rudolf; Plate, Erich J.; Radomski, Helge; Schwarz, Helmut; Vollmer, Ernst; Wildenhahn, Eberhard; 1967

8 Jumikis, Alfred: *Beitrag zur experimentellen Untersuchung des Wassernachschubs in einem gefrierenden Boden und die Beurteilung der Ergebnisse*, 1968

9 Marotz, Günter: *Technische Grundlagen einer Wasserspeicherung im natürlichen Untergrund*, 1968

10 Radomski, Helge: *Untersuchungen über den Einfluß der Querschnittsform wellenförmiger Spundwände auf die statischen und rammtechnischen Eigenschaften*, 1968

11 Schwarz, Helmut: *Die Grenztragfähigkeit des Baugrundes bei Einwirkung vertikal gezogener Ankerplatten als zweidimensionales Bruchproblem*, 1969

12 Erbel, Klaus: *Ein Beitrag zur Untersuchung der Metamorphose von Mittelgebirgsschneedecken unter besonderer Berücksichtigung eines Verfahrens zur Bestimmung der thermischen Schneequalität*, 1969

13 Westhaus, Karl-Heinz: *Der Strukturwandel in der Binnenschiffahrt und sein Einfluß auf den Ausbau der Binnenschiffskanäle*, 1969

14 Mayer-Vorfelder, Hans-Jörg: *Ein Beitrag zur Berechnung des Erdwiderstandes unter Ansatz der logarithmischen Spirale als Gleitflächenfunktion*, 1970

15 Schulz, Manfred: *Berechnung des räumlichen Erddruckes auf die Wandung kreiszylindrischer Körper*, 1970

16 Mobasseri, Manoutschehr: *Die Rippenstützmauer. Konstruktion und Grenzen ihrer Standsicherheit*, 1970

17 Benk, Dieter: *Ein Beitrag zum Betrieb und zur Bemessung von*

Hochwasserrückhaltebecken, 1970

18 Gàl, Attila: *Bestimmung der mitschwingenden Wassermasse bei überströmten Fischbauchklappen mit kreiszylindrischem Staublech*, 1971, vergriffen

19 Kuz, Klaus Dieter: *Ein Beitrag zur Frage des Einsetzens von Kavitationserscheinungen in einer Düsenströmung bei Berücksichtigung der im Wasser gelösten Gase*, 1971, vergriffen

20 Schaak, Hartmut: *Verteilleitungen von Wasserkraftanlagen*, 1971

21 *Sonderheft zur Eröffnung der neuen Versuchsanstalt des Instituts für Wasserbau der Universität Stuttgart mit Beiträgen von* Brombach, Hansjörg; Dirksen, Wolfram; Gàl, Attila; Gerlach, Reinhard; Giesecke, Jürgen; Holthoff, Franz-Josef; Kuz, Klaus Dieter; Marotz, Günter; Minor, Hans-Erwin; Petrikat, Kurt; Röhnisch, Arthur; Rueff, Helge; Schwarz, Helmut; Vollmer, Ernst; Wildenhahn, Eberhard; 1972

22 Wang, Chung-su: *Ein Beitrag zur Berechnung der Schwingungen an Kegelstrahlschiebern*, 1972

23 Mayer-Vorfelder, Hans-Jörg: *Erdwiderstandsbeiwerte nach dem Ohde-Variationsverfahren*, 1972

24 Minor, Hans-Erwin: *Beitrag zur Bestimmung der Schwingungsanfachungsfunktionen überströmter Stauklappen*, 1972, vergriffen

25 Brombach, Hansjörg: *Untersuchung strömungsmechanischer Elemente (Fluidik) und die Möglichkeit der Anwendung von Wirbelkammerelementen im Wasserbau*, 1972, vergriffen

26 Wildenhahn, Eberhard: *Beitrag zur Berechnung von Horizontalfilterbrunnen*, 1972

27 Steinlein, Helmut: *Die Eliminierung der Schwebstoffe aus Flußwasser zum Zweck der unterirdischen Wasserspeicherung, gezeigt am Beispiel der Iller*, 1972

28 Holthoff, Franz Josef: *Die Überwindung großer Hubhöhen in der Binnenschiffahrt durch Schwimmerhebewerke*, 1973

29 Röder, Karl: *Einwirkungen aus Baugrundbewegungen auf trog- und kastenförmige Konstruktionen des Wasser- und Tunnelbaues*, 1973

30 Kretschmer, Heinz: *Die Bemessung von Bogenstaumauern in Abhängigkeit von der Talform*, 1973

31 Honekamp, Hermann: *Beitrag zur Berechnung der Montage von Unterwasserpipelines*, 1973

32 Giesecke, Jürgen: *Die Wirbelkammertriode als neuartiges Steuerorgan im Wasserbau*, und
Brombach, Hansjörg: *Entwicklung, Bauformen, Wirkungsweise und Steuereigenschaften von Wirbelkammerverstärkern*, 1974

33 Rueff, Helge: *Untersuchung der schwingungserregenden Kräfte an zwei hintereinander angeordneten Tiefschützen unter besonderer Berücksichtigung von Kavitation*, 1974

34 Röhnisch, Arthur: *Einpreßversuche mit Zementmörtel für Spannbeton - Vergleich der Ergebnisse von Modellversuchen mit Ausführungen in Hüllwellrohren*, 1975

35 *Sonderheft anläßlich des 65. Geburtstages von Prof. Dr.-Ing. Kurt Petrikat mit Beiträgen von*: Brombach, Hansjörg; Erbel, Klaus; Flinspach, Dieter; Fischer jr., Richard; Gàl, Attila; Gerlach, Reinhard; Giesecke, Jürgen; Haberhauer, Robert; Hafner Edzard; Hausenblas, Bernhard; Horlacher, Hans-Burkhard; Hutarew, Andreas; Knoll, Manfred; Krummet, Ralph; Marotz, Günter; Merkle, Theodor; Miller, Christoph; Minor, Hans-Erwin; Neumayer, Hans; Rao, Syamala; Rath, Paul; Rueff, Helge; Ruppert, Jürgen; Schwarz, Wolfgang; Topal-Gökceli, Mehmet; Vollmer, Ernst; Wang, Chung-su; Weber, Hans-Georg; 1975

36 Berger, Jochum: *Beitrag zur Berechnung des Spannungszustandes in rotationssymmetrisch belasteten Kugelschalen veränderlicher Wandstärke unter Gas- und Flüssigkeitsdruck durch Integration schwach singulärer Differentialgleichungen*, 1975

37 Dirksen, Wolfram: *Berechnung instationärer Abflußvorgänge in gestauten Gerinnen mittels Differenzenverfahren und die Anwendung auf Hochwasserrückhaltebecken*, 1976

38 Horlacher, Hans-Burkhard: *Berechnung instationärer Temperatur- und Wärmespannungsfelder in langen mehrschichtigen Hohlzylindern*, 1976

39 Hafner, Edzard: *Untersuchung der hydrodynamischen Kräfte auf Baukörper im Tiefwasserbereich des Meeres*, 1977, ISBN 3-921694-39-6

40 Ruppert, Jürgen: *Über den Axialwirbelkammerverstärker für den Einsatz im Wasserbau*, 1977, ISBN 3-921694-40-X

41 Hutarew, Andreas: *Beitrag zur Beeinflußbarkeit des Sauerstoffgehalts in Fließgewässern an Abstürzen und Wehren*, 1977, ISBN 3-921694-41-8, vergriffen

42 Miller, Christoph: *Ein Beitrag zur Bestimmung der schwingungserregenden Kräfte an unterströmten Wehren*, 1977, ISBN 3-921694-42-6

43 Schwarz, Wolfgang: *Druckstoßberechnung unter Berücksichtigung der Radial- und Längsverschiebungen der Rohrwandung*, 1978, ISBN 3-921694-43-4

44 Kinzelbach, Wolfgang: *Numerische Untersuchungen über den optimalen Einsatz variabler Kühlsysteme einer Kraftwerkskette am Beispiel Oberrhein*, 1978, ISBN 3-921694-44-2

45 Barczewski, Baldur: *Neue Meßmethoden für Wasser-Luftgemische und deren Anwendung auf zweiphasige Auftriebsstrahlen*, 1979, ISBN 3-921694-45-0

46 Neumayer, Hans: *Untersuchung der Strömungsvorgänge in radialen Wirbelkammerverstärkern*, 1979, ISBN 3-921694-46-9

47 Elalfy, Youssef-Elhassan: *Untersuchung der Strömungsvorgänge in Wirbelkammerdioden und -drosseln*, 1979, ISBN 3-921694-47-7

48 Brombach, Hansjörg: *Automatisierung der Bewirtschaftung von Wasserspeichern*, 1981, ISBN 3-921694-48-5

49 Geldner, Peter: *Deterministische und stochastische Methoden zur Bestimmung der Selbstdichtung von Gewässern*, 1981, ISBN 3-921694-49-3, vergriffen

50 Mehlhorn, Hans: *Temperaturveränderungen im Grundwasser durch Brauchwassereinleitungen*, 1982, ISBN 3-921694-50-7, vergriffen

51 Hafner, Edzard: *Rohrleitungen und Behälter im Meer*, 1983, ISBN 3-921694-51-5

52 Rinnert, Bernd: *Hydrodynamische Dispersion in porösen Medien: Einfluß von Dichteunterschieden auf die Vertikalvermischung in horizontaler Strömung*, 1983, ISBN 3-921694-52-3, vergriffen

53 Lindner, Wulf: *Steuerung von Grundwasserentnahmen unter Einhaltung ökologischer Kriterien*, 1983, ISBN 3-921694-53-1, vergriffen

54 Herr, Michael; Herzer, Jörg; Kinzelbach, Wolfgang; Kobus, Helmut; Rinnert, Bernd: *Methoden zur rechnerischen Erfassung und hydraulischen Sanierung von Grundwasserkontaminationen*, 1983, ISBN 3-921694-54-X

55 Schmitt, Paul: *Wege zur Automatisierung der Niederschlagsermittlung*, 1984, ISBN 3-921694-55-8, vergriffen

56 Müller, Peter: *Transport und selektive Sedimentation von Schwebstoffen bei gestautem Abfluß*, 1985, ISBN 3-921694-56-6

57 El-Qawasmeh, Fuad: *Möglichkeiten und Grenzen der Tropfbewässerung unter besonderer Berücksichtigung der Verstopfungsanfälligkeit der Tropfelemente*, 1985, ISBN 3-921694-57-4, vergriffen

58 Kirchenbaur, Klaus: *Mikroprozessorgesteuerte Erfassung instationärer Druckfelder am Beispiel seegangsbelasteter Baukörper*, 1985, ISBN 3-921694-58-2

59 Kobus, Helmut (Hrsg.): *Modellierung des großräumigen Wärme- und Schadstofftransports im Grundwasser*, Tätigkeitsbericht 1984/85 (DFG-Forschergruppe an den Universitäten Hohenheim, Karlsruhe und Stuttgart), 1985, ISBN 3-921694-59-0, vergriffen

60 Spitz, Karlheinz: *Dispersion in porösen Medien: Einfluß von Inhomogenitäten und Dichteunterschieden*, 1985, ISBN 3-921694-60-4, vergriffen

61 Kobus, Helmut: *An Introduction to Air-Water Flows in Hydraulics*, 1985, ISBN 3-921694-61-2

62 Kaleris, Vassilios: *Erfassung des Austausches von Oberflächen- und Grundwasser in horizontalebenen Grundwassermodellen*, 1986, ISBN 3-921694-62-0

63 Herr, Michael: *Grundlagen der hydraulischen Sanierung verunreinigter Porengrundwasserleiter*, 1987, ISBN 3-921694-63-9

64 Marx, Walter: *Berechnung von Temperatur und Spannung in Massenbeton infolge Hydratation*, 1987, ISBN 3-921694-64-7

65 Koschitzky, Hans-Peter: *Dimensionierungskonzept für Sohlbelüfter in Schußrinnen zur Vermeidung von Kavitationsschäden*, 1987, ISBN 3-921694-65-5

66 Kobus, Helmut (Hrsg.): *Modellierung des großräumigen Wärme- und Schadstofftransports im Grundwasser*, Tätigkeitsbericht 1986/87 (DFG-Forschergruppe an den Universitäten Hohenheim, Karlsruhe und Stuttgart) 1987, ISBN 3-921694-66-3

67 Söll, Thomas: *Berechnungsverfahren zur Abschätzung anthropogener Temperaturanomalien im Grundwasser*, 1988, ISBN 3-921694-67-1

68 Dittrich, Andreas; Westrich, Bernd: *Bodenseeufererosion, Bestandsaufnahme und Bewertung*, 1988, ISBN 3-921694-68-X, vergriffen

69 Huwe, Bernd; van der Ploeg, Rienk R.: *Modelle zur Simulation des Stickstoffhaushaltes von Standorten mit unterschiedlicher landwirtschaftlicher Nutzung*, 1988, ISBN 3-921694-69-8, vergriffen

70 Stephan, Karl: *Integration elliptischer Funktionen*, 1988, ISBN 3-921694-70-1

71 Kobus, Helmut; Zilliox, Lothaire (Hrsg.): *Nitratbelastung des Grundwassers, Auswirkungen der Landwirtschaft auf die Grundwasser- und Rohwasserbeschaffenheit und Maßnahmen zum Schutz des Grundwassers*. Vorträge des deutsch-französischen Kolloquiums am 6. Oktober 1988, Universitäten Stuttgart und Louis Pasteur Strasbourg (Vorträge in deutsch oder französisch, Kurzfassungen zweisprachig), 1988, ISBN 3-921694-71-X

72 Soyeaux, Renald: *Unterströmung von Stauanlagen auf klüftigem Untergrund unter Berücksichtigung laminarer und turbulenter Fließzustände*,1991, ISBN 3-921694-72-8

73 Kohane, Roberto: *Berechnungsmethoden für Hochwasserabfluß in Fließgewässern mit überströmten Vorländern*, 1991, ISBN 3-921694-73-6

74 Hassinger, Reinhard: *Beitrag zur Hydraulik und Bemessung von Blocksteinrampen in flexibler Bauweise*, 1991, ISBN 3-921694-74-4, vergriffen

75 Schäfer, Gerhard: *Einfluß von Schichtenstrukturen und lokalen Einlagerungen auf die Längsdispersion in Porengrundwasserleitern*, 1991, ISBN 3-921694-75-2

76 Giesecke, Jürgen: *Vorträge, Wasserwirtschaft in stark besiedelten Regionen; Umweltforschung mit Schwerpunkt Wasserwirtschaft*, 1991, ISBN 3-921694-76-0

77 Huwe, Bernd: *Deterministische und stochastische Ansätze zur Modellierung des Stickstoffhaushalts landwirtschaftlich genutzter Flächen auf unterschiedlichem Skalenniveau*, 1992, ISBN 3-921694-77-9, vergriffen

78 Rommel, Michael: *Verwendung von Kluftdaten zur realitätsnahen Generierung von Kluftnetzen mit anschließender laminar-turbulenter Strömungsberechnung*, 1993, ISBN 3-92 1694-78-7

79 Marschall, Paul: *Die Ermittlung lokaler Stofffrachten im Grundwasser mit Hilfe von Einbohrloch-Meßverfahren*, 1993, ISBN 3-921694-79-5, vergriffen

80 Ptak, Thomas: *Stofftransport in heterogenen Porenaquiferen: Felduntersuchungen und stochastische Modellierung*, 1993, ISBN 3-921694-80-9, vergriffen

81 Haakh, Frieder: *Transientes Strömungsverhalten in Wirbelkammern,* 1993, ISBN 3-921694-81-7

82 Kobus, Helmut; Cirpka, Olaf; Barczewski, Baldur; Koschitzky, Hans-Peter: *Versucheinrichtung zur Grundwasser und Altlastensanierung VEGAS, Konzeption und Programmrahmen*, 1993, ISBN 3-921694-82-5

83 Zang, Weidong: *Optimaler Echtzeit-Betrieb eines Speichers mit aktueller Abflußregenerierung*, 1994, ISBN 3-921694-83-3, vergriffen

84 Franke, Hans-Jörg: *Stochastische Modellierung eines flächenhaften Stoffeintrages und Transports in Grundwasser am Beispiel der Pflanzenschutzmittelproblematik*, 1995, ISBN 3-921694-84-1

85 Lang, Ulrich: *Simulation regionaler Strömungs- und Transportvorgänge in Karstaquiferen mit Hilfe des Doppelkontinuum-Ansatzes: Methodenentwicklung und Parameteridentifikation*, 1995, ISBN 3-921694-85-X, vergriffen

86 Helmig, Rainer: *Einführung in die Numerischen Methoden der Hydromechanik*, 1996, ISBN 3-921694-86-8, vergriffen

87 Cirpka, Olaf: *CONTRACT: A Numerical Tool for Contaminant Transport and Chemical Transformations - Theory and Program Documentation* -, 1996, ISBN 3-921694-87-6

88 Haberlandt, Uwe: *Stochastische Synthese und Regionalisierung des Niederschlages für Schmutzfrachtberechnungen*, 1996, ISBN 3-921694-88-4

89 Croisé, Jean: *Extraktion von flüchtigen Chemikalien aus natürlichen Lockergesteinen mittels erzwungener Luftströmung*, 1996, ISBN 3-921694-89-2, vergriffen

90 Jorde, Klaus: *Ökologisch begründete, dynamische Mindestwasserregelungen bei Ausleitungskraftwerken*, 1997, ISBN 3-921694-90-6, vergriffen

91 Helmig, Rainer: *Gekoppelte Strömungs- und Transportprozesse im Untergrund - Ein Beitrag zur Hydrosystemmodellierung*-, 1998, ISBN 3-921694-91-4, vergriffen

92 Emmert, Martin: *Numerische Modellierung nichtisothermer Gas-Wasser Systeme in porösen Medien,* 1997, ISBN 3-921694-92-2

93 Kern, Ulrich: *Transport von Schweb- und Schadstoffen in staugeregelten Fließgewässern am Beispiel des Neckars*, 1997, ISBN 3-921694-93-0, vergriffen

94 Förster, Georg: *Druckstoßdämpfung durch große Luftblasen in Hochpunkten von Rohrleitungen 1997*, ISBN 3-921694-94-9

95 Cirpka, Olaf: *Numerische Methoden zur Simulation des reaktiven Mehrkomponententransports im Grundwasser*, 1997, ISBN 3-921694-95-7, vergriffen

96 Färber, Arne: *Wärmetransport in der ungesättigten Bodenzone: Entwicklung einer thermischen In-situ-Sanierungstechnologie*, 1997, ISBN 3-921694-96-5

97 Betz, Christoph: *Wasserdampfdestillation von Schadstoffen im porösen Medium: Entwicklung einer thermischen In-situ-Sanierungstechnologie*, 1998, ISBN 3-921694-97-3

98 Xu, Yichun: *Numerical Modeling of Suspended Sediment Transport in Rivers*, 1998, ISBN 3-921694-98-1, vergriffen

99 Wüst, Wolfgang: *Geochemische Untersuchungen zur Sanierung CKW-kontaminierter Aquifere mit Fe(0)-Reaktionswänden,* 2000, ISBN 3-933761-02-2

100 Sheta, Hussam: *Simulation von Mehrphasenvorgängen in porösen Medien unter Einbeziehung von Hysterese-Effekten*, 2000, ISBN 3-933761-03-4

101 Ayros, Edwin: *Regionalisierung extremer Abflüsse auf der Grundlage statistischer Verfahren*, 2000, ISBN 3-933761-04-2, vergriffen

102 Huber, Ralf: *Compositional Multiphase Flow and Transport in Heterogeneous Porous Media*, 2000, ISBN 3-933761-05-0

103 Braun, Christopherus: *Ein Upscaling-Verfahren für Mehrphasenströmungen in porösen Medien*, 2000, ISBN 3-933761-06-9

104 Hofmann, Bernd: *Entwicklung eines rechnergestützten Managementsystems zur Beurteilung von Grundwasserschadensfällen*, 2000, ISBN 3-933761-07-7

105 Class, Holger: *Theorie und numerische Modellierung nichtisothermer Mehrphasenprozesse in NAPL-kontaminierten porösen Medien,* 2001, ISBN 3-933761-08-5

106 Schmidt, Reinhard: *Wasserdampf- und Heißluftinjektion zur thermischen Sanierung kontaminierter Standorte*, 2001, ISBN 3-933761-09-3

107 Josef, Reinhold:, *Schadstoffextraktion mit hydraulischen Sanierungsverfahren unter Anwendung von grenzflächenaktiven Stoffen*, 2001, ISBN 3-933761-10-7

108 Schneider, Matthias: *Habitat- und Abflussmodellierung für Fließgewässer mit unscharfen Berechnungsansätzen*, 2001, ISBN 3-933761-11-5

109 Rathgeb, Andreas: *Hydrodynamische Bemessungsgrundlagen für Lockerdeckwerke an überströmbaren Erddämmen*, 2001, ISBN 3-933761-12-3

110 Lang, Stefan: *Parallele numerische Simulation instätionärer Probleme mit adaptiven Methoden auf unstrukturierten Gittern*, 2001, ISBN 3-933761-13-1

111 Appt, Jochen; Stumpp Simone: *Die Bodensee-Messkampagne 2001, IWS/CWR Lake Constance Measurement Program 2001*, 2002, ISBN 3-933761-14-X

112 Heimerl, Stephan: *Systematische Beurteilung von Wasserkraftprojekten,* 2002, ISBN 3-933761-15-8, vergriffen

113 Iqbal, Amin: *On the Management and Salinity Control of Drip Irrigation,* 2002, ISBN 3-933761-16-6

114 Silberhorn-Hemminger, Annette: *Modellierung von Kluftaquifersystemen: Geostatistische Analyse und deterministisch-stochastische Kluftgenerierung,* 2002, ISBN 3-933761-17-4

115 Winkler, Angela: *Prozesse des Wärme- und Stofftransports bei der In-situ-Sanierung mit festen Wärmequellen,* 2003, ISBN 3-933761-18-2

116 Marx, Walter: *Wasserkraft, Bewässerung, Umwelt - Planungs- und Bewertungsschwerpunkte der Wasserbewirtschaftung,* 2003, ISBN 3-933761-19-0

117 Hinkelmann, Reinhard: *Efficient Numerical Methods and Information-Processing Techniques in Environment Water,* 2003, ISBN 3-933761-20-4

118 Samaniego-Eguiguren, Luis Eduardo: *Hydrological Consequences of Land Use / Land Cover and Climatic Changes in Mesoscale Catchments*, 2003, ISBN 3-933761-21-2

119 Neunhäuserer, Lina: *Diskretisierungsansätze zur Modellierung von Strömungs- und Transportprozessen in geklüftet-porösen Medien*, 2003, ISBN 3-933761-22-0

120 Paul, Maren: *Simulation of Two-Phase Flow in Heterogeneous Poros Media with Adaptive Methods*, 2003, ISBN 3-933761-23-9

121 Ehret, Uwe: *Rainfall and Flood Nowcasting in Small Catchments using Weather Radar*, 2003, ISBN 3-933761-24-7

122 Haag, Ingo: *Der Sauerstoffhaushalt staugeregelter Flüsse am Beispiel des Neckars - Analysen, Experimente, Simulationen -,* 2003, ISBN 3-933761-25-5

123 Appt, Jochen: *Analysis of Basin-Scale Internal Waves in Upper Lake Constance,* 2003, ISBN 3-933761-26-3

124 Hrsg.: Schrenk, Volker; Batereau, Katrin; Barczewski, Baldur; Weber, Karolin und Koschitzky, Hans-Peter: *Symposium Ressource Fläche und VEGAS - Statuskolloquium 2003, 30. September und 1. Oktober 2003,* 2003, ISBN 3-933761-27-1

125 Omar Khalil Ouda: *Optimisation of Agricultural Water Use: A Decision Support System for the Gaza Strip,* 2003, ISBN 3-933761-28-0

126 Batereau, Katrin: *Sensorbasierte Bodenluftmessung zur Vor-Ort-Erkundung von Schadensherden im Untergrund*, 2004, ISBN 3-933761-29-8

127 Witt, Oliver: *Erosionsstabilität von Gewässersedimenten mit Auswirkung auf den Stofftransport bei Hochwasser am Beispiel ausgewählter Stauhaltungen des Oberrheins*, 2004, ISBN 3-933761-30-1

128 Jakobs, Hartmut: *Simulation nicht-isothermer Gas-Wasser-Prozesse in komplexen Kluft-Matrix-Systemen*, 2004, ISBN 3-933761-31-X

129 Li, Chen-Chien: *Deterministisch-stochastisches Berechnungskonzept zur Beurteilung der Auswirkungen erosiver Hochwasserereignisse in Flussstauhaltungen,* 2004, ISBN 3-933761-32-8

130 Reichenberger, Volker; Helmig, Rainer; Jakobs, Hartmut; Bastian, Peter; Niessner, Jennifer: *Complex Gas-Water Processes in Discrete Fracture-Matrix Systems: Up-scaling, Mass-Conservative Discretization and Efficient Multilevel Solution,* 2004, ISBN 3-933761-33-6

131 Hrsg.: Barczewski, Baldur; Koschitzky, Hans-Peter; Weber, Karolin; Wege, Ralf: *VEGAS - Statuskolloquium 2004,* Tagungsband zur Veranstaltung am 05. Oktober 2004 an der Universität Stuttgart, Campus Stuttgart-Vaihingen, 2004, ISBN 3-933761-34-4

132 Asie, Kemal Jabir: *Finite Volume Models for Multiphase Multicomponent Flow through Porous Media*. 2005, ISBN 3-933761-35-2

133 Jacoub, George: *Development of a 2-D Numerical Module for Particulate Contaminant Transport in Flood Retention Reservoirs and Impounded Rivers,* 2004, ISBN 3-933761-36-0

134 Nowak, Wolfgang: *Geostatistical Methods for the Identification of Flow and Transport Parameters in the Subsurface,* 2005, ISBN 3-933761-37-9

135 Süß, Mia: *Analysis of the influence of structures and boundaries on flow and transport processes in fractured porous media*, 2005, ISBN 3-933761-38-7

136 Jose, Surabhin Chackiath: *Experimental Investigations on Longitudinal Dispersive Mixing in Heterogeneous Aquifers,* 2005, ISBN: 3-933761-39-5

137 Filiz, Fulya: *Linking Large-Scale Meteorological Conditions to Floods in Mesoscale Catchments,* 2005, ISBN 3-933761-40-9

138 Qin, Minghao: *Wirklichkeitsnahe und recheneffiziente Ermittlung von Temperatur und Spannungen bei großen RCC-Staumauern*, 2005, ISBN 3-933761-41-7

139 Kobayashi, Kenichiro: *Optimization Methods for Multiphase Systems in the Subsurface - Application to Methane Migration in Coal Mining Areas*, 2005, ISBN 3-933761-42-5

140 Rahman, Md. Arifur: *Experimental Investigations on Transverse Dispersive Mixing in Heterogeneous Porous Media,* 2005, ISBN 3-933761-43-3

141 Schrenk, Volker: *Ökobilanzen zur Bewertung von Altlastensanierungsmaßnahmen,* 2005, ISBN 3-933761-44-1

142 Hundecha, Hirpa Yeshewatesfa: *Regionalization of Parameters of a Conceptual Rainfall-Runoff Model*, 2005, ISBN: 3-933761-45-X

143 Wege, Ralf: *Untersuchungs- und Überwachungsmethoden für die Beurteilung natürlicher Selbstreinigungsprozesse im Grundwasser,* 2005, ISBN 3-933761-46-8

144 Breiting, Thomas: *Techniken und Methoden der Hydroinformatik - Modellierung von komplexen Hydrosystemen im Untergrund*, 2006, 3-933761-47-6

145 Hrsg.: Braun, Jürgen; Koschitzky, Hans-Peter; Müller, Martin: *Ressource Untergrund: 10 Jahre VEGAS: Forschung und Technologieentwicklung zum Schutz von Grundwasser und Boden,* Tagungsband zur Veranstaltung am 28. und 29. September 2005 an der Universität Stuttgart, Campus Stuttgart-Vaihingen, 2005, ISBN 3-933761-48-4

146 Rojanschi, Vlad: *Abflusskonzentration in mesoskaligen Einzugsgebieten unter Berücksichtigung des Sickerraumes,* 2006, ISBN 3-933761-49-2

147 Winkler, Nina Simone: *Optimierung der Steuerung von Hochwasserrückhaltebecken-systemen,* 2006, ISBN 3-933761-50-6

148 Wolf, Jens: *Räumlich differenzierte Modellierung der Grundwasserströmung alluvialer Aquifere für mesoskalige Einzugsgebiete*, 2006, ISBN: 3-933761-51-4

149 Kohler, Beate: *Externe Effekte der Laufwasserkraftnutzung*, 2006, ISBN 3-933761-52-2

150 Hrsg.: Braun, Jürgen; Koschitzky, Hans-Peter; Stuhrmann, Matthias: *VEGAS-Statuskolloquium 2006,* Tagungsband zur Veranstaltung am 28. September 2006 an der Universität Stuttgart, Campus Stuttgart-Vaihingen, 2006, ISBN 3-933761-53-0

151 Niessner, Jennifer: *Multi-Scale Modeling of Multi-Phase - Multi-Component Processes in Heterogeneous Porous Media*, 2006, ISBN 3-933761-54-9

152 Fischer, Markus: *Beanspruchung eingeerdeter Rohrleitungen infolge Austrocknung bindiger Böden,* 2006, ISBN 3-933761-55-7

153 Schneck, Alexander: *Optimierung der Grundwasserbewirtschaftung unter Berücksichtigung der Belange der Wasserversorgung, der Landwirtschaft und des Naturschutzes*, 2006, ISBN 3-933761-56-5

154 Das, Tapash: *The Impact of Spatial Variability of Precipitation on the Predictive Uncertainty of Hydrological Models,* 2006, ISBN 3-933761-57-3

155 Bielinski, Andreas: *Numerical Simulation of CO_2 sequestration in geological formations*, 2007, ISBN 3-933761-58-1

156 Mödinger, Jens: *Entwicklung eines Bewertungs- und Entscheidungsunterstützungssystems für eine nachhaltige regionale Grundwasserbewirtschaftung*, 2006, ISBN 3-933761-60-3

157 Manthey, Sabine: *Two-phase flow processes with dynamic effects in porous media - parameter estimation and simulation,* 2007, ISBN 3-933761-61-1

158 Pozos Estrada, Oscar: *Investigation on the Effects of Entrained Air in Pipelines,* 2007, ISBN 3-933761-62-X

159 Ochs, Steffen Oliver: *Steam injection into saturated porous media – process analysis including experimental and numerical investigations*, 2007, ISBN 3-933761-63-8

160 Marx, Andreas: *Einsatz gekoppelter Modelle und Wetterradar zur Abschätzung von Niederschlagsintensitäten und zur Abflussvorhersage, 2007,* ISBN 3-933761-64-6

161 Hartmann, Gabriele Maria: *Investigation of Evapotranspiration Concepts in Hydrological Modelling for Climate Change Impact Assessment*, 2007, ISBN 3-933761-65-4

162 Kebede Gurmessa, Tesfaye: *Numerical Investigation on Flow and Transport Characteristics to Improve Long-Term Simulation of Reservoir Sedimentation*, 2007, ISBN 3-933761-66-2

163 Trifković, Aleksandar: *Multi-objective and Risk-based Modelling Methodology for Planning, Design and Operation of Water Supply Systems*, 2007, ISBN 3-933761-67-0

164 Götzinger, Jens: *Distributed Conceptual Hydrological Modelling - Simulation of Climate, Land Use Change Impact and Uncertainty Analysis*, 2007, ISBN 3-933761-68-9

165 Hrsg.: Braun, Jürgen; Koschitzky, Hans-Peter; Stuhrmann, Matthias: *VEGAS – Kolloquium 2007,* Tagungsband zur Veranstaltung am 26. September 2007 an der Universität Stuttgart, Campus Stuttgart-Vaihingen, 2007, ISBN 3-933761-69-7

166 Freeman, Beau: *Modernization Criteria Assessment for Water Resources Planning; Klamath Irrigation Project, U.S.*, 2008, ISBN 3-933761-70-0

167 Dreher, Thomas: *Selektive Sedimentation von Feinstschwebstoffen in Wechselwirkung mit wandnahen turbulenten Strömungsbedingungen*, 2008, ISBN 3-933761-71-9

168 Yang, Wei: *Discrete-Continuous Downscaling Model for Generating Daily Precipitation Time Series*, 2008, ISBN 3-933761-72-7

169 Kopecki, Ianina: *Calculational Approach to FST-Hemispheres for Multiparametrical Benthos Habitat Modelling,* 2008*,* ISBN 3-933761-73-5

170 Brommundt, Jürgen: *Stochastische Generierung räumlich zusammenhängender Niederschlagszeitreihen*, 2008, ISBN 3-933761-74-3

171 Papafotiou, *Alexandros: Numerical Investigations of the Role of Hysteresis in Heterogeneous Two-Phase Flow Systems*, 2008, ISBN 3-933761-75-1

172 He, Yi: *Application of a Non-Parametric Classification Scheme to Catchment Hydrology*, 2008, ISBN 978-3-933761-76-7

173 Wagner, Sven: *Water Balance in a Poorly Gauged Basin in West Africa Using Atmospheric Modelling and Remote Sensing Information*, 2008, ISBN 978-3-933761-77-4

174 Hrsg.: Braun, Jürgen; Koschitzky, Hans-Peter; Stuhrmann, Matthias; Schrenk, Volker: *VEGAS-Kolloquium 2008 Ressource Fläche III*, Tagungsband zur Veranstaltung am 01. Oktober 2008 an der Universität Stuttgart, Campus Stuttgart-Vaihingen, 2008, ISBN 978-3-933761-78-1

175 Patil, Sachin: *Regionalization of an Event Based Nash Cascade Model for Flood Predictions in Ungauged Basins*, 2008, ISBN 978-3-933761-79-8

176 Assteerawatt, Anongnart: *Flow and Transport Modelling of Fractured Aquifers based on a Geostatistical Approach,* 2008, ISBN 978-3-933761-80-4

177 Karnahl, Joachim Alexander: *2D numerische Modellierung von multifraktionalem Schwebstoff- und Schadstofftransport in Flüssen*, 2008, ISBN 978-3-933761-81-1

178 Hiester, Uwe: *Technologieentwicklung zur In-situ-Sanierung der ungesättigten Bodenzone mit festen Wärmequellen,* 2009, ISBN 978-3-933761-82-8

179 Laux, Patrick: *Statistical Modeling of Precipitation for Agricultural Planning in the Volta Basin of West Africa,* 2009, ISBN 978-3-933761-83-5

180 Ehsan, Saqib: *Evaluation of Life Safety Risks Related to Severe Flooding,* 2009, ISBN 978-3-933761-84-2

181 Prohaska, Sandra: *Development and Application of a 1D Multi-Strip Fine Sediment Transport Model for Regulated Rivers,* 2009, ISBN 978-3-933761-85-9

182 Kopp, Andreas: *Evaluation of CO_2 Injection Processes in Geological Formations for Site Screening,* 2009, ISBN 978-3-933761-86-6

183 Ebigbo, Anozie: *Modelling of biofilm growth and its influence on CO_2 and water (two-phase) flow in porous media,* 2009, ISBN 978-3-933761-87-3

184 Freiboth, Sandra: *A phenomenological model for the numerical simulation of multiphase multicomponent processes considering structural alterations of porous media*, 2009, ISBN 978-3-933761-88-0

185 Zöllner, Frank: *Implementierung und Anwendung netzfreier Methoden im Konstruktiven Wasserbau und in der Hydromechanik*, 2009, ISBN 978-3-933761-89-7

186 Vasin, Milos: *Influence of the soil structure and property contrast on flow and transport in the unsaturated zone*, 2010, ISBN 978-3-933761-90-3

187 Li, Jing: *Application of Copulas as a New Geostatistical Tool*, 2010, ISBN 978-3-933761-91-0

188 AghaKouchak, Amir: *Simulation of Remotely Sensed Rainfall Fields Using Copulas*, 2010, ISBN 978-3-933761-92-7

189 Thapa, Pawan Kumar: *Physically-based spatially distributed rainfall runoff modelling for soil erosion estimation*, 2010, ISBN 978-3-933761-93-4

190 Wurms, Sven: *Numerische Modellierung der Sedimentationsprozesse in Retentionsanlagen zur Steuerung von Stoffströmen bei extremen Hochwasserabflussereignissen*, 2011, ISBN 978-3-933761-94-1

191 Merkel, Uwe: *Unsicherheitsanalyse hydraulischer Einwirkungen auf Hochwasserschutzdeiche und Steigerung der Leistungsfähigkeit durch adaptive Strömungsmodellierung*, 2011, ISBN 978-3-933761-95-8

192 Fritz, Jochen: *A Decoupled Model for Compositional Non-Isothermal Multiphase Flow in Porous Media and Multiphysics Approaches for Two-Phase Flow*, 2010, ISBN 978-3-933761-96-5

193 Weber, Karolin (Hrsg.): *12. Treffen junger WissenschaftlerInnen an Wasserbauinstituten*, 2010, ISBN 978-3-933761-97-2

194 Bliefernicht, Jan-Geert: *Probability Forecasts of Daily Areal Precipitation for Small River Basins,* 2011, ISBN 978-3-933761-98-9

195 Hrsg.: Koschitzky, Hans-Peter; Braun, Jürgen: *VEGAS-Kolloquium 2010 In-situ-Sanierung - Stand und Entwicklung Nano und ISCO -,* Tagungsband zur Veranstaltung am 07. Oktober 2010 an der Universität Stuttgart, Campus Stuttgart-Vaihingen*,* 2010*,* ISBN 978-3-933761-99-6

196 Gafurov, Abror: *Water Balance Modeling Using Remote Sensing Information - Focus on Central Asia,* 2010, ISBN 978-3-942036-00-9

197 Mackenberg, Sylvia: *Die Quellstärke in der Sickerwasserprognose: Möglichkeiten und Grenzen von Labor- und Freilanduntersuchungen,* 2010, ISBN 978-3-942036-01-6

198 Singh, Shailesh Kumar: *Robust Parameter Estimation in Gauged and Ungauged Basins,* 2010, ISBN 978-3-942036-02-3

199 Doğan, Mehmet Onur: *Coupling of porous media flow with pipe flow,* 2011, ISBN 978-3-942036-03-0

200 Liu, Min: *Study of Topographic Effects on Hydrological Patterns and the Implication on Hydrological Modeling and Data Interpolation,* 2011, ISBN 978-3-942036-04-7

201 Geleta, Habtamu Itefa: *Watershed Sediment Yield Modeling for Data Scarce Areas,* 2011, ISBN 978-3-942036-05-4

202 Franke, Jörg: *Einfluss der Überwachung auf die Versagenswahrscheinlichkeit von Staustufen,* 2011, ISBN 978-3-942036-06-1

203 Bakimchandra, Oinam: *Integrated Fuzzy-GIS approach for assessing regional soil erosion risks,* 2011, ISBN 978-3-942036-07-8

204 Alam, Muhammad Mahboob: *Statistical Downscaling of Extremes of Precipitation in Mesoscale Catchments from Different RCMs and Their Effects on Local Hydrology,* 2011, ISBN 978-3-942036-08-5

205 Hrsg.: Koschitzky, Hans-Peter; Braun, Jürgen: *VEGAS-Kolloquium 2011 Flache Geothermie - Perspektiven und Risiken,* Tagungsband zur Veranstaltung am 06. Oktober 2011 an der Universität Stuttgart, Campus Stuttgart-Vaihingen, 2011, ISBN 978-3-933761-09-2

206 Haslauer, Claus: *Analysis of Real-World Spatial Dependence of Subsurface Hydraulic Properties Using Copulas with a Focus on Solute Transport Behaviour,* 2011, ISBN 978-3-942036-10-8

207 Dung, Nguyen Viet: *Multi-objective automatic calibration of hydrodynamic models – development of the concept and an application in the Mekong Delta,* 2011, ISBN 978-3-942036-11-5

208 Hung, Nguyen Nghia: *Sediment dynamics in the floodplain of the Mekong Delta, Vietnam,* 2011, ISBN 978-3-942036-12-2

209 Kuhlmann, Anna: *Influence of soil structure and root water uptake on flow in the unsaturated zone,* 2012, ISBN 978-3-942036-13-9

210 Tuhtan, Jeffrey Andrew: *Including the Second Law Inequality in Aquatic Ecodynamics: A Modeling Approach for Alpine Rivers Impacted by Hydropeaking,* 2012, ISBN 978-3-942036-14-6

211 Tolossa, Habtamu: *Sediment Transport Computation Using a Data-Driven Adaptive Neuro-Fuzzy Modelling Approach,* 2012, ISBN 978-3-942036-15-3

212 Tatomir, Alexandru-Bodgan: *From Discrete to Continuum Concepts of Flow in Fractured Porous Media,* 2012, ISBN 978-3-942036-16-0

213 Erbertseder, Karin: *A Multi-Scale Model for Describing Cancer-Therapeutic Transport in the Human Lung,* 2012, ISBN 978-3-942036-17-7

214 Noack, Markus: *Modelling Approach for Interstitial Sediment Dynamics and Reproduction of Gravel Spawning Fish,* 2012, ISBN 978-3-942036-18-4

215 De Boer, Cjestmir Volkert: *Transport of Nano Sized Zero Valent Iron Colloids during Injection into the Subsurface*, 2012, ISBN 978-3-942036-19-1

216 Pfaff, Thomas: *Processing and Analysis of Weather Radar Data for Use in Hydrology*, 2013, ISBN 978-3-942036-20-7

217 Lebrenz, Hans-Henning: *Addressing the Input Uncertainty for Hydrological Modeling by a New Geostatistical Method*, 2013, ISBN 978-3-942036-21-4

218 Darcis, Melanie Yvonne: *Coupling Models of Different Complexity for the Simulation of CO_2 Storage in Deep Saline Aquifers*, 2013, ISBN 978-3-942036-22-1

219 Beck, Ferdinand: *Generation of Spatially Correlated Synthetic Rainfall Time Series in High Temporal Resolution - A Data Driven Approach*, 2013, ISBN 978-3-942036-23-8

220 Guthke, Philipp: *Non-multi-Gaussian spatial structures: Process-driven natural genesis, manifestation, modeling approaches, and influences on dependent processes*, 2013, ISBN 978-3-942036-24-5

221 Walter, Lena: *Uncertainty studies and risk assessment for CO_2 storage in geological formations*, 2013, ISBN 978-3-942036-25-2

222 Wolff, Markus: *Multi-scale modeling of two-phase flow in porous media including capillary pressure effects,* 2013, ISBN 978-3-942036-26-9

223 Mosthaf, Klaus Roland: *Modeling and analysis of coupled porous-medium and free flow with application to evaporation processes,* 2014, ISBN 978-3-942036-27-6

224 Leube, Philipp Christoph: *Methods for Physically-Based Model Reduction in Time: Analysis, Comparison of Methods and Application*, 2013, ISBN 978-3-942036-28-3

225 Rodríguez Fernández, Jhan Ignacio: *High Order Interactions among environmental variables: Diagnostics and initial steps towards modeling*, 2013, ISBN 978-3-942036-29-0

226 Eder, Maria Magdalena: *Climate Sensitivity of a Large Lake*, 2013, ISBN 978-3-942036-30-6

227 Greiner, Philipp: *Alkoholinjektion zur In-situ-Sanierung von CKW Schadensherden in Grundwasserleitern: Charakterisierung der relevanten Prozesse auf unterschiedlichen Skalen*, 2014, ISBN 978-3-942036-31-3

228 Lauser, Andreas: *Theory and Numerical Applications of Compositional Multi-Phase Flow in Porous Media*, 2014, ISBN 978-3-942036-32-0

229 Enzenhöfer, Rainer: *Risk Quantification and Management in Water Production and Supply Systems*, 2014, ISBN 978-3-942036-33-7

230 Faigle, Benjamin: *Adaptive modelling of compositional multi-phase flow with capillary pressure*, 2014, ISBN 978-3-942036-34-4

231 Oladyshkin, Sergey: *Efficient modeling of environmental systems in the face of complexity and uncertainty*, 2014, ISBN 978-3-942036-35-1

232 Sugimoto, Takayuki: *Copula based Stochastic Analysis of Discharge Time Series*, 2014, ISBN 978-3-942036-36-8

233 Koch, Jonas: *Simulation, Identification and Characterization of Contaminant Source Architectures in the Subsurface*, 2014, ISBN 978-3-942036-37-5

234 Zhang, Jin: *Investigations on Urban River Regulation and Ecological Rehabilitation Measures, Case of Shenzhen in China*, 2014, ISBN 978-3-942036-38-2

235 Siebel, Rüdiger: *Experimentelle Untersuchungen zur hydrodynamischen Belastung und Standsicherheit von Deckwerken an überströmbaren Erddämmen,* 2014, ISBN 978-3-942036-39-9

236 Baber, Katherina: *Coupling free flow and flow in porous media in biological and technical applications: From a simple to a complex interface description,* 2014, ISBN 978-3-942036-40-5

237 Nuske, Klaus Philipp: *Beyond Local Equilibrium — Relaxing local equilibrium assumptions in multiphase flow in porous media,* 2014, ISBN 978-3-942036-41-2

238 Geiges, Andreas: *Efficient concepts for optimal experimental design in nonlinear environmental systems*, 2014, ISBN 978-3-942036-42-9

239 Schwenck, Nicolas: *An XFEM-Based Model for Fluid Flow in Fractured Porous Media*, 2014, ISBN 978-3-942036-43-6

240 Chamorro Chávez, Alejandro: *Stochastic and hydrological modelling for climate change prediction in the Lima region, Peru*, 2015, ISBN 978-3-942036-44-3

241 Yulizar: *Investigation of Changes in Hydro-Meteorological Time Series Using a Depth-Based Approach*, 2015, ISBN 978-3-942036-45-0

242 Kretschmer, Nicole: *Impacts of the existing water allocation scheme on the Limarí watershed – Chile, an integrative approach*, 2015, ISBN 978-3-942036-46-7

243 Kramer, Matthias: *Luftbedarf von Freistrahlturbinen im Gegendruckbetrieb*, 2015, ISBN 978-3-942036-47-4

244 Hommel, Johannes: *Modeling biogeochemical and mass transport processes in the subsurface: Investigation of microbially induced calcite precipitation*, 2016, ISBN 978-3-942036-48-1

245 Germer, Kai: *Wasserinfiltration in die ungesättigte Zone eines makroporösen Hanges und deren Einfluss auf die Hangstabilität*, 2016, ISBN 978-3-942036-49-8

246 Hörning, Sebastian: *Process-oriented modeling of spatial random fields using copulas*, 2016, ISBN 978-3-942036-50-4

247 Jambhekar, Vishal: *Numerical modeling and analysis of evaporative salinization in a coupled free-flow porous-media system, 2016, ISBN* 978-3-942036-51-1

248 Huang, Yingchun: *Study on the spatial and temporal transferability of conceptual hydrological models*, 2016, ISBN 978-3-942036-52-8

249 Kleinknecht, Simon Matthias: *Migration and retention of a heavy NAPL vapor and remediation of the unsaturated zone*, 2016, ISBN 978-3-942036-53-5

250 Kwakye, Stephen Oppong: *Study on the effects of climate change on the hydrology of the West African sub-region*, 2016, ISBN 978-3-942036-54-2

Die Mitteilungshefte ab der Nr. 134 (Jg. 2005) stehen als pdf-Datei über die Homepage des Instituts: www.iws.uni-stuttgart.de zur Verfügung.